AD-A141 983 THE SPOT OF ARAGO AND ITS ROLE IN ABERRATION ANALYSIS 1/4
(U) AIR FORCE INST OF TECH WRIGHT-PATTERSON AFB OH
D R ERBSCHLOE DEC 83 AFIT/CI/NR-84-7T

UNCLASSIFIED F/G 20/6 NL

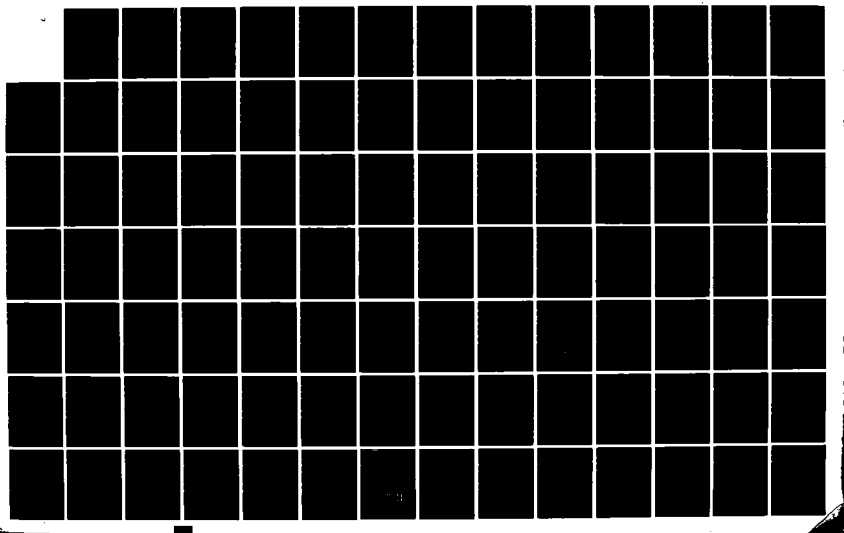

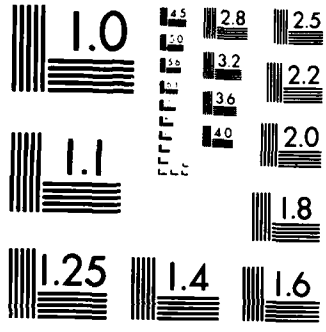

UNCLASS

SECURITY CLASSIFICATION OF THIS PAGE (When Data Entere

REPORT DOCUMENTATION PAGE

READ INSTRUCTIONS BEFORE COMPLETING FORM

1. REPORT NUMBER: AFIT/CI/NR 84-7T
2. GOVT ACCESSION NO.:
3. RECIPIENT'S CATALOG NUMBER:

4. TITLE (and Subtitle): The Spot Of Arago And Its Role In Aberration Analysis

5. TYPE OF REPORT & PERIOD COVERED: THESIS/DISSERTATION

6. PERFORMING ORG. REPORT NUMBER:

7. AUTHOR(s): Donald Ross Erbschloe

8. CONTRACT OR GRANT NUMBER(s):

9. PERFORMING ORGANIZATION NAME AND ADDRESS: AFIT STUDENT AT: Univ of New Mexico

10. PROGRAM ELEMENT, PROJECT, TASK AREA & WORK UNIT NUMBERS:

11. CONTROLLING OFFICE NAME AND ADDRESS: AFIT/NR WPAFB OH 45433

12. REPORT DATE: Dec 1983

13. NUMBER OF PAGES: 292

14. MONITORING AGENCY NAME & ADDRESS (if different from Controlling Office):

15. SECURITY CLASS. (of this report): UNCLASS

15a. DECLASSIFICATION DOWNGRADING SCHEDULE:

16. DISTRIBUTION STATEMENT (of this Report)

APPROVED FOR PUBLIC RELEASE; DISTRIBUTION UNLIMITED

17. DISTRIBUTION STATEMENT (of the abstract entered in Block 20, if different from Report)

18. SUPPLEMENTARY NOTES

APPROVED FOR PUBLIC RELEASE: IAW AFR 190-17

LYNN E. WOLAVER 15 May 84
Dean for Research and
Professional Development
AFIT, Wright-Patterson AFB OH

19. KEY WORDS (Continue on reverse side if necessary and identify by block number)

20. ABSTRACT (Continue on reverse side if necessary and identify by block number)

ATTACHED

DD FORM 1 JAN 73 1473 EDITION OF 1 NOV 65 IS OBSOLETE

UNCLASS

SECURITY CLASSIFICATION OF THIS PAGE (When Data Entered)

THE SPOT OF ARAGO AND ITS ROLE IN ABERRATION ANALYSIS

BY

DONALD ROSS ERBSCHLOE

B.A., University of Virginia, 1976

THESIS

Submitted in Partial Fulfillment of the
Requirements for the Degree of

Master of Science in Physics

The University of New Mexico
Albuquerque, New Mexico

December, 1983

Donald Ross Erbschloe

Candidate

Physics

Department

This thesis is approved, and it is acceptable in quality and form for publication on microfilm:

Approved by the Thesis Committee:

James E Harvey, Chairperson

Seymour J. Allen

Colston Chandler

Accepted:

Dean, Graduate School

March 8, 1984

Date

For Vickie, my bright spot.

ACKNOWLEDGEMENTS

The preparation of a thesis required a combined effort. I was very fortunate tc have a wealth of agencies and people supporting me. I would like to extend my thanks to the following:

First on the list is the Air Force Academy for giving me the opportunity to come back to school. The Air Force Weapons Lab at Kirtland Air Force Base provided computer funds. Some of the computer work was done under the supervision of Victor Gamiz and Joel Anspach of Rocketdyne. Rocketdyne also supplied the laboratory space and equipment for the experimental work and the computer analysis of interferogram data. Don Mullen and the personnel of the Optical Component Evaluation Laboratory (OCEL) gave tremendous support. Special thanks go to Larry Brooks and Johnny Johnson for their invaluable help.

My fellow graduate students followed the progress of this thesis with keen interest. I appreciated all their helpful ideas and suggestions. In particular, Barry Feldman and Roy Goeller helped with the preparation of the final draft. Also, Julio Gea-Banacloche contributed with his insight and his translation of several French articles. I talked with many faculty members about this thesis and would like to single out Dr. Seymour Alpert, Dr. Colston Chandler and Dr. George Lawrence for enlightening conversations. I want to thank Dr. James Harvey for suggesting this problem and for his continued enthusiastic guidance.

Finally, my family and in-laws were always there with patience, love and support. This thesis would have been impossible were it not for my wife, Vickie. She indulged and inspired me -- and typed.

THE SPOT OF ARAGO AND ITS ROLE

IN ABERRATION ANALYSIS

Donald Ross Erbschloe

B.A., Physics, University of Virginia, 1976
M.S., Physics, University of New Mexico, 1983

The Spot of Arago is the bright diffraction spot in the center of the shadow behind a circular obstacle. Because this pattern is the result of diffraction at the edge of the obstacle, the spot contains information about the incident beam. If the incident beam contains aberrations, the shape and intensity of the diffraction pattern should change.

For points on and near the optical axis, analytical solutions to the Rayleigh-Sommerfeld diffraction integral are possible for a circular obscuration and an annular aperture illuminated by a plane wave of uniform or gaussian intensity distribution and containing defocus and/or spherical aberration. Computer studies of these cases show excellent agreement with experiment. The amount of defocus and spherical aberration can be deduced by intensity measurements and shift in positions of on axis intensity extrema behind an annular aperture. An empirical study of astigmatism revealed a predictable change in the diffraction pattern allowing for the verification of the aberration to within .05 wavelengths.

The Spot of Arago is inherent in many optical systems due to the

geometry of components. The technique of aberration determination by changes in the diffraction pattern should be useful in such systems.

THE SPOT OF ARAGO AND ITS ROLE IN ABERRATION ANALYSIS

BY

DONALD ROSS ERBSCHLOE

ABSTRACT OF THESIS

Submitted in Partial Fulfillment of the
Requirements for the Degree of

Master of Science in Physics

The University of New Mexico
Albuquerque, New Mexico

December, 1983

TABLE OF CONTENTS

Page

APPENDICES

LIST OF FIGURES

LIST OF GRAPHS

LIST OF PHOTOGRAPHS

LIST OF TABLES

Chapter 1

INTRODUCTION

Annular apertures are commonplace in optical systems. For example, Cassegrain telescopes (reflecting) have a secondary mirror which acts as a central obscuration in an otherwise circular field. A circular stop deliberately placed on the objective of a refracting

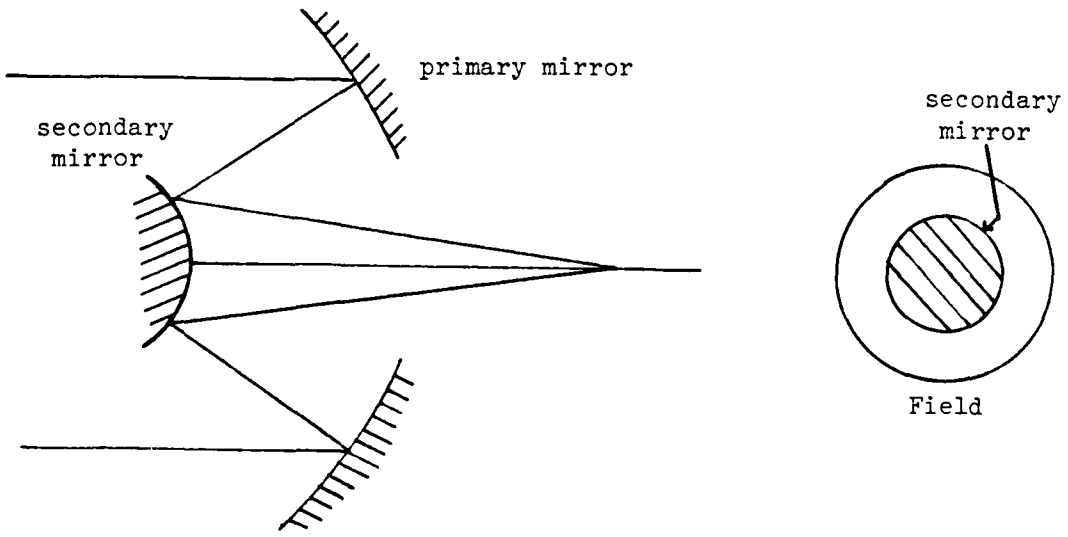

Figure 1.1

Cassegrain Mirror System and Cross-section of Field[1]

telescope can increase the depth of focus and the resolving power of the system.[2]

Statement of the Problem

Laser systems often have annular apertures as part of an optical resonator configuration. The diagram below depicts an elliptical out-coupling mirror set-up that acts as the optical analog of an annular aperture.

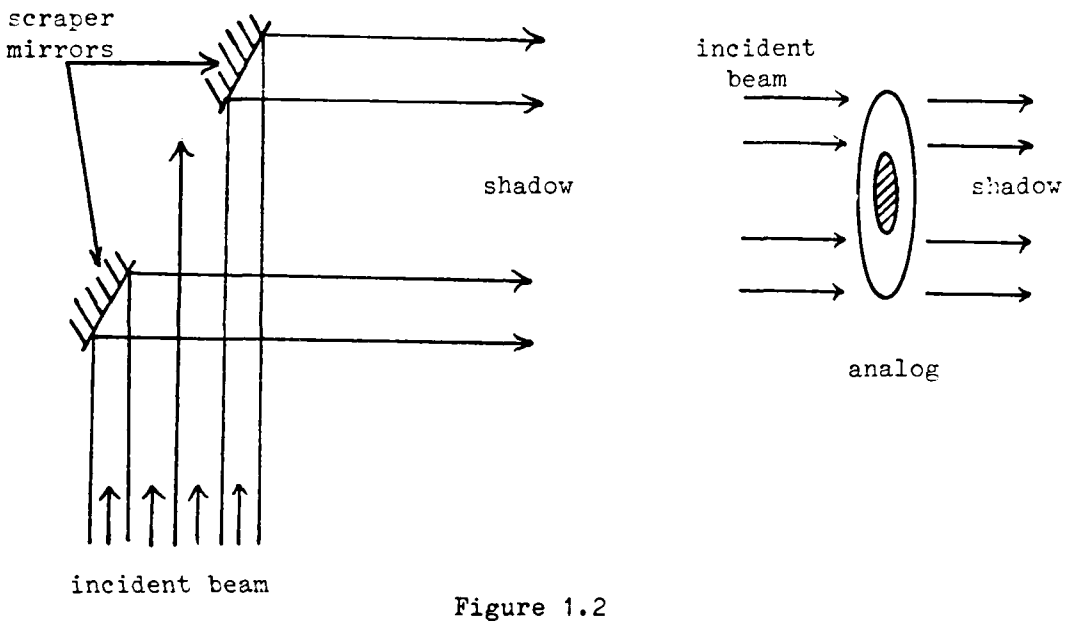

Figure 1.2

Elliptical Scraper Mirror and Its Optical Analog

This last configuration appears in the design of many High Energy Laser (HEL) resonators. It has created a particular nuisance for its developers. In the center of the shadow produced by this effective annular aperture is a hot spot. (The frequencies of the HEL output are in the infrared range.) The spot is a consequence of the constructive interference of radiation diffracted from the outer and

inner edges of the "aperture." This spot is related to the spot of Arago -- the diffraction spot formed by light incident upon a circular obstacle.[3] The intensity of the spot can be as high as four times the intensity of the incident beam. This makes it an unwanted addition to a designated "shadow" area. Left unchecked the spot can burn up vital optical components or produce thermal deformations in components. Designs must include provisions to diffract or reflect the aggravating manifestation into an optical dump. The attitude of the HEL workers is reminiscent of Lady Macbeth's plea "Out, damned spot! out, I say!"[4]

It is frequently necessary to perform real-time HEL diagnostics to test beam quality. This requires additional gratings, beam splitters, or other beam-sampling components which add to the overall weight, size and complexity of the design. If the hot spot contains information about beam quality, namely, if its shape and size is characteristic of aberrations in the incident wave front, it could be used as an integral part of the required diagnostic process. Such a scheme would eliminate the need for a lot of hardware.

James E. Harvey and James L. Forgham have demonstrated that the shape of the spot in the shadow of a circular obstacle illuminated by a plane wave does change with increased aberration (astigmatism).[5]

The feasibility of a diagnostic package using the spot as input depends on the answers to the following questions:

1. What types of aberrations produce measurable changes in the spot?
2. How sensitive are changes in the spot to changes in amount of aberration?

3. Given specific spot characteristics, can the aberrations present be determined?

Thesis Content

This thesis will address itself to the solutions of the preceding questions for the following Seidel aberrations: defocus, spherical aberration, coma and astigmatism. First the remarkable history of the spot of Arago will be traced from the eighteenth century to current research. A detailed analysis for the unaberrated cases of the spots produced by circular obscurations and annular apertures will serve as standards against which to compare the aberrated cases. It turns out that analytic solutions to the Rayleigh-Sommerfeld diffraction integral are possible for the rotationally symmetric aberrations (defocus, spherical aberration) for certain restrictive, but physically important cases. The non-rotationally symmetric aberrations (coma, astigmatism) require numerical or empirical analysis. Where possible, theory is tested against experimental results. Each aberration is handled separately but various strategies to separate combinations of aberrations are discussed. The main body of the thesis culminates in a discussion of experimental and theoretical results, suggestions for future research, and overall conclusions. Several appendices are included which contain material of historical interest, lengthy derivations and computer program listings.

Potential applications exist for a variety of optical systems;

however, the High Energy Laser was cited as a specific example of a system which might benefit from a sensor package capable of performing wavefront analysis upon the diffraction spot. This is because the diffraction spot is an inherent part of the output of any annular HEL beam and the use of a separate beam sampling component for diagnostic purposes can degrade the beam quality. The possibility that this diffraction pattern gives measurable and meaningful information is the incentive for the research that follows.

Notes

[1] Warren J. Smith, Modern Optical Engineering (New York: McGraw-Hill, 1966), p. 38.

[2] W. T. Welford, "Use of Annular Apertures to Increase Focal Depth," Journal of the Optical Society of America, 50 (August 1960), 749; E. H. Linfoot and E. Wolf, "Diffraction Images in Systems with an Annular Aperture," Procedings of the Physical Society B, 66 (1953), 145.

[3] Max Born and Emil Wolf, Principles of Optics, 6th ed. (Oxford: Pergamon Press, 1980), p. 375.

[4] Macbeth V.i.38.

[5] James E. Harvey and James L. Forgha..., "The Spot of Arago: New Relevance for an Old Phenomenon," American Journal of Physics, (January 1984).

Chapter 2

HISTORICAL BACKGROUND

The Wave Theory vs. the Corpuscular Theory of Light

One of the great ideological clashes in the history of physics is the controversy between the corpuscular and wave theories of light. The center of the conflict rested on the very nature of light. Advocates of the corpuscular theory agreed with Sir Isaac Newton that light was composed of minute particles. The wave theorists sided with Rene Descartes, Robert Hooke and Christian Huyghens who felt light was the result of waves undulating in a medium called the ether.[1]

By the beginning of the nineteenth century the corpuscular theory was firmly ensconced as the preferred theory. Peter Anton Pav proposes the popularity of the particle theory originated in the philosophical battle between inductivism and deductivism:

> What occupied scientists was not a battle of waves vs. corpuscles . . . nor blind allegiance to Newton's authority. Rather, it was a basic and deeply felt difference of opinion as to how and where scientific truth was to be found and whether the ultimate canons of scientific justification were to be experimental or deductive.[2]

Newton's approach in his work Opticks was experimental and this had great appeal for the scientists of the eighteenth century. The corpuscular theory was adopted almost by consequence.[3]

To win over the scientific community the wave theorists needed to

show experimentally the conclusive advantages of their theory. The first advance was made by Thomas Young. He conducted a series of experiments exploring a variety of diffraction effects (including the famous double slit experiment). Despite publication of his papers and the delivery of a lecture and demonstration before the Royal Society of London in 1801, Young's work won little immediate support for the wave theory.[4] However he did gain a very important convert -- the Frenchman Dominique Francois Jean Arago.

In 1811 Arago studied the Newton's rings phenomena in calcite in conjunction with his work on polarization. The failure of the corpuscular theory to explain many of his results encouraged him to consider the wave theory. He began a correspondence with Young and was soon convinced of the truth of Young's theory.[5]

The next advance in the cause of the wave theory came from Augustin Jean Fresnel. He met briefly with Arago in 1815. Arago introduced Fresnel to Young's treatises and persuaded him to come to Paris in 1816 to begin his researches in diffraction. The timing of the research was ripe, for in January 1817 a commission composed of Pierre Simon Laplace, Jean-Baptiste Biot, Claude Louis Berthollet and Jacques Alexandre César Charles chose diffraction as the subject for a prize sponsored by the Academié des Sciencès.[6]

Fresnel entered his memoir on diffraction in the contest. In July 1818 a panel of five was chosen to judge the entries. The panel members were Laplace, Biot, Arago, Simeón Denis Poisson and Joseph Louis Gay-Lussac. Laplace, Biot and Poisson were staunch adherents of the particle theory of light while Arago advocated Fresnel's view.

Gay-Lussac, a chemist, was impartial.[7]

In reviewing Fresnel's theory, Poisson saw that the simple geometry of light diffracted by an opaque circular disc suggested the existence of a bright spot of light in the center of the disc's shadow. This, he felt, was contrary to experience and thus Fresnel's theory must be wrong.[8]

Arago tested Poisson's prediction in the laboratory. He affixed a disc 2mm in diameter to a plate of glass and using sunlight observed the spot in the center of the shadow.[9] (This is an irony Pav should appreciate -- Poisson attempted to discredit Fresnel's wave theory based on deductive reasoning; Arago vindicated Fresnel through experiment.) Since this time the phenomena has been known as either Poisson's spot or Arago's spot. (This paper adopts the terminology of crediting Arago, who trusted in the spot's existence.) Arago's discovery was powerful evidence in favor of the wave theory of light. Fresnel won the prize from the Academié and his entry became known as his Crown Memoir.[10]

Although the demonstration of the spot did much to usurp the corpuscular theory, the controversy between waves and particles continued through the nineteenth century in a series of incarnations.

Earlier Observations of the Spot

Many sources mention that Arago was not the first to observe the bright point of light. John William Strutt (Lord Rayleigh) and

E. Verdet in his Leçons d'Optique Phisique note that Joseph Nicholas Delisle, a French astronomer, discovered a bright spot in the center of a circular shadow "in the earlier half of the 18th century," a discovery which subsequently "passed into oblivion."[11] John Strong, Max Born and Emil Wolf credit Maraldi, another French astronomer, with the finding. Born and Wolf say that Maraldi's observation occured "a century earlier" than Arago's experiment and "had bee- forgotten."[12] Strong claims that Maraldi found the bright spot "over half a century earlier."[13]

Joseph Nicholas Delisle (1688-1768) was one of a family of famous French scientists. One brother, Guillame, was a geographer and historian, another brother, Louis, was also an astronomer. Catherine the Great invited Joseph and Louis to come to Russia in 1726 to run the observatory at St. Petersburg. Louis died while in Russia and Joseph Nicholas came back to Paris. Delisle became a member of the Academié des Sciencès in 1714 and in 1724 was elected to the Royal Society of London.[14]

As a member of the Academie des Sciences, Deslisle could have met and worked with two Maraldis. Neither Born and Wolf's text nor Strong's book mentions Maraldi's first name.

Jacques-Phillipe Maraldi (1665-1729) was the nephew of Dominique Cassini -- the discoverer of the famous division in the rings of Saturn. Jacques-Phillipe also became an astronomer and joined the Academié des Sciencès in 1694.

Jean-Dominique Maraldi (1709-1788) was the nephew of Jacques-Phillip Maraldi. He was inducted into the Academié des Sciencès in

1731.[15]

The vague references from Rayleigh, Verdet, Strong and Born and Wolf do not allow one to pinpoint the date of the first observation, the circumstances surrounding the discovery, who made it or even which Maraldi was involved. Because Delisle and both Maraldis lived and worked in Paris at overlapping times and belonged to the same scientific organization it is possible that the "discovery" by the second party was actually a verification of a phenomenon observed by the first.

The sources also suggest the observations of Delisle and Maraldi about the spot faded into the limbo of untimely scientific discoveries. That Poisson was unaware of these findings is evident from the challenge he made against Fresnel's theory. Arago, however, did know about the earlier sightings. On February 26, 1816 (two years before he sat on the judging commission with Poisson) he presented to the National Institute observations about diffraction and an early draft of Fresnel's memoir. Here he mentions that besides Grimaldi, Maraldi and Delisle showed that light could penetrate the geometric shadow behind an opaque body.[16] This knowledge may have provided additional impetus for Arago to verify Poisson's skeptical prediction.

Rings Around the Spot

The ease with which one could produce the spot made it an ideal subject for study by the new legions of wave theorists. The following

is a description of an experiment by Richard Potter to test the intensity of the spot.

> I prepared . . . discs of brass of 1/10, 2/10, 3/10, 4/10 and 7/10 and with watch makers implements of 1/20 inch. The discs were attached by thin films of cement to a plate of glass. The sun's light was reflected horizontally through a window shutter of a darkened room, and the sun's image, formed by a lens of 1/6 inch focal length was at 60 inches distance from the disc at the same time the focus of the eyelens, by which the phenomena of diffraction were examined, was at 60 inches distance on the other side. When the whole was adjusted, on looking through an eyelens of about 1 inch focal length, at the centre of the shadow cast by the disc, there was seen a bright central spot, of a white color slightly tinged with brown, surrounded by a greater or lesser number of coloured rings, according to the size of the disc.[17]

The colors observed by Potter stem from the fact that light from the sun is not monochromatic.

The concentric ring structure was given a mathematical foundation by the British Astronomer Royal, George Biddell Airy. In a paper entitled "On the Diffraction of an Annular Aperture," Airy constructed a table by which one could deduce the spacing of the ring structure produced in three cases: monochromatic light falling on a circular aperture, a circular obscuration or an annular aperture.[18]

Lommel's Work

The definitive study of diffraction by a circular obstacle and a circular aperture was made by Emil Lommel in the 1880s. Lommel solved the diffraction integral by using Bessel functions. He found the intensity distribution of light in the shadow of a circular obstacle

satisfies the expression:

$$M^2 = C^2 + S^2 \qquad \text{(II-1)}$$

where M^2 is the intensity and C and S are integrals whose solutions contain the Lommel functions:

Born and Wolf list the Lommel functions as

$$U_n(u, v) = \sum_{s=0}^{\infty} (-1)^s \left(\frac{u}{v}\right)^{n+2s} J_{n+2s}(v) \qquad \text{(II-2)}$$

$$V_n(n, v) = \sum_{s=0}^{\infty} (-1)^s \left(\frac{u}{v}\right)^{n+2s} J_{n+2s}(v) \qquad \text{(II-3)}$$

where u and v are dimensionless parameters based on the geometry of the set-up and J_{n+2s} is the Bessel function of the first kind and $n + 2s^{th}$ order.[19] The Lommel functions have the disadvantage of being slowly convergent.

Lommel performed the experiment to verify his theory. He used sunlight and a prism to obtain fairly monochromatic light. With an eyelens etched with a micrometer he measured the ring structure of both the obstacle and the aperture and found it to be in excellent agreement with theory.[20]

Experiments at the Turn of the Century

It is interesting that Lommel relied on the somewhat crude method of sunlight and prism to make a light beam with narrow band width.

The nineteenth century saw major advances in the production of high intensity light sources. In 1825 Thomas Drummond invented lime-light.[21] The carbon arc-light was developed by a number of people. Frederick Holmes built a cumbersome working model in 1857. By the mid 1870s practical commercial arc-lamps were being sold.[22]

The widespread use of arc-lamps in laboratories at the turn of the century renewed interest in the spot of Arago. Using a spectrometer one could isolate an intense monochromatic signal from the carbon spectrum. This was important because photographs of the phenomenon were possible.

W. Arkadiew published a famous series of photographs in 1913. Using a variety of lens combinations he altered the virtual distance between object and image planes to observe the change in spot size.[23]

In April 1914 two papers appeared which demonstrated that a circular obstacle could be used in place of a lens to produce an image. Alfred W. Porter noticed that "the bright spot is in reality an image of the source of light."[24] Porter used a set-up similar to the one described by Mason E. Hufford and depicted below.

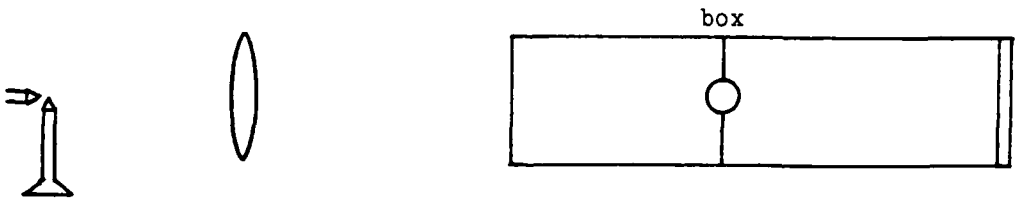

Figure 2.1

Experimental Set-up to Demonstrate Imaging by a Disc

Hufford reported that "each point in the aperture (opening to the box) produces a corresponding effect in the shadow. This suggests, therefore, that the aperture may be any sort of figure and in the shadow of the disc or sphere there should be an inverted image of it."[25] Porter used a triangular opening to produce a three-sided image. Hufford, with a bit more flair, made a monogram out of the letters I and U (he was a professor at Indiana University) as one opening and a transparency of the profile of Woodrow Wilson as another. The resultant image of the latter appears in Jenkins and White.[26]

Hufford also made photographs of the ring structure in the shadow of a circular obstacle. Lommel had only measured the radii of a few rings immediately surrounding the central spot. By exposing a photographic plate for several hours Hufford got photographs showing a large number of rings. These rings could be measured to check Lommel's theory. There was excellent agreement with theory (less than 2% difference in radius size for the outer rings).[27]

At a meeting of the Physical Society of London in 1925, A. O. Rankine projected several images using a 7mm ball bearing. He noted that each point in the light source produces an image in the shadow. Since only one source point is on the optical axis, a circular obstacle creates some aberration.[28] The aberrations can be understood by noticing that points in the source off the optical axis do not enjoy the special symmetry that the axial point does.

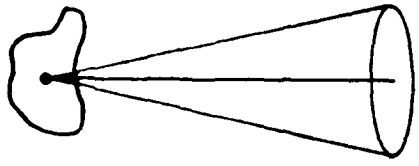

Figure 2.2

Disk Illuminated by
On-axis Source Point:
Equal Optical Path Distances

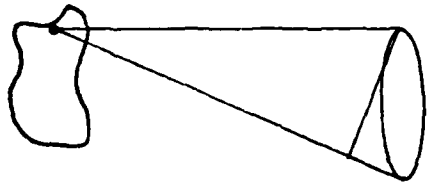

Figure 2.3

Disk Illuminated by
Off-axis Source Point:
Different Optical Path Distances

Optical path differences in Figure 2.3 lead to phase differences upon diffraction. If one substitutes a spherical obstacle, the circular cross section restores the symmetry for every source point.

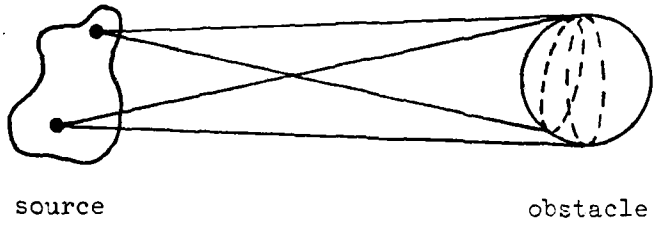

Figure 2.4

Sphere Illuminated by Off-axis Source Points:
Equal Optical Path Distances for Each Point

Dissimilarities in the intensities of the Arago spots for circular obstacles and spherical obstacles was the subject of a 1926 paper by C. V. Raman and K. S. Krishnan. They mounted a sphere and a disc to a

glass plate and measured the central spot intensities for both cases. If the observation distance behind the obstacles was small, the circular obstacle produced a brighter central spot than the spherical obstacle. Raman and Krishnan explained it this way. Rays diffracted by the edge of a circular obstacle can reach the observation point directly. For a spherical obstacle one must construct a cone tangent

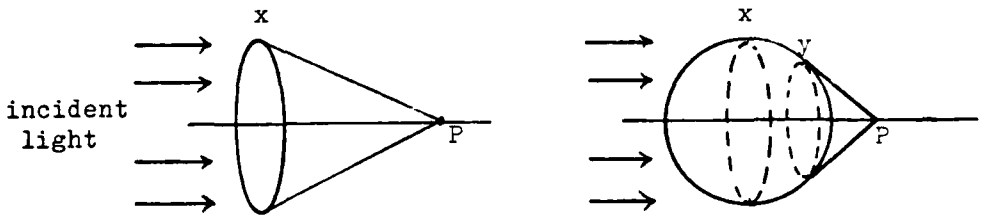

Circular obstacle Spherical obstacle

Figure 2.5

Diffraction Edge Sources for Rays Converging at Point P

to the back side of the sphere with the observation point as the apex. "The disturbance incident on the surface of the sphere has to creep round it, as it were, over the arc XY before the rays diffracted out by the sphere can reach the point of observation, and must suffer a very considerable dimunation in the process." As the distance from the obstacle to P increases, the arc XY decreases in length and the difference in intensity between the spherical and circular obstacle diffraction spots becomes smaller.[29]

The promise of imaging by a disc or sphere was never fully realized. The ring structure associated with each image point led to

smearing and poor image quality. With no forseeable practical application, interest in the spot of Arago waned until the next major advance in production of monochromatic light.

The Advent of the Laser

A laser is a source of coherent, intense, monochromatic light. It provides a simple means of observing the spot of Arago. A circular or spherical obstacle placed in an expanded beam from a laser creates a bright spot and ring structure that in many cases is visible with the naked eye.[30]

The importance of the laser prompted innovative uses for the spot. One area with great potential is the use of the spot in the detection of aberrations.

In an interdepartmental correspondence from Hughes Aircraft, J. A. Jenny showed a way to detect tilt in a wavefront. A plane wave propagating in the direction of an optical axis normal to a circular obstacle will image a bright spot at every point on axis behind the obstacle. If the incident wave direction vector makes a small angle with the optical axis the spot is offset from the axis by a calculable distance. Thus a circular obstacle placed in a wavefront to be tested can be used to measure the amount of tilt present.[31]

Harvey and Forgham solved the Fresnel region Rayleigh-Sommerfeld diffraction integral for a spherical obstacle with an incident plane wave of uniform or gaussian distribution of intensity. The intensity

pattern in the image plane has a J_0^2 dependence, where J_0 is the zeroth order Bessel function. They also derived a formula for the intensity on axis behind an annular aperture. Introducing known amounts of aberration (astigmatism) in the incident wavefront they demonstrated the shape and pattern of the spot and ring structure changes.[32]

This last experiment is the embarkation point for this thesis.

Notes

[1] Stanley B. Brown, ed., "The Interference of Light," Foundations of Physics (Louisville: Touchstone, 1972), p. 99.

[2] Peter Anton Pav, "Eighteenth Century Optics: The Cartesian-Newton Conflict," Applied Optics, 14 (December 1975), 3104.

[3] Ibid., p. 3103.

[4] Charles G. Fraser, Half-hours with Great Scientists (Toronto: University of Toronto Press, 1948), p. 276.

[5] Maurice Crosland, The Society of Arcueil (Cambridge, Mass.: Harvard University Press, 1967), p. 321.

[6] Ibid., p. 408.

[7] Ibid., p. 409.

[8] John Strong, Concepts of Classical Optics (San Francisco: W. H. Freeman, 1958), p. 186.

[9] Augustin Fresnel, De La Lumière (Paris: Librairie Armand Colin, 1914), p. 61.

[10] Brown, op. cit., p. 126.

[11] Lord Rayleigh, "The Wave Theory of Light," in his Scientific Papers, Vol. III (New York: Dover, 1964), p. 78.

[12] Max Born and Emil Wolf, Principles of Optics, 6th ed. (Oxford: Pergamon, 1980), p. 375.

[13] Strong, loc. cit.

[14] "Deslisle, Joseph Nicholas," The American Cyclopedia, rev. ed.

[15] "Maraldi, Jacques-Phillipe" and "Maraldi, Jean-Dominique," La Grand Encyclopedie.

[16] Francois Dominique Arago, "Note sur un phénomène remarquable qui s'observe dans diffraction de la lumière," in his Oeuvres Completes des Memoires Notices Scientifiques, Vol. IV (Amsterdam: Lees-Museum Bibliothek, 1858), p. 99.

[17] Richard Potter, "On the Phenomena of Diffraction in the Centre of the Shadow of a Circular Disc," The Philosophical Magazine, 19 (1841), 153-154.

[18] George Biddell Airy, "On the Diffraction of an Annular Aperture," The Philosophical Magazine, 18 (1841), 1-10.

[19] Born and Wolf, op. cit, p. 438.

[20] E. Lommel, "Die Beugungerscheinungen einer kreisrunden Oeffnung und eines kreisrunden Schirmchens," Abhandlungen der Mathematisch - Physikalischen classe der Koniglich. Bayerischen Akademie der Wissenschaft, (1886), 298.

[21] James Burke, Connections (Boston: Little Brown, 1978), pp. 269-271.

[22] Ibid., p. 276.

[23] W. Arkadiew, "Die Fresnelschen Beugungerscheinungen," Physikalische Zeitschrift, XIV (1913), 833; George S. Monk, Light: Principles and Experiments (New York: Dover, 1963), p. 168.

[24] Alfred W. Porter, "On the Formation of Images by Means of an Opaque Disk," The Philosophical Magazine, 27 (April 1914), 673.

[25] Mason E. Hufford, "Some New Diffraction Photographs," The Physical Review, III (Apr 1914), 242.

[26] Francis A. Jenkins and Harvey E. White, Fundamentals of Optics, 4th ed. (New York: McGraw-Hill, 1976), p. 385.

[27] Mason E. Hufford, "The Diffraction Ring Pattern in the Shadow of a Circular Object," The Physical Review, VII (May 1916), 549.

[28] A. O. Rankine, "Demonstration on the Diffraction of Light by a Spherical Obstacle," Procedings of the Physical Society, 37 (August 1925), 267.

[29] C. V. Raman and K. S. Krishnan, "On the Diffraction of Light by Spherical Obstacles," Proceedings of the Physical Society, 38 (August 1926), 352.

[30] H. Schober and R. Krusche, "Einfacher Demonstrationsversuch zum Poissonschen Fleck," Optik, 30 (1969), 314-317; John B. Johnston, "Projecting Poisson's Spot," The Physics Teacher, 16 (March 1978), 179.

[31] J. A. Jenney, "Diffraction Disk Imaging Resolution and Image Quality," Interdepartmental Correspondence, Hughes Aircraft (29 July 1974).

[32] James E. Harvey and James E. Forgham, "The Spot of Arago: New Relevance for an Old Phenomenon," The American Journal of Physics, (January 1984).

Chapter 3

THEORY I: UNABERRATED CASES

Consider a monochromatic plane wave incident upon an aperture in an otherwise opaque plane screen. The disturbance at a point P_2 behind the screen is given by the Rayleigh-Sommerfeld diffraction integral:[1]

$$U(P_2) = \frac{1}{i\lambda} \int\int_{\text{plane}} U(P_1) \frac{e^{ikl}}{l} \cos(\underset{\sim}{n}, \underset{\sim}{l})\, r_1 dr_1 d\phi_1 \qquad \text{(III-1)}$$

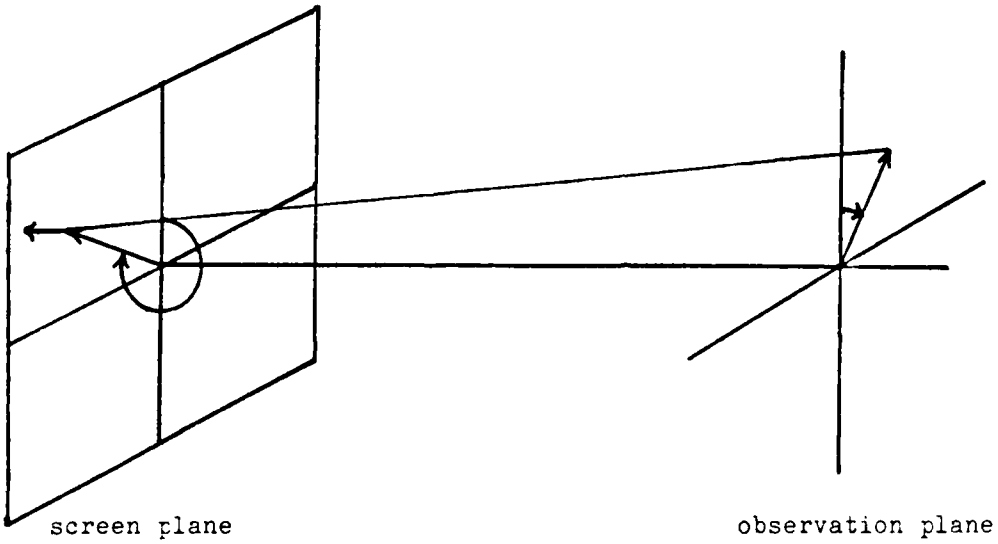

Figure 3.1

Diffraction by an Aperture in a Plane Screen

λ is the wavelength of the incident wave. $U(P_1)$ is the disturbance function in the plane of screen where:

$$U(P_1) = A(r_1, \phi_1)\, e^{ikW(r_1, \phi_1)}\, T(r_1, \phi_1) \qquad \text{(III-2)}$$

$A(r_1, \phi_1)$ = amplitude function

$W(r_1, \phi_1)$ = aberration function

$T(r_1, \phi_1)$ = aperture function = 1 if (r_1, ϕ_1) is in the aperture

= 0 otherwise

$\underset{\sim}{n}$ is a unit vector normal to the plane of the screen

$\cos(\underset{\sim}{n}, \underset{\sim}{l})$ is the cosine obliquity factor

$\underset{\sim}{l}$ is the vector from point P_1 to point P_2

It is possible to obtain $|\underset{\sim}{l}|$ in terms of the factors r_1, r_2, ϕ_1, ϕ_2 and z, the normal distance from point P_2 to the screen plane.

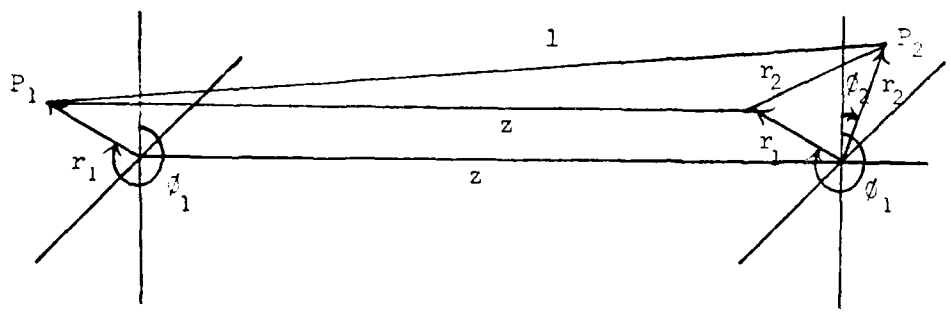

Figure 3.2

General Geometrical Layout

As shown in the above diagram:

$$l^2 = z^2 + r_2^2 \qquad \text{(III-3)}$$

But by the law of cosines:

$$r_3^2 = r_1^2 + r_2^2 - 2r_1r_2\cos(\phi_2 - \phi_1) \qquad \text{(III-4)}$$

$$\therefore\ l^2 = z^2 + r_1^2 + r_2^2 - 2r_1r_2\cos(\phi_2 - \phi_1) \qquad \text{(III-5)}$$

Case 1: Circular Obstacle with Uniform Illumination

The first case to consider is that of a circular obstacle in the screen plane. The diameter of the obstacle is d. The optical axis will be defined as the line normal to the obstacle and passing through the center of the obstacle, which is the origin of a cylindrical coordinate system.

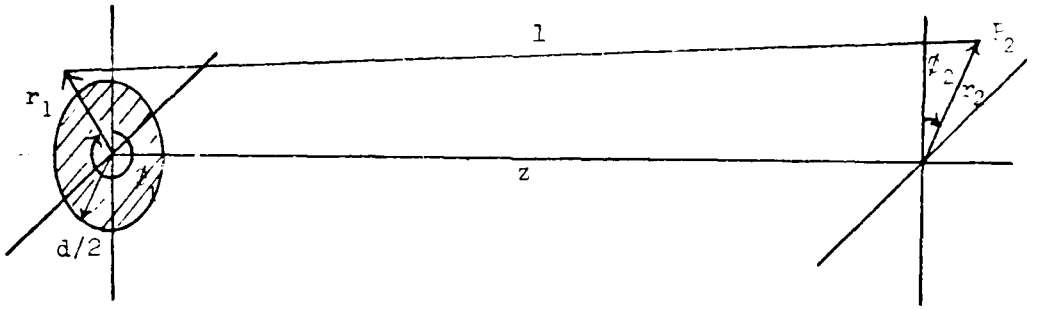

Figure 3.3

Geometrical Layout for Diffraction by a Circular Obstacle

If the incident plane wave is of uniform illumination (constant amplitude A) and contains no aberrations then the disturbance function U in the obstacle plane is given by:

$$U(r_1, \phi_1) = AT(r_1, \phi_1) \qquad \text{(III-6)}$$

The aperture function T can be transferred to the limits of integration and the Rayleigh-Sommerfeld diffraction integral becomes:

$$U(r_2, \phi_2, z) = \frac{A}{i\lambda} \int_{d/2}^{\infty} \int_{0}^{2\pi} \frac{e^{ikl}}{l} \cos(\underset{\sim}{n}, \underset{\sim}{l})\, r_1 dr_1 d\phi_1 \qquad \text{(III-7)}$$

Intensity on Axis

The cosine obliquity factor can be replaced by the term $\frac{z}{l}$. It is convenient to change the variable of integration to l.

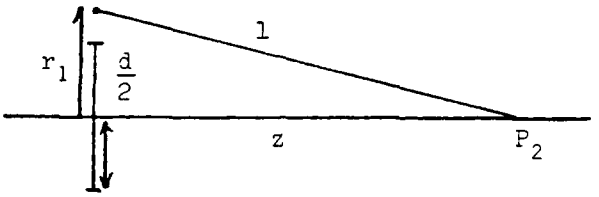

Figure 3.4

Determination of l for On-axis Points

$$l^2 = z^2 + r_1^2 \qquad dl = \frac{r_1}{l}\, dr_1 \qquad \text{(III-8)}$$

Thus the integral becomes:

$$U(0, 0, z) = \frac{Az}{i} \int_{\sqrt{z^2+d^2/4}}^{\infty} \int_{0}^{2\pi} \frac{e^{ikl}}{l}\, dl d\phi_1$$

$$= \frac{2\pi Az}{i} \int_{\sqrt{z^2+d^2/4}}^{\infty} \frac{e^{ikl}}{l}\, dl \qquad \text{(III-9)}$$

To evaluate this integral, integrate by parts:

$$f(1) = \frac{1}{1} \qquad g'(1) = e^{ikl}$$

$$f'(1) = -\frac{1}{l^2} \qquad g(1) = \frac{1}{ik}\ e^{ikl}$$

$$U(0, 0, z) = \frac{2\pi Az}{i\lambda}\left[\frac{1}{ikl}\ e^{ikl}\ \Bigg|_{\sqrt{z^2+d^2/4}}^{\infty} + \frac{1}{i}\int_{\sqrt{z^2+d^2/4}}^{\infty} \frac{1}{kl}\ \frac{e^{ikl}}{l}\ dl\right] \qquad \text{(III-10)}$$

This second integral contains a $\frac{1}{kl}$ term, otherwise it is identical to the original integral. Unless one looks immediately behind the obstacle (a distance on the order of a few wavelengths or less) then kl is much greater than 1. Thus the second integral is negligibly small. The expression for the disturbance at P_2 is:

$$U(0, 0, z) = \frac{2\ Az}{k\sqrt{z^2+d^2/4}}\ e^{ik\sqrt{z^2+d^2/4}}$$

but since $k = \frac{2\pi}{\lambda}$

$$U(0, 0, z) = A\ \frac{z}{\sqrt{z^2+d^2/4}}\ e^{ik\sqrt{z^2+d^2/4}} \qquad \text{(III-11)}$$

What does this expression mean physically? The factor A is the amplitude for the incident plane wave. $z/\sqrt{z^2 + d^2/4}$ is the cosine obliquity factor for rays diffracted by the edge of the obstacle to

P_2. $e^{ik\sqrt{z^2+d^2/4}}$ is the phase difference from the edge points to the point P_2. This indicates only the rays diffracted from the edge of the obstacle cause a disturbance on axis. Since the optical path length is identical for each edge-diffracted ray converging at P_2 the overall interference effect will be constructive.

The on-axis intensity distribution is given by the expression:

$$I(0, 0, z) = |U(0, 0, z)|^2$$

$$= A^2 \frac{z^2}{z^2+d^2/4} \qquad \text{(III-12)}$$

Substituting the incident intensity $I_0 = A^2$ in the expression yields:

$$I(0, 0, z) = \frac{1}{1 + \frac{d^2}{4z^2}} \; I_0 \qquad \text{(III-13)}$$

Thus the intensity on axis behind a circular obscuration is equal to the incident intensity times the square of the cosine obliquity factor for edge diffracted rays. For large values of z, $d^2/4z^2$ is much less than 1 (the cosine obliquity factor in essence becomes 1) and the intensity on axis is the same as if no obstacle were present.

Below is a graph of $I(0, 0, z) / I_0$ as a function of z for a 1cm diameter obstacle.

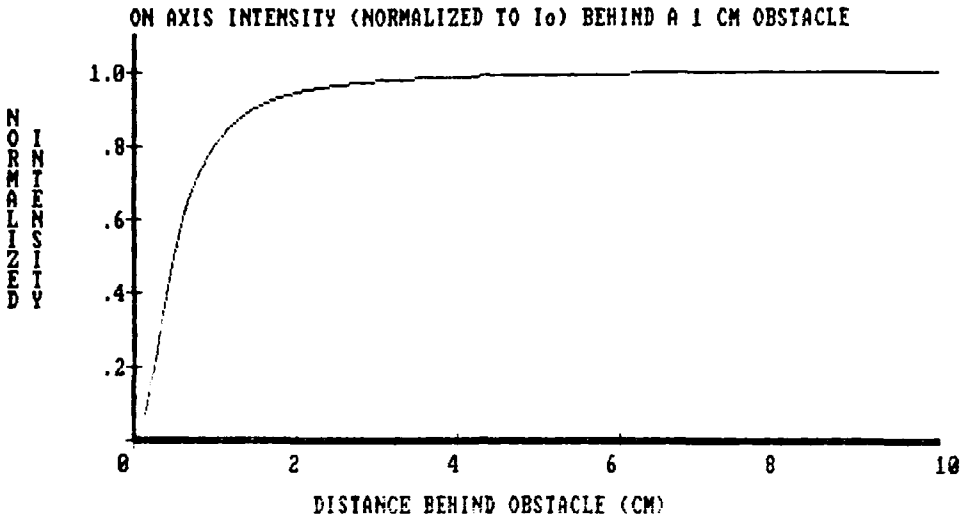

Graph 3.1

The intensity rapidly approaches its normalized value of 1. In fact it has reached a value of .9 at a distance of one and one half times the obstacle diameter behind the obstacle.[2]

$$I(0, 0, 1.5d) / I_0 = \frac{1}{1 + d^2/(4x2.25d^2)} = \frac{1}{1 + 1/9}$$

$$= .9 \qquad \text{(III-14)}$$

Off Axis Intensity Function

To find the disturbance at a point P_2 near the optical axis, but off it, it is necessary to impose restrictions. The observation plane is placed a distance z behind the obstacle plane such that:

$$\frac{d/2}{z} << 1 \qquad \text{(III-15)}$$

Looking only at points near the optical axis implies the restriction:

$$\frac{r_2}{d/2} << 1 \qquad \text{(III-16)}$$

These two restrictions insure that the cosine obliquity factor is approximately equal to 1.

With these restrictions it is possible to expand l. By III-5

$$l^2 = z^2 + r_1^2 + r_2^2 - 2r_1 r_2 \cos(\phi_2 - \phi_1)$$

For the region where $\frac{r_1}{z} << 1$ then

$$l \simeq z + \frac{r_1^2}{2z} + \frac{r_2^2}{2z} - \frac{r_1 r_2}{z} \cos(\phi_2 - \phi_1) \qquad \text{(III-17)}$$

If l is multiplied by a large number (like k) then all the above expansion terms must be kept, otherwise l is approximately equal to z.

The Rayleigh-Sommerfeld integral of interest is:

$$U(r_2, \phi_2, z) = \frac{A}{i\lambda} \int_{d/2}^{\infty} \int_0^{2\pi} \frac{e^{ikl}}{l} \cos(\underset{\sim}{n}, \underset{\sim}{l})\, r_1 dr_1 d\phi_1 \qquad \text{(III-7)}$$

Inserting the cosine obliquity factor of 1 and the approximate expansions of l yields:

$$U(r_2, \phi_2, z) = \frac{A}{i\lambda z} e^{ikz} e^{ik\frac{r_2^2}{2z}} \int_{d/2}^{\infty} \int_0^{2\pi} e^{ik\frac{r_2^2}{2z}} \times e^{-ik\frac{r_1 r_2}{z}\cos(\phi_2 - \phi_1)}\, r_1 dr_1 d\phi_1 \qquad \text{(III-18)}$$

To solve the integral over ϕ, one can use the identity for the Bessel function:[3]

$$J_n(x) = \frac{i^{-n}}{2\pi} \int_0^{2\pi} e^{ix\cos\alpha}\, e^{in\alpha}\, d\alpha \qquad \text{(III-19)}$$

When $n = 0$ and $\alpha = (\phi_2 - \phi_1)$ then

$$J_0\left(-\frac{kr_1r_2}{z}\right) = J_0\left(\frac{k\, r_1r_2}{z}\right)$$

$$= \frac{1}{2\pi}\int_0^{2\pi} e^{ik\frac{r_1r_2}{z}\cos(\phi_2 - \phi_1)}\, d\phi_1 \qquad \text{(III-20)}$$

Substituting the above in III-18 gives:

$$U(r_2, \phi_2, z) = \frac{2\pi A}{i\lambda z}\, e^{ikz}\, e^{ik\frac{r_2^2}{2z}}$$

$$x\int_{d/2}^{\infty} r_1 e^{ikr_1^2}\, J_0\left(\frac{kr_1r_2}{z}\right) dr_1 \qquad \text{(III-21)}$$

(Up to this point the treatment is identical to Lommel's formulation. He proceeded to solve the integral by substituting in a Bessel function identity and integrating by parts to obtain a series of cascading higher order Bessel functions.)

The integral to be evaluated is:

$$\int_{d/2}^{\infty} e^{ik\frac{r_1^2}{2z}}\, J_0\left(\frac{kr_1r_2}{z}\right)\, r_1 dr_1$$

Both the exponential term and the zero order Bessel function are oscillatory of similar period. (The period of the Bessel function

approaches 2π.) The argument of the Bessel function is $\frac{2r_2}{r_1}$ times the argument of the exponential. When $\frac{r_2}{r_1} << 1$ the Bessel function will oscillate much more slowly than the exponential term. One can divide the interval $[d/2, \infty]$ into subintervals sufficiently small that the Bessel function term is essentially constant over the subinterval. One can also impose the restriction that for neighboring subintervals the Bessel function terms are approximately equal. That is, if $J_0\left(\frac{kr_i r_2}{z}\right)$ represents the Bessel term for the i^{th} subinterval then:

$$J_0\left(\frac{kr_i r_2}{z}\right) \approx J_0\left(\frac{kr_{i+1} r_2}{z}\right) \qquad \text{(III-22)}$$

Since this term is taken as constant it can be pulled out of the integral. The integral over the i^{th} subinterval is thus:

$$\int_{r_i}^{r_{i+1}} e^{ik\frac{r_1^2}{2z}} J_0\left(\frac{kr_1 r_2}{z}\right) r_1 dr_1 \approx J_0\left(\frac{kr_i r_2}{z}\right) \int_{r_i}^{r_{i+1}} e^{ik\frac{r_1^2}{2z}} r_1 dr_1$$

$$\approx J_0\left(\frac{kr_i r_2}{z}\right) \frac{z}{ik} e^{ik\frac{r_1^2}{2z}} \Bigg|_{r_i}^{r_{i+1}}$$

$$\approx \frac{z}{ik} J_0\left(\frac{kr_i r_2}{z}\right)\left[e^{ik\frac{(r_{i+1})^2}{2z}} - e^{ik\frac{r_i^2}{2z}} \right] \qquad \text{(III-23)}$$

It is clear by III-22 that the upper integration limit for the i^{th} subinterval will negate the lower integration limit for the $i = 1^{th}$ subinterval. This pairwise cancellation will continue over the

subintervals and leave two unpaired terms corresponding to $r_1 = d/2$ and $r_1 = \infty$. Thus the original integral becomes:

$$\int_{d/2}^{D/2} e^{ik\frac{r_1^2}{2z}} J_0\left(\frac{kr_1r_2}{z}\right) r_1 dr_1 \simeq -\frac{z}{ik} J_0\left(\frac{kdr_2}{2z}\right) e^{ik\frac{d^2}{8z}} \qquad \text{(III-24)}$$

The final, radially symmetric form for the disturbance at P_2 is:

$$U(r_2, z) = \frac{2\pi A}{i\lambda z} e^{ikz} e^{ikr_2^2/2z} \frac{z}{ik} J_0\left(\frac{kdr_2}{2z}\right) e^{ik\frac{d^2}{8z}}$$

$$= -A e^{ikz} e^{ikr_2^2/2z} e^{ikd^2/8z} J_0\left(\frac{kdr_2}{2z}\right) \qquad \text{(III-25)}$$

(Notice the disturbance function is independent of angle ϕ_2).

The intensity at P_2 is:

$$I(r_2, z) = |U(r_2, z)|^2 = A^2 J_0^2\left(\frac{kdr_2}{2z}\right) \qquad \text{(III-26)}$$

Since $J_0(0) = 1$, it is readily apparent the intensity on axis equals the incident intensity (A^2), which is expected for the region where $\frac{d}{2z} \ll 1$.

An intensity contour plot and related radial intensity profile for a 3/16 inch diameter obstacle viewed 50cm away is given below.

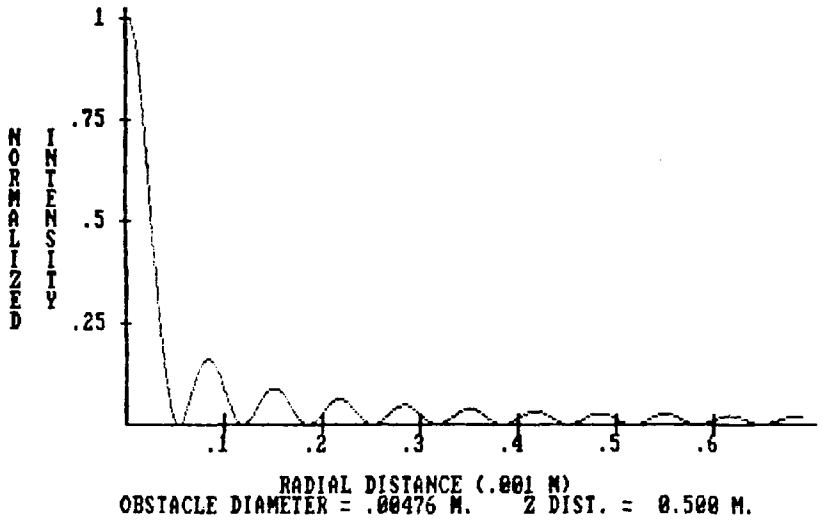

Graph 3.2

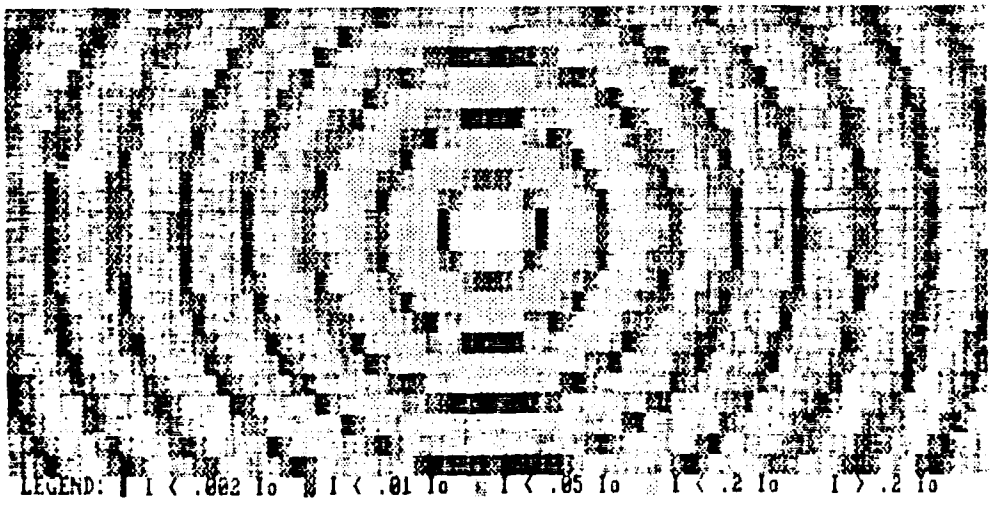

Graph 3.3

As is characteristic of an Airy pattern, the spot of Arago is surrounded by a series of increasingly dimmer rings. (The reference to the Airy pattern is intentional. Both the pattern and the spot are images of a light source produced by a circular aperture and obstacle respectively.) The ratios of the maximum intensities to the intensity on axis as well as the positions of the maxima and minima can be determined readily from a table of zeroes for J_0 and J_1.

Extrema occur when:

$$\frac{d}{dr_2} \; A^2 J_0{}^2 \left(\frac{kdr_2}{2z}\right) = 0$$

$$-A^2 \frac{kd}{2z} J_0\left(\frac{kdr_2}{2z}\right) J_1\left(\frac{kdr_2}{2z}\right) = 0 \qquad \text{(III-27)}$$

Minima occur when $J_0\left(\frac{kdr_2}{2z}\right) = 0$ and maxima when $J_0\left(\frac{kdr_2}{2z}\right) = 0$. The table below shows the radial distances (in terms of $\frac{2z}{kd}$) and normalized intensities (normalized to I(0, 0, Z)) for the first fourteen intensity extrema based on the table of values for J_0 and J_1 found in the CRC Standard Math Tables, 13th student edition, pages 326-329.

Table 3.1

Extrema of Diffraction Ring Structure

Radial distance $x \frac{kd}{2z}$	$I(r/z) / I(0,z) = J_0^2\left(\frac{kdr_2}{2z}\right)$	Extremum type
0	1.0	Maximum
2.405	0.0	Minimum
3.832	0.162	Maximum
5.502	0.0	Minimum
7.016	0.09	Maximum
8.654	0.0	Minimum
10.174	0.062	Maximum
11.792	0.0	Minimum
13.324	0.048	Maximum
14.931	0.0	Minimum
16.471	0.039	Maximum
18.071	0.0	Minimum
19.616	0.032	Maximum
21.212	0.0	Minimum

An examination of the factors k, r_2, d and z in the argument of the Bessel function provides insight into characteristics of the spot and its ring structure. The argument is:

$$\frac{kdr_2}{2z} = \frac{\pi dr_2}{\lambda z} \qquad \text{(III-28)}$$

If the argument is set equal to a constant, then r_2 is proportional to

λ and z and inversely proportional to d. The larger r_2 is for a given argument the more "spread out" the ring pattern is in the observation plane. The pattern will increase in size the longer the wavelength of incident light, the farther along the optical axis the observation is made or the smaller the diameter of the obstacle. Likewise the pattern shrinks if one has a shorter wavelength light, moves closer to the obstacle or uses a larger diameter obstruction.

For a given obstacle diameter and incident wavelength, the spot of Arago (the central maximum) can be thought of as a slowly widening sheath surrounding the optical axis for increasing distance z. This concept has an intriguing consequence. If one observes the spot at a sufficient distance, the diameter of the spot will be equal to or greater than the diameter of the shadow. In short, the shadow will disappear. If the preceding theory is valid in this range then this will occur when:

$$\frac{kr_2 d}{2z} = 2.405 \qquad \text{with } r_2 \geq \frac{d}{2}$$

$$z \geq .653 \frac{d^2}{\lambda} \tag{III-29}$$

For a 1cm diameter obstacle illuminated by He-Ne laser light of 6328Å wavelength, then theory predicts shadow saturation when:

$$z \geq 103\text{m} \tag{III-30}$$

One must view the above numbers with some caution. One restriction the theory was based on was $\frac{2r_2}{d} << 1$. The theory may not be valid for this large a value of r_2.

The graphs below show the change in radial intensity distribution for variations in λ, d and z. Unless specified, the wavelength is taken to be 6328Å.

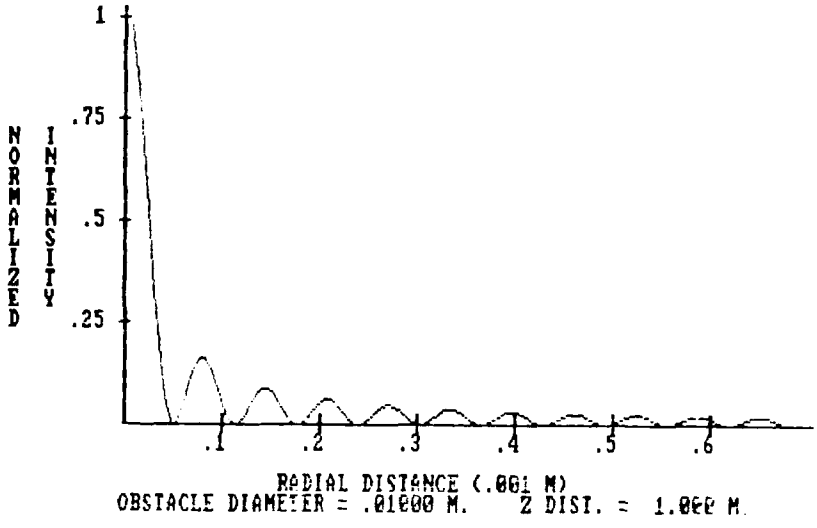

Graph 3.4

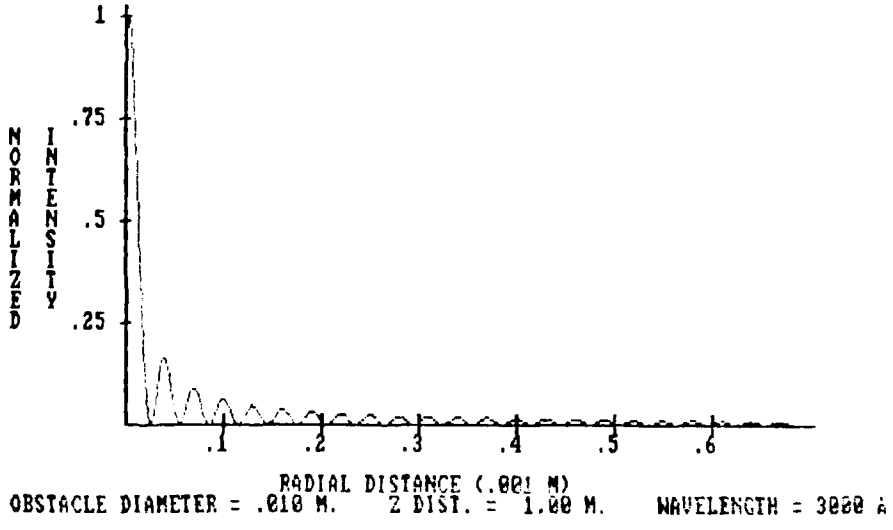

Graph 3.5

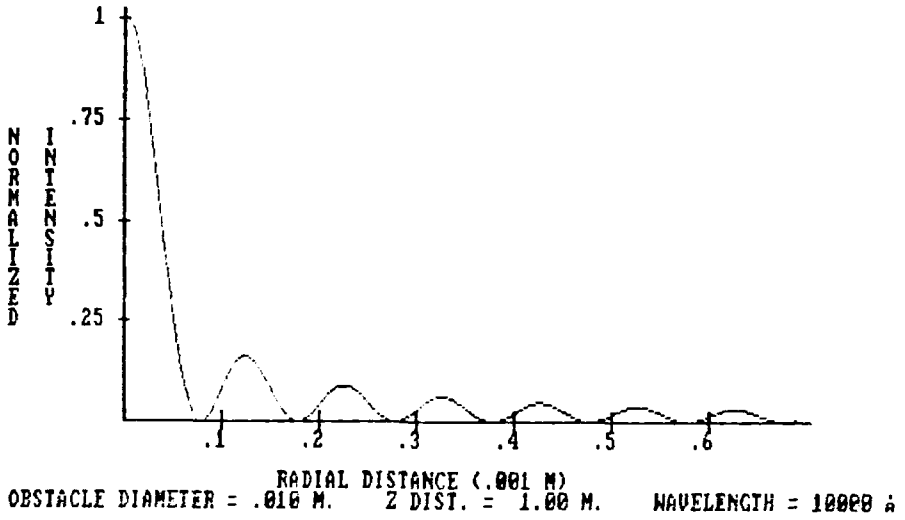

Graph 3.6

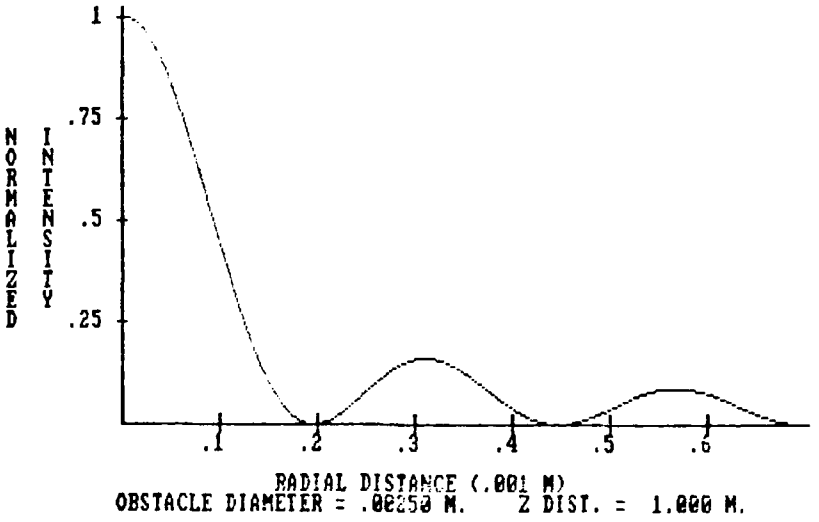

Graph 3.7

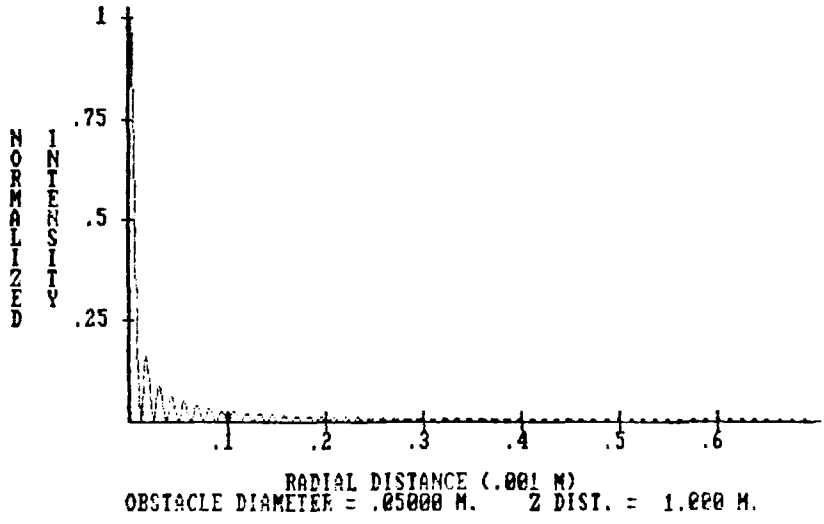

Graph 3.8

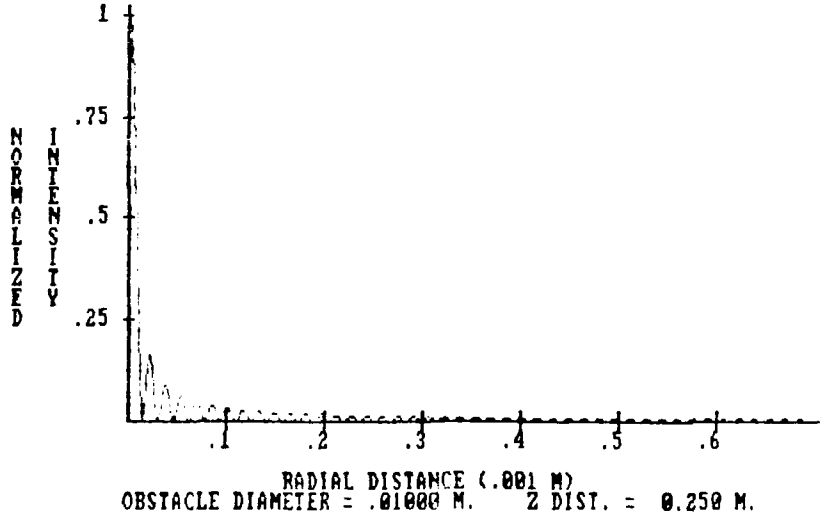

Graph 3.9

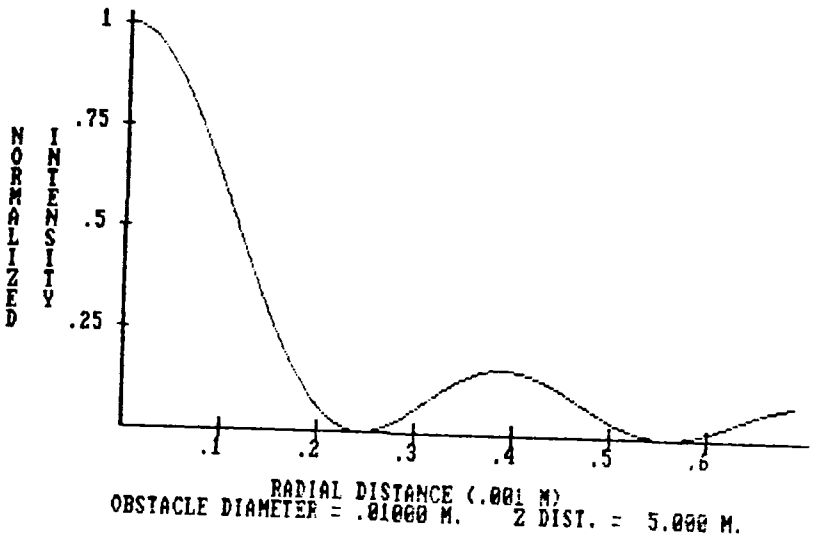

Graph 3.10

Case 2: Circular Obstacle Illuminated with Gaussian Intensity Distribution

Up to this point the formulation has depended upon an incident plane wave of uniform intensity. Light from a laser has a characteristic gaussian distribution. Consider an incident plane wave with a gaussian intensity distribution centered on the optical axis. Let the gaussian distribution be of the form:

$$e^{-c\,\frac{r^2}{d^2}}$$

where d is the diameter of the obstacle

r is the radial distance off the optical axis

c is a characteristic constant.

Thus when $r = \frac{d}{2}$ the gaussian factor becomes:

$$e^{-\frac{c}{4}}$$

The edge diffracted rays define the disturbance at points in the shadow. One expects a reproduction of the previous results multiplied by the gaussian factor $e^{-\frac{c}{4}}$ for the diffraction of a wave with a gaussian distribution.

The Rayleigh-Sommerfeld integral is:

$$U(r_2, z) = \frac{A}{i\lambda z} e^{ik\frac{r_2^2}{2z}} e^{ikz} \int_{d/2}^{\infty} \int_{0}^{2\pi} e^{-c\frac{r_1^2}{d^2}}$$

$$x\, e^{ik\frac{r_1^2}{2z}} e^{-ik\frac{r_1 r_2}{z}\cos(\phi_2 - \phi_1)} r_1 dr_1 d\phi_1$$

$$= \frac{2\pi A}{i\lambda z} e^{ik\frac{r_2^2}{2z}} e^{ikz} \int_{d/2}^{\infty} e^{\left[\frac{ik}{2z} - \frac{c}{d^2}\right] r_1^2} J_0\left(\frac{kr_1 r_2}{z}\right) r_1 dr_1$$

(III-31)

The evaluation of the integral follows the method presented in the preceding section with the result for the disturbance function:

$$U(r_2, z) = -\frac{2\pi A}{i\lambda z} \frac{zd^2}{ikd^2 - 2zc} e^{ik\frac{r_2^2}{2z}} e^{ikz} e^{-\frac{c}{4}} e^{ik\frac{d^2}{8z}} J_0\left(\frac{kdr_2}{2z}\right)$$

$$= \frac{A}{1 - i\frac{2zc}{kd^2}} e^{-\frac{c}{4}} e^{ik\left[\frac{r_2^2}{2z} + z + \frac{d^2}{8z}\right]} J_0\left(\frac{kdr_2}{2z}\right)$$

(III-32)

The intensity distribution is:

$$I(r_2, z) = \frac{A^2}{1-4\frac{z^2c^2}{k^2d^4}} \; e^{-\frac{c}{2}} \; J_0^2\left(\frac{kdr_2}{2z}\right) \qquad \text{(III-33)}$$

For most cases of interest $4\frac{z^2c^2}{k^2d^4} << 1$ and can be neglected. (For z on the order of 1 meter, C = 10 and d on the order of .01m then $\frac{z^2c^2}{k^2d^4} \approx 10^{-4}$ Then the intensity distribution reduces to the anticipated form:

$$I(r_2, z) = A^2 \; e^{-\frac{c}{2}} \; J_0^2\left(\frac{kdr_2}{2z}\right) \qquad \text{(III-34)}$$

The resulting intensity on axis and radial intensity distributions are reduced by the gaussian factor $e^{-\frac{c}{2}}$.

The following graphs demonstrate the intensity distribution on and off the optical axis for different values of the gaussian constant c.

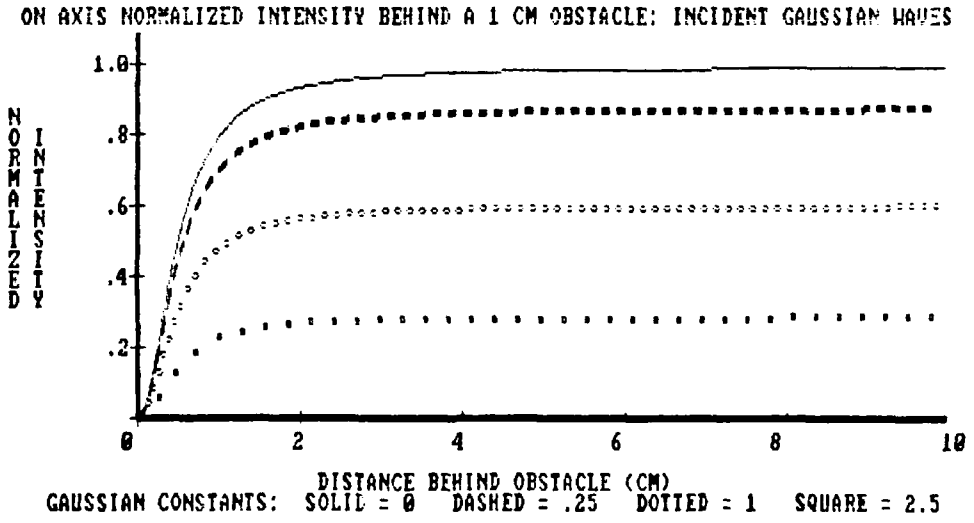

Graph 3.11

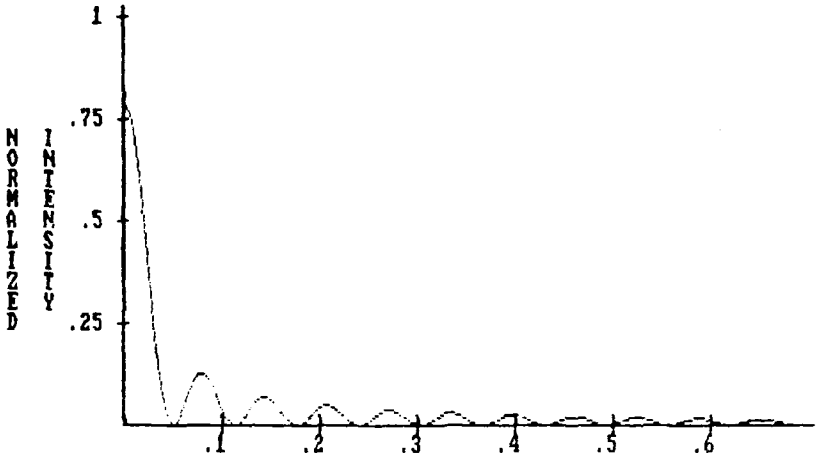

OBSTACLE DIAMETER = .010 M. Z DIST. = 1.00 M. GAUSSIAN CONSTANT = 0.5

Graph 3.12

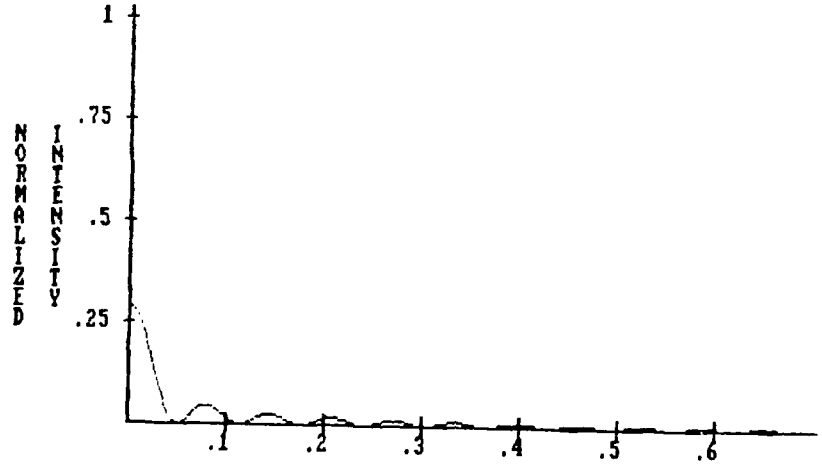

OBSTACLE DIAMETER = .010 M. Z DIST. = 1.00 M. GAUSSIAN CONSTANT = 2.5

Graph 3.13

Case 3: Annular Aperture with Uniform Illumination

The geometrical layout for diffraction by an annular aperture is depicted below. The Rayleigh-Sommerfeld integral is given by III-7

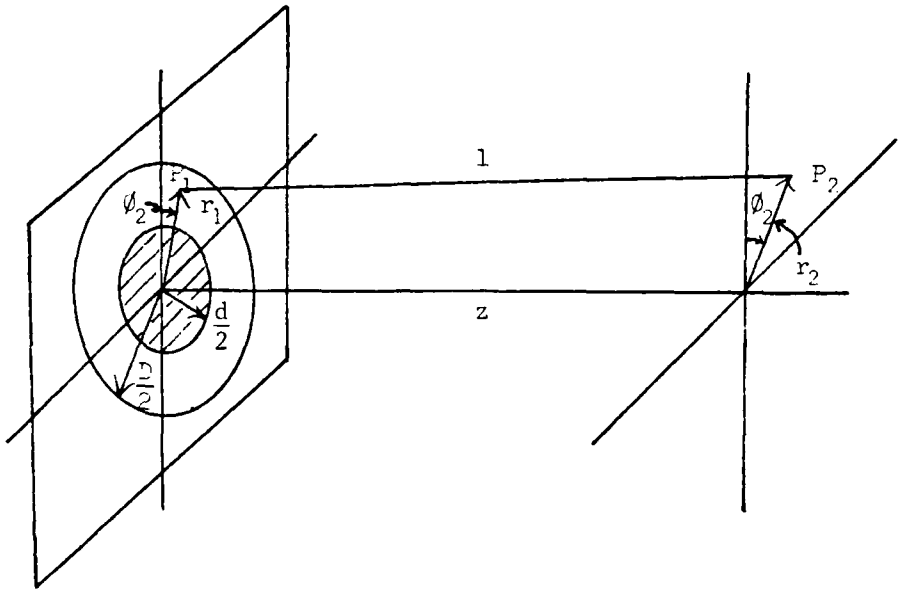

Figure 3.5

Geometrical Layout for Diffraction by an Annular Aperture

substituting $\frac{D}{2}$ in for the upper limit for the integral over r_1.

$$U(r_2, \emptyset_2, z) = \frac{A}{i\lambda} \int_{d/2}^{D/2} \int_{0}^{2} \frac{e^{ikl}}{l} \cos(\underset{\sim}{n}, \underset{\sim}{l})\, r_1 dr_1 d\emptyset_1 \qquad \text{(III-35)}$$

On Axis Intensity

The arguments follow those for the circular obscuration with the final result for the disturbance at point P_2 (from III-10) being:

$$U(0,\ 0,\ z) = \frac{2\pi Az}{i\lambda}\left[\frac{1}{ikl}\ e^{ikl}\right]\frac{\sqrt{z^2+D^2/4}}{\sqrt{z^2+d^2/4}}$$

$$U(0,\ 0,\ z) = -A\left[\frac{z}{\sqrt{z^2+D^2/4}}\ e^{ik\sqrt{z^2+D^2/4}} - \frac{z}{\sqrt{z^2+d^2/4}}\ e^{ik\sqrt{z^2+d^2/4}}\right] \qquad \text{(III-36)}$$

The on axis intensity distribution is thus:

$$I(0,\ 0,\ z) = \left|U(0,\ 0,\ z)\right|^2 = A^2\left[\frac{z^2}{z^2+D^2/4} + \frac{z^2}{z^2+d^2/4} - \frac{z^2}{\sqrt{z^2+D^2/4}\sqrt{z^2+d^2/4}}\left(e^{ik\sqrt{z^2+D^2/4}}\ e^{-ik\sqrt{z^2+d^2/4}} + e^{-ik\sqrt{z^2+D^2/4}}\ e^{ik\sqrt{z^2+d^2/4}}\right)\right]$$

$$= A^2\left[\frac{1}{1+\frac{D^2}{4z^2}} + \frac{1}{1+\frac{d^2}{4z^2}} - \frac{1}{\sqrt{1+\frac{D^2}{4z^2}}\sqrt{1+\frac{d^2}{4z^2}}}\right.$$

$$\left.\times\ \left(\cos\left(k\left(\sqrt{z^2+D^2/4} - \sqrt{z^2+d^2/4}\right)\right) + \cos\left(k\left(\sqrt{z^2+d^2/4} - \sqrt{z^2+D^2/4}\right)\right)\right)\right]$$

$$= A^2\left[\frac{1}{1+\frac{D^2}{4z^2}} + \frac{1}{1+\frac{d^2}{4z^2}} - \frac{2}{\sqrt{1+\frac{D^2}{4z^2}}\sqrt{1+\frac{d^2}{4z^2}}}\right.$$

$$\left. \times \cos\left(kz\left[\sqrt{1+\frac{D^2}{4z^2}} - \sqrt{1+\frac{d^2}{4z^2}}\right]\right)\right] \qquad \text{(III-37)}$$

The above expression is valid for z greater that a few wavelengths. If the observation plane is in the region where $\frac{D^2}{4z^2} << 1$ and $\frac{d^2}{4z^2} << 1$, one can employ the expansions:

$$\left(1 + \frac{D^2}{4z^2}\right)^{\frac{1}{2}} \simeq 1 + \frac{D^2}{8z^2} \qquad \left(1 + \frac{d^2}{4z^2}\right)^{\frac{1}{2}} \simeq 1 + \frac{d^2}{8z^2}$$

to obtain:

$$I(0, 0, z) = A^2\left[2 - \frac{1}{8z^2}(D^2 + d^2) - 2\cos\left(\frac{k}{z}(D^2 - d^2)\right)\right] \qquad \text{(III-38)}$$

which, upon neglecting the second term, reduces to:

$$I(0, 0, z) = A^2\left[2 - 2\cos\left(\frac{k}{z}(D^2 - d^2)\right)\right] \qquad \text{(III-39)}$$

To gain physical insight into these results one should look at III-36.

$$U(0, 0, z) = -A\left[\frac{z}{\sqrt{z^2+D^2/4}}\, e^{ik\sqrt{z^2+D^2/4}} -\right.$$

$$\frac{z}{\sqrt{z^2+d^2/4}}\ e^{ik\sqrt{z^2+d^2/4}}\ \Bigg]$$

A is the amplitude for the disturbance of the incident wave in the aperture plane. The coefficients in front of the exponentials are the cosine obliquity factors for points on the edges of the aperture. The exponential terms are the phase factors for rays reaching P_2 from the inside and outside boundaries (through distances $\sqrt{z^2+d^2/4}$ and $\sqrt{z^2+D^2/4}$ respectively). As with the case for the circular obstacle the edge diffracted rays cause the disturbance at P_2. Those for the circular obstacle are all in phase for axial points and thus interfere constructively. For the annular aperture the rays from the inside and outside borders will interfere to varying degrees based on the relative phases. This phase difference is given by $\frac{k}{z}\left(\sqrt{z^2+\frac{D^2}{4}} - \sqrt{z^2+\frac{d^2}{4}}\right)$. For large z the phase difference will vary slowly with changes in z. Thus one has a disturbance function that oscillates between -2A and 2A, rapidly close behind the aperture. The intensity oscillates between 0 and 4 times the incident intensity.

In the region where $\frac{D^2}{4z^2} \ll 1$ and $\frac{d^2}{4z^2} \ll 1$, maxima will occur on axis when the cosine term equals -1. This happens when the argument is an odd multiple of π.

$$\frac{k}{8z}\,(D^2 - d^2) = (2n+1)\pi \qquad n = 0, 1, 2, \ldots$$

$$z = \frac{D^2-d^2}{4\lambda(2n+1)} \qquad \text{(III-40)}$$

Minima will occur when:

$$z = \frac{D^2-d^2}{8m\lambda} \qquad m = 1, 2, \ldots \tag{III-41}$$

The last maximum on axis occurs when n = 0 or when:

$$z = \frac{D^2-d^2}{4\lambda} \tag{III-42}$$

The last miminum (before the intensity is driven to zero at infinite z) occurs when m = 1 or:

$$z = \frac{D^2-d^2}{8\lambda} \tag{III-43}$$

The last maximum defines the boundary for the oscillatory behavior of the intensity on axis. The distance to the last maximum will decrease for increased wavelength or decreased factor $(D^2 - d^2)$. $(D^2 - d^2)$ can be written as $D^2(1 - \varepsilon^2)$ where ε is the obscuration ratio, the ratio of the inner to outer diameters. Thus a smaller obscuration ratio (for fixed D) will decrease the distance to the last maximum and a smaller outer diameter (for fixed ε) will accomplish the same thing.

Below are graphs depicting the intensity on axis for variations in the parameters λ, D and ε. (Unless specified, the wavelength is assumed to be 6328Å.)

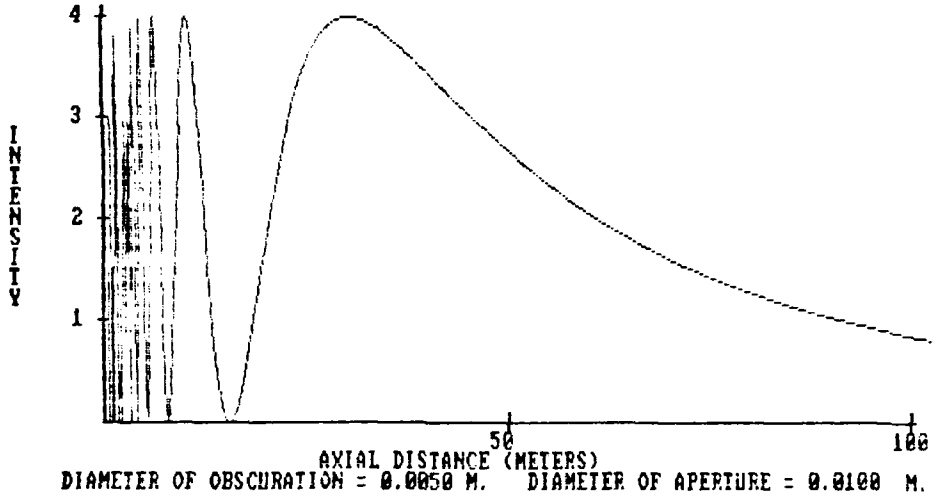

Graph 3.14

D = .01m ε = .5

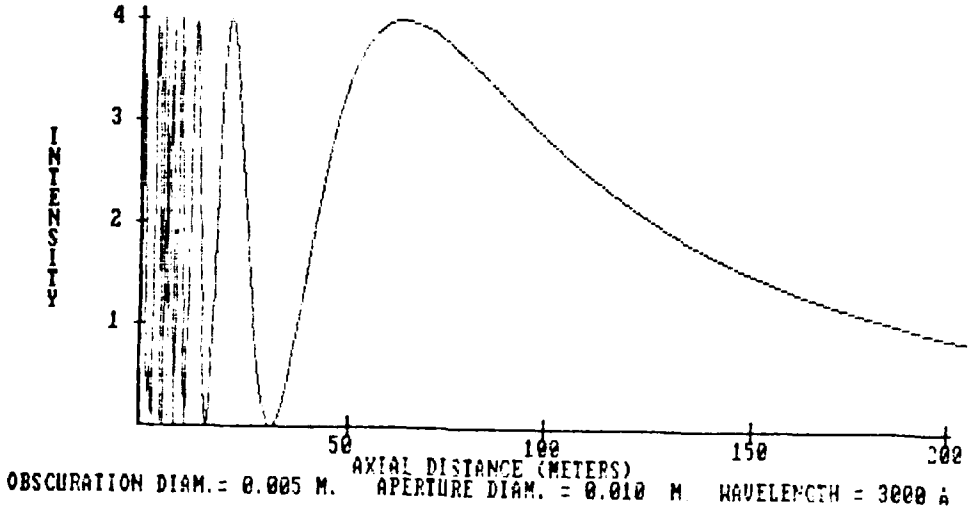

Graph 3.15

λ = 3000 Å

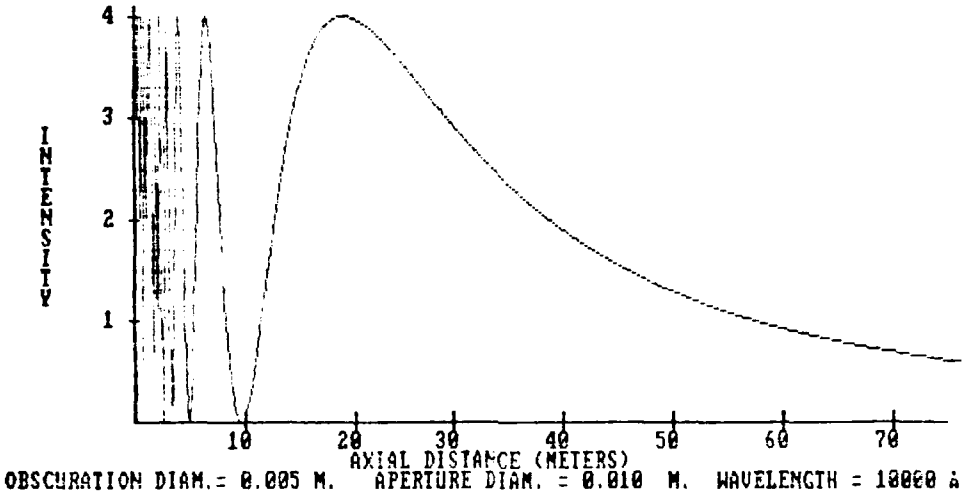

Graph 3.16

λ = 10000 Å

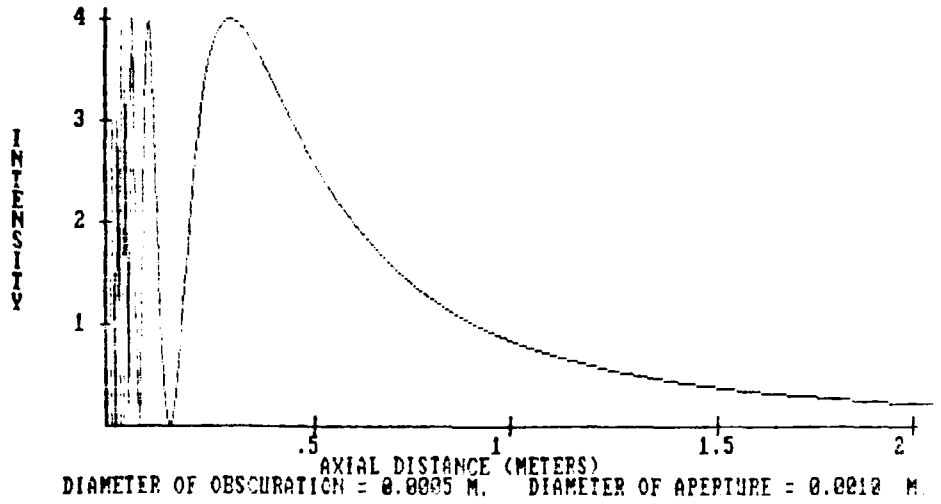

Graph 3.17

D = .001m

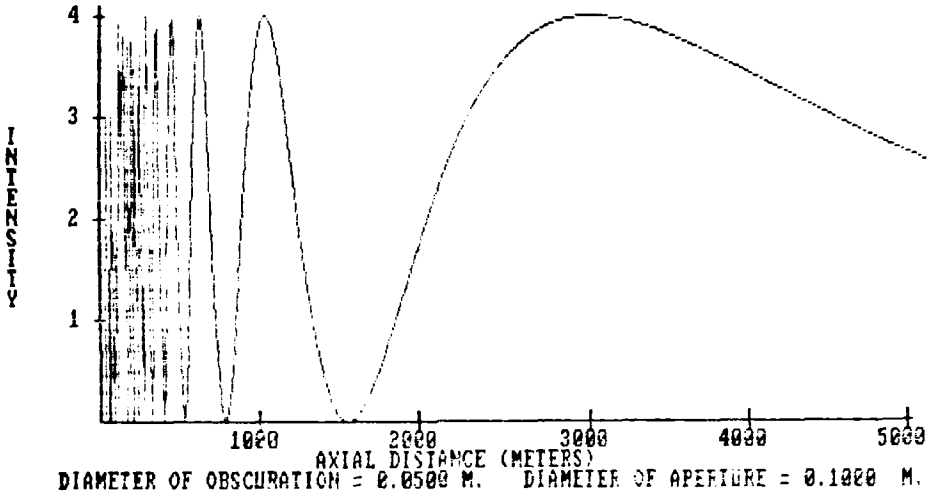

Graph 3.18

D = .1m

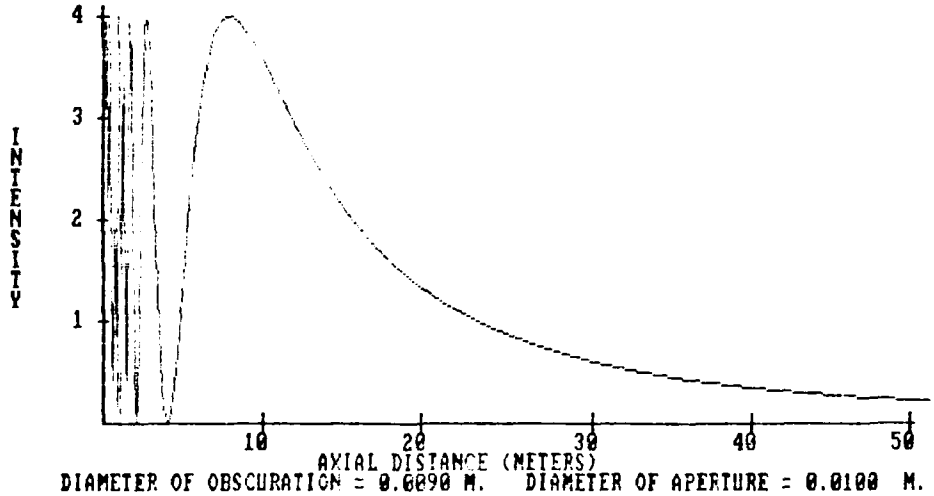

Graph 3.19

ε = .9

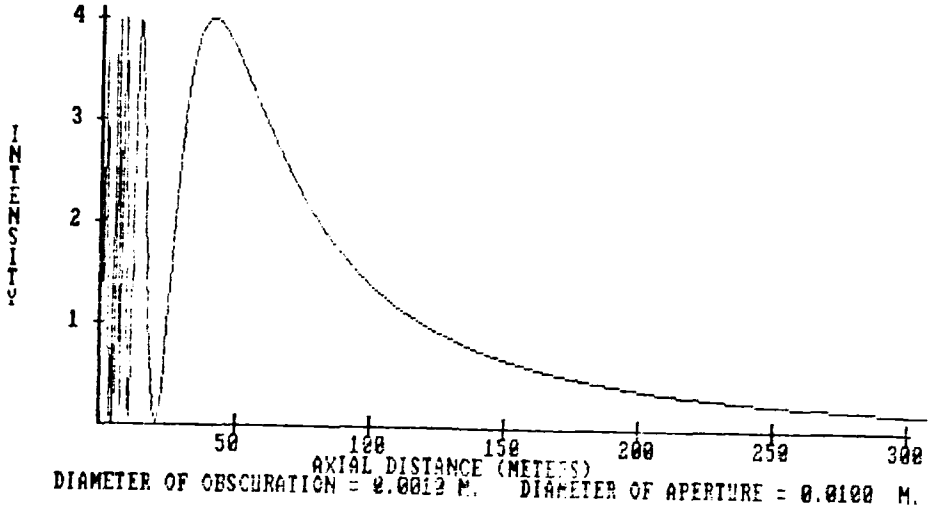

Graph 3.20

$\varepsilon = .1$

The circular aperture as a special case of the annular aperture. If there is no central obscuration the annular aperture problem reduces to that for a circular aperture. This is equivalent to letting d equal zero in the preceeding treatment. Then III-36 reduces to:

$$U(0, 0, z) = -A\left[\frac{z}{\sqrt{z^2+D^2/4}}\ e^{ik\sqrt{z^2+D^2/4}} - e^{ikz}\right] \qquad \text{(III-44)}$$

The first term in the parenthesis reflects the edge diffracted rays. The second term is the phase factor due to the distance a ray travels down the optical axis (notice for this case the cosine obliquity factor equals 1). Thus the disturbance at an on axis point P_2 behind

a circular obstacle results from interference between rays diffracted from the edge and from the center of the aperture.

The intensity on axis is given by:

$$I(0,\ 0,\ z) = A^2\left[\frac{1}{1+\frac{D^2}{4z^2}} + 1 - \frac{2}{\sqrt{1+\frac{D^2}{4z^2}}}\ \cos\left(kz\left[\sqrt{1+\frac{D^2}{4z^2}} - 1\right]\right)\right] \qquad \text{(III-45)}$$

When $\frac{D^2}{4z^2} << 1$ this reduces to:

$$I(0,\ 0,\ z) = A^2\left[2 - 2\cos\left(\frac{k}{8z}\ D^2\right)\right] \qquad \text{(III-46)}$$

For the circular aperture the last maximum on axis occurs when

$$z = \frac{D^2}{4\lambda(2n+1)} \qquad \text{(III-47)}$$

A graph of the intensity on axis behind a 1cm aperture appears below.

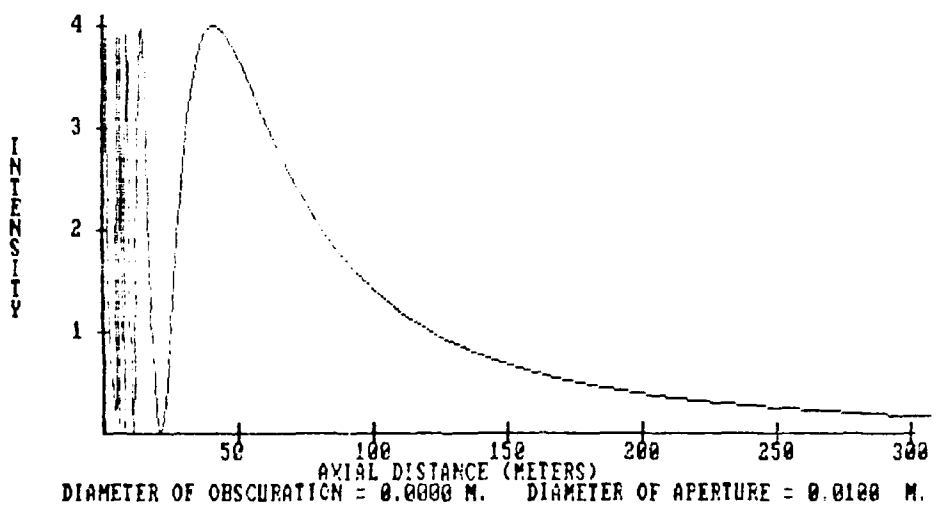

Graph 3.21

The Circular Obscuration as a Special Case of the Annular Aperture. If the diameter of the outside rim of the aperture is taken to infinity the problem of the annular aperture reduces to that of the circular obscuration. Equation III-36 becomes:

$$U(0, 0, z) = A \frac{z}{\sqrt{z^2+d^2/4}} \; e^{ik\sqrt{z^2+d^2/4}} \qquad \text{(III-48)}$$

which is the same expression as in III-11. Thus all previously derived results for the intensity on axis behind a circular obscuration can be reproduced.

Off Axis Intensity

The derivation of the disturbance function $U(r_2, \phi_2, z)$ for the annular aperture case follows that for the circular obscuration. The only difference is the upper limit of integration is now $\frac{D}{2}$. Making this substitution, equation III-25 becomes:

$$U(r_2, z) = \frac{2\pi A}{i\lambda z} e^{ikz} \, e^{ik\frac{r_2^2}{2z}} \, \frac{z}{ik} \left[J_0\left(\frac{kDr_2}{2z}\right) e^{ik\frac{D^2}{8z}} - J_0\left(\frac{kdr_2}{2z}\right) e^{ik\frac{d^2}{8z}} \right]$$

$$= -Ae^{ikz} \, e^{ik\frac{r_2^2}{2z}} \left[J_0\left(\frac{kDr_2}{2z}\right) e^{ik\frac{D^2}{8z}} - J_0\left(\frac{kdr_2}{2z}\right) e^{ik\frac{d^2}{8z}} \right] \qquad \text{(III-49)}$$

The intensity at $P_2 = (r_2, \phi_2, z)$ is given by:

$$I(r_2, z) = |U(r_2, z)|^2$$

$$= A^2 \left[J_0^2\left(\frac{kDr_2}{2z}\right) + J_0^2\left(\frac{kdr_2}{2z}\right) - 2J_0\left(\frac{kDr_2}{2z}\right) J_0\left(\frac{kdr_2}{2z}\right) \right.$$
$$\left. \times \cos\left(\frac{k}{8z}\,(D^2 - d^2)\right) \right] \qquad \text{(III-50)}$$

If $r_2 = 0$ then the above reduces to equation III-39. If D becomes infinite then $J_0\left(\frac{kDr_2}{2z}\right)$ goes to zero and the above reduces to the result for the circular obscuration. When d equals zero one obtains the intensity function for diffraction by a circular aperture.

$$I(r_2, z) = A^2 \left[J_0^2\left(\frac{kDr_2}{2z}\right) + 1 - 2J_0\left(\frac{kDr_2}{2z}\right) \cos\left(\frac{k}{8z}\,D^2\right) \right] \qquad \text{(III-51)}$$

The intensity pattern produced by an annular aperture is a complicated series of bright, dim and dark rings of various radii. The following intensity contour plots and radial intensity profiles show the diffraction patterns for a .3333cm diameter circular obstacle, a 1cm diameter circular aperture and their resultant annular aperture combination at .5 meters.

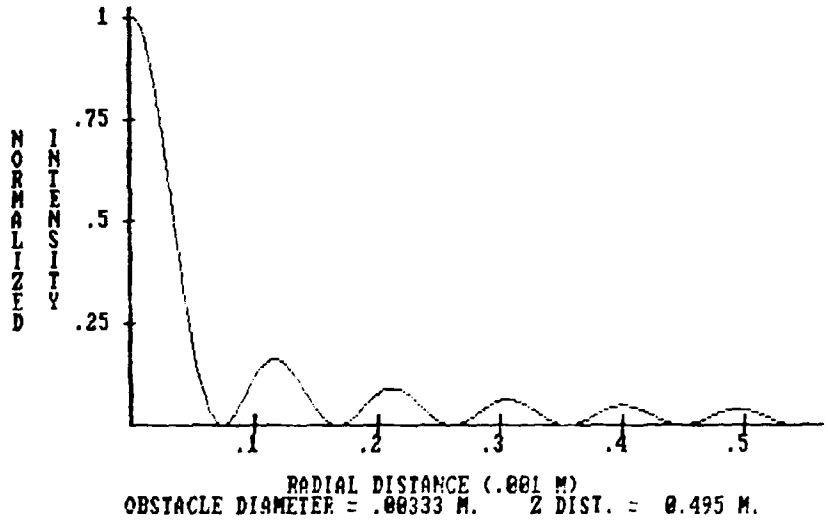

Graph 3.22

Circular Obscuration Intensity Pattern

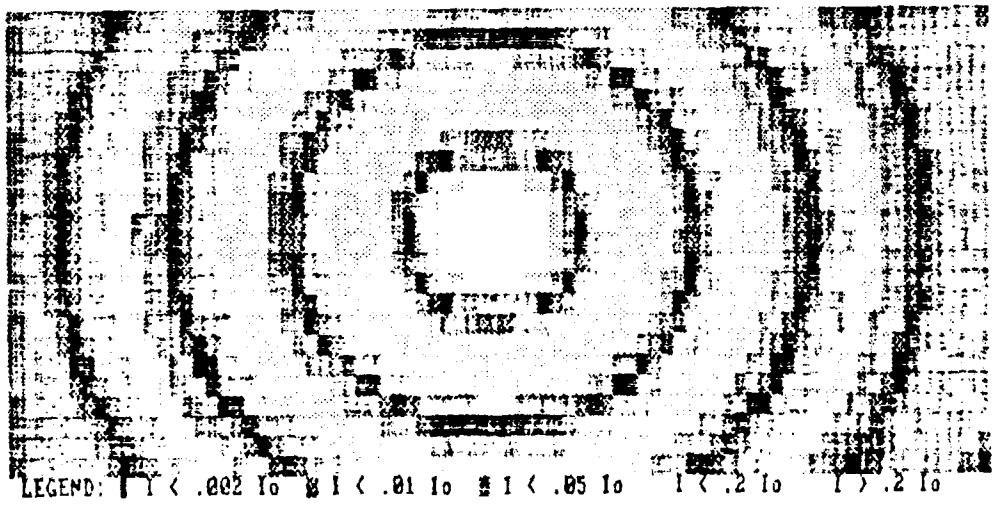

Graph 3.23

Circular Obscuration Pattern

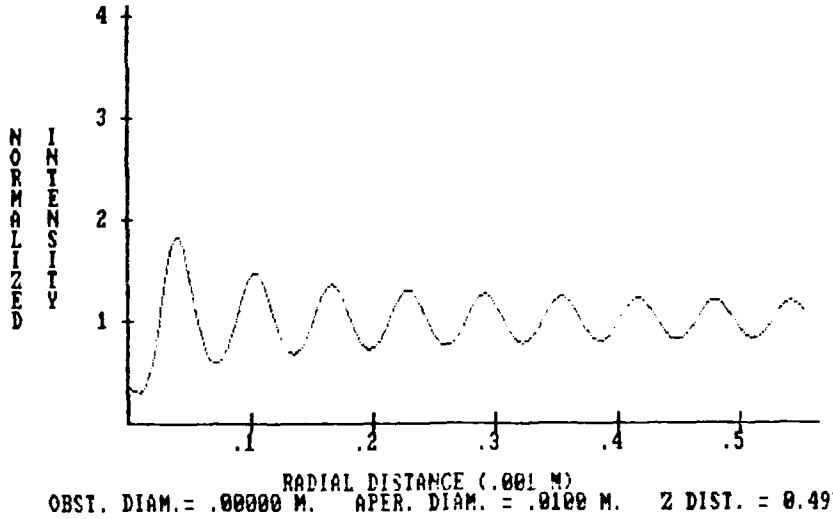

Graph 3.24

Circular Aperture Intensity Distribution

Graph 3.25

Circular Aperture Pattern

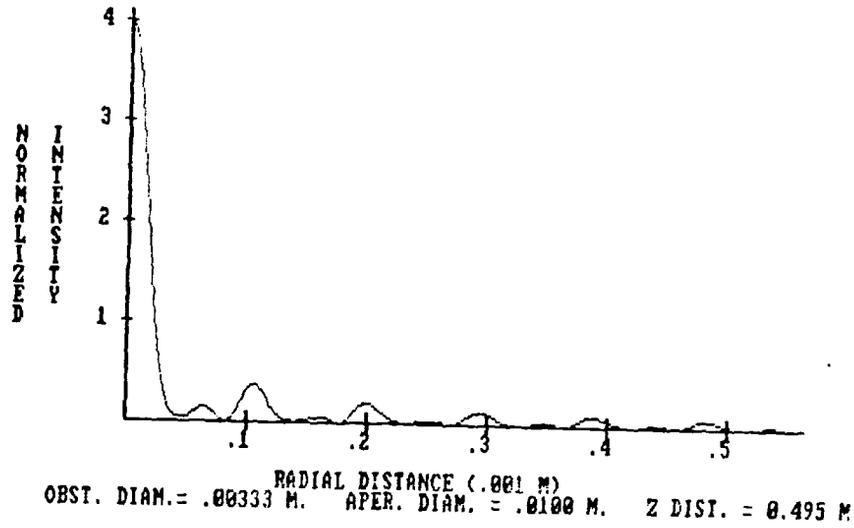

Graph 3.26

Annular Aperture Intensity Distribution

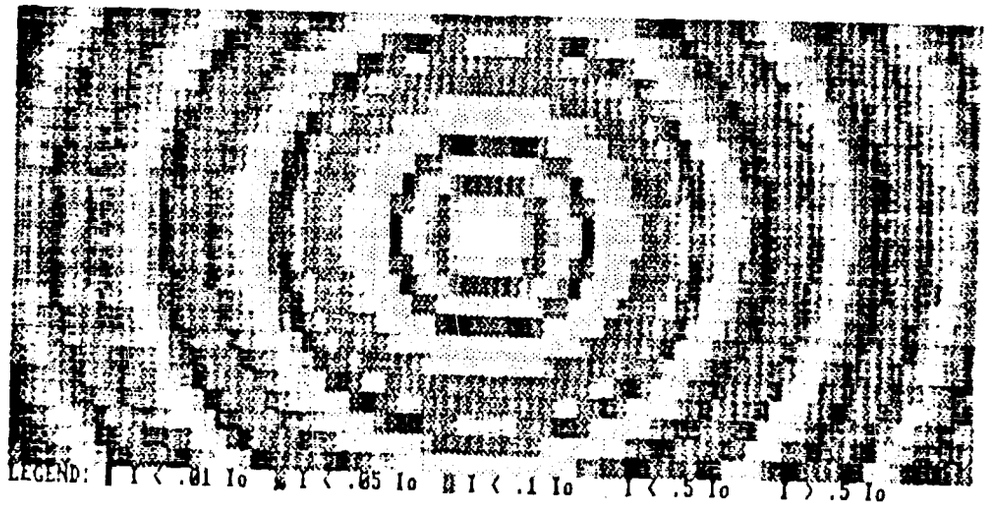

Graph 3.27

Annular Aperture Pattern

Beats and the ring structure. The radial intensity plot for the annular aperture of obscuration ratio 1/3 above yields zeroes for intensity at the radial distances depicted in the table below.

Table 3.2

Radial Positions of Intensity Zeroes for Annular Aperture

(D = .01, ε = 1/3, z = .495m)

Radial distance from center (mm)	Distance to next zero (mm)
.081	.094
.175	.094
.269	.093
.362	.094
.456	
	average .09375mm ± .0005

This very regular pattern also appears in the spacing of minima for the circular aperture. A table of the radial positions of these appear below.

Table 3.3

Radial Position of Intensity Minima for Circular Aperture

(D = .01, z = .495m)

Radial distance from center (mm)	Distance to next minima (mm)
.009	.061
.070	.064
.134	.061
.195	.064
.259	.062
.321	.063
.384	.062
.446	.063
.509	
	average .0625mm $\pm$ .0012

The frequency of zeroes for the annular case is:

$$\nu_{ann.} = \frac{1}{9.375 \times 10^{-5} m} = 10666.7 m^{-1} \qquad \text{(III-52)}$$

The frequency of minima for the circular aperture case is:

$$\nu_{circ.} = \frac{1}{6.25 \times 10^{-5} m} = 16000 m^{-1} \qquad \text{(III-53)}$$

$$\nu_{ann.} / \nu_{circ.} = 2/3 \qquad \text{(III-54)}$$

To understand the above ratio, one can approximate the Bessel function as a sinusoidal function. The period for J_0 for large arguments approaches 2π. The amplitude for large arguments is essentially constant (very slowly decreasing). The Bessel functions in equation III-51 are of the form:

$$J_0(2\pi\nu_i r_2) \approx c\sin(2\pi\nu_i r_2) \qquad i = 1, 2$$

where $\nu_1 = \frac{D}{2\lambda z}$ and $\nu_2 = \frac{d}{2\lambda z}$. The sinusoidal approximations are thus:

$$J_0(2\pi\nu_i r_2) \approx c \sin(2\pi\nu_i r_2) \qquad i = 1, 2 \qquad \text{(III-55)}$$

ν_1 is different than ν_2 and the combination of the two periodic patterns will lead to beating. This beat frequency is given by the expression:[4]

$$\nu_{beat} = \nu_1 - \nu_2 \qquad \text{(III-56)}$$

$$= \frac{1}{2\lambda z}(D - d)$$

$$= \frac{D}{2\lambda z}(1 - \varepsilon)$$

$$= \nu_1 (1 - \varepsilon) \qquad \text{(III-57)}$$

For the case where $\varepsilon = 1/3$ then:

$$\nu_{beat} = \nu_1 \left(1 - \frac{1}{3}\right) = \frac{2}{3}\nu_1 \qquad \text{(III-58)}$$

The frequency, ν_{beat}, corresponds to the frequency of intensity zeroes radially for the annular aperture case. The frequency ν_1 corresponds to the frequency of minima for the circular aperture case.

The frequency ν_2 applies to the circular obscuration case.

$$\nu_{circ.} \equiv \nu_1 = \frac{D}{2\lambda z} = \frac{.01m}{2 \times 6.328 \times 10^{-7}m \times .495m} = 15962m^{-1}$$

(III-59)

$$\nu_{ann.} \equiv \nu_{beat} = \frac{D-d}{2\lambda z} = \frac{(.01 - .003333)m}{2 \times 6.328 \times 10^{-7}m \times .495m} = 10642m^{-1}$$

(III-60)

The concept of beats provides insight into the outlying ring structure of the diffraction pattern of an annular aperture. The ring structure will oscillate within a beat envelope whose radial width is given by $1 / \nu_{ann.}$ or $\frac{2\lambda z}{D-d}$. The intensity pattern is the square of the beat structure from the disturbance function. The result is a series of dark bands (corresponding to the regions around the zeroes of the beat envelopes) and bright bands (corresponding to the regions around the maxima of the beat envelopes) which contain an underlying dark and bright ring structure. These bands will be wide for large obscuration ratios. (The beat envelope width is inversely proportional to $(1 - \varepsilon)$). For ε very close to 1 the beat envelope is very broad and one will observe a ring structure whose frequency of intensity zeroes approaches that of the frequency of minima for the circular aperture and circular obstacle. For very small ε the beat envelope is very narrow. (The study of aberration effects on the diffraction pattern will involve changes in the ring structure. A wide beat envelope will provide a better opportunity to observe deviations. Thus an aperture with a high obscuration ratio is better for aberration testing.

The graphs and table below illustrate the concepts discussed in this section.

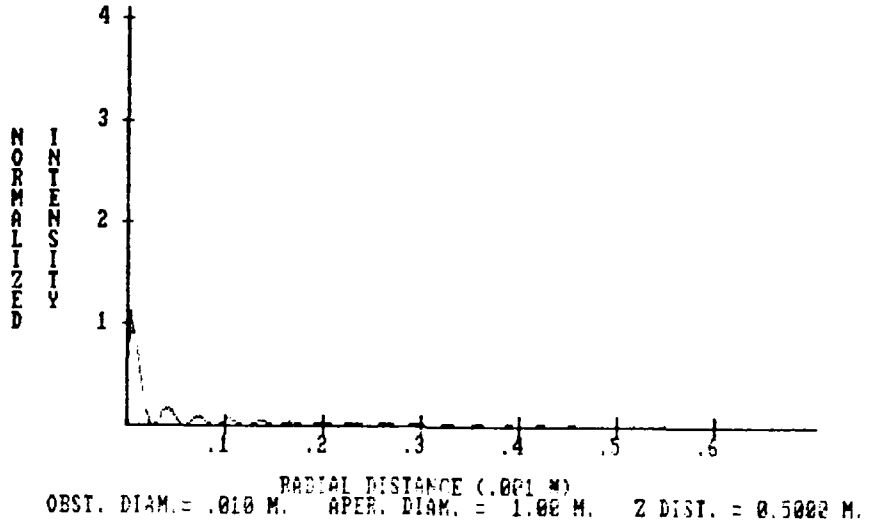

Graph 3.28

Intentisy Distribution for ε = .01

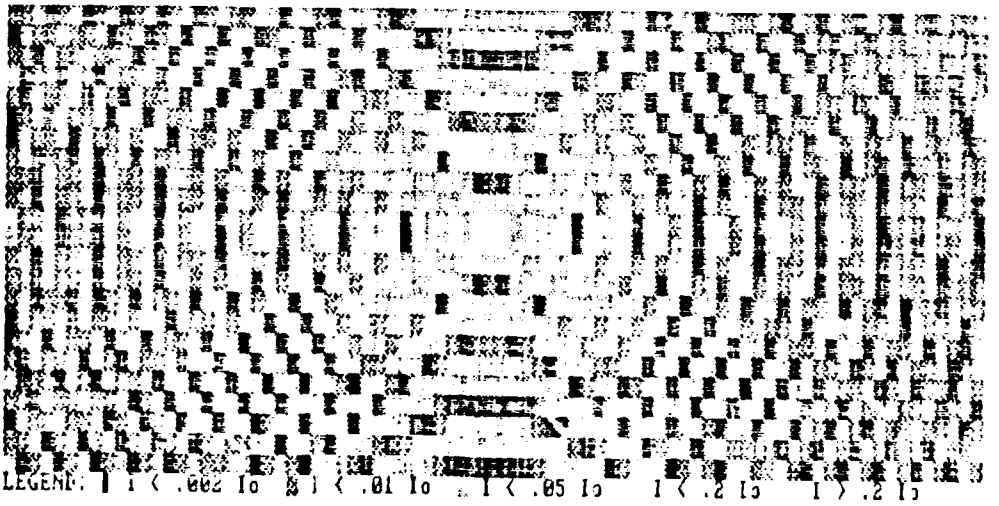

Graph 3.29

Annular Aperture Pattern for ε = .01

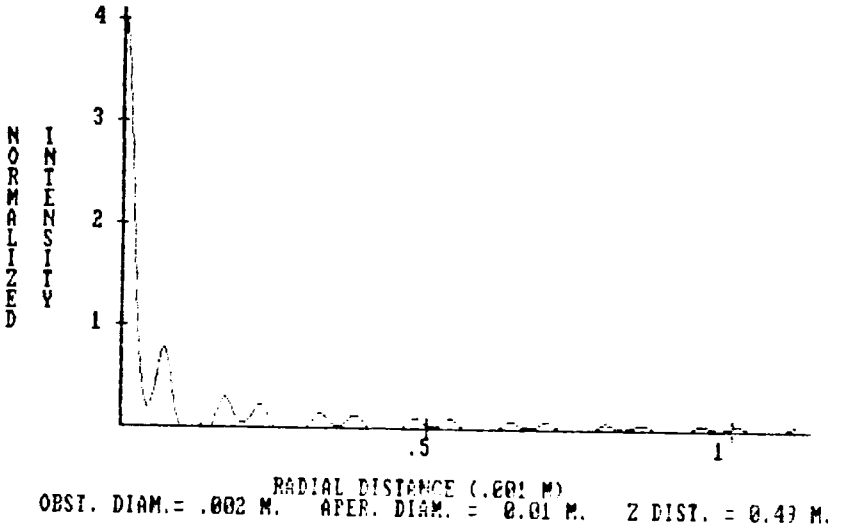

Graph 3.30

Intensity Distribution for ε = .2

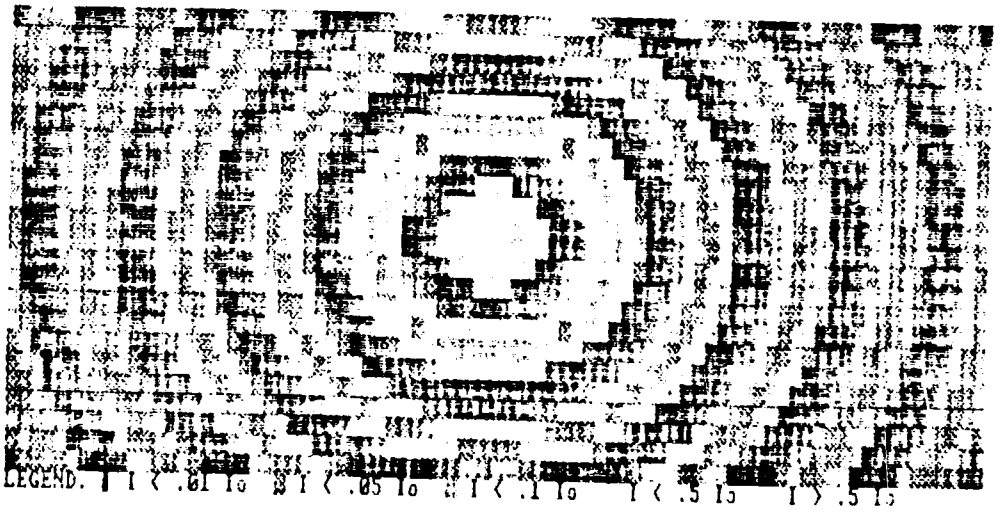

Graph 3.31

Annular Aperture Pattern for ε = .2

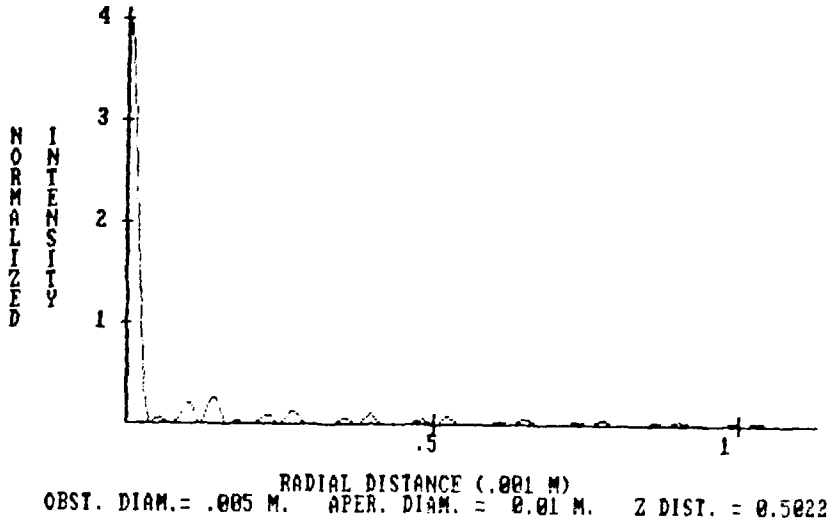

Graph 3.32

Intensity Distribution for ε = .5

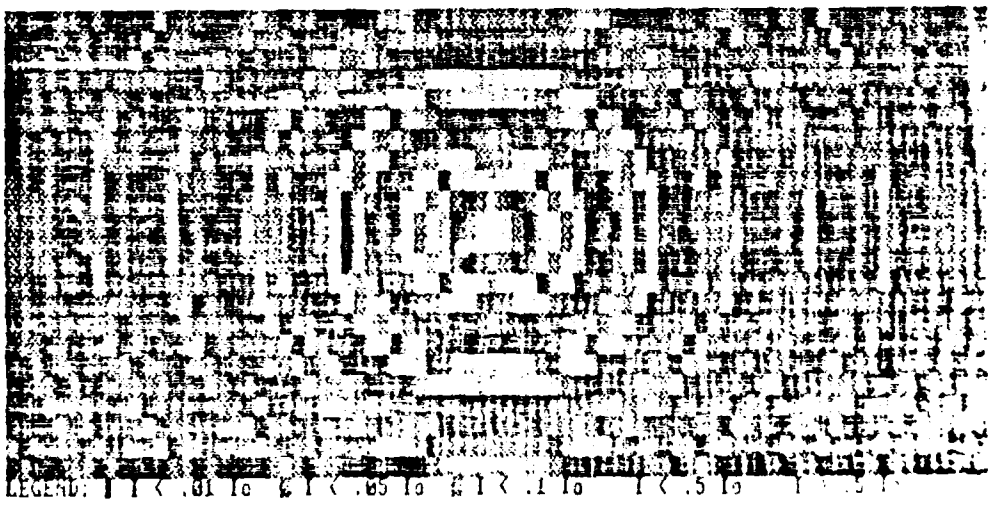

Graph 3.33

Annular Aperture Pattern

AD-A141 983 THE SPOT OF ARAGO AND ITS ROLE IN ABERRATION ANALYSIS 2/4
(U) AIR FORCE INST OF TECH WRIGHT-PATTERSON AFB OH
D R ERBSCHLOE DEC 83 AFIT/CI/NR-84-7T

UNCLASSIFIED F/G 20/6 NL

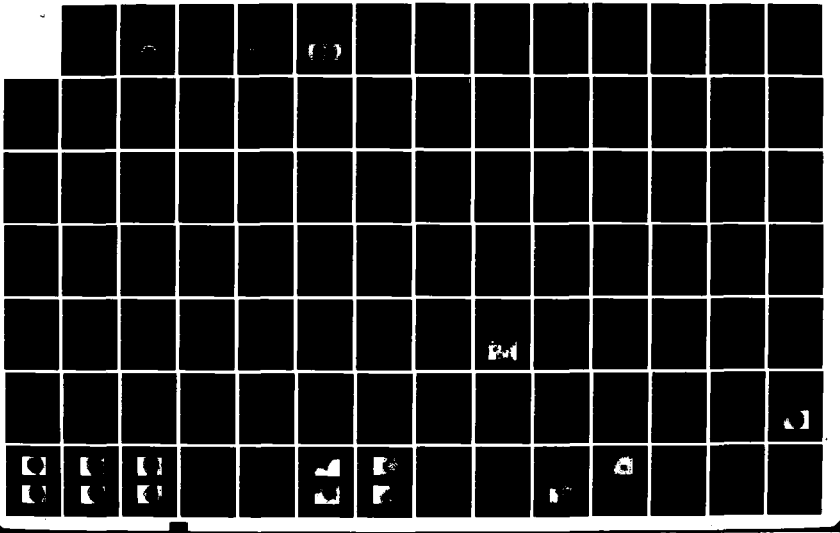

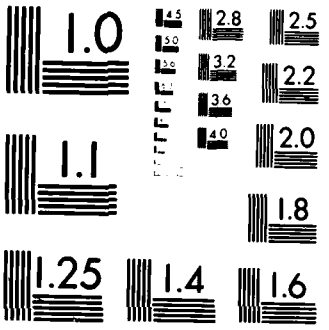

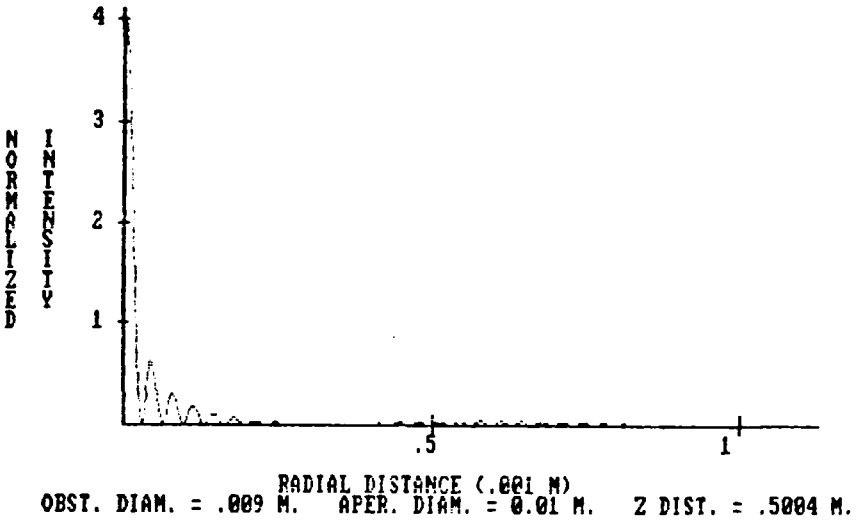

Graph 3.34

Intensity Distribution for $\varepsilon = .9$

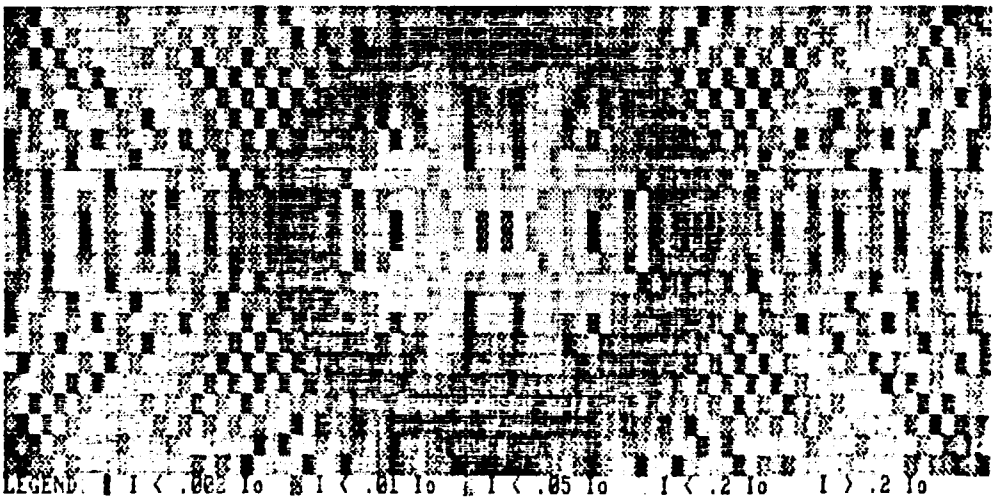

Graph 3.35

Annular Aperture Pattern for $\varepsilon = .9$

Table 3.4

Comparison of Measured Envelope Widths to Theory

Graph from which measurements taken	Average measured distance between beat zeroes (mm)	Theoretical distance $2\delta z$ D-d	Percent Difference	Measured $\frac{\nu_{ann.}}{\nu_{circ.}}$	$(1-\varepsilon)$
Graph 3.30	.0784 ± .0019	.0779	.6 %	.795	.8
Graph 3.32	.1270 ± .0011	.1271	.08%	.500	.5
Graph 3.34	.5330 ± .0005	.6333	.05%	.100	.1
Graph 3.36	.9053 ± .0009	.9052	.11%	.666	.667
Graph 3.38	.665 ± .0005	.679	2.1%	.102	.1

Tolerances in patterns with on-axis shifts. The preceding charts and graphs were made for planes at positions of maxima along the optical axis behind the annular apertures. The intensity of the central spot changes with distance z. Mathematically this stems from the cosine interference term in equation III-50. One can view the argument for the cosine, $\frac{k}{\delta z}(D^2 - d^2)$, as a phase term. For constant z, D and d this phase term will be fixed. This phase term will affect the intensity of the rings and their positions. A null on axis will push ring structure out from the center.

Below are graphs which demonstrate the change in the diffraction patterns for shifts to the next minima on axis for two previously calculated cases for $\varepsilon = 1/3$ and $\varepsilon = .9$.

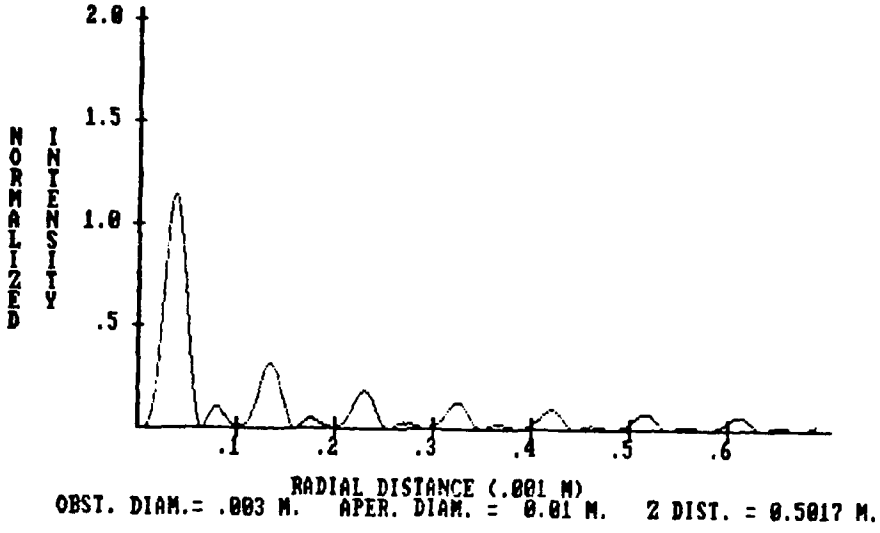

Graph 3.36

Intensity Distribution for $\varepsilon = 1/3$

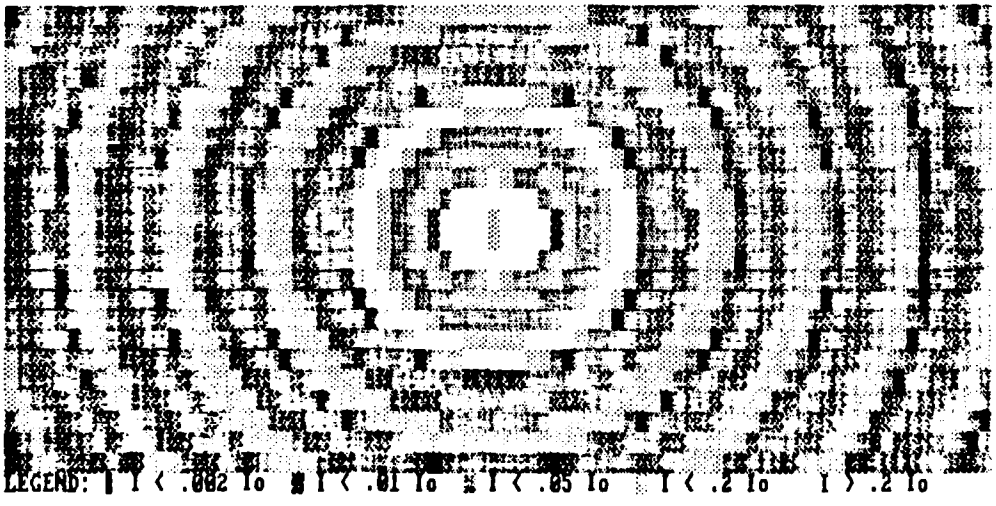

Graph 3.37

Annular Aperture Pattern for $\varepsilon = 1/3$

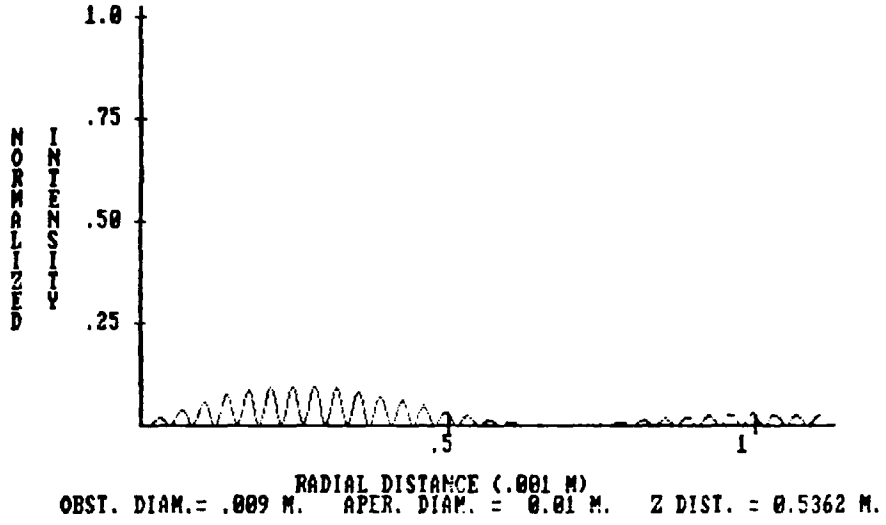

Graph 3.38

Intensity Distribution for ϵ = .9

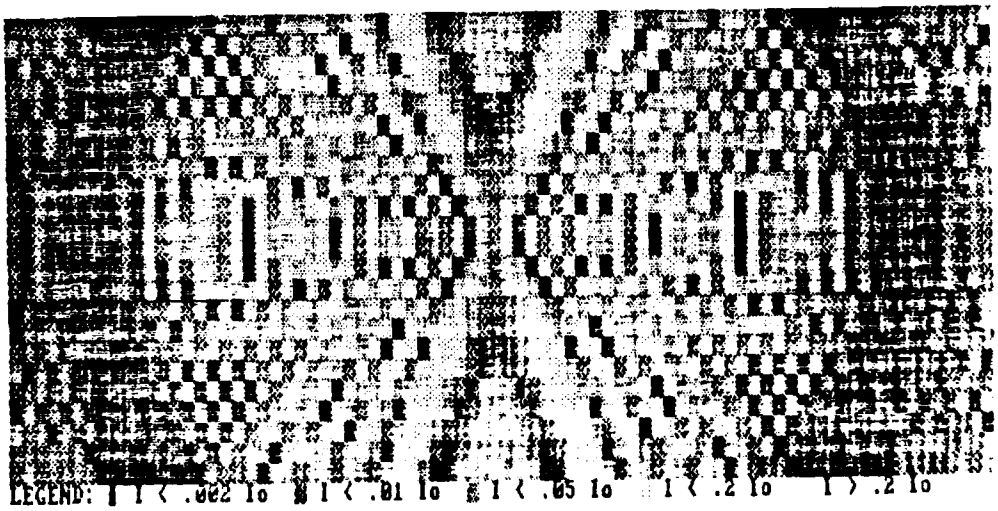

Graph 3.39

Annular Aperture Pattern for ϵ = .9

The diffraction pattern makes its most dramatic change as the central spot shifts from on-axis maximum to on-axis minimum. This relates to a change in the argument of the cosine term by π. Designating the argument by α one has:

$$\alpha = \frac{k}{8z}(D^2 - d^2)$$

$$\Delta\alpha = -\frac{k}{8z^2}(D^2 - d^2)\,\Delta z$$

(keeping k, D and d constant) (III-61)

Let $\Delta\alpha = a\pi$. Then:

$$\Delta z = -\frac{4a\lambda}{D^2-d^2}z^2 \qquad \text{(III-62)}$$

Thus the necessary shift on axis by a phase factor a π is quadratic in the initial distance z. As z increases a greater shift on axis is necessary to produce a given change in the diffraction pattern.

Case 4: Annular Aperture Illuminated with Gaussian Intensity Distribution

The treatment of an annular aperture illuminated by a plane wave with a gaussian intensity of the form $e^{-c\frac{r^2}{D^2}}$ follows that already done for the circular obscuration with the substitution of $\frac{D}{2}$ for the upper limit of the integral in equation III-31. The disturbance function becomes:

$$U(r_2, z) = \frac{A}{1-i\frac{2zc}{kD^2}} e^{ikz} e^{ik\frac{r_2^2}{2z}} \left[e^{-\frac{c}{4}} e^{ik\frac{D^2}{8z}} J_0\left(\frac{kDr_2}{2z}\right) - e^{-\frac{c}{4}\frac{d^2}{D^2}} e^{ik\frac{d^2}{8z}} J_0\left(\frac{kdr_2}{2z}\right) \right] \quad \text{(III-63)}$$

The intensity function is:

$$I(r_2, z) = \frac{A^2}{1+4\frac{z^2c^2}{k^2D^4}} \left[e^{-\frac{c}{2}} J_0^2\left(\frac{kDr_2}{2z}\right) + e^{-\frac{c}{2}\frac{d^2}{D^2}} J_0^2\left(\frac{kdr_2}{2z}\right) - 2e^{-\frac{c}{4}}\left[1+\frac{d^2}{D^2}\right] J_0\left(\frac{kDr_2}{2z}\right) J_0\left(\frac{kdr_2}{2z}\right) \cos\left(\frac{k}{8z}(D^2 - d^2)\right) \right] \quad \text{(III-64)}$$

As with the circular obscuration case, the term $4\frac{z^2c^2}{k^2D^4} << 1$ for small z and can be neglected.

On axis $r_2 = 0$ and the Bessel functions go to 1. The intensity function becomes:

$$I(0, z) = A^2 \left[e^{-\frac{c}{2}} + e^{-\frac{c}{2}\frac{d^2}{D^2}} - 2e^{-\frac{c}{4}}\left[1+\frac{d^2}{D^2}\right] \cos\left(\frac{k}{8z}(D^2 - d^2)\right) \right] \quad \text{(III-65)}$$

The positions of maxima on axis are given by equation III-40. At the maxima, the intensity is:

$$I(0, z_{max}) = A^2 \left[e^{-\frac{c}{4}} + e^{-\frac{c}{4}\frac{d^2}{D^2}} \right]^2 \quad \text{(III-66)}$$

The position of minima on axis are given by equation III-41. At the minima, the intensity is:

$$I(0, z_{min}) = A^2 \left[e^{-\frac{c}{4}} - e^{-\frac{c}{4}\frac{d^2}{D^2}} \right]^2 \qquad \text{(III-67)}$$

Thus for a gaussian intensity distribution the intensity on axis oscillates between the two limits given by the equations above. If c is not zero then the intensity on axis never reaches zero. Likewise the intensity at the maxima is always less than four times the incident intensity.

Physically the above result stems from difference in amplitude of the diffracted rays from the inner and outer edges. The amplitude of light rays reaching an aperture point a distance r from the center are diminished by the gaussian term $e^{-c\frac{r^2}{D^2}}$. The amplitudes of rays at the outer edge are decreased more than amplitudes of rays at the inner edge. Therefore the destructive interference of diffracted rays is not total. The constructive interference of diffracted rays is reduced by a combination of the gaussian terms.

The following graphs show the intensity on axis behind an annular aperture of obscuration ratio .5 for gaussian constants c of .5, 2 and 5.

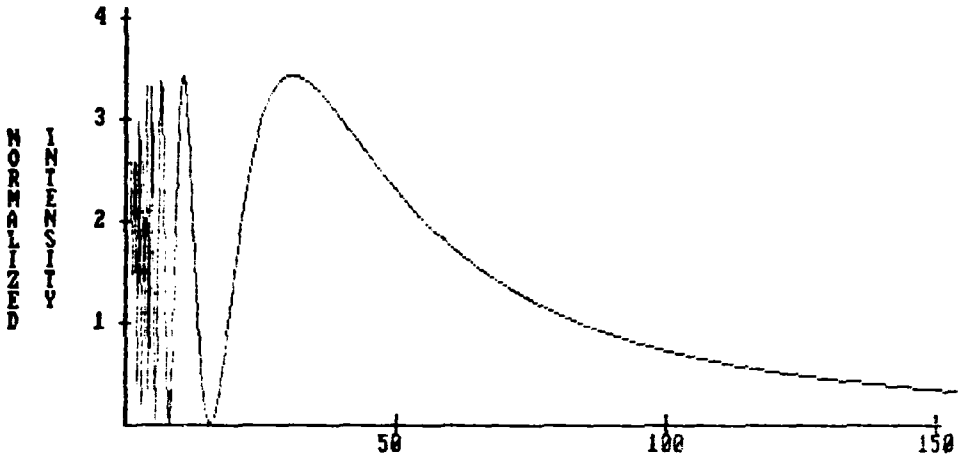

OBS. DIAM. = 0.005 M. APER. DIAM. = 0.010 M. GAUSSIAN CON. = 0.5

Graph 3.40

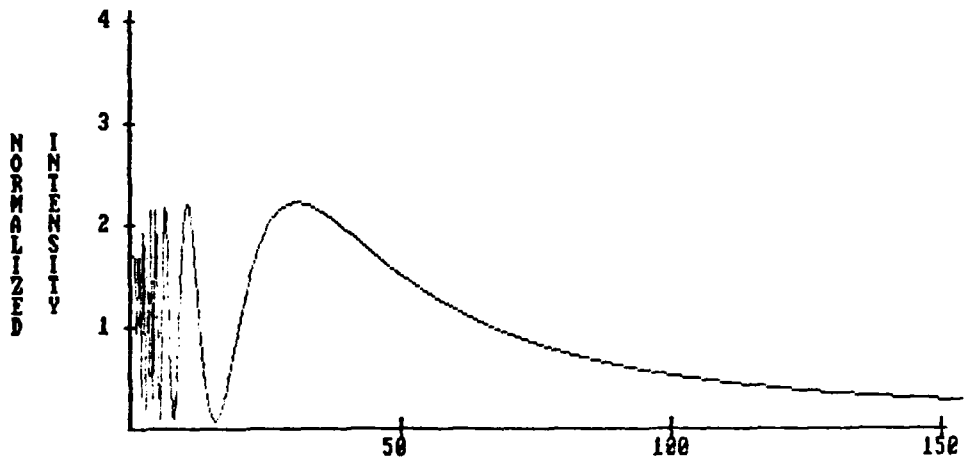

OBS. DIAM. = 0.005 M. APER. DIAM. = 0.010 M. GAUSSIAN CON. = 2.0

Graph 3.41

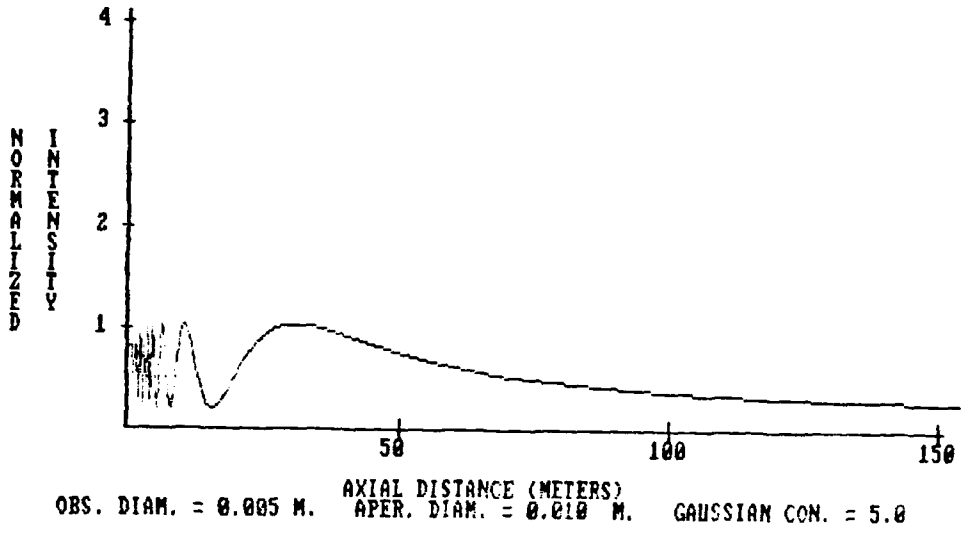

Graph 3.42

For large z or for large gaussian constants c the term $4\frac{z^2c^2}{k^2D^4}$ in the denominator in equation III-64 is no longer negligible. This drives the intensity on axis to zero at large observing distances.

As the gaussian constant c increases the maximum intensity on axis decreases. The minimum intensity starts at zero for c equal to zero and increases as c does. But it reaches a maximum value beyond which the exponential decrease starts to drive the minimum intensity back to zero. For fixed obscuration ratios one can maximize the minimum intensity on axis by changing the gaussian constant. The following graphs depict the maximum and minimum on axis intensities as functions of gaussian constants for obscuration ratios of .1, .2, .4, .6 and .8.

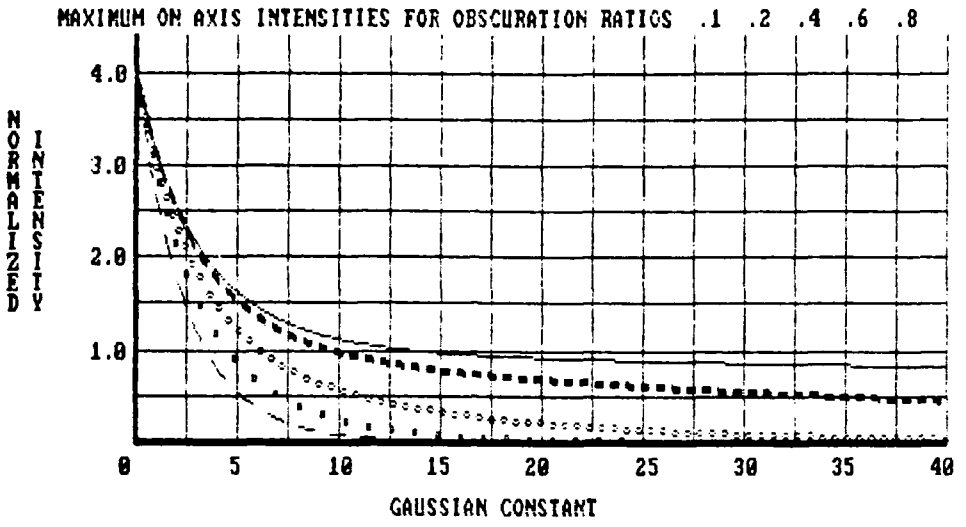

Solid line: $\varepsilon = .1$ Squared line: $\varepsilon = .6$
Heavy dashed line: $\varepsilon = .2$ Thin dashed line: $\varepsilon = .8$
Dotted line: $\varepsilon = .4$

Graph 3.43

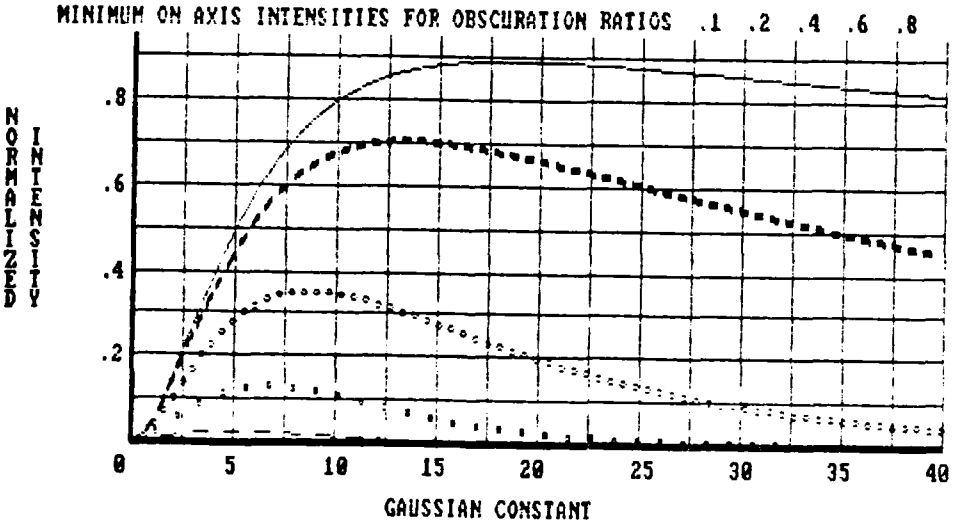

Solid line: $\varepsilon = .1$ Squared line: $\varepsilon = .6$
Heavy dashed line: $\varepsilon = .2$ Thin dashed line: $\varepsilon = .8$
Dotted line: $\varepsilon = .4$

Graph 3.44

Case 5: Displaced Obstacle and Aperture Illuminated with Uniform Intensity

If the obstacle and aperture do not lie in the same plane, it is still possible to derive expressions for the on and off axis intensity distribution functions. The layout depicted below corresponds to the eventual experimental set-up. As with the previous treatment the origin of the cylindrical coordinate system is taken to be the center of the aperture.

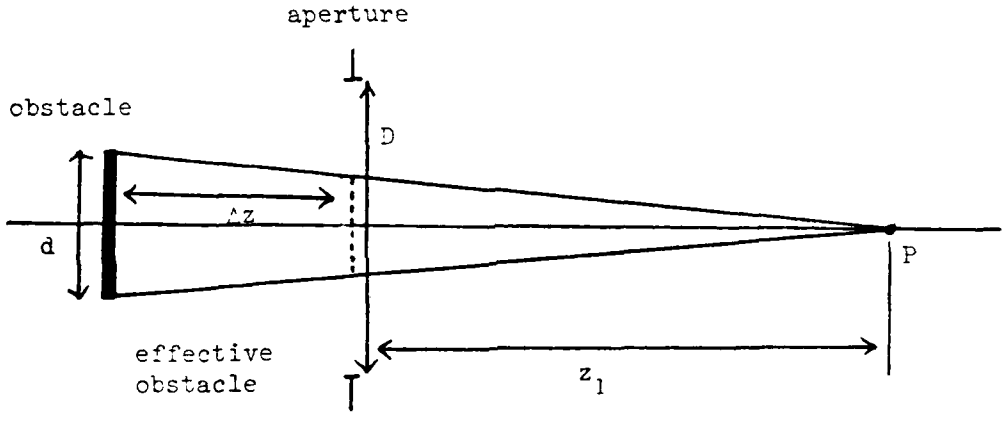

Figure 3.6

Geometrical Layout for Diffraction by Displaced Aperture and Obstacle

The observation plane lies a distance z_1 behind the aperture and a distance $z_2 = z_1 + \Delta z$ behind the obstacle. The rays diffracted by the obstacle which converge at point P project an effective obstacle in the aperture plane. By similar triangles, the diameter of this phantom obstacle is $d' = \frac{z_1}{z_2} d$. The light rays striking the aperture are parallel to the optical axis, but those striking the effective

obscuration are converging to the axis, thus there will be a phase difference.

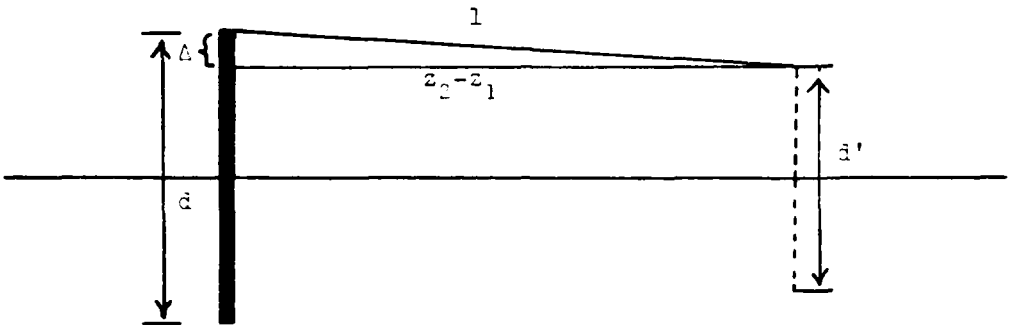

Figure 3.7

Phase Difference for Obstacle Diffracted Rays

The diffracted rays travel through distance l to the effective obstacle.

$$l = \sqrt{\Delta^2 + (z_2 - z_1)^2}$$

$$= \sqrt{\frac{d^2}{4}\left(1 - \frac{z_1}{z_2}\right)^2 + (z_2 - z_1)^2}$$

$$= (z_2 - z_1)\sqrt{1 + \frac{d^2}{4z_2^2}} \qquad \text{(III-68)}$$

Taking $\frac{d^2}{4z_2^2} << 1$ this becomes

$$l \approx (z_2 - z_1)\left(1 + \frac{d^2}{8z_2^2}\right) \qquad \text{(III-69)}$$

The phase difference of the rays striking the edge of the effective obstacle is then:

$$k(l - (z_2 - z_1)) \approx \frac{kd^2}{8z_2^2}(z_2 - z_1) \qquad \text{(III-70)}$$

To evaluate the Rayleigh-Sommerfeld integral for the effective annular aperture, the following assumptions are made:

1. $\frac{D^2}{4z_2^2} << 1, \quad \frac{d^2}{4z_2^2} << 1$

2. The effect from rays diffracted by the obstacle striking the aperture is negligible. The rays striking the aperture are considered parallel to the optical axis.

3. As with previous treatments only those rays diffracted by the outer aperture edge and the inner effective edge contribute to the ultimate diffraction pattern.

4. The rays hitting the inside and outside edges of the effective annular aperture have a phase difference given by equation III-68.

The Rayleigh-Sommerfeld integral for the disturbance at a point P in the observation plane is:

$$U(r_2, z_1, z_2) = \frac{A}{i\lambda} \int_0^{2\pi} d\phi_1 \int_{\frac{z_1}{z_2}\frac{d}{2}}^{D/2} \frac{e^{ikl}}{l} \cos(\underset{\sim}{n}, \underset{\sim}{l})\, \beta(r_1)\, r_1 dr_1 \qquad \text{(III-71)}$$

where:

$$\beta(r_1) = 1 \qquad \text{for } r_1 = \frac{D}{2}$$

$$= e^{ik\frac{d^2}{8z_1^2}(z_2 - z_1)} \qquad \text{for } r_1 = \frac{z_1}{z_2}\frac{d}{2} \qquad \text{(III-72)}$$

The result follows from previous derivations:

$$U(r_2, z_1, z_2) = Ae^{ikz_1}\, e^{ikr_2^2/2z_1} \left[e^{ik\frac{D^2}{8z_1}}\, J_0\left(\frac{kDr_2}{2z_1}\right) - e^{i\frac{k}{8z_1}\left[\frac{z_1}{z_2}d\right]^2}\, e^{ik\frac{d^2}{8z_2^2}(z_2-z_1)}\, J_0\left(\frac{kr_2}{z_1}\,\frac{z_1}{z_2}\,\frac{d}{2}\right)\right]$$

$$= Ae^{ikz_1}\, e^{ikr_2^2/2z_1} \left[e^{ik\frac{D^2}{8z_1}}\, J_0\left(\frac{kDr_2}{2z_1}\right) - e^{i\frac{kd^2}{8z_2}}\, J_0\left(\frac{kr_2 d}{2z_2}\right)\right] \qquad \text{(III-73)}$$

Thus the disturbance function has the reassuring form of having the effect from the aperture edge at distance Z_1, coupled with the effect from the obstacle edge at distance Z_2. The intensity distribution function is:

$$I(r_2, z_1, z_2) = A^2 \left[J_0^2\left(\frac{kDr_2}{2z_1}\right) + J_0^2\left(\frac{kdr_2}{2z_2}\right) - 2J_0\left(\frac{kDr_2}{2z_1}\right) J_0\left(\frac{kdr_2}{2z_2}\right) \times \cos\left(\frac{k}{8}\left[\frac{D^2}{z_1} - \frac{d^2}{z_2}\right]\right)\right] \qquad \text{(III-74)}$$

Notes

[1] Joseph W. Goodman, Introduction to Fourier Optics (San Francisco: McGraw-Hill, 1968), p. 44.

[2] James E. Harvey and James E. Forgham, "The Spot of Arago: New Relevance for an Old Phenomenon," American Journal of Physics, (January 1984).

[3] Max Born and Emil Wolf, Principles of Optics, 6th ed. (Oxford: Pergamon, 1980), p. 395.

[4] Harvey E. White, Modern College Physics, 6th ed. (New York: Van Nostrand Reinhold, 1972), p. 304.

Chapter 4

THEORY I. THE ABERRATED CASES

General Aberration Considerations

Wavefront aberrations are deviations from spherical wavefront behavior. Consider an arbitrary wavefront in space. (A wavefront is defined as a surface of constant phase.) It is convenient to project this wavefront onto a spherical wavefront. This reference wavefront shares the phase and optical axis point with the arbitrary wavefront. The radius of curvature is the distance to the source if a diverging wavefront or the distance to the focal point if a converging wavefront. The projections onto the reference wavefront reflect phase

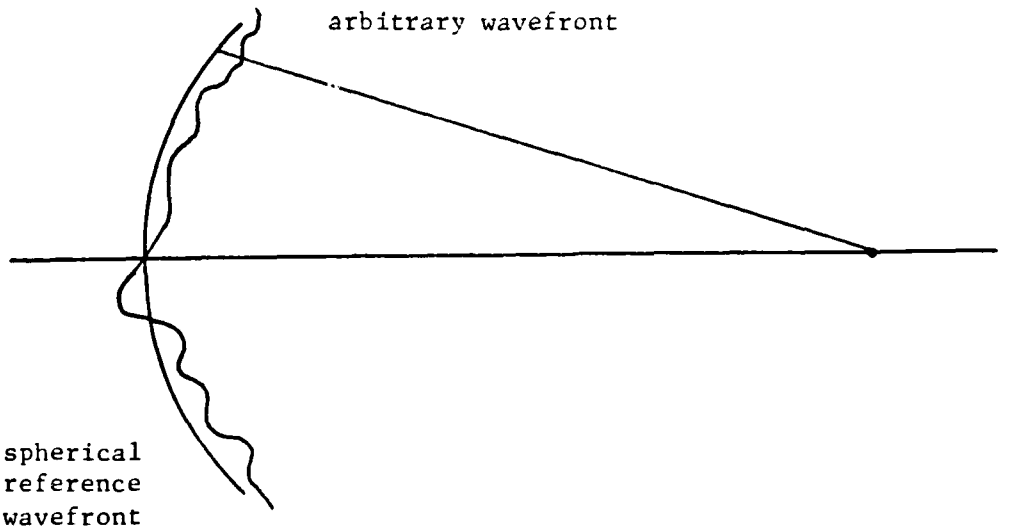

Figure 4.1

Aberrated Wavefront

differences due to the optical path differences between corresponding points on the two wavefronts. The phase differences can be characterized by an aberration function W where W(r, β, $\emptyset$) is the optical path difference between the point (r, β, $\emptyset$) on the reference wavefront and its complement on the arbitrary wavefront. Thus the phase differences appear in the form:

$$e^{ikW}$$

First Order and Seidel Aberrations

The aberration function can be expanded in terms of a complete set of polynomials called the Zernicke polynomials.[1] In many cases it is sufficient to expand the aberration function in terms of primary aberrations. Convenient expressions for these primary aberrations were made by Seidel and the third order aberrations now bear his name. The wavefront aberration representations appear in Table 4.1. The coefficients W_{abc} are constants with the dimension of length. $\emptyset$ is the polar coordinate angle of points in the reference plane. r is the radial distance in the reference plane normalized to a given pupil radius. When the pupil is the outer edge of an annular aperture $r = \frac{r_1}{D/2}$. Similarly, β is a normalized field parameter. When the source is a point source β is a constant and can be absorbed into the coefficients W_{abc}. Table 4.2 lists field independent wavefront aberrations. In the field independent situation field curvature acts like defocus and distortion like tilt.

Table 4.1

The Primary Wavefront Aberrations

Aberration type	Representation	
Defocus	$W_{020}r^2$	First order
Tilt	$W_{111}\beta r\cos\phi$	aberrations
Spherical aberration	$W_{040}r^4$	
Coma	$W_{131}\beta r^3\cos\phi$	Third order
Astigmatism	$W_{222}\beta^2 r^2\cos^2\phi$	(Seidel)
Field curvature	$W_{220}\beta^2 r^2$	aberrations
Distortion	$W_{311}\beta^3 r\cos\phi$	

Table 4.2

Field Independent Wavefront Aberrations

Aberration type	Representation
Defocus / Field Curvature	$4W_{20}r_1^2/D^2$
Tilt / Distortion	$2W_{11}r_1\cos\phi/D$
Spherical aberration	$16W_{40}r_1^4/D^4$
Coma	$8W_{31}r_1^3\cos\phi/D^3$
Astigmatism	$4W_{22}r_1^2\cos^2\phi/D^2$

Aberrations Produced by Plane Parallel Plates

Consider a diverging wavefront incident upon a tilted plane parallel plate. The tilt angle is given by θ and u is the half angle

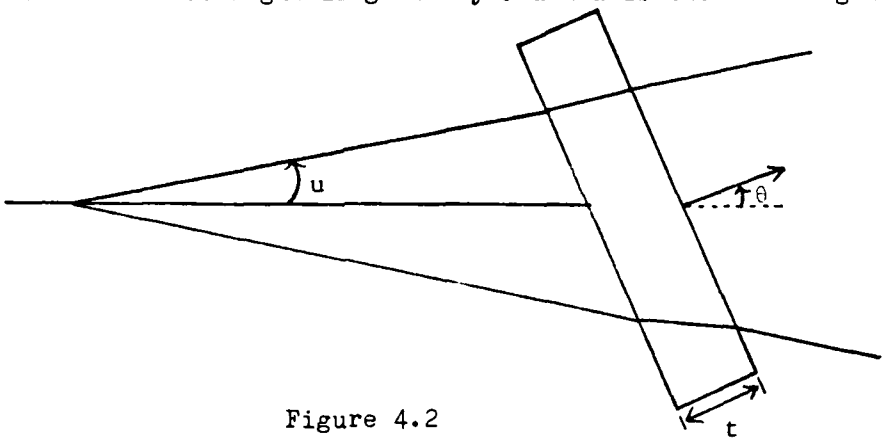

Figure 4.2

Aberration Production by Plane Parallel Plate

of the cone of illumination. u is related to the f-number by the formula:[2]

$$F^{\#} = \frac{1}{2u} \qquad \text{(IV-1)}$$

The thickness of the plate is t. It is clear to see that phase differences result from passage through the plate by breaking up the wavefront into rays. Rays corresponding to different f-numbers will strike the plate at different angles. By Snell's law the refraction angles will not be the same and the path lengths through the plate will differ. Because light moves more slowly in glass than in air, transit times vary and phase differences ensue. The phase differences appear as aberrations in the wavefront. A table of the primary wavefront aberrations coefficients as functions of n, u, θ and t produced by a plane parallel plate appears below:[3]

Table 4.3

Aberration Coefficients Due to Tilted Plane Parallel Plate

Aberration Coefficient	Expression
W_{22} (Astigmatism)	$-\frac{1}{2}\frac{n^2-1}{n^3} tu^2\theta^2$
W_{31} (Coma)	$-\frac{1}{2}\frac{n^2-1}{n^3} tu^3\theta$
W_{40} (Spherical Aberration)	$-\frac{1}{8}\frac{n^2-1}{n^3} tu^4$

Notice the coefficient for coma is an odd function of the tilt angle θ. By *countertilting* two plane parallel plates of equal indices of refraction and thickness comatic effects can be neutralized. At the same time the coefficients for astigmatism and spherical aberration double.

Table 4.4

Aberration Coefficients for Two Countertilted Plane Parallel Plates

Aberration coefficient	Expression
W_{22} (Astigmatism)	$-\frac{n^2-1}{n^3} tu^2\theta^2$
W_{31} (Coma)	0
W_{40} (Spherical Aberration)	$-\frac{1}{4}\frac{n^2-1}{n^3} tu^4$

Typically the aberration coefficients are very small numbers, having the magnitude of order of optical wavelengths. It is convenient to express the aberration coefficients in terms of wavelengths of the incident light. The two graphs below illustrate the aberration coefficient curves for a single plate and two counter tilted plates. The incident wavelength is taken as 6328Å, the thickness of one plate is 12.7mm (1/2 inch), the index of refraction n = 1.517 and the angle u = .1 (5.74°). The aberration coefficients are plotted as functions of the plate tilt angle θ.

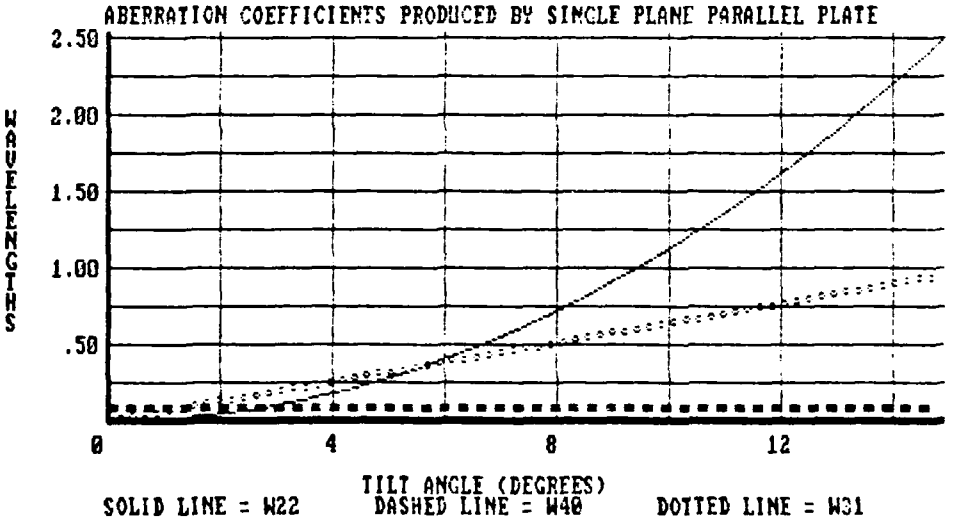

Graph 4.1

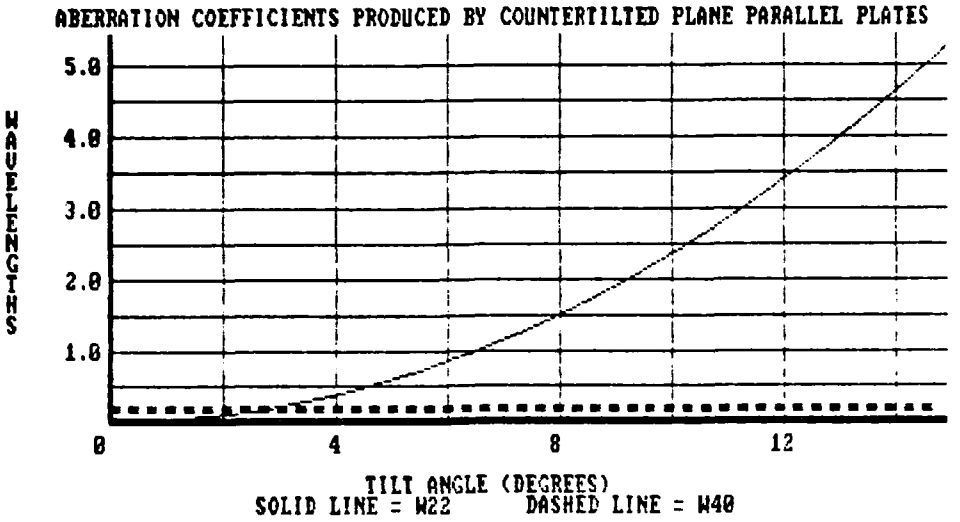

Graph 4.2

Symmetries in the Primary Aberrations

The primary aberrations have characteristic symmetries which will ultimately determine their contributions to the diffraction pattern. Both defocus and spherical aberration are independent of θ. They are rotationally symmetric and as such should have little or no effect on the rotationally symmetric diffraction patterns discussed in Chapter 3. Tilt and coma are products of odd functions in r and even functions in θ. Because $\cos\phi = \cos(-\phi)$, the aberration terms for tilt and coma will have equal values for fixed r and $\pm\phi$. This means there is one plane of symmetry for these terms. Astigmatism is the product of an even function in r and the even function $\cos^2\phi$. Because $\cos^2(\phi) = \cos^2(\pi - \phi) = \cos^2(\pi + \phi) = \cos^2(2\pi - \phi)$ astigmatism exhibits two planes of symmetry.

Each primary aberration will be discussed separately.

Defocus

Defocus can best be discribed as a shift of the focal point on the optical axis. In effect the reference spherical wavefront is changed as the radius of curvature changes. If the focal point shift on optical axis is designated as Δz then the coefficient of defocus for a point on the reference spherical wavefront with f-number $F^{\#}$ is:[4]

$$W_{20} = - \frac{\Delta z}{8(F^{\#})^2} \tag{IV-2}$$

Case 6: Circular Obscuration

The Rayleigh-Sommerfeld integral of interest is:

$$U(r_2, \emptyset_2, z) = \frac{A}{i\lambda z} e^{ikz} e^{ikr_2^2/2z} \int_0^{2\pi} \int_{d/2}^{\infty} e^{ik \frac{r_1^2}{2z}} e^{ik4W_{20}\frac{r_1^2}{d^2}}$$

$$x\ e^{-ik \frac{r_1 r_2}{z} \cos(\emptyset_2 - \emptyset_1)}\ r_1 dr_1 d\emptyset_1$$

$$= \frac{2\pi A}{i\lambda} e^{ikz} e^{ikr_2^2/2z} \int_{d/2}^{\infty} e^{ik\left[\frac{1}{2z} + \frac{4W_{20}}{d^2}\right]r_1^2}$$

$$x\ J_0\left(\frac{kr_1 r_2}{z}\right) r_1 dr_1 \tag{IV-3}$$

The solution of the above integral follows the procedures set forth in Chapter 3.

$$U(r_2, z) = \frac{kA}{i\lambda z} \frac{zd^2}{ik(d^2+8W_{20}z)} e^{ikz} e^{ik\frac{r_2^2}{2z}} e^{ik\left[\frac{1}{2z}+\frac{4W_{20}}{d^2}\right]\frac{d^2}{4}} \times J_0\left(\frac{kdr_2}{2z}\right)$$

$$= -A \frac{1}{1+\frac{8W_{20}z}{d^2}} e^{ik(z+\frac{r_2^2}{2z}-\frac{d^2}{8z}+W_{20})} J_0\left(\frac{kdr_2}{2z}\right) \qquad \text{(IV-4)}$$

The intensity distribution is:

$$I(r_2, z) = \frac{A^2}{\left(1+\frac{8W_{20}z}{d^2}\right)^2} J_0^2\left(\frac{kdr_2}{2z}\right) \qquad \text{(IV-5)}$$

If no defocus is present $W_{20} = 0$ and the above expression becomes equivalent to the unaberrated case in equation III-26. The Bessel function term is identical to that for the unaberrated case -- as expected this rotationally symmetric aberration does not affect the rotationally symmetric diffraction pattern. Where defocus does enter is in the overall intensity. For positive defocus the factor $1 / \left(1 + \frac{8W_{20}z}{d^2}\right)^2$ decreases as the distance along the optical axis z increases. The effect of positive defocus is to decrease the overall intensity for large z. Something interesting happens when the coefficient of defocus is negative. At one value of z the intensity on axis goes to infinity. This z corresponds the focal point of the system. To see this, the denominater goes to zero when:

$$z = -\frac{d^2}{8W_{20}} \qquad \text{(IV-6)}$$

The obscuration (or aperture) will act as a focusing system. With no aberration present it would obey the lens law.

$$\frac{1}{s} + \frac{1}{i} - \frac{1}{f} = 0 \qquad \text{(IV-7)}$$

where s is the distance to the source, i is the distance to the image and f is the focal distance of the system. With defocus present the lens law is replaced by:[4]

$$\frac{1}{s} + \frac{1}{i} - \frac{1}{f} = \varepsilon \qquad \text{(IV-8)}$$

Where $$\varepsilon = 2\,\frac{W(r_1, \phi_1)}{r_1^2} = 2\,\frac{4W_{20}r_1^2}{r_1^2 d^2}$$

$$= \frac{8W_{20}}{d^2} \qquad \text{(IV-9)}$$

With no aberration present the terms s, i and f in equation IV-7 are all infinite. With defocus s and i remain infinite and f changes. Then:

$$-\frac{1}{f} = \varepsilon$$

$$f = -\frac{d^2}{8W_{20}} \qquad \text{(IV-10)}$$

Thus the focal point of the system is the singularity on the optical axis.

As the magnitude of defocus is increased, the focal point moves in from infinity and approaches the aperture. For negative defocus the on axis intensity will increase until the focal point is reached.

Then it will decrease. (If the coefficient of defocus is positive the system focal point occurs at negative z and the decreasing intensity already discussed is an extension of the decrease from the focal point.)

The singularity intensity is reminiscent of the geometrical optics limit where the intensity at the focal point is infinite. Appendix 5 demonstrates the infinite intensity is a result of an infinite plane wave striking a circular obscuration. Physically the extent of the incident wave is always finite so the intensity at $z = -\frac{d^2}{8W_{20}}$ will never go to infinity. The graphs below demonstrate these effects for on and off axis intensity plots.

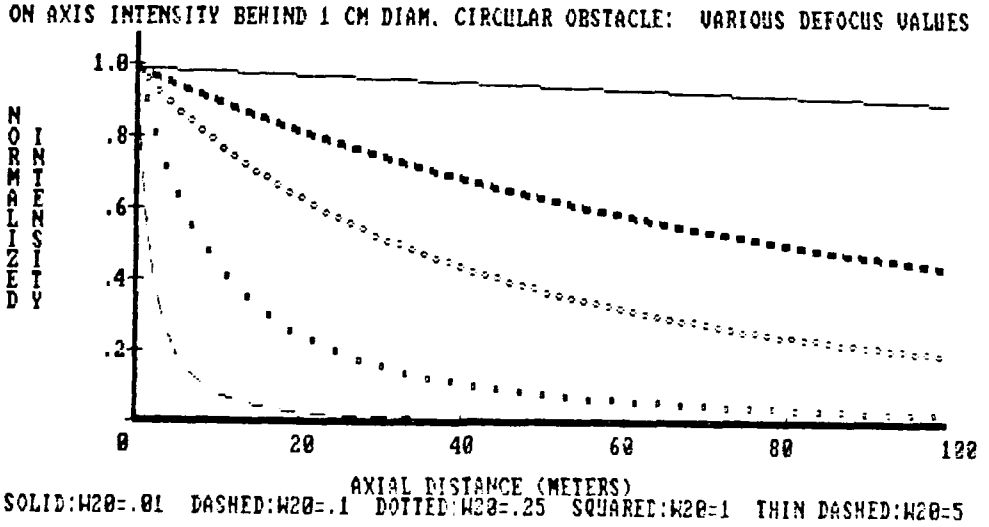

Graph 4.3

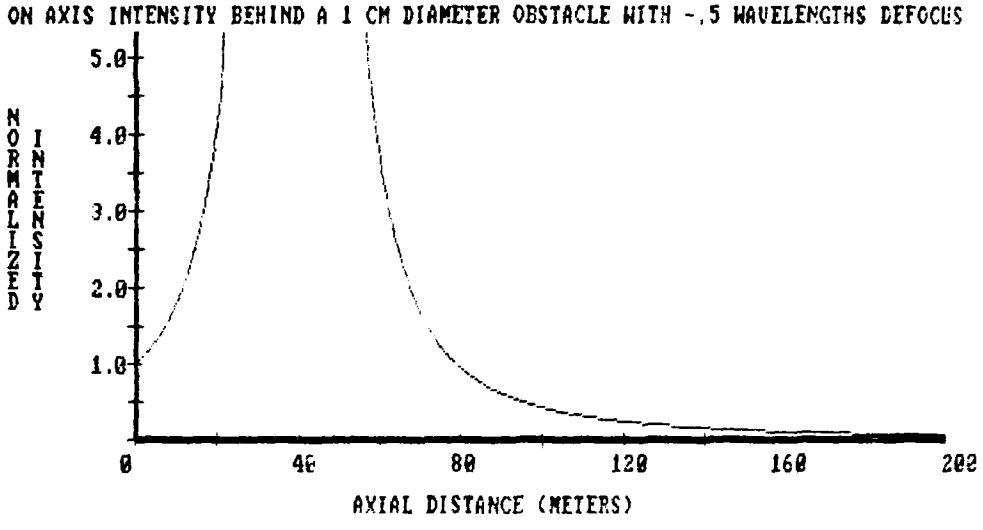

Graph 4.4

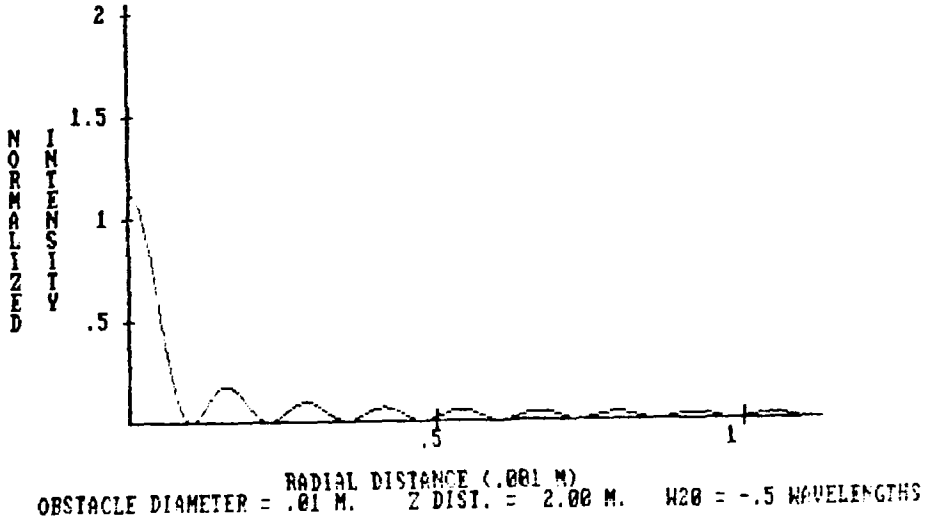

Graph 4.5

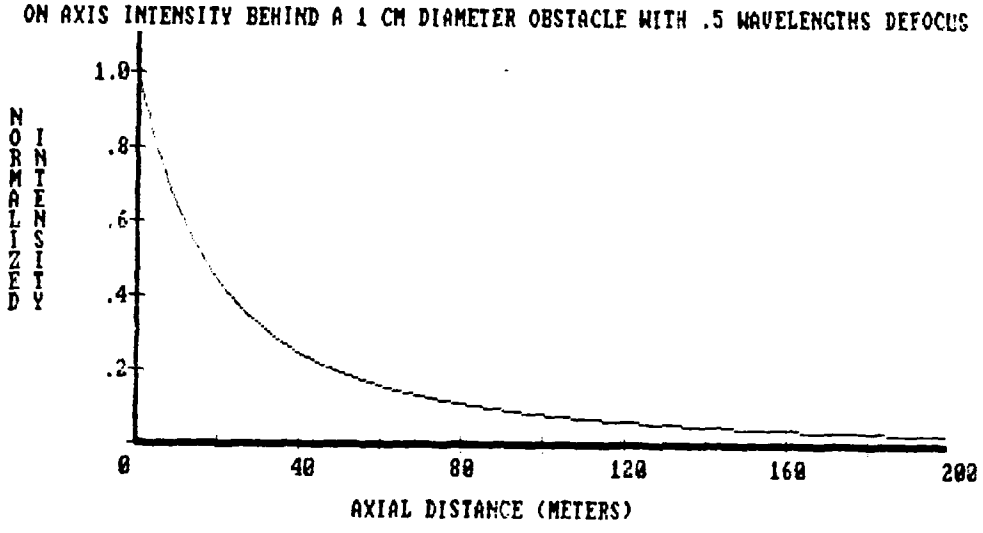

Graph 4.6

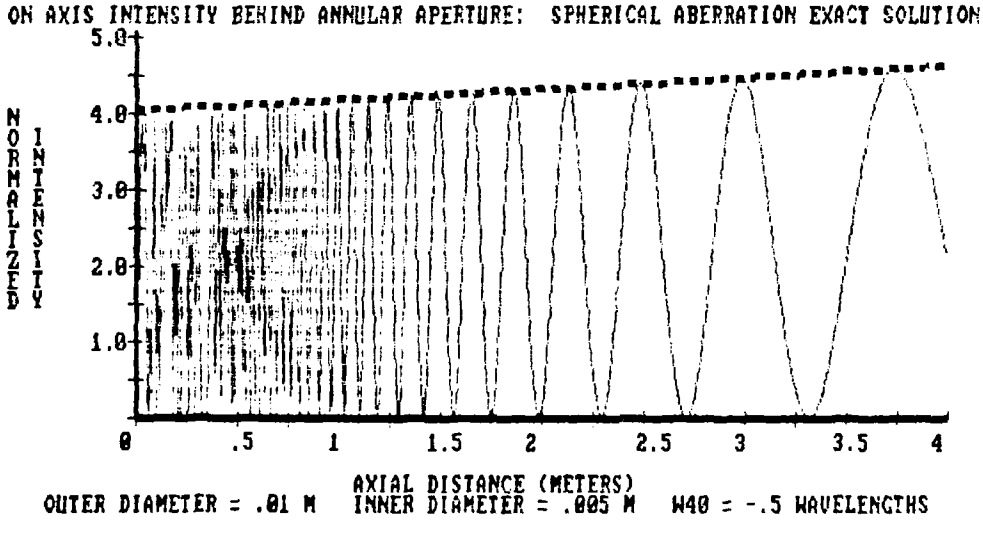

Graph 4.7

The on axis intensity is characteristic of the defocus present. By measuring the intensity a given distance z along the optical axis one can readily determine the amount of defocus in the incident beam. From equation IV-5:

$$I_{meas.} = \frac{I_0}{\left(1 + \frac{8W_{20}z}{d^2}\right)^2}$$

$$W_{20} = \frac{d^2}{8z}\left(\sqrt{\frac{I_0}{I_{meas.}}} - 1\right)$$

$$= -\frac{d^2}{8z}\left(\sqrt{\frac{I_0}{I_{meas.}}} + 1\right) \qquad \text{for } W_{20} < 0 \text{ and } z > \frac{d^2}{8|W_{20}|}$$

(IV-11)

Case 7: Annular Aperture

In the case of the annular aperture the aberration function is normalized to the aperture outer radius. The expression for W is:

$$W = 4W_{20}\frac{r_1^2}{D^2} \qquad \text{(IV-12)}$$

Substituting the above into equation IV-3 and changing the upper integration limit for r_1 to D/2 allows one to write out the disturbance function from equation IV-4.

$$U(r_2, z) = \frac{A}{1+\frac{8W_{20}z}{D^2}} e^{ik\left[z+\frac{r_2^2}{2z}\right]}\left[e^{ik\left[\frac{D^2}{8z}+W_{20}\right]} J_0\left(\frac{kDr_2}{2z}\right) - e^{ik\left[\frac{d^2}{8z}+W_{20}\frac{d^2}{D^2}\right]} J_0\left(\frac{kdr_2}{2z}\right)\right] \quad \text{(IV-13)}$$

The intensity distribution is:

$$I(r_2, z) = \frac{A^2}{\left(1+\frac{8W_{20}z}{D^2}\right)^2}\left[J_0^2\left(\frac{kDr_2}{2z}\right) + J_0^2\left(\frac{kdr_2}{2z}\right) - 2J_0\left(\frac{kDr_2}{2z}\right) x\, J_0\left(\frac{kdr_2}{2z}\right) \cos\left(\frac{k}{8z}(D^2 - d^2) + kW_{20}\left[1-\frac{d^2}{D^2}\right]\right)\right] \quad \text{(IV-14)}$$

The cosine term can be rewritten in a somewhat more condensed form:

$$\cos\left(\frac{k}{8z}(D^2 - d^2) + kW_{20}\left[1-\frac{d^2}{D2}\right]\right) = \cos\left(\frac{k}{8z}(D^2 - d^2) x \left[1+\frac{8W_{20}z}{D^2}\right]\right) \quad \text{(IV-15)}$$

When no defocus is present the intensity distribution reduces to that for the unaberrated case.

Defocus will affect the diffraction pattern of an annular aperture in two ways. The first is in the change of the overall intensity. The intensity distribution is multiplied by the same term $1 / (1 + 8W_{20}z/D^2)^2$ as for the circular obscuration case. The coefficient

for defocus also enters the cosine term. Thus the second effect defocus has is to shift the positions of maxima and minima on axis.

Maxima will occur when the argument of the cosine term equals an odd multiple of π.

$$\frac{k}{8z}(D^2 - d^2)\left[1 + \frac{8W_{20}z}{D^2}\right] = (2n + 1)\pi \qquad n = 0, 1, 2, \ldots$$

$$z = \frac{kD^2(D^2-d^2)}{8\pi(2n+1)D^2 - 8W_{20}k(D^2-d^2)}$$

$$z = \frac{D^2(1-\varepsilon^2)}{4\lambda(2n+1) - 8W_{20}(1-\varepsilon^2)} \qquad \text{(IV-16)}$$

Minima occur for:

$$z = \frac{D^2(1-\varepsilon^2)}{8n\lambda - 8W_{20}(1-\varepsilon^2)} \qquad \text{(IV-17)}$$

The last maximum on axis occurs when n = 0 at a distance

$$z = \frac{D^2(1-\varepsilon^2)}{4\lambda - 8W_{20}(1-\varepsilon^2)} \qquad \text{(IV-18)}$$

The above formula suggests the last maximum on axis will occur at infinite z when the denominater goes to zero, or when:

$$W_{20} = \frac{1}{2(1-\varepsilon^2)}\ \lambda \qquad \text{(IV-19)}$$

But there is a second effect to consider. The coefficient $1 / (1 + 8W_{20}z/D^2)^2$ goes to zero for infinite z. This term is the upper limit for the on-axis intensity. The intensity oscillates between 0 and this upper bound. The result that the last maximum on axis occurs at infinite z is a statement that there is no last maximum on axis behind the aperture -- the oscillations continue to infinity. In general this will be the case whenever:

$$8W_{20}\,(1 - \epsilon^2) \geq 4\lambda\,(2n + 1)$$

$$W_{20} \geq \frac{(2n+1)}{2(1-\epsilon^2)}\,\lambda \qquad n = 0,\ 1,\ 2,\ \ldots \qquad \text{(IV-20)}$$

Notice this implies positive defocus.

Although the positions of the maxima on axis have changed from the unaberrated case, the spacing of the maxima has the same form. From equation III-62 the spacing between adjacent maxima for the unaberrated case is:

$$\Delta z = -\frac{4a\lambda}{D^2-d^2}\,z^2 \qquad \text{(III-62)}$$

With defocus present:

$$\Delta\,\frac{k}{8z}\,(D^2 - d^2)\left[1 - \frac{8W_{20}z}{D^2}\right] = \Delta \text{ argument}$$

$$-\frac{k}{8z^2}\,(D^2 - d^2)\left[1 - \frac{8W_{20}z}{D^2}\right]\Delta z + \frac{k}{8z}\,(D^2 - d^2)\,\frac{8W_{20}}{D^2}\,\Delta z = 2\pi$$

$$-\frac{k}{8z^2}(D^2 - d^2)\,\Delta z = 2\pi$$

$$\Delta z = -\frac{8\lambda}{D^2-d^2}\,z^2 = \frac{8}{(1-\varepsilon^2)}\,\frac{z^2}{D^2}\,\lambda \qquad \text{(IV-21)}$$

The following graphs demonstrate the on axis intensities behind a one centimeter outer diameter annular aperture with $\varepsilon = .5$ and with defocus coefficients of $.5\lambda$, $-.5\lambda$, $.667\lambda$ and 2λ. ($.667\lambda$ corresponds to the case where the last maximum occurs at infinity.) The envelope $1 / (1 + 8W_{20}z/D^2)^2$ is also plotted.

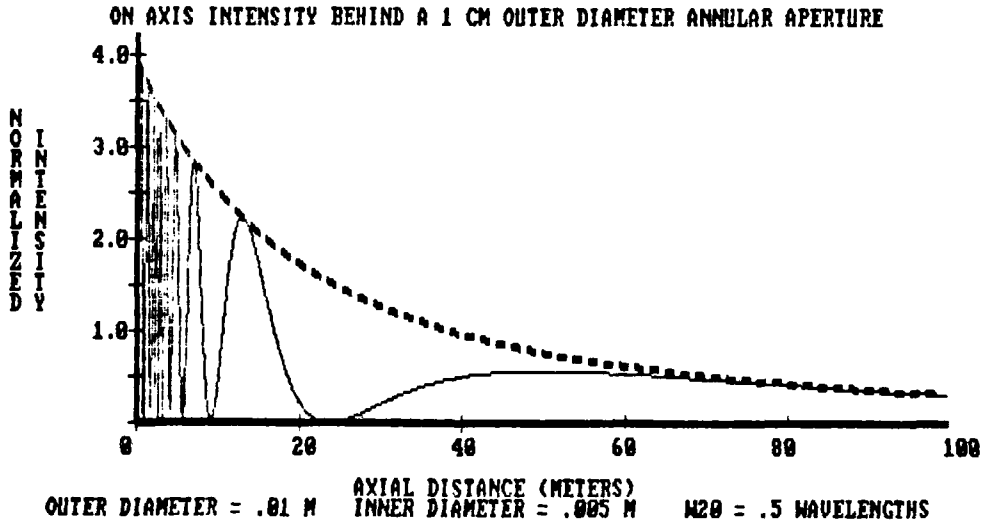

Graph 4.8

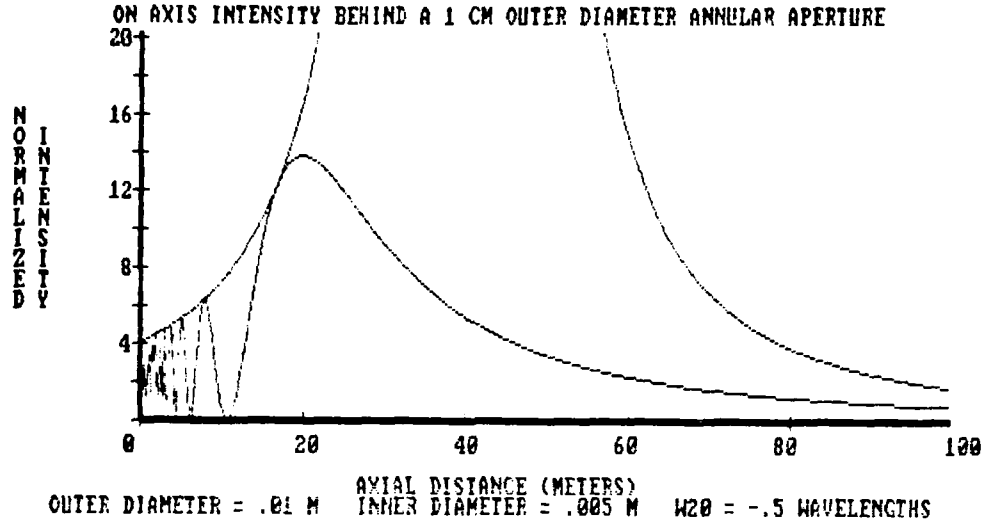

Graph 4.9

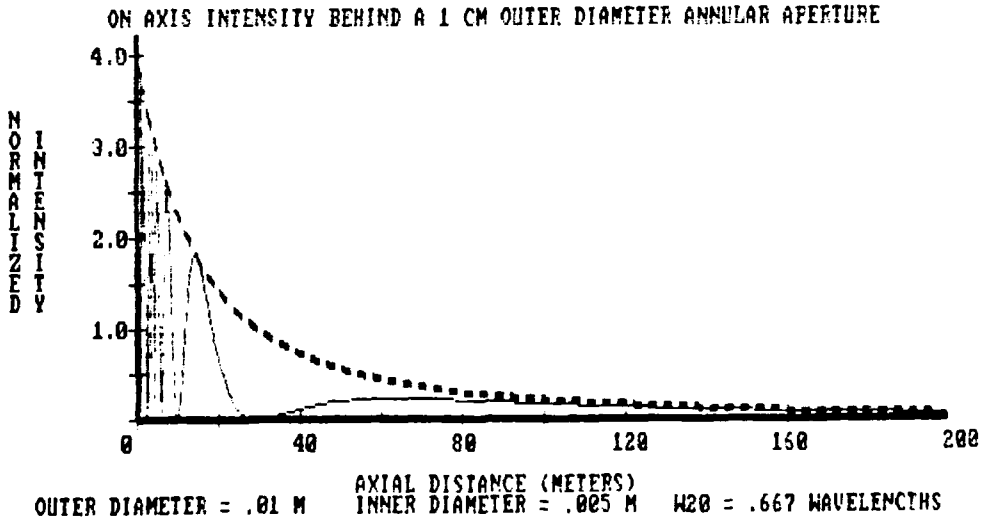

Graph 4.10

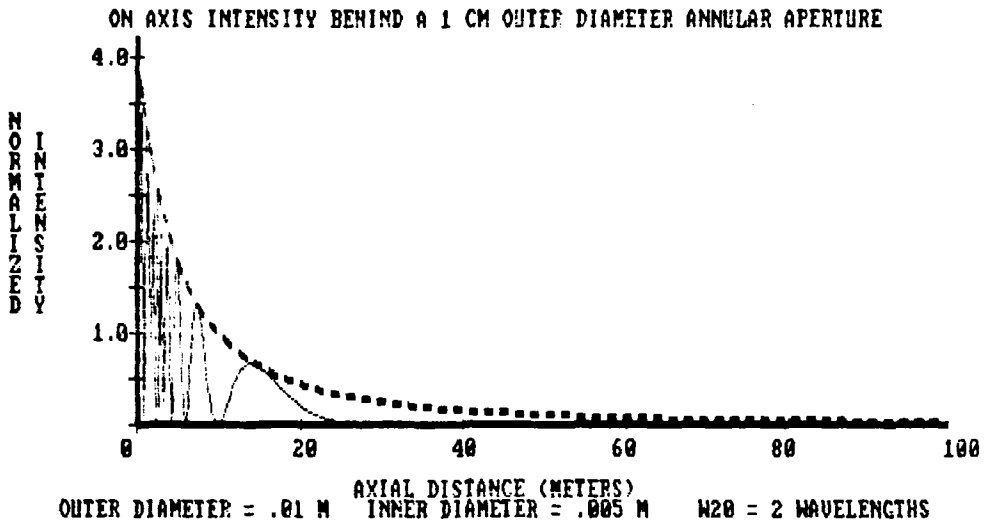

Graph 4.11

The annular aperture provides two methods of determining the coefficient of defocus. The first is to seek out an on axis maximum and measure the intensity. This intensity must lie on the curve:

$$I(0, z) = \frac{1}{\left(1+ \frac{8W_{20}z}{D^2}\right)^2} \qquad \text{(IV-22)}$$

The amount of defocus present can be found in the same way discussed for the circular obscuration. The previous graphs show the limitations of measuring the intensity at a maximum to find the coefficient for defocus. The curve defining the upper bound for the oscillations is very steep around the focal point. This curve is tangent to the on-axis intensity distribution and the actual intensity maximum does not necessarily coincide with this tangent point. For example, from

Graph 4.9 for minus one half wavelength of defocus the last maximum on axis as given by equation IV-18 occurs at:

$$z = \frac{D^2(1-\varepsilon^2)}{4\lambda - 8W_{20}(1-\varepsilon^2)} = 16.93\text{m} \qquad \text{(IV-23)}$$

The actual (measured) intensity maximum occurs at z = 20m with a normalized intensity of 13.6. Putting these values into equation IV-11 yields a calculated value for W_{20}:

$$W_{20} = \frac{D^2}{8z}\left(\sqrt{\frac{I_0}{I_{meas.}}} - 1\right) = -4.6 \times 10^{-7}\text{m} = -.72\lambda \qquad \text{(IV-24)}$$

-- a 44% difference from the actual value. When using this technique to find the coefficient for defocus one should take measurements at values of z far away from the effective focal point of the system. The second method is to measure the shift of extrema on axis. With no defocus the n^{th} maximum occurs at:

$$z_0 = \frac{D^2(1-\varepsilon^2)}{4\lambda(2n+1)} \qquad \text{(IV-25)}$$

With defocus it occurs at:

$$z' = \frac{D^2(1-\varepsilon^2)}{4\lambda(2n+1) - 8W_{20}(1-\varepsilon^2)} \qquad \text{(IV-26)}$$

The shift on axis is then:

$$\Delta z = z' - z_0 = \frac{D^2(1-\varepsilon^2)}{4\lambda(2n+1)}\left[\frac{4\lambda(2n+1)}{4\lambda(2n+1) - 8W_{20}(1-\varepsilon^2)} - 1\right]$$

$$= z_0 \frac{2W_{20}(1-\varepsilon^2)}{\lambda(2n+1) - 2W_{20}(1-\varepsilon^2)} \qquad \text{(IV-27)}$$

$$W_{20} = \frac{(2n+1)\lambda}{2(1-\varepsilon^2)} \frac{\Delta z}{z'} \qquad \text{(IV-28)}$$

This method will be effective if the maximum of order n for the aberrated case can be determined. A good criterion for this is if the shift on axis is less than the spacing to the next maximum. Comparing equations IV-21 and IV-25, one must satisfy (W_{20} in this case is negative):

$$z_0 \frac{2W_{20}(1-\varepsilon^2)}{\lambda(2n+1) - 2W_{20}(1-\varepsilon^2)} > -\frac{8}{(1-\varepsilon^2)} \frac{z_0^2}{D^2} \lambda$$

$$W_{20}(1 - \varepsilon^2) > 2W_{20} \frac{(1-\varepsilon^2)}{(2n+1)} - \lambda$$

$$|W_{20}| < \frac{\lambda}{(1-\varepsilon^2)} \frac{2n+1}{2n-1} \qquad \text{(IV-29)}$$

For large n $\frac{2n+1}{2n-1} \approx 1$ and the coefficient for defocus should be less than half the minimum value in equation IV-19.

Tilt

When tilt is present in the incident beam the center of the diffraction pattern moves off the optical axis without changing its functional form. Tilt will not be investigated in the experimental phase.

Spherical Aberration

Spherical aberration is a rotationally symmetric aberration. As with defocus the presence of spherical aberration should not affect the overall diffraction pattern. However the intensities and positions of on-axis extrema should be influenced.

Case 8: Circular Obscuration

The Rayleigh-Sommerfeld integral for this case is:

$$U(r_2, \phi_2, z) = \frac{A}{i\lambda z} e^{ikz} e^{ikr_2^2/2z} \int_0^{2\pi} \int_{d/2}^{\infty} e^{ik \frac{r_1^2}{2z}} e^{ik16W_{40}\frac{r_1^4}{d^4}}$$

$$x\ e^{-ik \frac{r_1 r_2}{z} \cos(\phi_2 - \phi_1)}$$

$$= \frac{kA}{iz} e^{ikz} e^{ikr_2^2/2z} \int_{d/2}^{\infty} e^{ik\left[\frac{1}{2z} + 16W_{40}\frac{r_1^2}{d^2}\right]r_1^2}$$

$$x\ J_0\left(\frac{kr_1 r_2}{z}\right) r_1 dr_1 \qquad \text{(IV-30)}$$

The evaluation of the integral requires several steps. Consider the function:

$$g(r_1) = \frac{z}{ik} e^{ikr_1^2\left[\frac{1}{2z} + 16W_{40}\frac{r_1^2}{d^4}\right]}$$

$$g'(r_1) = \left(1 + \frac{32W_{40}r_1^2 z}{d^4}\right) r_1 e^{ik\frac{r_1^2}{2z}\left[1 + \frac{32W_{40}r_1^2 z}{d^4}\right]}$$

(IV-31)

Then rewrite the original integral as:

$$\int_{d/2}^{\infty} e^{ik\frac{r_1^2}{2z}}\left[1+\frac{32W_{40}r_1^2z}{d^4}\right] J_0\left(\frac{kr_1r_2}{z}\right) r_1 dr_1$$

$$= \int_{d/2}^{\infty} g'(r_1)\, J_0\left(\frac{kr_1r_2}{z}\right) dr_1 - \frac{32W_{40}z}{d^4}$$

$$\times \int_{d/2}^{\infty} e^{ik\frac{r_1^2}{2z}}\left[1+\frac{32W_{40}r_1^2z}{d^4}\right] J_0\left(\frac{kr_1r_2}{z}\right) r_1^3 dr_1$$

(IV-32)

The first integral on the left side is solved as in Chapter 3 with the solution:

$$\int_{d/2}^{\infty} g'(r_1)\, J_0\left(\frac{kr_1r_2}{z}\right) dr_1 = \frac{z}{ik} J_0\left(\frac{kr_1r_2}{z}\right) e^{ik\frac{d^2}{8z}}\left[1+8W_{40}\frac{z}{d^2}\right]$$

(IV-33)

Consider the second integral. Let $g(r_1)$ be the same as in IV-31 and

$$f(r_1) = r_1^2 J_0\left(\frac{kr_1r_2}{z}\right) \qquad \text{(IV-34)}$$

Then:

$$\int_{d/2}^{\infty} e^{ik\frac{r_1^2}{2z}}\left[1+\frac{32W_{40}r_1^2z}{d^4}\right] J_0\left(\frac{kr_1r_2}{z}\right) r_1^3 dr_1$$

$$x\int_{d/2}^{\infty} g'(r_1)\, f(r_1)\, dr_1 - \frac{32W_{40}z}{d^4} \int_{d/2}^{\infty} e^{ik\frac{r_1^2}{2z}}$$

$$x\left[1+\frac{32W_{40}r_1^2z}{d^4}\right] f(r_1)\, r_1^3 dr_1 \qquad \text{(IV-35)}$$

The diffraction effects come from the edge where $r_1 = d/2$. Making the assumption $f(r_1)$ oscillates slowly compared to $g'(r_1)$ the first integral is solved by the method of Chapter 3.

$$\int_{d/2}^{\infty} g'(r_1)\, f(r_1)\, dr_1 = \frac{z}{ik}\frac{d^2}{4} e^{ik\frac{d^2}{8z}}\left[1+8\frac{W_{40}z}{d^2}\right] J_0\left(\frac{kdr_2}{2z}\right)$$

(IV-36)

Grouping the terms thus evaluated yields for the original integral:

$$\int_{d/2}^{\infty} e^{ik\frac{r_1^2}{2z}}\left[1 + 32\frac{W_{40}r_1^2z}{d^4}\right] J_0\left(\frac{kr_1r_2}{z}\right) r_1 dr_1$$

$$= \frac{z}{ik} J_0\left(\frac{kdr_2}{2z}\right) e^{ik\frac{d^2}{8z}}\left[1 + \frac{8W_{40}z}{d^2}\right]\left(1 - \frac{8W_{40}z}{d^2}\right)$$

$$+\left(\frac{32W_{40}z}{d^4}\right)^2 \int_{d/2}^{\infty} e^{ik\frac{r_1^2}{8z}}\left[1 + \frac{32W_{40}r_1^2z}{d^4}\right]$$

$$x\, J_0\left(\frac{kr_1r_2}{z}\right) r_1^5 dr_1 \qquad \text{(IV-37)}$$

If the last integral is evaluated using the function:

$$h(r_1) = r_1^4 J_0\left(\frac{kr_1 r_2}{z}\right) \tag{IV-38}$$

one obtains the next term in the series $(1 - (8W_{40}z/d2) + \ldots)$ which is:

$$\left(\frac{32W_{40}z}{d^4}\right)^2 r_1^4\Big|_{r_1=d/2} = \left(\frac{8W_{40}z}{d^2}\right)^2 \tag{IV-39}$$

The expected solution to the original integral is:

$$\frac{z}{ik} J_0\left(\frac{kdr_2}{2z}\right) e^{ik\frac{d^2}{8z}\left[1+\frac{8W_{40}z}{d^2}\right]} \sum_{n=0}^{\infty} \left(-\frac{8W_{40}z}{d^2}\right)^n$$

$$= \frac{z}{ik} J_0\left(\frac{kdr_2}{2z}\right) e^{ik\frac{d^2}{8z}\left[1+8\frac{W_{40}z}{d^2}\right]} \left(1+\frac{8W_{40}z}{d^2}\right)^{-1} \tag{IV-40}$$

for $\left|\frac{8W\ z}{d^2}\right| < 1$

Notice this implies $z < \left|\frac{d^2}{8W_{40}}\right|$. $z = -\frac{d^2}{8W_{40}}$ is the effective focal point of the system. The disturbance function is therefore:

$$U(r_2, z) = -\frac{A}{\left(1+\frac{8W_{40}z}{d^2}\right)} e^{ikz} e^{ik\frac{r_2^2}{2z}} e^{ik\frac{d^2}{8z}\left[1+8\frac{W_{40}z}{d^2}\right]}$$

$$\times J_0\left(\frac{kdr_2}{2z}\right) \tag{IV-41}$$

The intensity function is:

$$I(r_2, z) = \frac{A^2}{\left(1+\frac{8W_{40}z}{d^2}\right)^2} J_0^2\left(\frac{kdr_2}{2z}\right) \qquad \text{(IV-42)}$$

The intensity distribution behind a circular obscuration has an identical form spherical aberration and defocus. In fact if both defocus and spherical aberration are present the intensity distribution is:

$$I(r_2, z) = \frac{A^2}{\left(1+\frac{8W'z}{d^2}\right)^2} J_0^2\left(\frac{kdr_2}{2z}\right) \qquad \text{(IV-43)}$$

where $W' = W_{20} + W_{40}$ (IV-44)

All previously derived results for defocus in this case hold for spherical aberration for the region of validity $z < \left| \frac{d^2}{8W_{40}} \right|$. This region of validity includes normal laboratory conditions for typical amounts of spherical aberration. If an upper limit of $W_{40} = |5\lambda|$ is assumed for a one centimeter diameter obscuration then equation IV-42 will hold for $z < 4$ meters.

Case 9: Annular Aperture

The aberration function for spherical aberration for the annular aperture case is:

$$W = 16W_{40}\frac{r_1^4}{D^4} \qquad \text{(IV-45)}$$

The disturbance function is found from expression IV-38 with the upper limit evaluation of $r_1 = \frac{D}{2}$.

$$U(r_2, z) = -Ae^{ikz}\, e^{ik\frac{r_2^2}{2z}} \left[\frac{1}{1+8\frac{W_{40}z}{D^2}}\; e^{ik\frac{D^2}{8z}\left[1+\frac{8W_{40}z}{D^2}\right]} \right.$$

$$\times J_0\left(\frac{kDr_2}{2z}\right) - \frac{1}{1+\frac{8W_{40}zd^2}{D^4}}\; e^{ik\frac{d^2}{8z}\left[1+8\frac{W_{40}zd^2}{D^4}\right]}$$

$$\left. \times J_0\left(\frac{kdr_2}{2z}\right) \right] \qquad \text{(IV-46)}$$

The intensity distribution is:

$$I(r_2, z) = A^2 \left[\frac{1}{\left(1+\frac{8W_{40}z}{D^2}\right)^2}\; J_0^2\left(\frac{kDr}{2z}\right) + \frac{1}{\left(1+\frac{8W_{40}zd^2}{D^4}\right)^2} \right.$$

$$\times J_0^2\left(\frac{kdr_2}{2z}\right) - 2\,\frac{J_0\left(\frac{kDr_2}{2z}\right) J_0\left(\frac{kdr_2}{2z}\right)}{\left(1+\frac{8W_{40}z}{D^2}\right)\left(1+\frac{8W_{40}zd^2}{D^4}\right)} \cos\left(\frac{k}{8z}\right.$$

$$\left. \left. \times (D^2 - d^2) + kW_{40}\left[1 - \frac{d^4}{D^4}\right]\right)\right] \qquad \text{(IV-47)}$$

Intensity on axis. The intensity on axis is described by the following:

$$I(0, z) = A^2 \left[\frac{1}{\left(1+ \frac{8W_{40}z}{D^2}\right)^2} + \frac{1}{\left(1+ \frac{8W_{40}zd^2}{D^4}\right)^2} - \frac{2}{\left(1+ \frac{8W_{40}z}{D^2}\right)\left(1+ \frac{8w_{40}zd^2}{D^4}\right)} \right.$$

$$\left. x \cos\left(\frac{k}{8z}(D^2 - d^2) + kW_{40}\left[1 - \frac{d^4}{D^4}\right]\right)\right] \qquad \text{(IV-48)}$$

The intensities for the maxima and minima lie on the curves

$$I(0, z_{max}) = A^2 \left[\frac{1}{1+ \frac{8W_{40}z}{D^2}} + \frac{1}{1+ \frac{8W_{40}zd^2}{D^2}} \right]^2$$

$$I(0, z_{min}) = A^2 \left[\frac{1}{1+ \frac{8W_{40}z}{D^2}} - \frac{1}{1+ \frac{8W_{40}zd^2}{D^2}} \right]^2 \qquad \text{(IV-49)}$$

As with the case of the annular aperture illuminated by a plane wave with a gaussian intensity distribution the on-axis intensity distribution oscillates between an upper and lower bound with the lower bound non-zero (except for z = 0 and z = ∞). For positive W_{40} the upper bound is a decreasing function with increasing z. The lower bound will increase to a maximum value then go to zero for large z. This maximum occurs when:

$$\frac{dI_{min}}{dz} = 0 = 2A^2 \left[\frac{1}{1+ \frac{8W_{40}z}{D^2}} - \frac{1}{1+ \frac{8W_{40}zd^2}{D^4}} \right]\left[- \frac{8W_{40}/D^2}{\left(1+ \frac{8W_{40}z}{D^2}\right)^2} + \right.$$

$$\frac{8W_{40}d^2/D^4}{\left(1+\frac{8W_{40}zd^2}{D^4}\right)^2}\Bigg]$$

$$\left[1+\frac{8W_{40}zd^2}{D^4}\right] = \left[1+\frac{8W_{40}z}{D^2}\right]\frac{d^2}{D^2}$$

$$z = \frac{D^3}{8W_{40}d} \qquad \text{(IV-50)}$$

Since $\frac{D}{d} > 1$

$$\frac{D^3}{8W_{40}d} > \frac{D^2}{8W_{40}} \qquad \text{(IV-51)}$$

Thus the maximum lies beyond the limit where equation IV-43 is valid. In the region where the equation holds the minimum intensity boundary curve is a constantly increasing function.

The amount of spherical aberration produced by plane parallel plates is very small. In addition the experimental phase will involve distances z on the order of one meter. In all cases of concern the following approximations are valid:

$$\frac{8W_{40}z}{D^2} << 1$$

$$\frac{8W_{40}zd^2}{D^4} << 1 \qquad \text{(IV-52)}$$

With these restrictions the denominators in equation IV-48 are

replaced by their expansions to first order. The intensity on axis then is:

$$I(0, z) \approx A^2 \left[2 - \frac{16W_{40}z}{D^2} \left(1 + \frac{d}{D^2}\right) - 2 \left(1 - \frac{8W_{40}z}{D^2} \left[1 + \frac{d^2}{D^2} \right] \right) \right.$$

$$\left. \times \cos \left(\frac{k}{8z} (D^2 - d^2) + kW_{40} \left[1 - \frac{d^4}{D^4} \right] \right) \right] \qquad \text{(IV-53)}$$

If one measures the intensity at a maximum on axis the spherical aberration coefficient is found to be:

$$W_{40} = \frac{D^2}{32z(1+\varepsilon^2)} \left[4 - \frac{I_m}{I_0} \right] \qquad \text{(III-54)}$$

As with the defocus case, spherical aberration also causes an axial shift of maxima and minima. Maxima will occur when:

$$\frac{k}{8z} (D^2 - d^2) + kW_{40} (1 - \varepsilon^4) = (2n + 1)\pi$$

$$z = \frac{D^2(1-\varepsilon^2)}{4\lambda(2n+1) - 8W_{40}(1-\varepsilon^4)} \qquad \text{(IV-55)}$$

Minima occur when

$$z = \frac{D^2(1-\varepsilon^2)}{8m\lambda - 8W_{40}(1-\varepsilon^4)} \qquad \text{(IV-56)}$$

The spacing on axis from the n^{th} order maximum to the $n + 1^{th}$ order maximum is:

$$\Delta z = - \frac{4}{(1-\varepsilon^2)} \frac{z^2}{D^2} \lambda \qquad \text{(IV-57)}$$

As before the spacing is independent of aberration. The coefficient for spherical aberration can be calculated from the axial shift of maxima on axis. Following the argument in the section on defocus:

$$W_{40} = \frac{(2n+1)\lambda}{2(1-\epsilon^4)} \frac{\Delta z}{z'} \qquad \text{(IV-58)}$$

where Δz is the axial shift and z' is the new position of the n^{th} order maximum. By measuring minima the above becomes:

$$W_{40} = \frac{m\lambda}{1-\epsilon^4} \frac{\Delta z}{z'} \qquad \text{(IV-59)}$$

The following graphs show the differences between equations IV-45 and IV-53 for a 1cm annular aperture with $\epsilon = .5$ and $W_{40} = \pm .5\lambda$ (for $z \leq 4m$. $\left| \frac{8W_{40}z}{D^2} \right| < .1$).

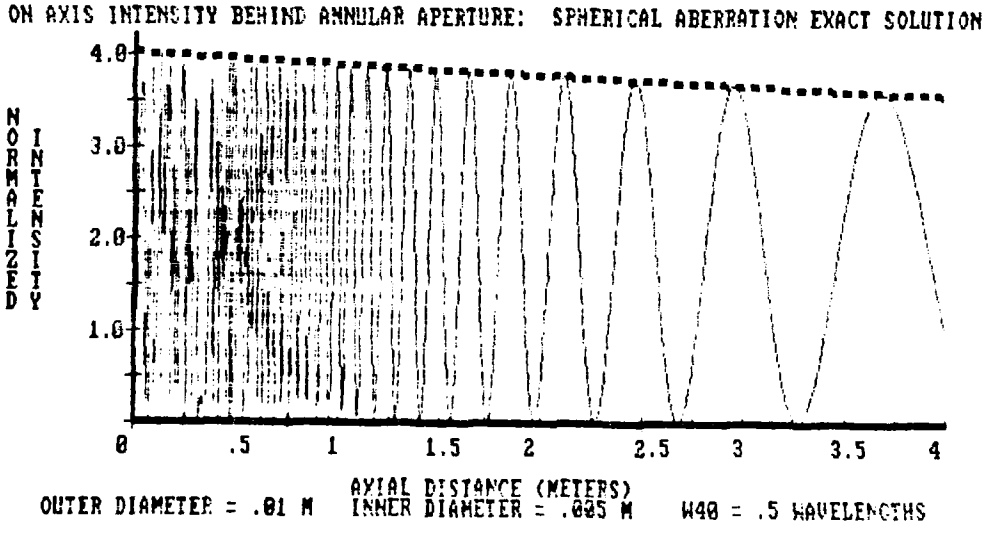

Graph 4.12

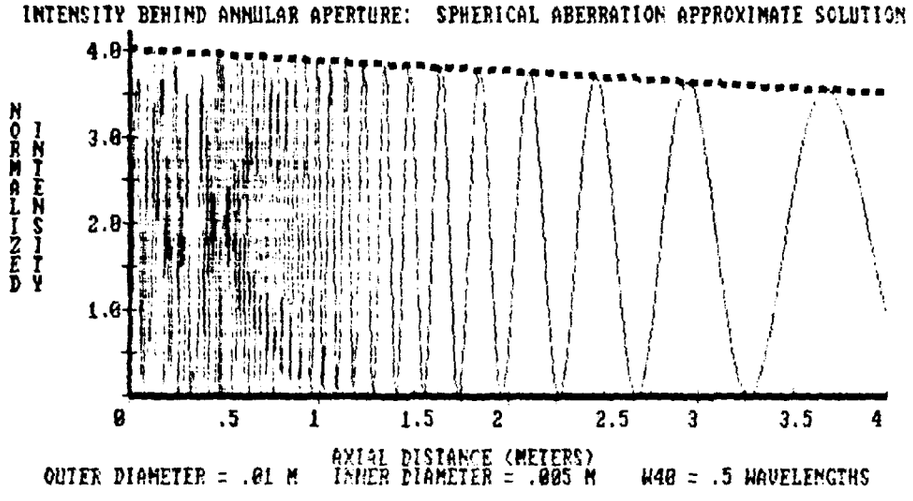

Graph 4.13

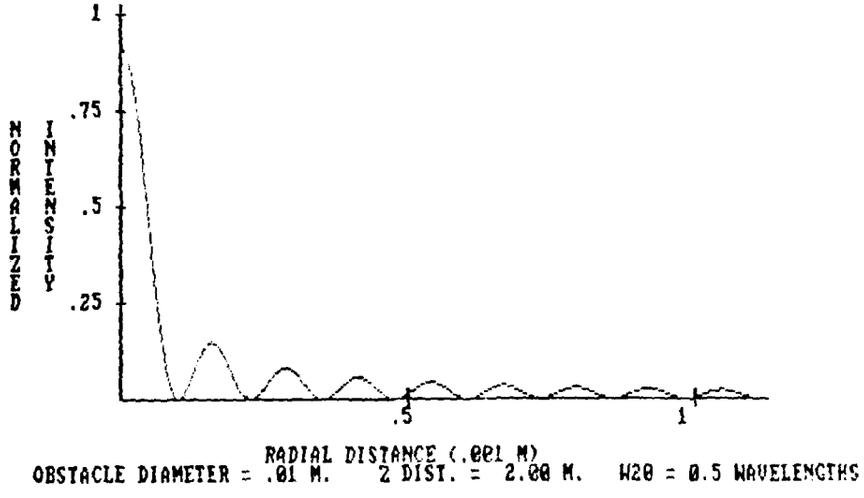

Graph 4.14

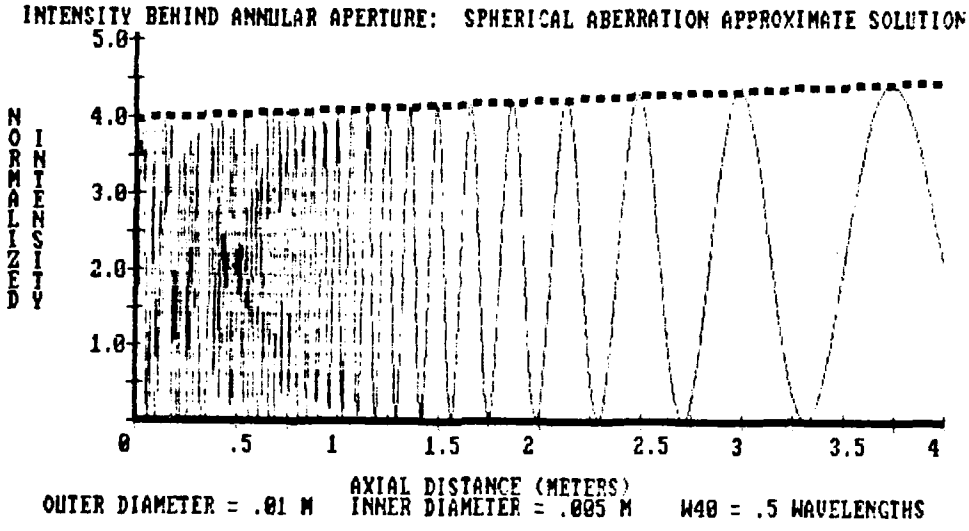

Graph 4.15

Off axis intensity distribution. Off axis, the intensity behind the annular aperture is:

$$I(r_2, z) = A^2\left[\left(1 - 16W_{40}\frac{z}{D^2}\right)J_0{}^2\left(\frac{kDr_2}{2z}\right) + \left(1 - 16W_{40}\frac{zd^2}{D^4}\right)\right.$$

$$\times J_0{}^2\left(\frac{kdr_2}{2z}\right) - 2\left[1 - 8W_{40}\frac{z}{D^2}\left(1 + \frac{d^2}{D^2}\right)\right]J_0\left(\frac{kDr_2}{2z}\right)$$

$$\left.\times J_0\left(\frac{kdr_2}{2z}\right)\cos\left(\frac{k}{8z}(D^2 - d^2) + kW_{40}(1 - \varepsilon^4)\right)\right] \qquad \text{(IV-60)}$$

The following graphs show the patterns for an on axis maximum with $W_{40} = .25\lambda$, 2.5λ and -2.5λ. There is very little change in the patterns.

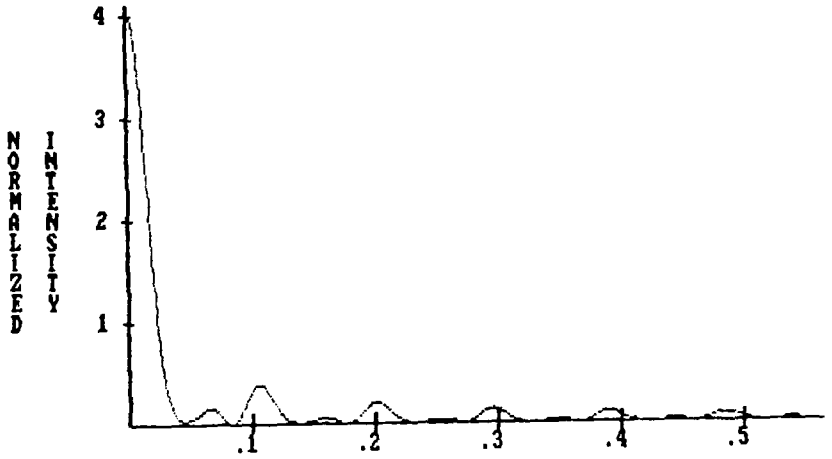

O.D.= 0.01 M. I.D. = .003 M. Z DIST. = .493 M. W40 = 0.25 WAVELENGTHS

Graph 4.16

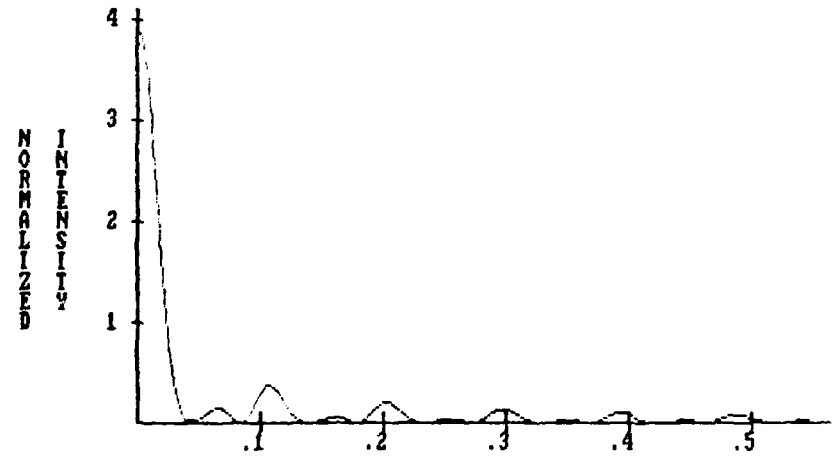

O.D.= 0.01 M. I.D. = .003 M. Z DIST. = .501 M. W40 = 2.50 WAVELENGTHS

Graph 4.17

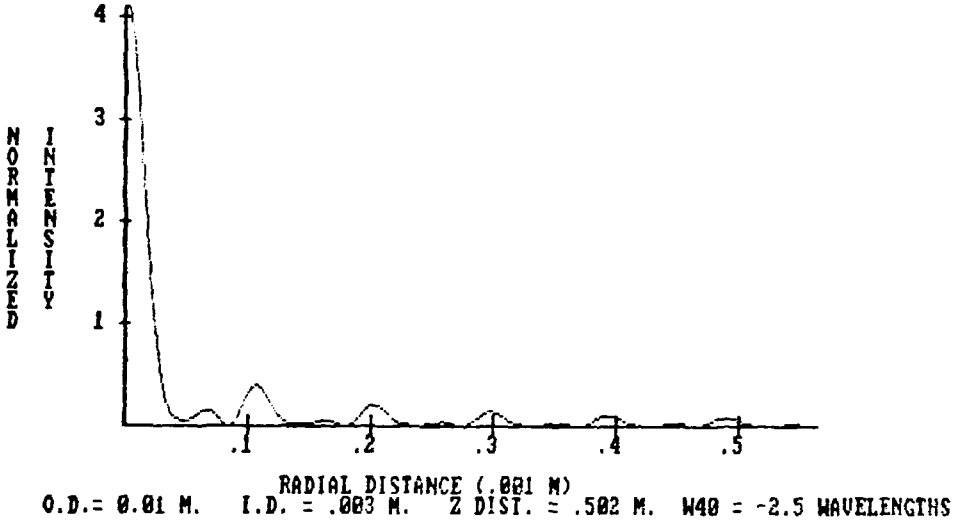

Graph 4.18

Defocus and Spherical Aberration Combined

Earlier the restriction $\frac{8W_{40}z}{D^2} << 1$ was imposed. A resonable assumption under this restriction is that $\frac{8W_{20}z}{D^2} << 1$ (the amount of defocus is of a similar order as that of spherical aberration). When this is the case the intensity distribution becomes:

$$I(r_2, z) = A^2 \left[\left(1 - 16 \frac{z}{D^2} (W_{20} + W_{40})\right) J_0{}^2 \left(\frac{kDr_2}{2z}\right) + \right.$$

$$\left. \left(1 - 16 \frac{z}{D^2} (W_{20} + W_{40} \frac{d^2}{D^2})\right) J_0{}^2 \left(\frac{kdr_2}{2z}\right) - \right.$$

$$2(1 - 8\frac{z}{D^2}(W_{20} + W_{40}(1 + \frac{d^2}{D^2}))\ J_0\left(\frac{kDr_2}{2z}\right) J_0\left(\frac{kdr_2}{2z}\right)$$

$$\times \cos\left(\frac{k}{8z}(D^2 - d^2) + kW_{20}\left[1 - \frac{d^2}{D^2}\right] + kW_{40}\left[1 - \frac{d^4}{D^4}\right]\right)\Bigg] \qquad \text{(IV-61)}$$

To separate the two aberrations one must capitalize on the basic difference between them. Spherical aberration has a r_1^4 dependence while defocus has only a r_1^2 dependence. Varying the obscuration ratio (that is varying the inner diameter of the aperture, keeping the outer diameter constant) will change the intensity of maxima on axis.

Measure two maxima on axis. These will occur at z_1 and z_2. The first measurement will be I_1 with obscuration ratio $\varepsilon_1 = \frac{d_1}{D}$ and the second will be I_2 with $\varepsilon_2 = \frac{d_2}{D}$. Then:

$$I_1 = I_0\Bigg[(1 - 16\frac{z_1}{D^2}(W_{20} + W_{40})) + (1 - 16\frac{z_1}{D^2}(W_{20} + W_{40}\varepsilon_1^2)) +$$

$$2(1 - 8\frac{z_1}{D^2}(W_{20} + W_{40}(1 + \varepsilon_1^2))\Bigg]$$

$$\frac{I_1}{I_0} = 4 - W_{20}\ 48\frac{z_1}{D^2} - W_{40}(32\frac{z_1}{D^2}(1 + \varepsilon_1^2))$$

$$W_{20} = \frac{D^2}{48z}\left(4 - \frac{I_1}{I_0}\right) - W_{40}\frac{2}{3}(1 + \varepsilon_1^2) \qquad \text{(IV-62)}$$

A second measurement will replace I_1, z_1 and ε_1 by I_2, z_2 and ε_2. Then subtracting the two and solving for W_{40} yields:

$$W_{40}\frac{2}{3}(\varepsilon_1^2 - \varepsilon_2^2) = \frac{D^2}{48}\left(4\left[\frac{1}{z_1} - \frac{1}{z_2}\right] - \frac{1}{I_0}\left[\frac{I_1}{z_1} - \frac{I_2}{z_2}\right]\right)$$

$$W_{40} = \frac{D^2}{32z_1z_2(\varepsilon_1^2-\varepsilon_2^2)I_0} \quad (4I_0(z_2 - z_1) + (I_2z_1 - I_1z_2)) \tag{IV-63}$$

Putting this result back into IV-62 yields:

$$W_{20} = \frac{D^2}{48z}\left(4 - \frac{I_0}{I_0}\right) - \frac{2}{3}\frac{D^2}{32z_1z_2(\varepsilon_1^2-\varepsilon_2^2)I_0}(4I_0(z_2 - z_1) +$$

$$(I_2z_1 - I_1z_2))(1 + \varepsilon_1^2)$$

$$= \frac{D^2}{48z_1z_2I_0(\varepsilon_1^2-\varepsilon_2^2)}\left[z_1(1 + \varepsilon_1^2)(4I_0 - I_2) +\right.$$

$$\left. z_2(1 + \varepsilon_2^2)(I_1 - 4I_0)\right] \tag{IV-64}$$

The separation of the aberrations is also possible by considering axial shifts of maxima, with different obscuration ratios. It is clear by looking at equation IV-61 that the term in the cosine $k(W_{20}(1-\varepsilon^2) + W_{40}(1-\varepsilon^4))$ acts like a phase factor. Unless one varies ε the two cannot be separated.

Maxima on axis will occur when

$$\frac{kD^2}{8z}(1 - \varepsilon^2) + kW_{20}(1-\varepsilon^2) + kW_{40}(1 - \varepsilon^4) = (2n + 1)\pi$$

$$z = \frac{D^2(1-\varepsilon^2)}{4\lambda(2n+1) - 8W_{20}(1-\varepsilon^2) - 8W_{40}(1-\varepsilon^4)} \tag{IV-65}$$

If the n^{th} maximum is measured at z_1 with obscuration ratio ε_1 and at z_2 with obscuration ratio ε_2 then the respective axial shifts from the

unaberrated case are:

$$\Delta z_i = \frac{D^2(1-\varepsilon_i^2)}{4}\left[\frac{1}{\lambda(2n+1) - 2W_{20}(1-\varepsilon_i^2) - 2W_{40}(1-\varepsilon_i^4)} - \frac{1}{\lambda(2n+1)}\right]$$

$$i = 1, 2$$

$$= \frac{D^2(1-\varepsilon_i^2)}{4}\;\frac{W_{20} + W_{40}(1+\varepsilon_i^2)}{\lambda(2n+1)\left[\lambda(2n+1) - 2W_{20}(1-\varepsilon_i^2) - 2W_{40}(1-\varepsilon_i^4)\right]}$$

(IV-66)

After much algebra (see Appendix 6) the resolved aberration coefficients are:

$$W_{20} = \frac{2\lambda^2(2n+1)^2}{(\varepsilon_1^2-\varepsilon_2^2)(1-\varepsilon_1^2)(1-\varepsilon_2^2)}$$

$$\times \left(D^2\left[\Delta z_1(1-\varepsilon_2^2)^2(1-\varepsilon_1^2) - \Delta z_2(1-\varepsilon_1^2)^2(1-\varepsilon_2^2)\right] - 4\lambda(2n+1)\Delta z_1\Delta z_2(\varepsilon_1^4-\varepsilon_2^4)\right)$$

$$\div (D^2(1-\varepsilon_1^2) + \Delta z_1 4\lambda(2n+1))(D^2(1-\varepsilon_2^2) + \Delta z_2 4\lambda(2n+1))$$

(IV-67)

$$W_{40} = \frac{2\lambda^2(2n+1)^2}{(\varepsilon_1^2-\varepsilon_2^2)(1-\varepsilon_1^2)(1-\varepsilon_2^2)}$$

$$\times \frac{D^2\left[\Delta z_1(1-\varepsilon_2^2)^2 - \Delta z_2(1-\varepsilon_1^2)^2\right] + 4\lambda(2n+1)\Delta z_1\Delta z_2(\varepsilon_1^2-\varepsilon_2^2)}{(D^2(1-\varepsilon_1^2) + \Delta z_1 4\lambda(2n+1))(D^2(1-\varepsilon_2^2) + \Delta z_2 4\lambda(2n+1))}$$

(IV-68)

Solving the above expressions is a tedious task. There is another drawback to separating the aberration coefficients using axial shifts -- the difficulty of locating the n^{th} order maximum. With the restrictions at the beginning of this section imposed, small values of z are implied. Small z means high orders of maxima and small spacing between maxima. To verify the order of the maxima in both cases will require assiduous measurements.

Astigmatism

The aberration function for astigmatism is:

$$W = 4W_{22} \frac{r_1^2}{D^2} \cos^2\phi_1 \tag{IV-69}$$

The Rayleigh-Sommerfeld formula for the disturbance function with

$$U(r_2, z) = \frac{A}{i\lambda} e^{ikz} e^{ik\frac{r_2^2}{2z}} \int_0^{2\pi} \int_{d/2}^{D/2} e^{ikr_2^2/2z} e^{-ik\frac{r_1 r_2}{z}\cos(\phi_2-\phi_1)} \times e^{i4kW_{22}\frac{r_1^2}{D^2}\cos^2\phi_1} r_1 dr_1 d\phi_1 \tag{IV-70}$$

The above must be evaluated numerically. As explained earlier the expected diffraction pattern will have two planes of symmetry. Astigmatism is the predominant aberration generated by tilting parallel plates. Thus an empirical study of this aberration is possible.

Coma

The aberration function for coma is:

$$W = 8W_{31} \frac{r_1^3}{D^3} \cos\phi_1 \qquad \text{(IV-71)}$$

The Rayleigh-Sommerfeld formula with coma is:

$$U(r_2, z) - \frac{A}{i\lambda} e^{ikz} e^{ik \frac{r_2^2}{2z}} \int_0^{2\pi} \int_{d/2}^{D/2} e^{ik \frac{r_1^2}{2z}} e^{-ik \frac{r_1 r_2}{z} \cos(\phi_2 - \phi_1)}$$

$$x\, e^{ik8W_{31} \frac{r_1^3}{D^3} \cos\phi_1} r_1 dr_1 d\phi_1 \qquad \text{(IV-72)}$$

The above has no apparent analytic solution and must be evaluated numerically. The amount of coma produced by the plane parallel plates is small particularly in comparison to the amount of astigmatism. It is doubtful any comatic effects will be observable during the experimental phase.

Summary

Chapters 3 and 4 included many formulas for intensity distributions on and off axis. Below is a review of the formulas and equation numbers.

Unaberrated Cases

Uniform intensity plane wave incident upon circular obscurration:

On axis:

$$I(0, 0, z) = A^2 \frac{z^2}{z^2+d^2/4} \qquad \text{(III-12)}$$

Off axis:

$$I(r_2, z) = A^2 J_0^2 \left(\frac{kdr_2}{2z}\right) \qquad \text{(III-26)}$$

Uniform intensity plane wave incident upon annular aperture:

On axis:

$$I(0, 0, z) = A^2 \left[2 - 2\cos\left(\frac{k}{z}(D^2 - d^2)\right)\right] \qquad \text{(III-39)}$$

Off axis:

$$I(r_2, z) = |U(r_2, z)|^2$$
$$= A^2 \left[J_0^2\left(\frac{kDr_2}{2z}\right) + J_0^2\left(\frac{kdr_2}{2z}\right) - 2J_0\left(\frac{kDr_2}{2z}\right) J_0\left(\frac{kdr_2}{2z}\right) \right.$$
$$\left. \times \cos\left(\frac{k}{8z}(D^2 - d^2)\right)\right] \qquad \text{(III-50)}$$

Gaussian intensity plane wave incident upon circular obscuration:

On axis:

$$I(0, z) = A^2 \frac{1}{1+ d^2/4z^2} e^{-c/2} \qquad \text{(IV-73)}$$

Off axis:

$$I(r_2, z) = A^2 e^{-\frac{c}{2}} J_0^2\left(\frac{kdr_2}{2z}\right) \qquad \text{(III-34)}$$

Gaussian intensity plane wave incident upon annular obscuration:

On axis:

$$I(0, z) = A^2\left[e^{-\frac{c}{2}} + e^{-\frac{c}{2}\frac{d^2}{D^2}} - 2e^{-\frac{c}{4}}\left[1+\frac{d^2}{D^2}\right]\cos\left(\frac{k}{8z}(D^2 - d^2)\right)\right]$$

(III-65)

Off axis:

$$I(r_2, z) = A^2\left[e^{-\frac{c}{2}} J_0^2\left(\frac{kDr_2}{2z}\right) + e^{-\frac{c}{2}\frac{d^2}{D^2}} J_0^2\left(\frac{kdr_2}{2z}\right) - 2e^{-\frac{c}{4}}\left[1+\frac{d^2}{D^2}\right] J_0\left(\frac{kDr_2}{2z}\right) J_0\left(\frac{kdr_2}{2z}\right)\cos\left(\frac{k}{8z}(L^2 - d^2)\right)\right]$$

(IV-74)

Uniform plane wave incident upon displaced obstacle and aperture:

On axis:

$$I(0, z_1, z_2)\ A^2\ \ 2 - 2\cos\ \frac{k}{8}\ \ \frac{D^2}{z_1} - \frac{d^2}{z_2} \qquad \text{(IV-75)}$$

Off axis:

$$I(r_2, z_1, z_2) = A^2\left[J_0^2\left(\frac{kDr_2}{2z_1}\right) + J_0^2\left(\frac{kdr_2}{2z_2}\right) - 2J_0\left(\frac{kDr_2}{2z_1}\right)\right.$$

$$x\ J_0\left(\frac{kdr_2}{2z_2}\right)\ \cos\left(\frac{k}{8}\left[\frac{D^2}{z_1}-\frac{d^2}{z_2}\right]\right)\Bigg] \qquad \text{(III-74)}$$

Aberrated Cases

Uniform intensity plane wave containing defocus incident upon circular obscuration:

On axis:

$$I(0,\ z) = \frac{A^2}{\left(1+\frac{8W_{20}z}{d^2}\right)^2} \qquad \text{(IV-76)}$$

Off axis:

$$I(r_2,\ z) = \frac{A^2}{\left(1+\frac{8W_{20}z}{d^2}\right)^2}\ J_0^{\,2}\left(\frac{kdr_2}{2z}\right) \qquad \text{(IV-5)}$$

Uniform intensity plane wave containing defocus incident upon annular aperture:

On axis:

$$I(0,\ z) = \frac{A^2}{\left(1+\frac{8W_{20}z}{D^2}\right)^2}\left[2-2\cos\left(\frac{k}{8z}\left(D^2-d^2\right)\left[1+\frac{8W_{20}z}{D^2}\right]\right)\right] \qquad \text{(IV-77)}$$

Off axis:

$$I(r_2, z) = \frac{A^2}{\left(1+ \frac{8W_{20}z}{D^2}\right)^2}\left[J_0{}^2\left(\frac{kDr_2}{2z}\right) + J_0{}^2\left(\frac{kdr_2}{2z}\right) - 2J_0\left(\frac{kDr_2}{2z}\right)\right.$$

$$\left. x\ J_0\left(\frac{kdr_2}{2z}\right)\ \cos\left(\frac{k}{8z}\ (D^2\ - d^2) + kW_{20}\left[1 - \frac{d^2}{D^2}\right]\right)\right] \qquad \text{(IV-14)}$$

Uniform intensity plane wave containing spherical aberration incident upon circular obscuration

On axis:

$$I(0, z) = A^2\left[1 - 16\ \frac{W_{40}z}{d^2}\right] \qquad \text{(IV-78)}$$

Off axis:

$$I(r_2\ , z) = A^2\left[1 - 16\ \frac{W_{40}z}{d^2}\right]\ J_0{}^2\ \ \frac{kdr_2}{2z} \qquad \text{(IV-79)}$$

Uniform intensity plane wave containing spherical aberration incident upon annular apertue

On axis:

$$I(0, z) = A^2\left[2 - \frac{16W_{40}z}{D^2}\ (1 + \frac{d}{D^2}) - 2\left(1 - \frac{8W_{40}z}{D^2}\left[1 + \frac{d^2}{D^2}\right]\right)\right.$$

$$\left. x\ \cos\left(\frac{k}{8z}\ (D^2 - d^2) + kW_{40}\left[1 - \frac{d^4}{D^4}\right]\right)\right] \qquad \text{(IV-53)}$$

Off axis:

$$I(r_2, z) = A^2\left[\left(1 - 16W_{40}\frac{z}{D^2}\right)J_0^2\left(\frac{kDr_2}{2z}\right) + \left(1 - 16W_{40}\frac{zd^2}{D^4}\right)\right.$$

$$\times J_0^2\left(\frac{kdr_2}{2z}\right) - 2\left[1 - 8W_{40}\frac{z}{D^2}\left(1 + \frac{d^2}{D^2}\right)\right]J_0\left(\frac{kDr_2}{2z}\right)$$

$$\left.\times J_0\left(\frac{kdr_2}{2z}\right)\cos\left(\frac{k}{8z}\left(D^2 - d^2, + kW_{40}(1 - \varepsilon^4)\right)\right)\right] \qquad \text{(IV-60)}$$

From all the preceding, one can construct a general formula containing all of the soluble elements discussed in the two chapters:

$$I(r_2\ ,\ z\ ) = A^2\left[\frac{1-16\ \frac{W_{40}z_1}{D^2}}{\left[1+8\ \frac{W_{20}z_1}{D^2}\right]^2}\ e^{-\frac{c}{2}}\ J_0^2\left(\frac{kDr}{2z_2}\right) + \right.$$

$$\frac{1-16W_{40}\frac{z_2d^2}{D^2}}{\left[1+8\ \frac{W_{20}z_2d^2}{D^4}\right]^2}\ e^{-\frac{c}{2}\frac{d^2}{D^2}}\ J_0^2\left(\frac{kdr}{2z_2}\right) -$$

$$2\frac{\left[1-16\ \frac{W_{40}}{D^2}\left(z_1+ z_2\ \frac{d^2}{D^2}\right)\right]}{\left[1+\frac{8W_{20}z_1}{D^2}\right]\left[1+\frac{8W_{20}z_2d^2}{D^4}\right]}\ e^{-\frac{c}{4}\left[1+\frac{d^2}{D^2}\right]}$$

$$\times J_0\left(\frac{kDr_2}{2z}\right)\ J_0\left(\frac{kdr_2}{2z}\right)\ \cos\left(\frac{k}{8}\left[\frac{D^2}{z_1} - \frac{d^2}{z_2}\right] + \right.$$

$$\left.\left. kW_{20}\left[1 - \frac{d^2}{D^2}\right] + kW_{40}\left[1 - \frac{d^4}{D^4}\right]\right)\right] \qquad \text{(IV-80)}$$

Notes

[1] Max Born and Emil Wolf, Principles of Optics 6th ed. (Oxford: Pergamon, 1980), p. 470.

[2] Warren J. Smith, Modern Optical Engineering (New York: McGraw-Hill, 1966), p. 132.

[3] H. H. Hopkins, Wave Theory of Aberrations (Oxford: Oxford University, 1950), p. 141.

[4] James E. Harvey, "An Introduction to Aberration Theory," Class handout, University of New Mexico, Albuquerque.

[5] Joseph W. Goodman, "Introduction to Fourier Optics," (San Francisco: McGraw-Hill, 1968), pp. 123-124.

Chapter 5

EXPERIMENTAL PROCEDURES

The experiment contained three phases. The first phase involved calibrating the aberration generator and determining the gaussian constants for the beams used. The second phase included preliminary runs which suggested the ultimate tests for the final (testing) phase.

Laboratory Equipment

Below is a photograph of the laboratory set-up. The next page is a diagram labelling the components.

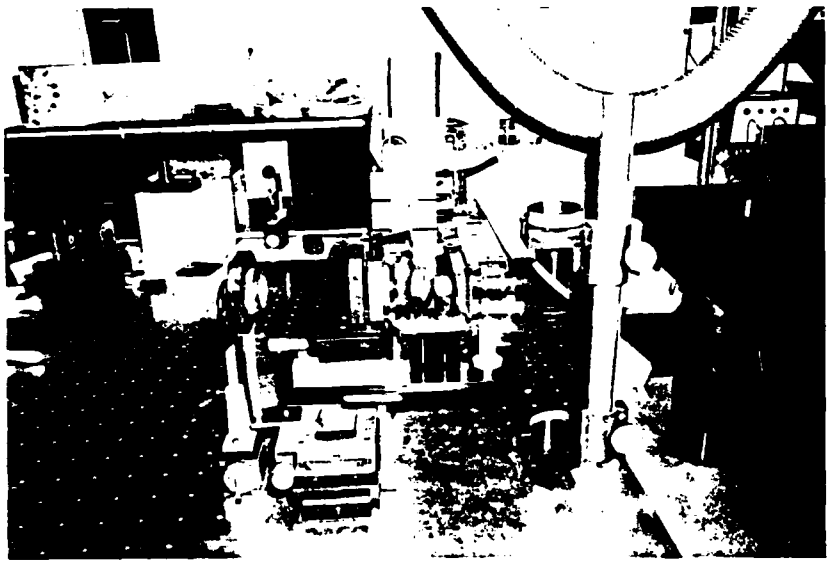

Photograph 5.1: Laboratory Set-up

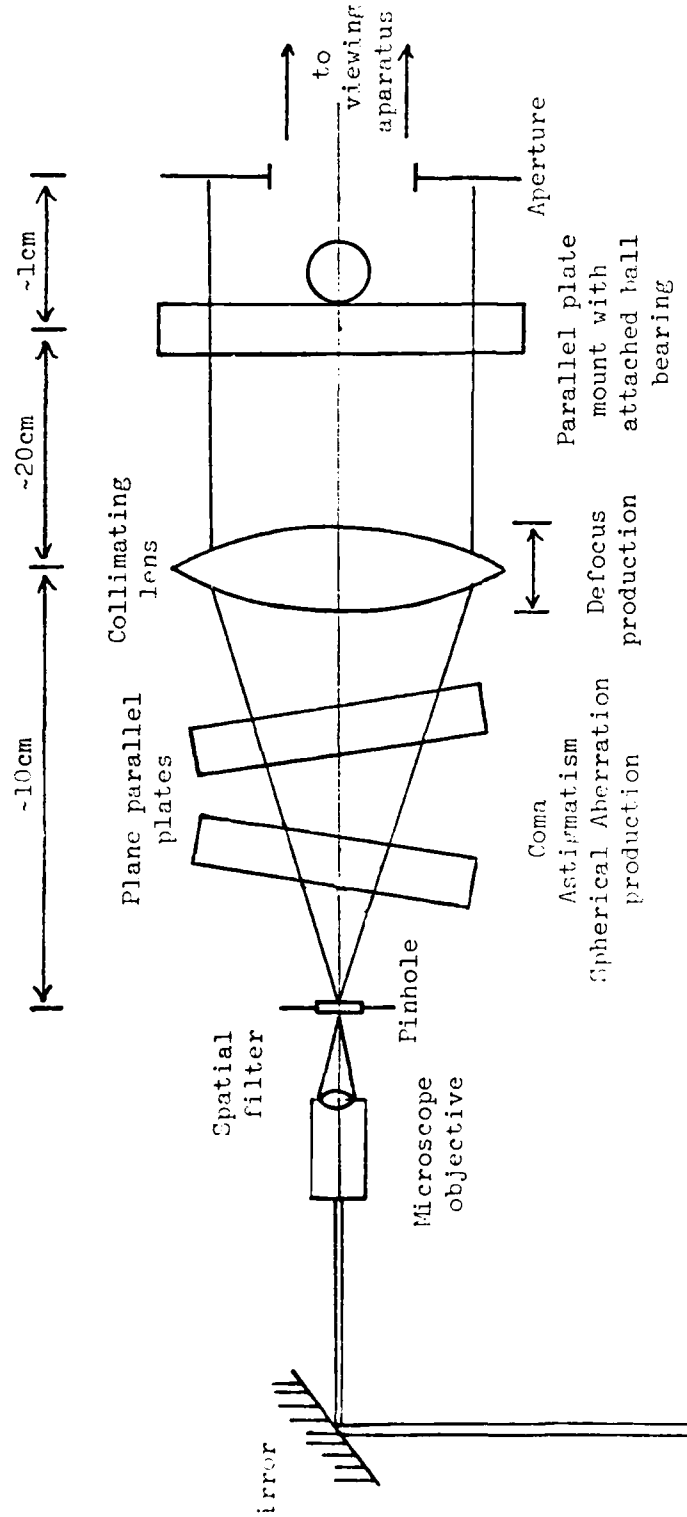

Figure 5.1
Laboratory Set-up Schematic

The laser used was a Spectra-physics helium-neon laser with a .5mW power output. The spatial filter was composed of either a 20X or 60X microscope objective (to change the gaussian distribution constant for the incident beam) and a 25 micron pinhole. The plane parallel plates were half-inch thick and made of BK-17 glass with index of refraction 1.517. The plates were mounted on posts allowing for somewhat precise ($\pm$ half degree) tilt angles. The collimating lens was a 100mm focal length achromatic doublet. The lens could be translated to introduce defocus. The obstacles were ball bearings of diameters 3/16, 5/16, 1/2 and 3/4 inches mounted on plane parallel plates. Disks drilled with different sized holes provided the apertures. A Gaertner travelling microscope with a 20X objective was used to make measurements of the diffraction structure on and off the optical axis. Photographs of the spot and ring patterns were made with a Bausch and Lomb stereo viewer with Polaroid camera attachment. The camera attachment had adjustable shutter speed and used Polaroid 3000 black and white film.

Calibration

The aberration coefficients for given parallel plate tilt angles in tables 4.3 and 4.4 were verified by taking and analyzing interferograms produced by aberrated wavefronts. A Smartt point diffraction interferometer created the interferograms. The interferograms included a variety of tilt angles using one plate, two plates counter-rotated or two plates rotated in the same direction. Photographs were made of the interference pattern using Polaroid 3000 black and white film. The photographs were digitized and run through an analysis

program called FRINGE at the Fringe Reduction Facility at the Air Force Weapons Laboratory at Kirtland AFB. The results were then compared with theory (see Chapter 6).

The gaussian intensity widths of the two microscope objectives used in the spatial filter were investigated using two methods. The first method was the knife edge test. A collecting lens focused the plane wave output of the lab set-up (no plane parallel plates or target) into a power meter (a hν 6328Å meter). A razor blade on a translation stage is introduced into the beam before the collecting lens.

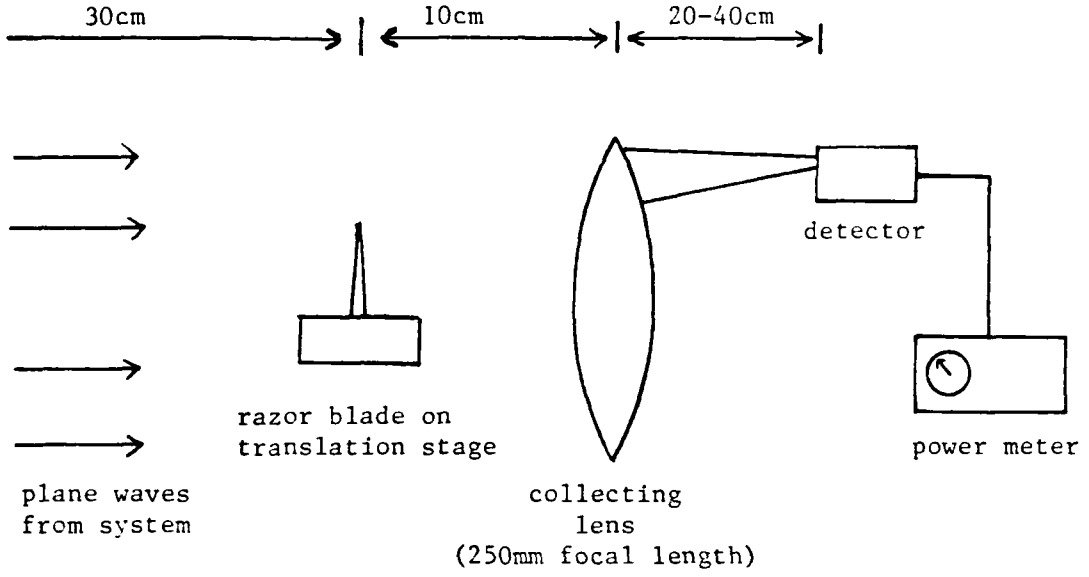

Figure 5.2

Set-up for Determination of Gaussian Constants

As the razor blade is moved farther into the beam the percent of the beam still reaching the power meter is measured as a function of the distance of translation of the blade. A best fit line for the data

points is calculated. The distance between the position where 84.2% transmission occurs and the point where 15.8% transmission occurs is designated Δx. This difference corresponds to the radius of the beam at the e^{-2} points (the radius at which the intensity drops to e^{-2} times the maximum value). The desired form of the gaussian distribution is given by $e^{-c\frac{r^2}{D^2}}$. Equating the two and substituting Δx for r yields:

$$e^{-2} = e^{-c\frac{(\Delta x)^2}{D^2}}$$

$$C = \frac{2D^2}{(\Delta x)^2} \qquad \text{(V-1)}$$

As expected the gaussian constant will depend on the size of the aperture D taken as the normalization value.

The second method of finding the gaussian constant is a method by Stijns.[1] A wire or cylindrical object is used in place of the blade. Instead of wholescale screening of the incident beam, selective shading is possible. The wire is moved across the beam until a minimum in power registered by the meter occurs. As the figures below suggest this minimum corresponds to the point at which the wire is centered in

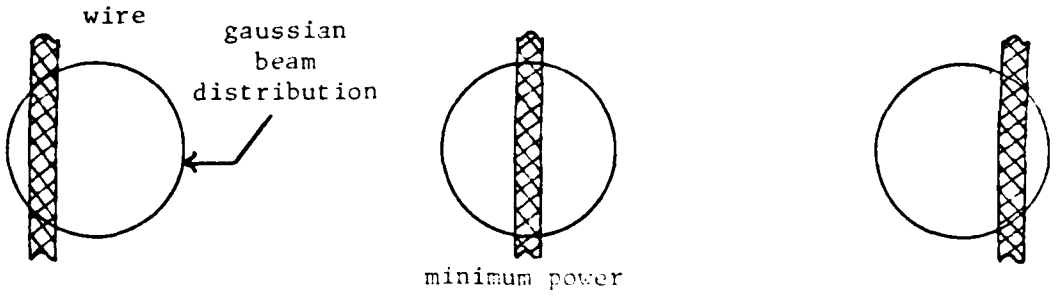

Figure 5.3

Wire Method of Gaussian Constant Detemination

the beam. The ratio of the power at the minimum to the unobstructed power is compared to an error function. Use of a graph enables one to obtain a value for the ratio of the wire diameter to the radius W_o of the e^{-2} points. In a similar method to equation V-1, the gaussian constant can be determined.

Preliminary Runs

The dry run phase involved taking measurements to verify theory and to perfect experimental techniques for the final trials.

Final Tests

The ultimate experiment involved:

1) Verification of theory for the unaberrated case.

2) Measurement of defocus aberration coefficients by axial shifting of on-axis extrema.

3) Measurement of spherical aberration coefficients by shifting of on-axis extrema.

4) Study of astigmatism.

Verification of theory. The testing of the theory presented in Chapter 3 was accomplished by varying a number of parameters. These parameters were the obstacle diameter, the aperture diameter (for the annular aperture), the gaussian constant, the distance along the optical axis and the separation of the obstacle and aperture. The travelling microscope allowed for on and off axis measurements. In addition, some photographs were taken to compare with computer generated intensity contour plots.

Measurement of defocus coefficients. The positions of maxima and minima on axis behind various annular apertures were measured, marked and their orders determined. Defocus was introduced by moving the collimating lens. The shift of the lens position becomes the Δz term in equation IV-2. The coefficient of defocus thus obtained can be compared to the coefficient found by equation IV-28 from the shift on axis.

It is important to note that by decollimating the incident beam the wavefront is no longer planar. The beam will diverge or converge depending on the sign of defocus. But the spherical obscuration is mounted on a plane parallel plate. Will the now diverging or converging wave contain more aberrations upon plate passage? Since the plate is not tilted some spherical aberration will be produced but only a negligible amount. The non-converging rays still strike the plate at essentially perpendicular angles.

Measurement of spherical aberration coefficients. Spherical aberration was introduced by inserting one or two parallel plates in the diverging beam from the spatial filter. Measurements were taken using the same method employed for defocus. The aberration coefficients were calculated from the expression for spherical aberration in tables 4.3 and 4.4. These were compared with the results obtained from equations IV-58 and IV-59.

Study of astigmatism. Astigmatism was introduced into the wavefront by countertilting two plane parallel plates. Photographs were

taken of the diffraction pattern of a circular obstacle for one degree increments in tilt angle. This became the standard by which every other photograph was evaluated. Various axial distances and obstacle diameters were tried. To investigate the annular aperture, the obstacle was purposely offset from center so the diffraction patterns from the outer and inner edges were separated. The changes in each pattern by the addition of astigmatism were photographed. The effect of the aberration was then observed for a variety of annular apertures and these were compared with the circular obscuration cases. Finally it was demonstrated that astigmatism also shifts the position of extrema on axis.

Numerical Studies

The unaberrated cases and those with defocus and spherical aberration lent themselves to study using an IBM PC computer. Appendix 8 contains program listings of the routines used to generate the plots and graphs in this thesis. Appendix 7 gives a comparison of the use of single precision numbers versus double precision numbers for the analysis.

Notes

[1] Erik Stijns, "Measuring the Spot Size of Gaussian Beam with an Oscillating Wire." IIEE Journal of Quantum Electronics, QE-16 (December 1980), 1298-1299.

Chapter 6

EXPERIMENTAL RESULTS

The presentation of the results of the experiment will follow the order presented in Chapter 5.

Determination of the Beam Parameters

Two different microscope objectives were used in the spatial filter. The 60X objective produced a wide intensity pattern, suggesting a low gaussian constant. This objective was employed to study annular apertures. If no aperture was used then the 13/16 inch diameter mount for the collimating lens became the aperture stop for the system. To minimize the edge-diffracted effects from the mount, the objective used was by the 20X objective. This produces a narrow gaussian beam.

The methods employed to find the gaussian constants were the knife-edge test and the wire test.

Knife-edge Test

The power of the uninterrupted beam reaching the detector was 0.418mW. The table below gives the knife edge position, the power measurement and the percent transmission past the knife edge.

Table 6.1

Knife Edge Test Data for 60X Objective

Knife Edge Position (mm)	Power (mW)	% Transmission
44	.418	100
46	.400	95.7
47	.396	94.7
48	.390	93.3
49	.379	90.7
50	.362	86.6
51	.345	82.5
52	.328	78.5
53	.300	71.8
54	.281	67.2
55	.253	60.5
56	.223	53.3
57	.209	50.0
58	.185	44.2
59	.146	34.9
60	.104	24.9
61	.050	12.0

The percent transmission levels off at the extremes of the knife edge position. The best fit line for the data points should neglect these regions. The suggested procedure is to consider data points between 15.8% and 84.2% transmission and extrapolate. A least squares linear fit of the data from 51mm to 60mm yields a percent transmission function of the form:

$$(\% \text{ transmission}) = 400 - 6.184 \times (\text{knife edge position}) \qquad \text{(VI-1)}$$

The coefficient of determination is .9883. The 15.8% and 84.2% transmission points occur at 62.13 and 51.06mm respectively giving a x of 11.07mm. Then by equation V-1, the gaussian constant is:

$$C_{60x} = \frac{2D^2}{(\Delta x)^2} = 16320\ D^2 m^{-2} \qquad \text{(VI-2)}$$

For example, a one centimeter diameter aperture will yield a gaussian constant of 1.632.

The 20X objective yielded a total beam power of .438mW. The table of data for this objective appears below:

Table 6.2

Knife Edge Test Data for 20X Objective

Knife Edge Position (mm)	Power (mW)	% Transmission
61	.431	98.4
62	.421	96.1
63	.405	92.5
64	.379	86.5
65	.341	77.9
66	.300	68.5
67	.249	56.8
68	.184	42.0
69	.136	31.1
70	.090	20.5
71	.048	11.0

The least squares linear fit through the data points from 65mm to 70mm gives a linear function:

$$(90 \text{ transmission}) = 847.9 - 11.8 \times (\text{knife edge position}) \quad \text{(VI-3)}$$

The coefficient of determination is .9967. The x term is 5.87mm, the difference between the 15.8% point at 70.43mm and the 84.2% point at 64.56mm. The gaussian constant for the 20X objective is:

$$C_{20x} = 58044\ D^2 m^{-2} \quad \text{(VI-4)}$$

Wire Test

Four cylindrical objects of different diameters were used in this test. These are listed in the table below:

Table 6.3

Diameters of Objects Used in Wire Test

	Measured Diameter	
Object	Inches	Millimeters
Paper clip wire	.0345 ± .0005	.876 ± .013
Nail #1	.0950 ± .0005	2.413 ± .013
Nail #2	.1178 ± .0005	2.992 ± .013
Pen insert	.1246 ± .0005	3.165 ± .013

The measured unobstructed power for the 60X objective was .418mW.

This is designated P_0. The wire was moved into the beam until the minimum power P_a was reached. By Stijns' method:

$$\frac{P_a}{P_0} = 1 - \frac{2}{\pi} \int_0^{a/\sqrt{2}W_0} e^{-t^2} dt \qquad \text{(VI-5)}$$

where a is the radius of the wire and W_0 is the radius of the e^{-2} points. The table below gives the measured minimum power, and the related parameters used find W_0.

Table 6.4

Wire Test Parameters for 60X Objective

Paperclip wire	.376	.900	.125	7.01
Nail #1	.295	.706	.370	6.52
Nail #2	.275	.658	.445	6.72
Pen insert	.268	.641	.460	6.88

The average gaussian radius for the e^{-2} points is 6.78mm ($\pm$ .21mm). (The term in parentheses is the standard deviation.) Using this average value to find the gaussian constant C yields:

$$C = \frac{2D^2}{W_0^2} = 43510\ D^2m^{-2} \qquad \text{(VI-6)}$$

This differs from the result found by the knife edge test by a factor of over 2.5.

The comparison between the two tests was much closer for the 20X objective. In this test the background power was .448mW. The table below shows the parameters to find w .

Table 6.5

Wire Test Parameters for 20X Objective

Object	Minimum Power (mW)	P_a /P	a/W	W (mm)
Paperclip wire	.389	.868	.160	5.48
Nail #1	.300	.670	.435	5.55
Nail #2	.271	.605	.515	5.81
Pen insert	.266	.594	.540	5.86

The average gaussian radius for the e^{-2} points is 5.68mm ($\pm$ .19mm). Notice the radius measured using the knife edge method (5.87mm) is within one standard deviation of the above. The gaussian constant determined by the wire test is:

$$C = 61990\ D^2m^{-2} \qquad \text{(VI-7)}$$

The wire test method gave very consistent results. Unfortunately, the results were much too high. For a 16mm aperture the gaussian

constant for a 60X microscope objective is 11.14 using the wire method value. This constant is sufficiently large to eliminate the effects of the outer aperture. The diffraction pattern should be just that of an obstacle alone. This is not what is observed. There are diffraction effects from the outer edge. One possibility for the difference between the two tests is the beam might not be perfectly gaussian. In this case the results from both tests are suspect. For the purpose of plotting graphs, the values of the gaussian constants from the knife-edge test will be used as the standards.

Aberration Coefficient Curves

Defocus

The coefficient of defocus as a function of the shift in position of the collimating lens is given by equation IV-2.

$$W = -\frac{\Delta z}{8(F^{\#})^2} \qquad \text{(IV-2)}$$

The f number is determined by the radius of aperture used. The aberration coefficient curves for aperture diameters of 7mm (solid line), 10mm (dashed line) and 16mm (dotted line) appear below.

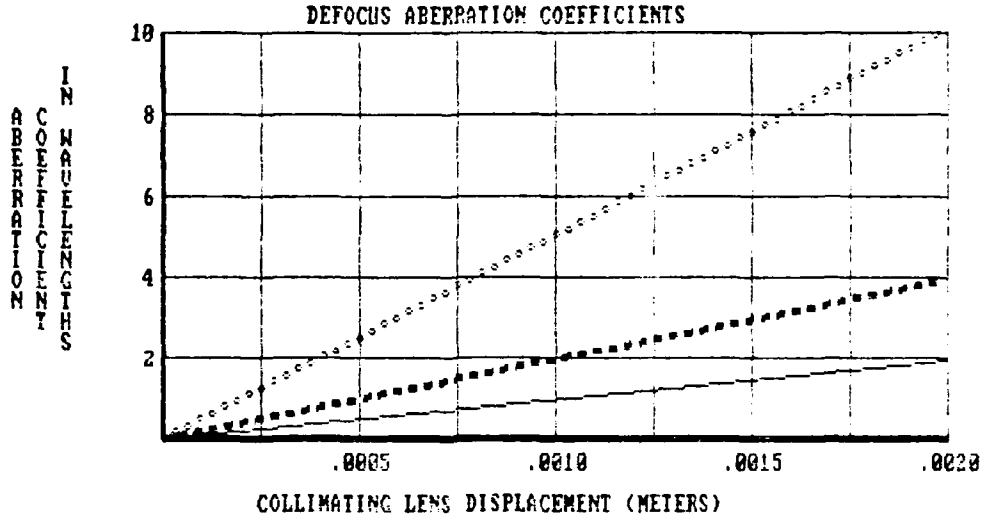

Graph 6.1

Spherical Aberration

As shown in Chapter 4, the coefficient of spherical aberration will be constant. The table below lists the spherical aberration coefficients for apertures of diameters 7, 10 and 16mm.

Table 6.6

Spherical Aberration Coefficients

Aperture Diameter (mm)	W_{40}-one plate (wavelengths)	W_{40}-two plates (wavelengths)
7	- .0014	- .0028
10	- .0056	- .0117
16	- .0383	- .0766

Astigmatism

Early in the experiment the laboratory set-up was found to contain background astigmatism. The majority of this astigmatism seemed to come from the plane parallel plates. With the plates removed the diffraction patterns of all obstacles were the symmetric ring patterns predicted by theory. When the plates were inserted the patterns were aberrated to various degrees depending on the diameter of the obstacle. The residual astigmatism seemed to be positive. The astigmatism produced by countertilting two plates has a negative sign. Thus one can balance out the background positive astigmatism by introducing negative aberration. By measuring these required plate tilt angles for various sized obstacles the amount of background astigmatism can be determined. The table below lists the countertilt angles using obstacles of diameters 5/16, 1/2 and 5/8 inches and the associated aberration coefficients. The error term in the aberration coefficient

Table 6.7

Measure of Background Astigmatism

Obstacle Diameter (mm)	Tilt angle required to balance out background aberration (°)	W_{22} (wavelengths)
7.938	5 ± .5	.090 ± .018
12.7	3.5 ± .5	.113 ± .032
15.875	2.5 ± .5	.090 ± .036

is the average deviation based upon the half angle uncertainty in the tilt angle. The aberration coefficient for the background astigmatism is taken as .0975 , the average of the above values. This is added to the expression from Table 4.4 for W_{22}.

$$W_{22} = .0975\lambda - \frac{n^2-1}{n^3} \frac{tu^2\theta^2}{\lambda} \lambda \qquad \text{(VI-8)}$$

Interferograms using the point diffraction interferometer were made to verify the above. The data points obtained from interferogram analysis are plotted against the curve of equation VI-3 for a 13/16 inch diameter aperture. The error bars reflect the uncertainty in tilt angles and the associated uncertainty in W_{22}.

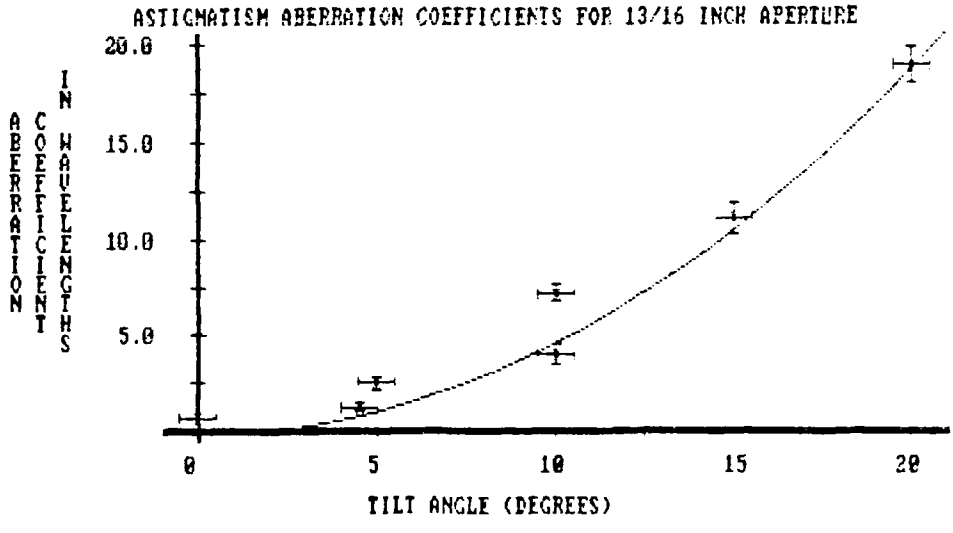

Graph 6.2

Seven interferograms were selected from over thirty taken to be reduced. These are shown below. The first is of one plate inserted with no tilt. The next three show two countertilted plates of 4.5°, 10° and 20° each. The effect of increasing astigmatism is seen to compress the interferogram pattern from concentric circles to concentric ellipses. The last three show the effects of two plates tilted in the same direction at angles of 5°, 10° and 15°. Coma enters into these patterns and sweeps the fringes to one side. Photograph 6.6 contains a dark spot in the center of the pattern. This is the result of the photograph being taken of the pattern on the side of negative defocus. All the other photographs show patterns on the positive defocus side of the null (zero focus) position.

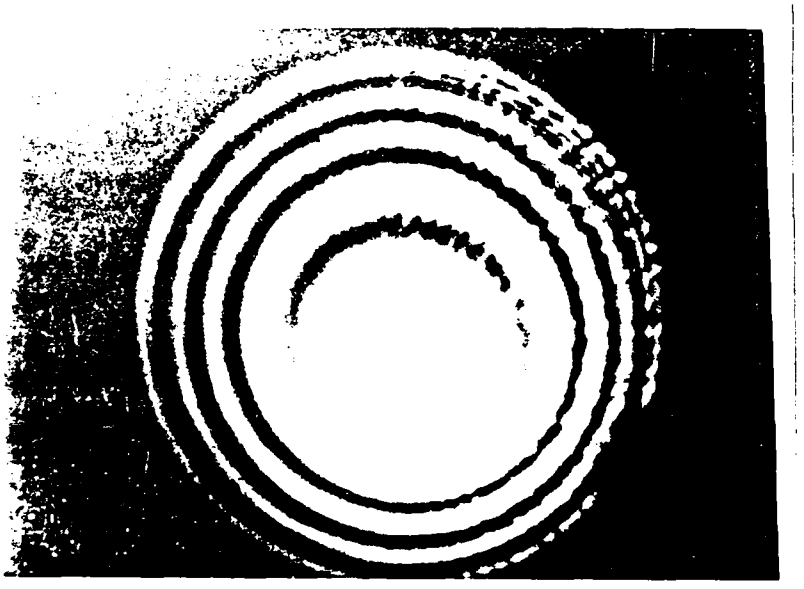

Photograph 6.1

One plate - no tilt

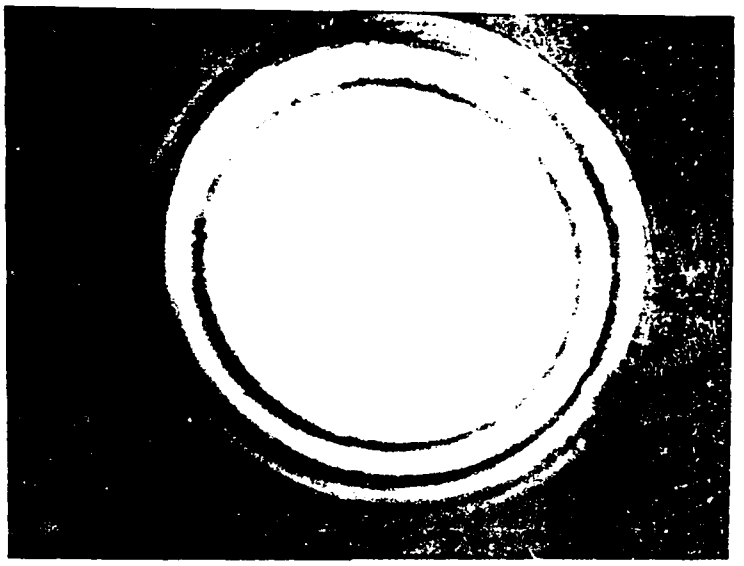

Photograph 6.2

Two plates - 4.5° countertilt

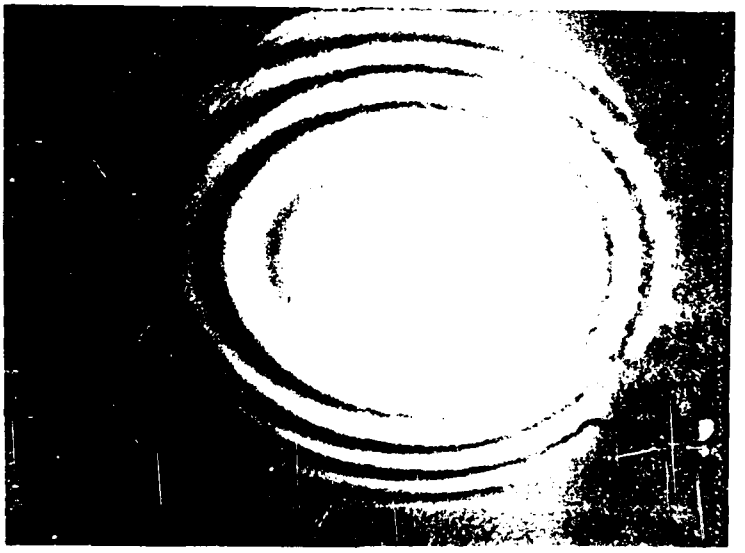

Photograph 6.3

Two plates - 10° countertilt

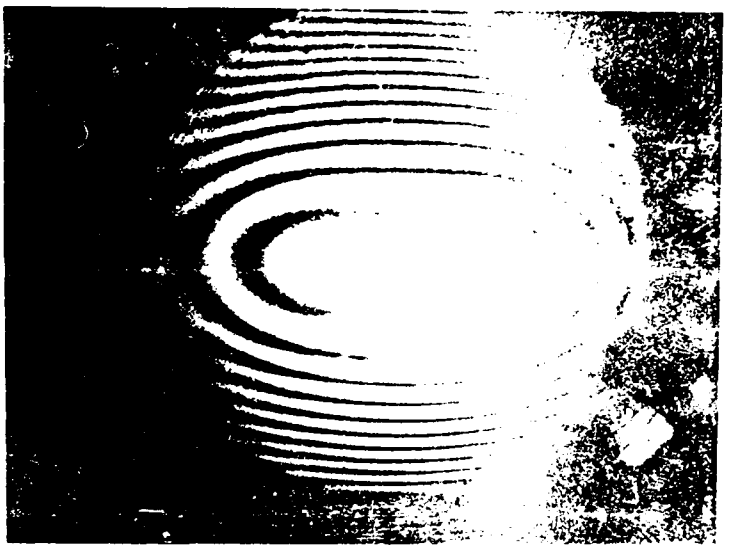

Photograph 6.4

Two plates - 20° countertilt

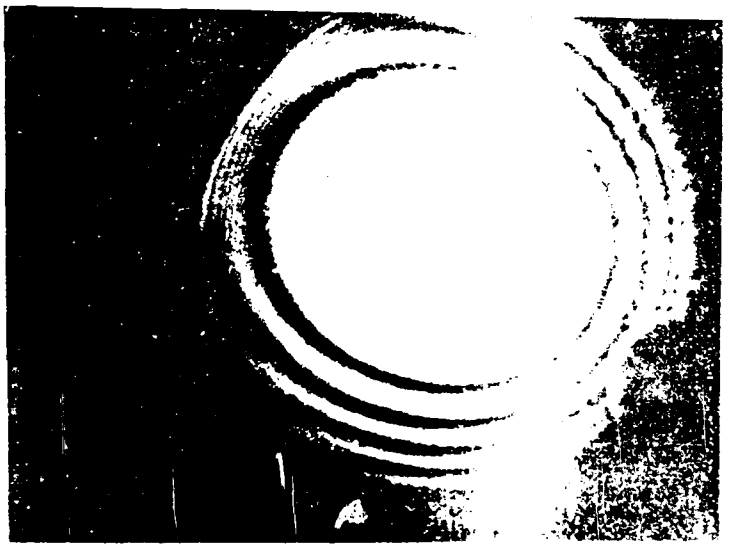

Photograph 6.5

Two plates - 5° tilt in same direction

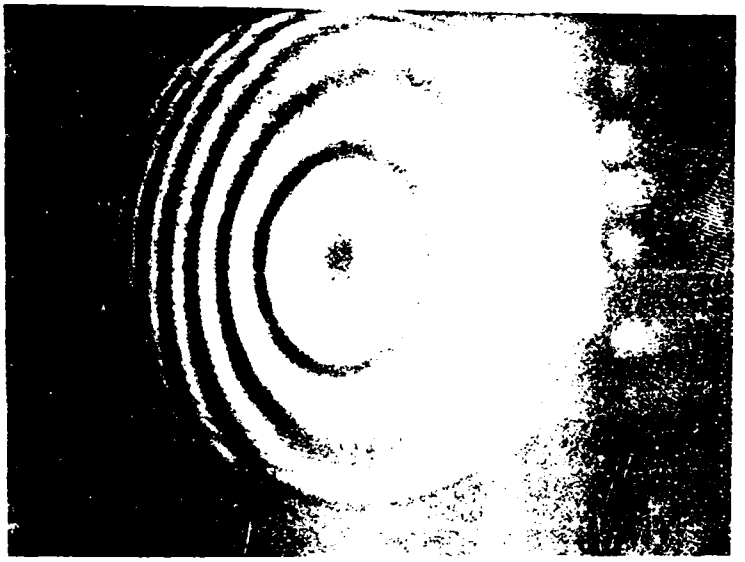

Photograph 6.6

Two plates - 10° tilt in same direction

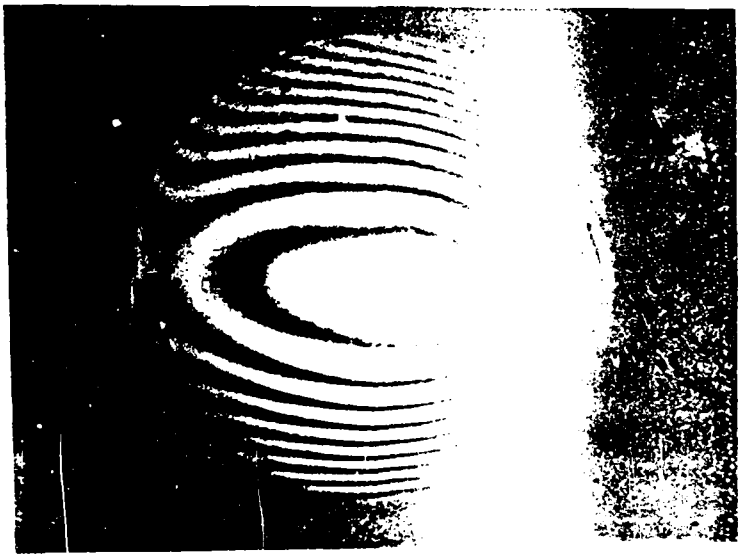

Photograph 6.7

Two plates - 15° tilt in same direction

In each photograph the center of the pattern was measured. (In the case of Photograph 6.7 which is not symmetric, the position of center had to be estimated.) This became the center of the pattern to be digitized for the computer analysis. This was necessary because a shift in position from the center will introduce extraneous aberrations. To see this take a simple example. Assume the only aberration present is defocus. Let the x-position of the center be shifted by Δx, ($\Delta x \ll 1$). Then the aberration function becomes:

$$W = W_{20}r^2 = W_{20}(x^2 + y^2) \Rightarrow W_{20}((x + \Delta x)^2 + y^2)$$

$$= W_{20}(x^2 + 2x\Delta x + 0 + y^2)$$

$$= W_{20}(x^2 + y^2) + 2\Delta x W_{20}x$$

$$= W_{20}r^2 + 2\Delta x W_{20}r\cos\phi$$

$$= W_{20}r^2 + W_{11}'r\cos\phi \qquad \text{(VI-9)}$$

A shift in the x-direction manifests itself by the introduction of an extraneous tilt term. If the pattern is not centered when put into the reduction program the output will contain many of these manufactured aberrations.

Verification of Theory for the Unaberrated Case

Three features of the diffraction pattern predicted by the theory of Chapter 3 were investigated. The first was the position and spacing

of the rings in the diffraction pattern. This was accomplished in conjunction with the observations of the other two features. The second was the increase of the overall pattern size for increased optical axis distance Z. The third was the decrease in the overall pattern size for increased obstacle diameter.

Circular Obstacle

The following photographs show the diffraction patterns behind a 3/16 inch diameter circular obstacle observed at 20, 25, 50 and 75 centimeters. The 20X microscope objective was used in the spatial filter. The stereo-viewer was set at a magnification of 6X. The exposure times were all 1/2 second. The photographs demonstrate not only the increase in pattern size with increased z, but the regular spacing of the ring structure and the brightness of the central spot in comparison to the rings.

Quantitative measurements of the increased pattern size came from looking behind a 5/16 inch diameter ball bearing at 40cm and at 75cm. The tables below compare experiment and theory for these cases. The calibrations on the travelling microscope allowed for measurement accuracy within $\pm$ .005mm. Additional uncertainty arose from the judgement of where the brightest and darkest points in the ring structure occurred.

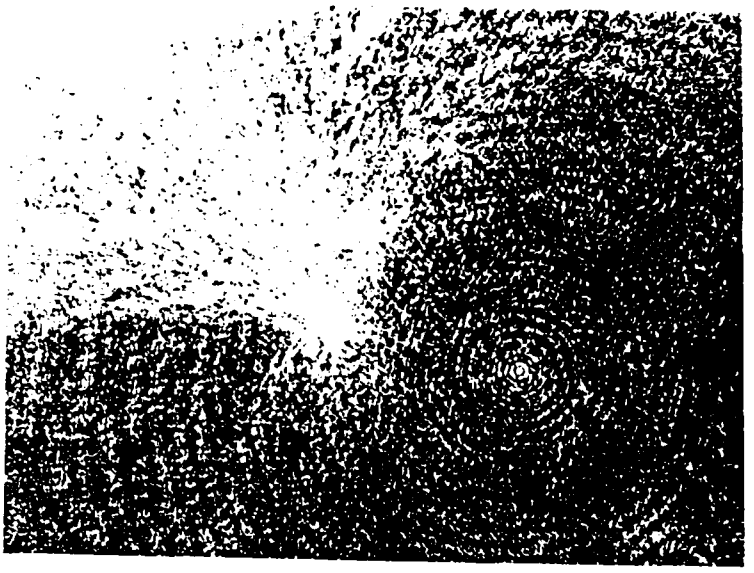

Photograph 6.8

z = 20cm

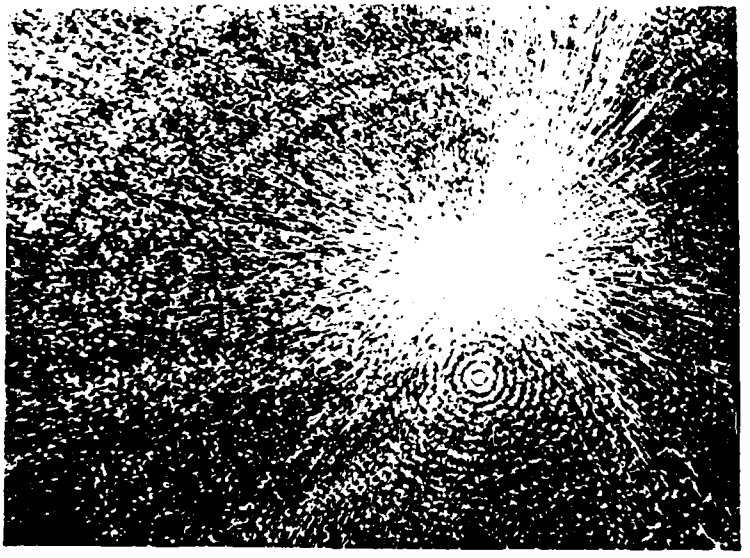

Photograph 6.9

z = 25cm

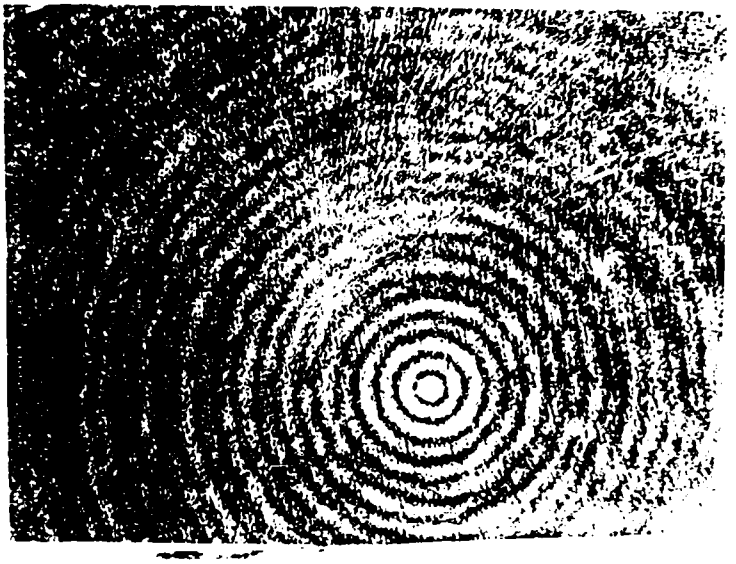

Photograph 6.10

z = 50cm

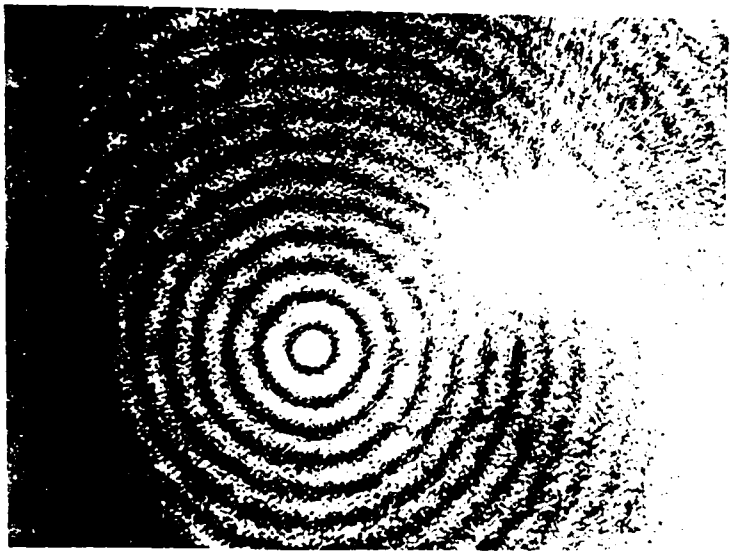

Photograph 6.11

z = 75cm

Table 6.8

Comparison of Theory and Experiment:
Positions of Ring Minima and Maxima.
5/16 Inch Diameter Obstacle Viewed at 40cm

Ring Structure	Distance from Center (mm)		Percent Difference
	Experiment	Theory	
Minimum #1	.023	.024	4.2
Maximum #1	.046	.039	17.9
Minimum #2	.057	.056	1.8
Maximum #2	.072	.071	1.4
Minimum #3	.091	.088	3.4
Maximum #3	.108	.103	4.9
Minimum #4	.126	.120	5.0
Maximum #4	.143	.135	5.9
Minimum #5	.154	.152	1.3
Maximum #5	.172	.167	6.0
Minimum #6	.194	.183	6.0
Maximum #6	.209	.199	5.0
Minimum #7	.227	.215	5.6

Table 6.9

Comparison of Theory and Experiment:
Positions of Ring Minima and Maxima.
5/16 Inch Diameter Obstacle Viewed at 75cm

Ring Structure	Distance from Center (mm)		Percent Difference
	Experiment	Theory	
Minimum #1	.045	.046	2.2
Maximum #1	.070	.073	4.1
Minimum #2	.103	.105	1.9
Maximum #2	.134	.134	0.0
Minimum #3	.162	.164	1.2
Maximum #3	.189	.194	2.6
Minimum #4	.230	.224	2.7
Maximum #4	.256	.254	0.8
Minimum #5	.287	.284	1.1
Maximum #5	.317	.313	1.3
Minimum #6	.344	.344	0.0
Maximum #6	.374	.373	0.3
Minimum #7	.405	.404	0.2

The above tables show that the experiment agrees with predicted values. The spacing between the rings shows almost a 100% increase from the 40cm measurements to the respective 75cm measurements. There

were larger deviations from theory for the pattern viewed at 40cm than for the 75cm pattern. This is reasonable because the uncertainty in measurements results in a larger percentage of difference.

The photographs on the next page show the diffraction patterns behind a 3/16 inch diameter obstacle and a 5/16 inch diameter obstacle viewed at a distance of 60cm. A 20X microscope objective was used and the binocular viewer set to magnification 6X. Photograph 6.12 had an exposure time of 1/8 second while photograph 6.13 was timed for 1/2 second. The diffraction pattern for the 3/16 inch obstacle is much larger than that for the 5/16 inch obstacle.

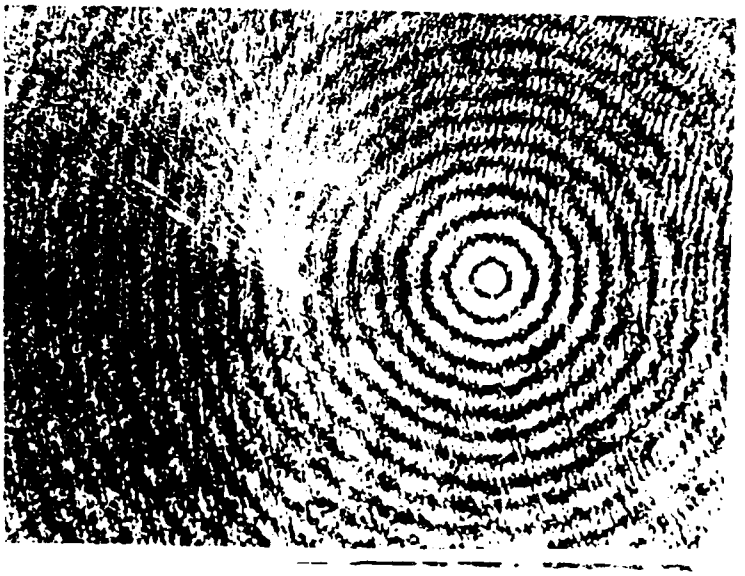

Photograph 6.12

3/16" diameter obstacle at 60cm

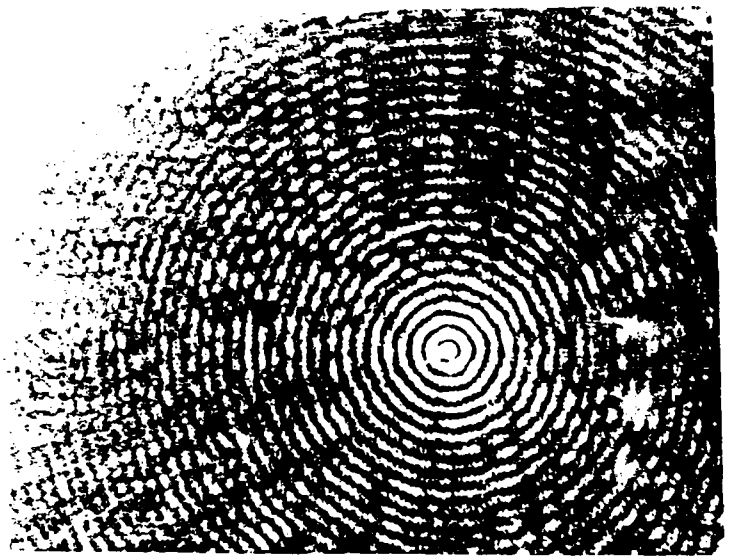

Photograph 6.13

5/16" diameter obstacle at 60cm

The positions of the first six ring intensity maxima were taken for the above cases as well as for a 1/2 inch diameter obstacle. The comparisons with theory appear in the tables below.

Table 6.10

Comparison of Theory and Experiment:
Positions of Ring Maxima.
3/16 Inch Diameter Obstacle Viewed at 60cm

Ring # (Maximum)	Distance from Center (mm)		Percent Difference
	Experiment	Theory	
1	.095	.097	2.1
2	.180	.178	1.1
3	.262	.258	1.6
4	.345	.338	2.1
5	.415	.418	0.7
6	.511	.498	2.6

Table 6.11

Comparison of Theory and Experiment:
Positions of Ring Maxima.
5/16 Inch Diameter Obstacle Viewed at 60cm

Ring # (Maximum)	Distance from Center (mm)		Percent Difference
	Experiment	Theory	
1	.057	.058	1.7
2	.107	.107	0.0
3	.153	.155	1.3
4	.203	.203	0.0
5	.252	.251	0.4
6	.299	.299	0.0

Table 6.12

Comparison of Theory and Experiment:
Positions of Ring Maxima.
1/2 Inch Diameter Obstacle Viewed at 60cm

Ring # (Maximum)	Experiment	Theory	Percent Difference
1	.034	.036	5.6
2	.069	.067	3.0
3	.100	.127	3.1
4	.123	.127	3.1
5	.154	.157	1.9

As the diameter of the obstacle increases the scale of the pattern diminishes. As previously seen the smallest pattern has the largest average percent difference from theory.

Annular Aperture

To test the theory for the annular aperture, three obstacle sizes and six aperture sizes were used. The table below lists the obscuration ratios ϵ for the possible combinations.

Table 6.13

Obscuration Ratios

ε / Aperture Diameters (cm)	Obstacle Diameters (cm)		
	3/16" (.47625)	5/16" (.79375)	1/2" (1.27)
.7	.68	—	—
3/8" (.9525)	.5	.833	—
1.0	.476	.794	—
1/2" (1.27)	.375	.625	1.00
5/8" (1.5875)	.3	.5	.8
1.6	.198	.496	.794

The following photographs and graphs compare the experimental results with theoretical predictions for a variety of combinations. The scale factors in the intensity contour plots were reduced from those used in Chapters 3 and 4 in consideration of the reduced overall intensity resulting from a gaussian intensity distribution of the incident wave. They were reduced again by half in the contour plots accompanying the last two photographs.

AD-A141 983 THE SPOT OF ARAGO AND ITS ROLE IN ABERRATION ANALYSIS 3/4
(U) AIR FORCE INST OF TECH WRIGHT-PATTERSON AFB OH
D R ERBSCHLOE DEC 83 AFIT/CI/NR-84-7T

UNCLASSIFIED F/G 20/6 NL

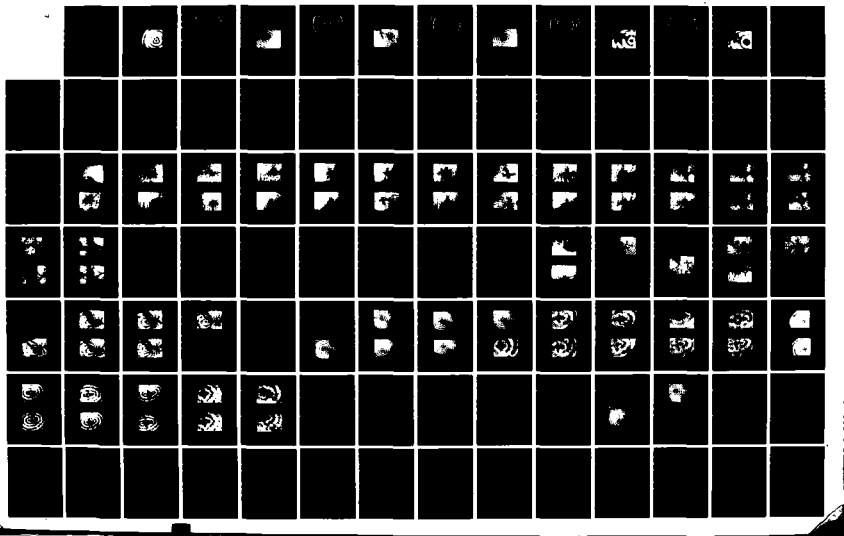

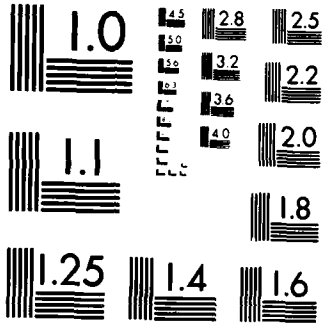

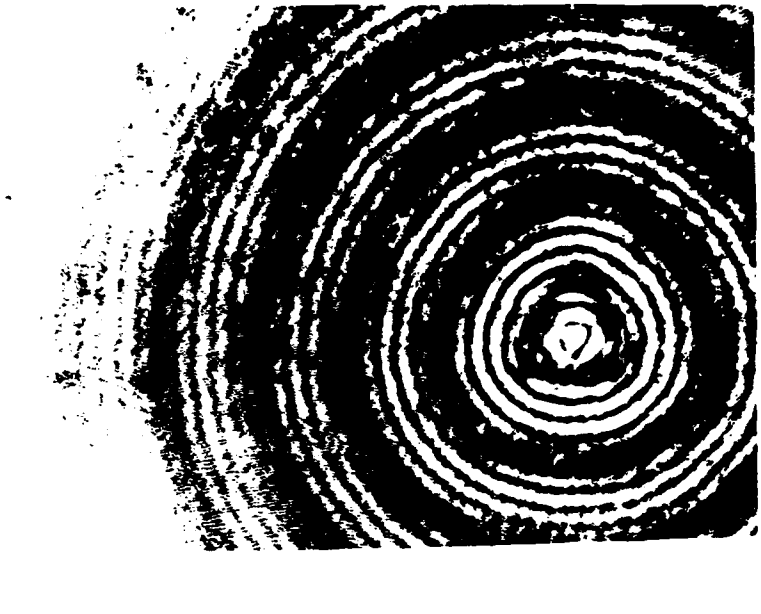

Photograph 6.14

3/16" diameter obstacle with 7mm diameter aperture.
Viewing distance = 62cm. Obstacle-aperture separation = 1cm.
Magnification 5X. Exposure time = 1/2 sec.

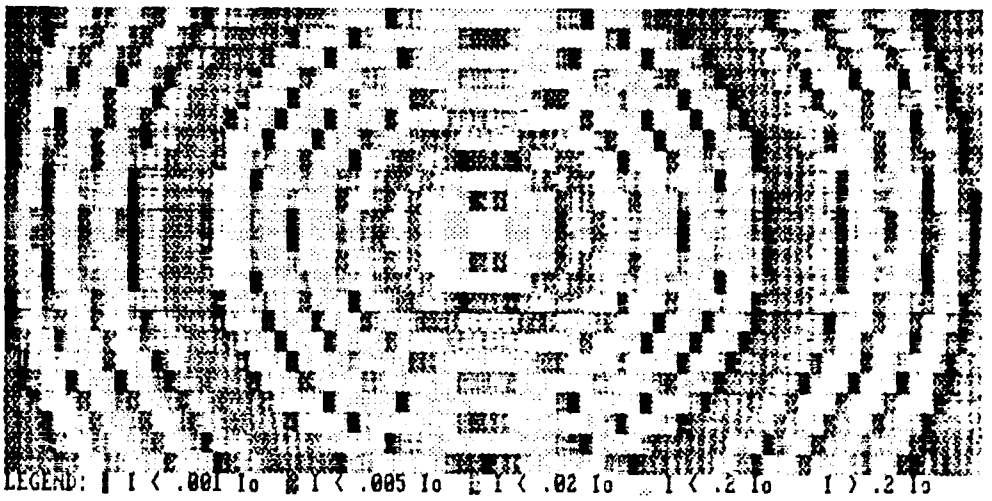

Graph 6.3

3/16" obstacle with 7mm aperture

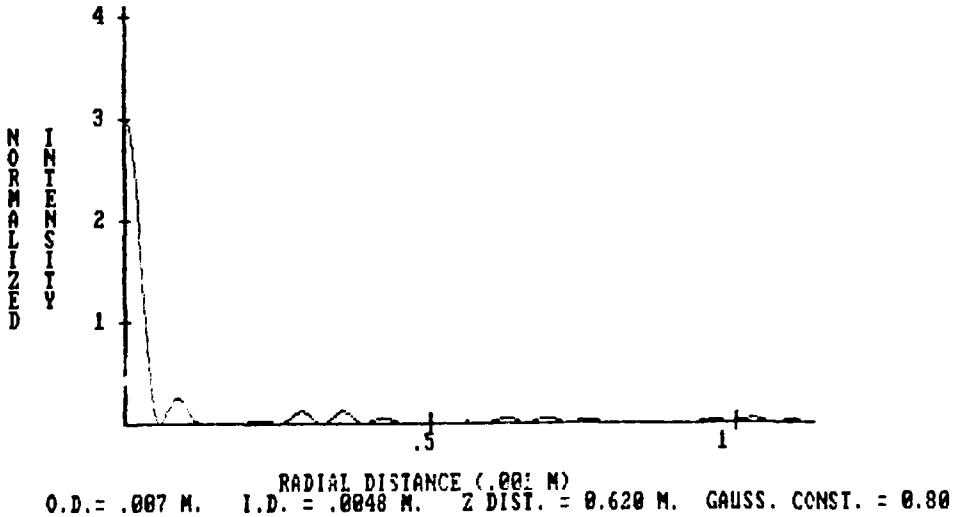

Graph 6.4

Intensity profile for 3/16" obstacle with 7mm aperture

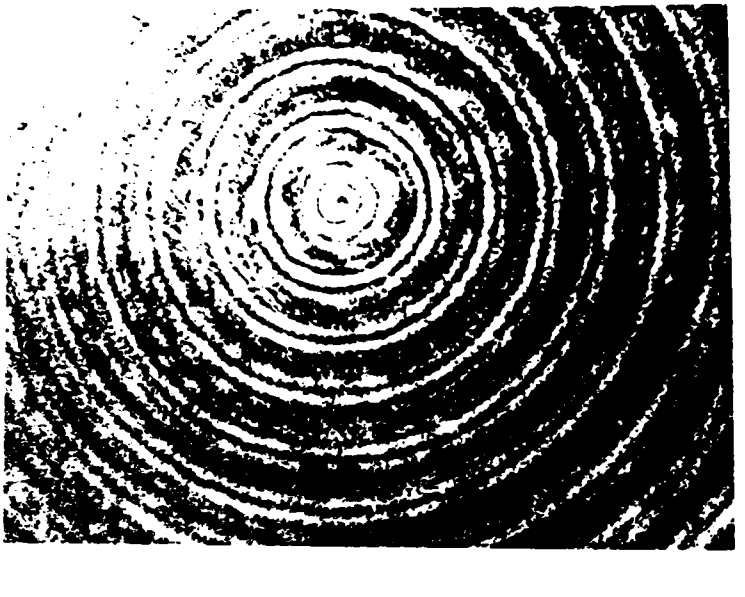

Photograph 6.15

3/16" diameter obstacle with 10mm diameter aperture.
Viewing distance = 59.1cm. Obstacle-aperture separation = 1.3cm.
Magnification 6X. Exposure time = 1 sec.

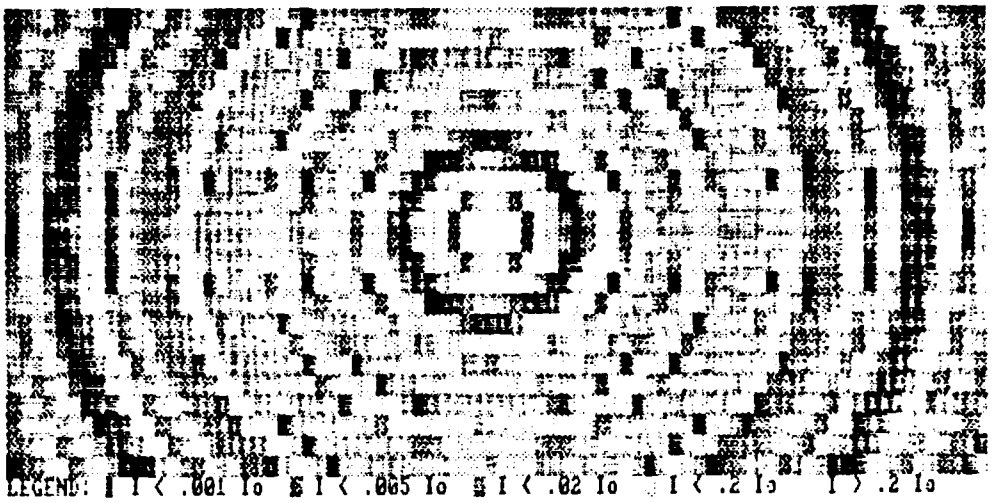

Graph 6.5

3.16" diameter obstacle with 10mm aperture

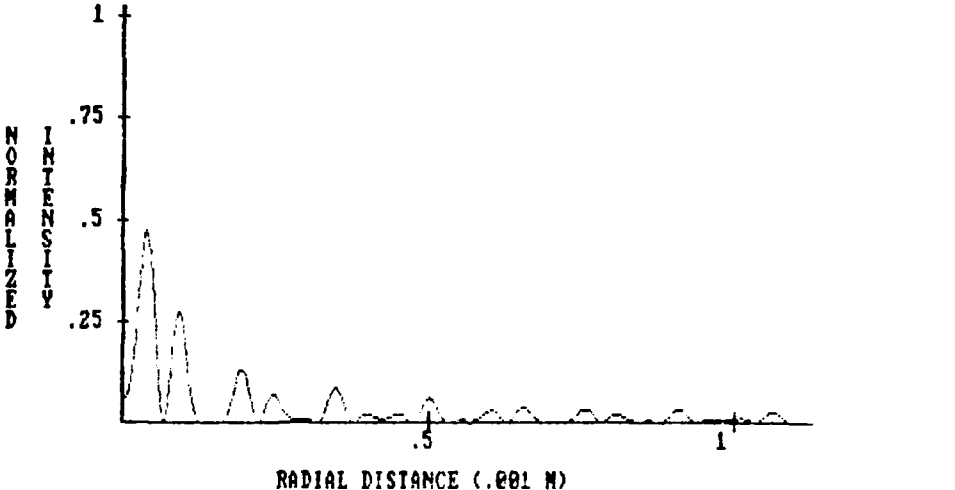

Graph 6.6

Intensity profile for 3/16" obstacle with 10mm aperture

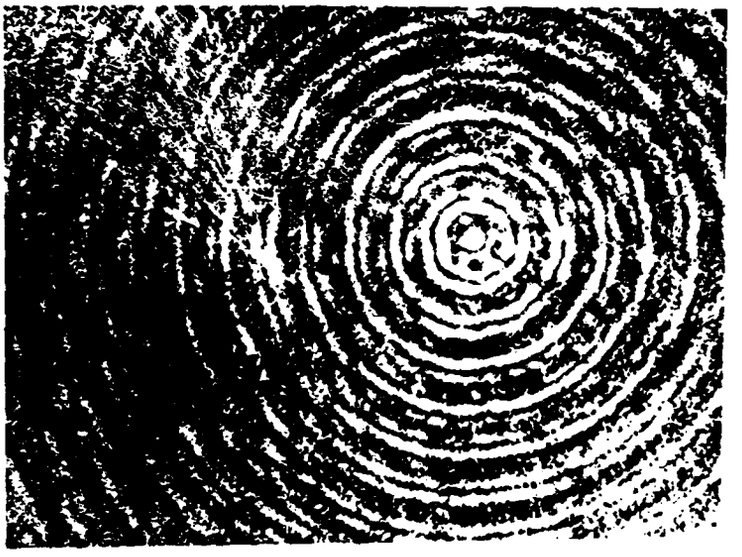

Photograph 6.16

3/16" diameter obstacle with 10mm diameter aperture.
Viewing distance = 60.3cm. Obstacle-aperture separation = 1.3cm.
Magnification 6X. Exposure time = 1 sec.

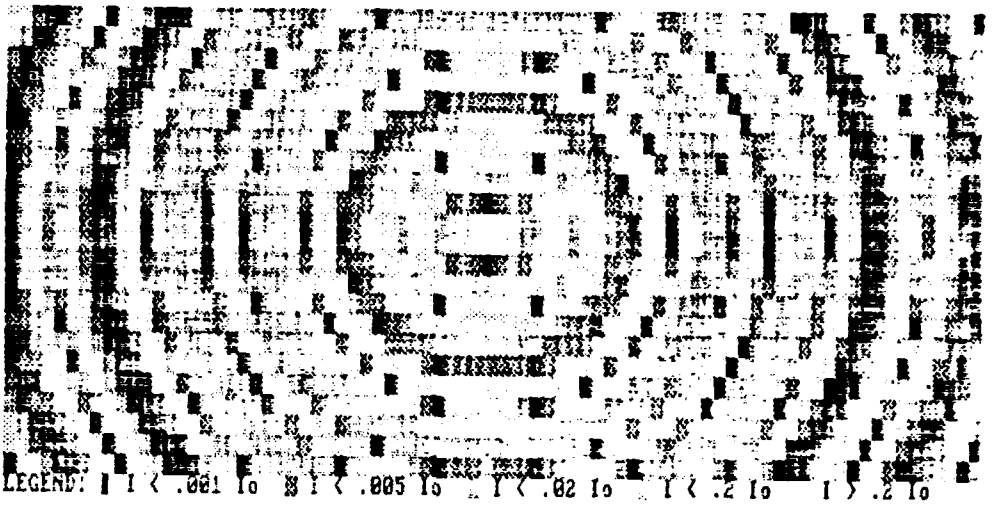

Graph 6.7

3/16" diameter obstacle with 10mm aperture

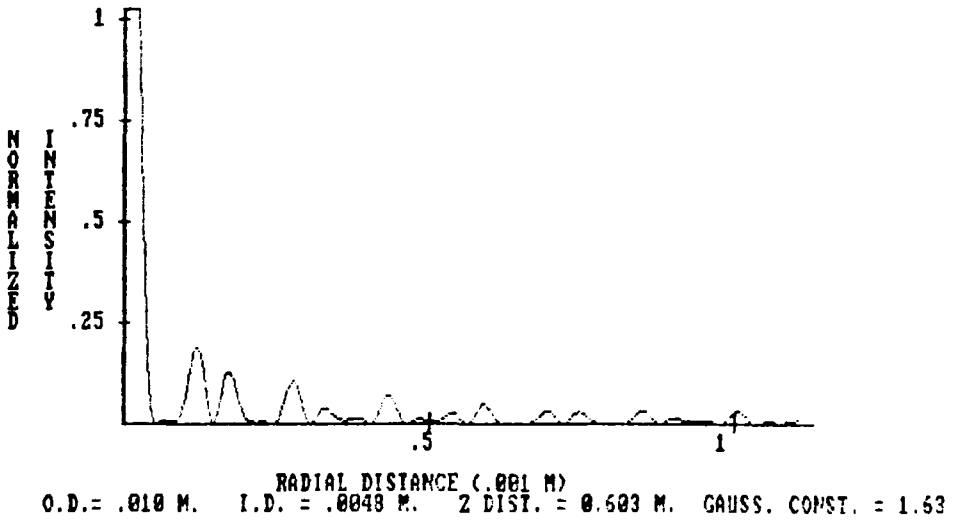

Graph 6.8

Intensity profile for 3/16" obstacle with 10mm aperture

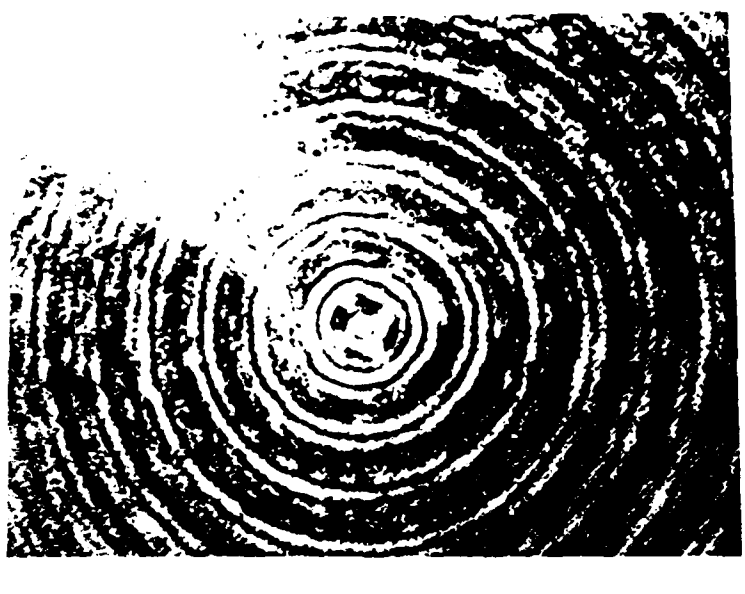

Photograph 6.17

3/16" diameter obstacle with 3/8" diameter aperture.
Viewing distance = 60.2cm. Obstacle-aperture separation = 1.3cm.
Magnification 6X. Exposure time = 1 sec.

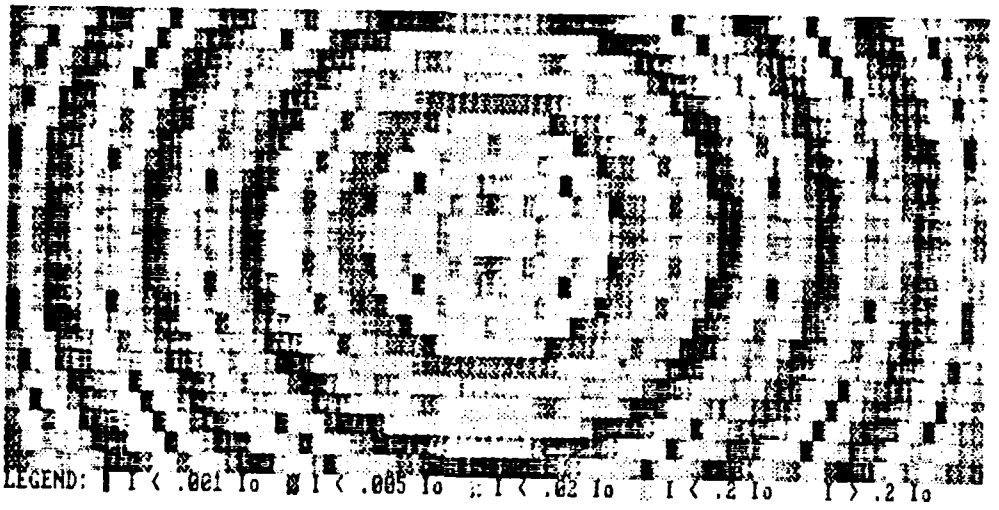

Graph 6.9

3/16" diameter obstacle with 3/8" diameter aperture

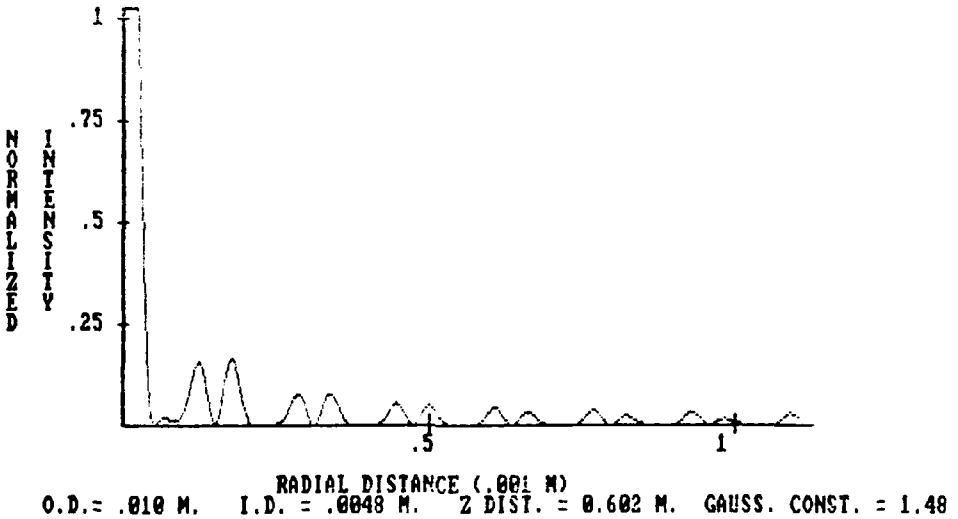

Graph 6.10

Intensity profile for 3/16" obstacle
with 3/8" diameter aperture

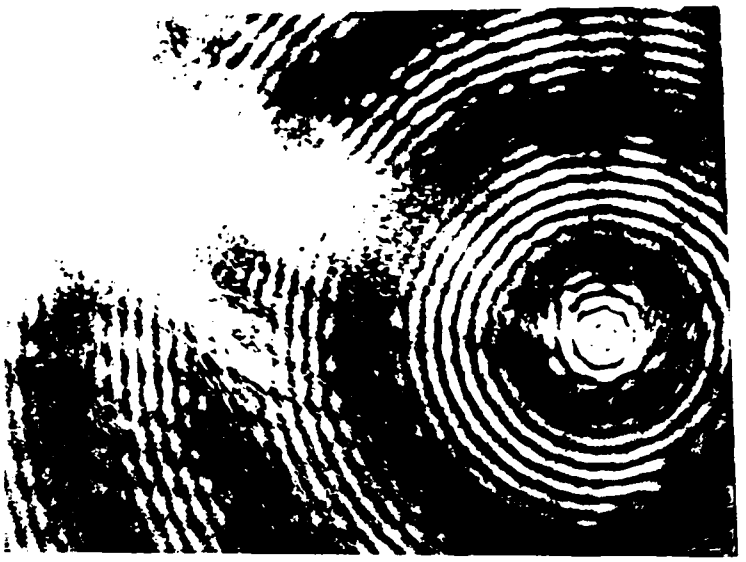

Photograph 6.18

1/2" diameter obstacle with 5/8" diameter aperture.
Viewing distance = 2.120m. Obstacle-aperture centered.
Magnification 6X. Exposure time = 1 sec.

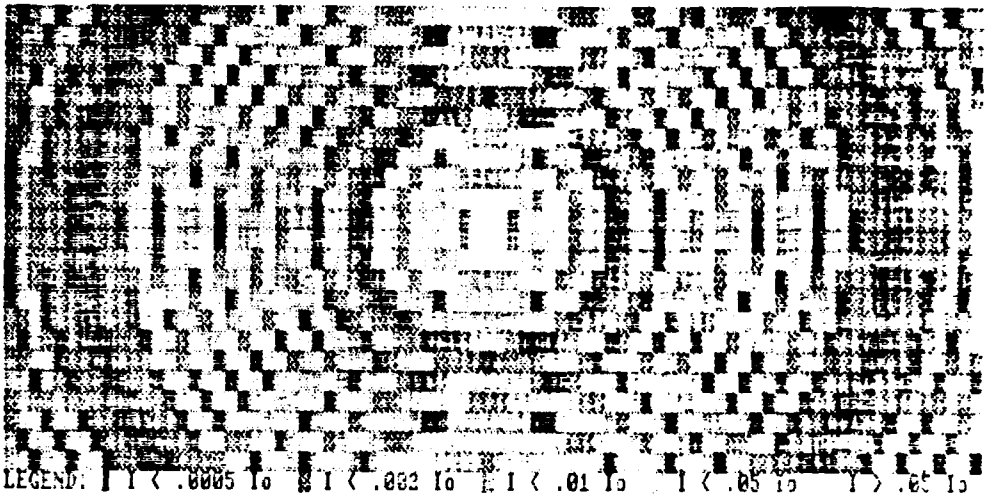

Graph 6.11

1/2" diameter obstacle with 5/8" diameter aperture

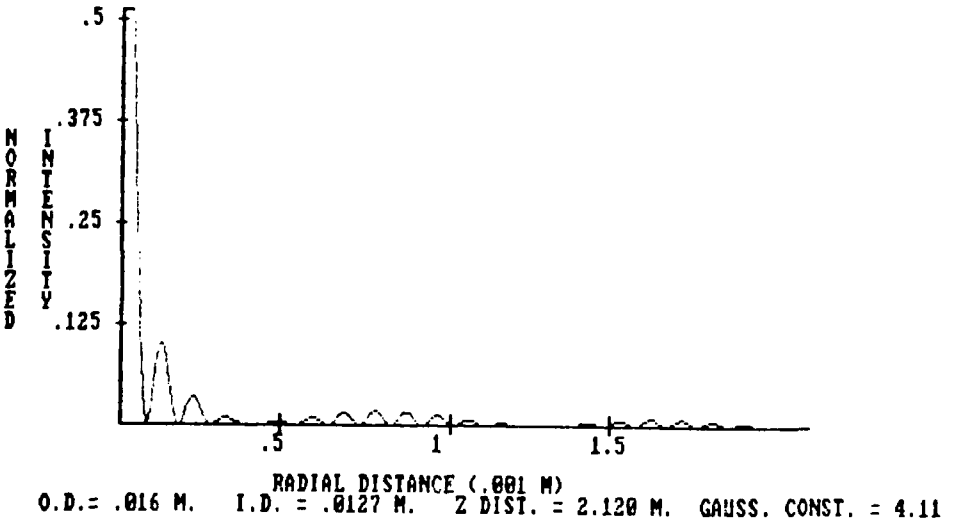

Graph 6.12

Intensity profile of 1/2" diameter obstacle
with 5/8" diameter aperture

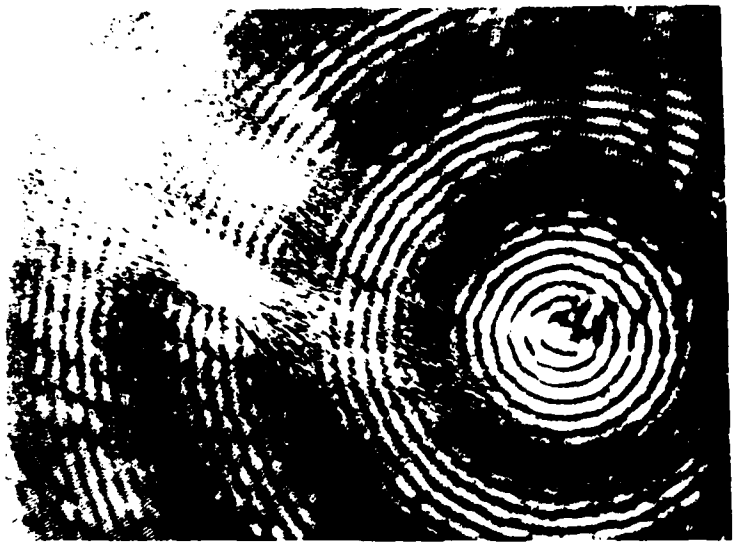

Photograph 6.19

1/2" diameter obstacle with 5/8" diameter aperture.
Viewing distance = 2.003m. Obstacle-aperture centered.
Magnification 6X. Exposure time = 1 sec.

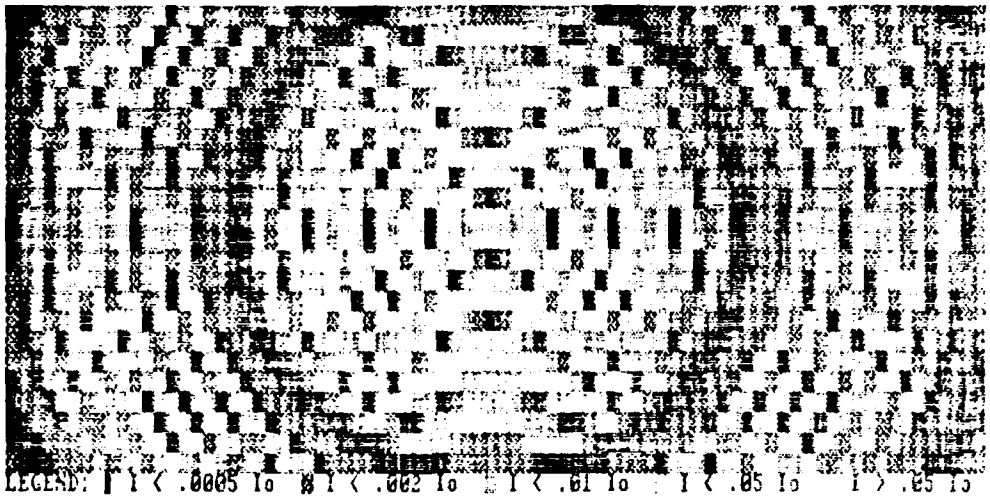

Graph 6.13

1/2" diameter obstacle with 5/8" aperture

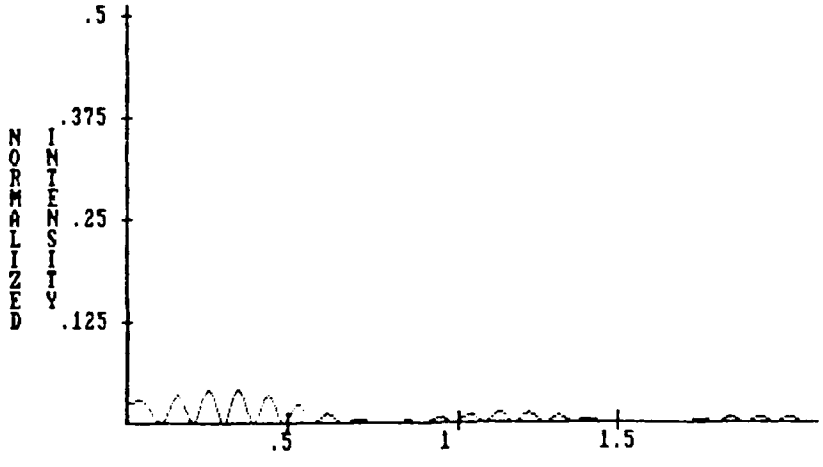

Graph 6.14

Intensity profile for 1/2" diameter obstacle
with 5/8" diameter aperture

The photographs show excellent agreement with theory. Photograph 6.15 depicts a 3/16 inch diameter obstacle with a 10mm diameter aperture at an on-axis minimum. The corresponding intensity contour plot does not have a dark center. This is due to the resolution of the contour plotting routine. The central minimum in this plot is too narrow for the routine to observe. It does show up in the companion intensity distribution curve. Of interest is the fact that the on-axis intensities are non-zero in the minimum on-axis plots. This is a consequence of the gaussian nature of the incident beam. This effect is most easily seen in photograph 6.19 where the center of the diffraction pattern is not dark. Photographs 6.16 and 6.17 show very similar patterns. This is expected because of similar obscuration ratios. Photograph 6.15 corresponds to a ratio of .48 and photograph 6.16 to a ratio of .5.

A quantitative comparison of radial positions of diffraction pattern minima and maxima for theory and experiment follows.

Table 6.14

Comparison of Theory and Experiment:
Positions of Ring Maxima and Minima.
3/16 Inch Diameter Obstacle with
1cm Diameter Aperture, Viewing Distance = 50.2cm,
Obstacle-Aperture Separation = 1cm

Qualitative Description	Normalized Intensity (Theory)	Distance from Center (mm)		Percent Difference
		Experiment	Theory	
Center (minimim)	.061	.000	.000	--
Maximum ring 1	.475	.030	.031	3.2
Minimum	.000	.059	.055	7.3
Maximum ring 2	.277	.073	.076	3.9
Dark band	~ .0	.092-.154	.118-.130	--
Maximum ring 3	.132	.171	.165	3.6
Minimum	.000	.190	.188	1.1
Maximum ring 4 (faint)	.071	.208	.209	.5
Dark band	~ .0	.216-.282	.242-.271	—
Maximum ring 5	.086	.296	.298	.7
Minimum	.000	.317	.323	1.9
Maximum ring 6 (faint)	.023	.332	.341	2.6

Table 6.15

Comparison of Theory and Experiment:
Positions of Ring Maxima and Minima.
3/16 Inch Diameter Obstacle with 1.6cm Diameter Aperture,
Viewing Distance = 59.9cm, Obstacle-Aperture Separation = .8cm

Qualitative Description	Normalized Intensity (Theory)	Distance from Center (mm)		Percent Difference
		Experiment	Theory	
Center (minimim)	.314	.000	.000	--
Maximum ring 1	.697	.027	.023	17.4
Minimum	.000	.051	.057	10.5
Maximum ring 2	.196	.102	.099	3.0
Minimum	.000	.159	.147	8.2
Maximum ring 3	.103	.172	.174	1.1
Minimum	.000	.227	.226	0.4
Maximum ring 4	.056	.245	.248	1.2
Minimum	.000	.304	.303	0.3
Maximum ring 5	.026	.322	.323	0.3
Minimum	.000	.378	.380	0.5

Table 6.16

Comparison of Theory and Experiment:
Positions of Ring Maxima and Minima.
5/16 Inch Diameter Obstacle with 5/8 Inch Diameter Aperture,
Viewing Distance = 62.8cm

Qualitative Description	Normalized Intensity (Theory)	Distance from Center (mm)		Percent Difference
		Experiment	Theory	
Center (minimim)	1.280	.000	.000	--
Minimum	.000	.035	.034	2.9
Maximum ring 1	.079	.073	.071	2.8
Minimum	.000	.090	.090	0.0
Maximum ring 2	.041	.111	.109	1.8
Minimum	.000	.131	.132	0.3
Maximum ring 3	.033	.174	.172	1.2
Minimum	.000	.190	.190	0.0
Maximum ring 4	.048	.208	.209	0.5
Maximum ring 5	.020	.274	.272	0.7
Minimum	.000	.291	.290	0.3
Maximum ring 6	.032	.313	.309	0.3
Maximum [illegible]	.015	.371	.372	0.3
Minimum	.000	.389	.390	0.3
Maximum ring 8	.024	.408	.409	0.2

The above tables demonstrate close agreement between experiment and theory. An interesting feature is the relative nature of minima and maxima. Table 6.15 shows the central minimum has an intensity (theoretical) higher than the maximum intensity in most of the surrounding rings! Clearly the appearance of a maximum or minimum depends on the immediate intensity background.

The final study for the unaberrated case involved the positions and spacing of maxima and minima on axis behind annular apertures. Three combinations of apertures and obstacles were employed. The first was a 3/16 inch diameter obstacle with a 7mm diameter aperture. A maximum or minimum on axis was found and its postion measured to the nearest centimeter. The corresponding position on the scale of the travelling microscope was noted. The microscope was translated along the optical axis and the spacings between the extrema measured. (The microscope could be moved a total distance of 5.5cm.) The scale allowed for a maximum uncertainty in measurement of approximately .01cm. The first case includes measurements starting at various positions along the optical axis. The last two involve just one starting position. A quirk of the scale on the travelling microscope is that scale measurements are inversely related to optical axis distances. A decrease of position by 2cm on the microscope scale means an increase of 2cm along the optical axis.

Table 6.17

Comparison of Theory and Experiment:
Positions and Spacing of On Axis Extrema.
3/16 Inch Diameter Obstacle with 7mm Aperture Separated by 1cm

Measured Starting Position (± .5cm): 33cm

	Experiment		Theory		
Extremum Type	Scale Reading (cm)	Distance from Starting point (cm)	Optical axis Distance (cm)	Distance from Starting Point (cm)	% Difference
Minimum	4.85	0.0	33.31	0.0	--
Maximum	3.94	.91	34.36	1.05	13.3
Minimum	2.68	2.17	35.48	2.17	0.0
Maximum	1.60	3.25	36.67	3.36	3.3
Minimum	.33	4.52	37.96	4.65	2.8

Measured Starting Position (± .5cm): 40cm

	Experiment		Theory		
Extremum Type	Scale Reading (cm)	Distance from Starting point (cm)	Optical axis Distance (cm)	Distance from Starting Point (cm)	% Difference
Maximum	5.22	0.0	39.33	0.0	--
Minimum	3.76	1.46	40.82	1.49	2.0
Maximum	2.07	3.17	42.42	3.09	2.6
Minimum	.37	4.87	44.15	4.82	1.0

Table 6.17 (Cont.)

Comparison of Theory and Experiment:
Positions and Spacing of On Axis Extrema.
3/16 Inch Diameter Obstacle with 7mm Aperture Separated by 1cm

Measured Starting Position (± .5cm): 50cm

	Experiment		Theory		
Extremum Type	Scale Reading (cm)	Distance from Starting point (cm)	Optical axis Distance (cm)	Distance from Starting Point (cm)	% Difference
Maximum	5.85	0.0	50.34	0.0	--
Minimum	3.20	2.65	52.82	2.48	6.6
Maximum	.64	5.21	55.56	5.22	0.2

Measured Starting Position (± .5cm): 75cm

	Experiment		Theory		
Extremum Type	Scale Reading (cm)	Distance from Starting point (cm)	Optical axis Distance (cm)	Distance from Starting Point (cm)	% Difference
Minimum	4.36	0.0	75.11	0.0	∞
Maximum	.89	3.47	80.82	5.71	28.8

Table 6.18

Comparison of Theory and Experiment:
Positions and Spacing of On Axis Extrema.
3/16 Inch Diameter Obstacle with 5/8 Inch Diameter Aperture
Separated by .25cm. Starting Position = Minimum at 76cm (± .5cm)

	Experiment		Theory		
Extremum Type	Scale Reading (cm)	Distance from Starting point (cm)	Optical axis Distance (cm)	Distance from Starting Point (cm)	% Difference
Minimum	5.34	0.0	75.53	0.0	--
Maximum	4.71	.63	76.16	.63	0.0
Minimum	4.09	1.25	76.81	1.28	2.3
Maximum	3.38	1.96	77.46	1.93	1.6
Minimum	2.74	2.60	78.13	2.60	0.0
Maximum	2.03	3.31	78.81	3.28	0.9
Minimum	1.35	3.99	79.50	3.97	0.5
Maximum	.57	4.77	80.20	4.67	2.1

Table 6.19

Comparison of Theory and Experiment:
Positions and Spacing of On Axis Extrema.
5/16 Inch Diameter Obstacle Centered with 5/8 Inch Diameter Aperture.
Starting Position = Minimum at 60cm (± .5cm)

	Experiment		Theory		
Extremum Type	Scale Reading (cm)	Distance from Starting point (cm)	Optical axis Distance (cm)	Distance from Starting Point (cm)	% Difference
Minimum	5.43	0.0	60.22	0.0	--
Maximum	4.94	.49	60.71	.49	0.0
Minimum	4.43	1.00	61.21	.99	1.0
Maximum	3.94	1.49	61.71	1.49	0.0
Minimum	3.41	2.02	62.23	2.01	0.5
Maximum	2.87	2.56	62.75	2.53	1.2
Minimum	2.35	3.08	63.28	3.06	0.7
Maximum	1.84	3.59	63.82	3.60	0.3
Minimum	1.23	4.20	64.37	4.15	1.2
Maximum	.73	4.70	64.93	4.71	0.2
Minimum	.14	5.29	65.50	5.28	0.2

The above tables show excellent agreement between theory and experiment. Table 6.17 demonstrates the increased spacing between extrema with increased distance along the optical axis. This table had the highest average percent difference as well as the largest

single deviation from theory (almost 30% difference between theory and experiment for the spacing of extrema at 75cm). This table illustrates the major difficulty in measuring the positions of on axis extrema. When the spacing between adjacent maxima and minima is large (more than 2cm), it becomes difficult to judge the exact position of the extremum. The pattern changes so slowly with z translation large amounts of uncertainty in measurements are introduced. This source of potential error can be avoided by limiting measurements to the region on the optical axis where extremum spacing is small. The extent of this region increases with larger aperture size and smaller obscuration ratio.

Verification of Theory for the Aberrated Case

Defocus

Defocus was introduced by axially translating the collimating lens. For each shift of the lens the change in the on-axis position of a minimum of known order was measured. This was possible by shifting the lens in .1mm movements so as to make the resulting on-axis change be less than the spacing between adjacent minima. The aberration coefficient W_{20} for each measurement was calculated from equation IV-28. These points were plotted against the aberration coefficient curve given by equation IV-2. There was an uncertainty of $\pm$ .05cm in the measurements of the on-axis extrema. The error bars based on this uncertainty were included in the plots, but the error range for any

given point is practically negligible.

The following graphs illustrate the comparison of theory and experiment for three cases: The first was a 3/16 inch diameter obstacle with a 7mm diameter aperture. The measurements were based on the 7^{th} order minimum at 75.11cm behind the aperture. The second was a 3/16 inch diameter obstacle with a 10mm diameter aperture. The measurements were based on the 20^{th} order minimum at 76.65cm. The final case involved a 3/16 inch diameter obstacle and a 16mm diameter aperture. The 60^{th} order minimum at 76.69cm was used.

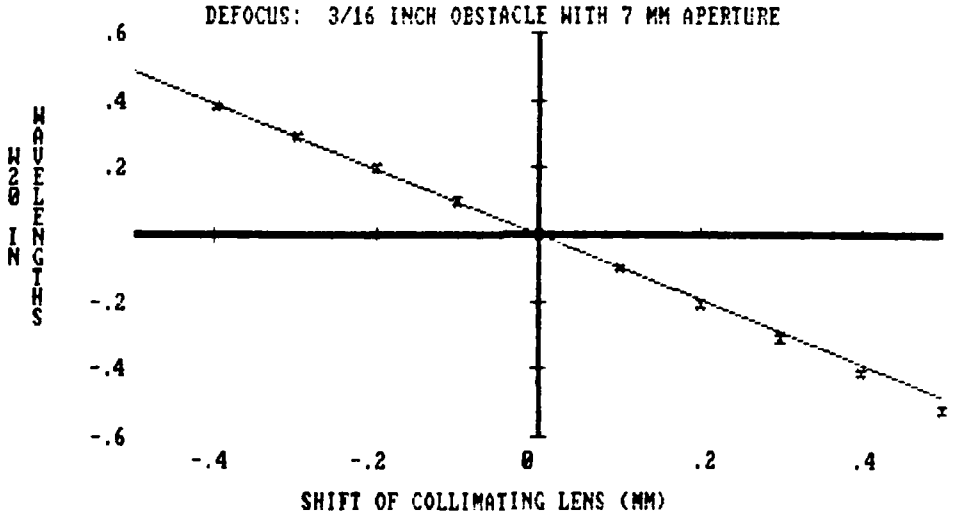

Graph 6.15

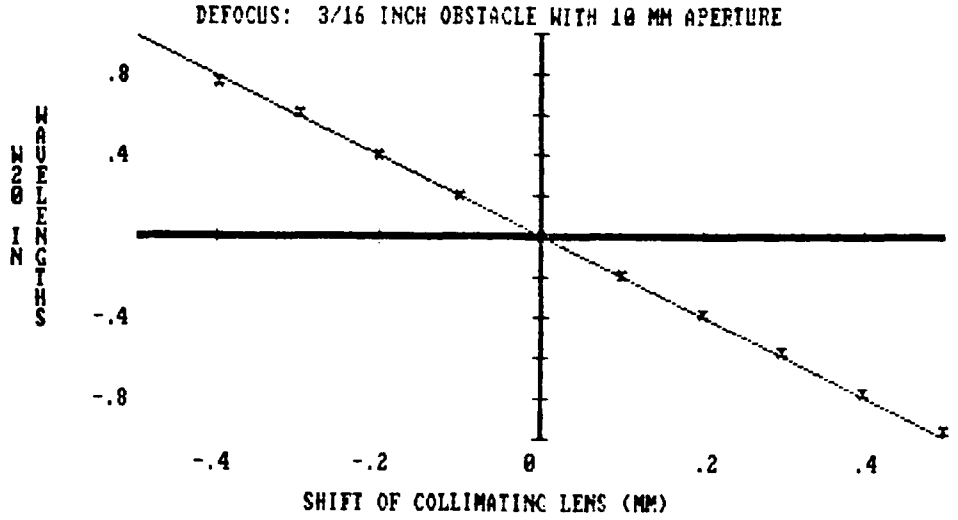

Graph 6.16

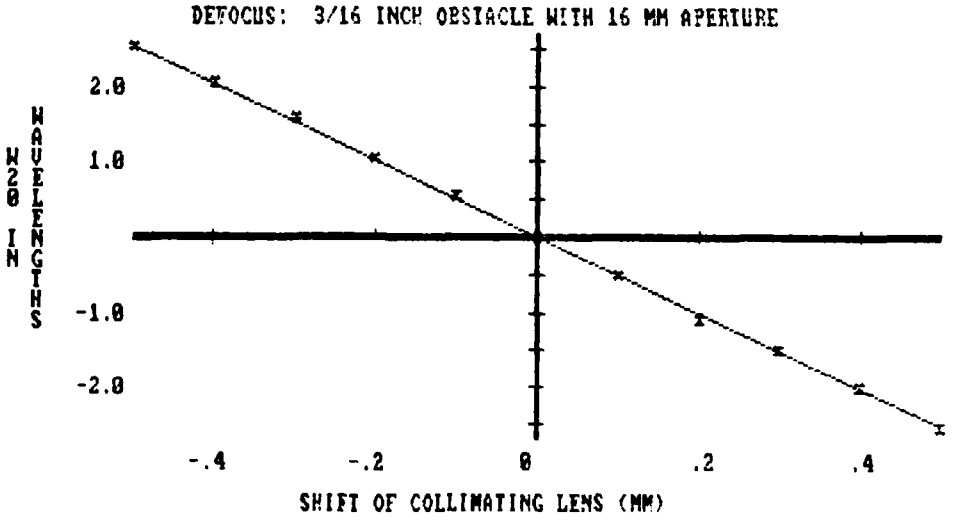

Graph 6.17

The graphs show remarkable agreement between theory and experiment. The shift of extrema on axis is a very effective method of measuring defocus.

Spherical Aberration

The attempts to verify the theory for spherical aberration were mostly unsuccessful. Because the coefficient of spherical aberration is proportional to the fourth power of the diameter of the outer edge of the annular aperture the largest sized apertures were used. A 16mm diameter aperture had W_{40} equal to -.0766 wavelengths when two half inch thick plates were inserted in the system. From equation IV-58, the shift on axis for the n^{th} order maximum with spherical aberration present is:

$$\Delta z = \frac{2W_{40}(1-\varepsilon^4)}{(2n+1)\lambda} z' \qquad \text{(VI-10)}$$

A 1/2 inch diameter obstacle with a 16mm diameter aperture has its 9^{th} order maximum at 1.97m. The addition of two plates will result in a shift of position of nearly 1cm. Even a shift as large as this is hard to distinguish when one considers the distance to the nearest minimum is 8cm. To pinpoint the position of the maximum is very difficult without intensity measurements. The uncertainty is at least on the order of a centimeter. In short, the best case gives a predicted shift less than the experimental error.

Many of the results were conflicting, e.g., the insertion of one plate seemed to move the 11^{th} order maximum at 1.7m a distance of

0.4cm. This gave a value for W_{40} of .043λ -- a 13% error. When remeasured, the shifts for one and two plates appeared to be 1.18cm and 3.1cm, giving values for W_{40} of .127λ and .338λ -- 4 times larger than actual.

Additional uncertainty arose from the need to reposition the collimating lens when a plate was inserted or removed. For each plate the lens had to be moved:[1]

$$d = \frac{n-1}{n} t$$

$$= \frac{1.517-1}{1.517} \quad 1.27\text{cm}$$

$$= .433\text{cm} \qquad \text{(VI-11)}$$

This displacement was verified by observing the size of the beam at various distances along the optical axis, and by observing the interference pattern produced by a shear plate (when the beam is collimated, one obtains a null pattern). As demonstrated in the previous section on defocus, a change in the position of the collimating lens introduces defocus which also shifts the on-axis position of minima. For a 16mm diameter aperture, an error of .1mm in the position of the collimating lens from the proper position will yield a defocus term on the order of .1λ which will shift the positions of extrema at 1.7m by nearly 2cm.

One can introduce a substantial amount of spherical aberration by reversing the achromatic collimating lens. Unfortunately, this involves realigning the system. This technique was considered impractical.

Study of Astigmatism

Circular Aperture

To study the effect of astigmatism on the diffraction pattern of a circular obstacle, a standard had to be established. The 5/16 inch diameter obstacle provided this standard. There were two benefits to using this obstacle. Because this diameter fell in the center of the range of obstacle diameters used (3/16 inch, 5/16 inch and 1/2 inch), one could investigate the change in pattern by increasing or decreasing the diameter. In addition, the diffraction pattern of the 5/16 inch diameter obstacle changed at a convenient rate with the increase of parallel plate tilt angle. An increase of one degree in tilt angle resulted in a noticeable, but not dramatic, change. A series of photographs of degree increments in tilt angle offered a wide spectrum of astigmatic effects and yet allowed one to observe subtle differences.

The following photographs are of a 5/16 inch diameter obstacle observed at 60cm. The first photograph used magnification of 6X and an exposure time of 1/2 seconds. All the other photographs were magnified seven times and had one second exposure times. The astigmatism was produced by two half-inch plane parallel plates. In the range from tilt angles of 10^{o} to 18^{o} photographs were made of plates countertilted and tilted in the same direction. This was to observe whether coma had any effect on the diffraction pattern. Each caption lists the amount of astigmatism present (given by equation VI-3) as well as the upper and lower bounds of the aberration (in parentheses) based upon an uncertainty of $\pm .5^{o}$ in the tilt angle.

Photograph 6.20

0^{o} tilt. $W_{22} = .098\lambda$ $(.097\lambda, .097\lambda)$

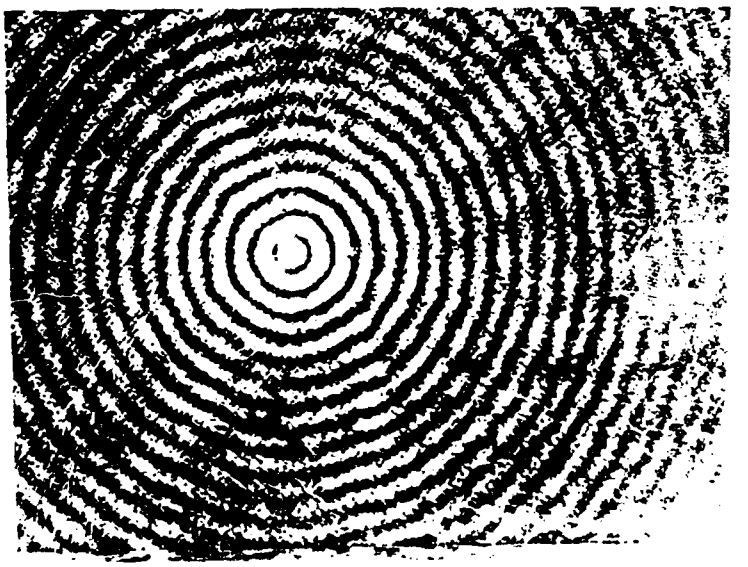

Photograph 6.21

5^{o} countertilt. $W_{22} = .088\lambda$ $(.025\lambda, -.011\lambda)$

Photograph 6.22

10^{o} countertilt. $W_{22} = -.261\lambda$ $(-.226\lambda, -.298\lambda)$

Photograph 6.23

10^{o} tilt same direction. $W_{22} = -.261\lambda$ $(-.226\lambda, -.298\lambda)$

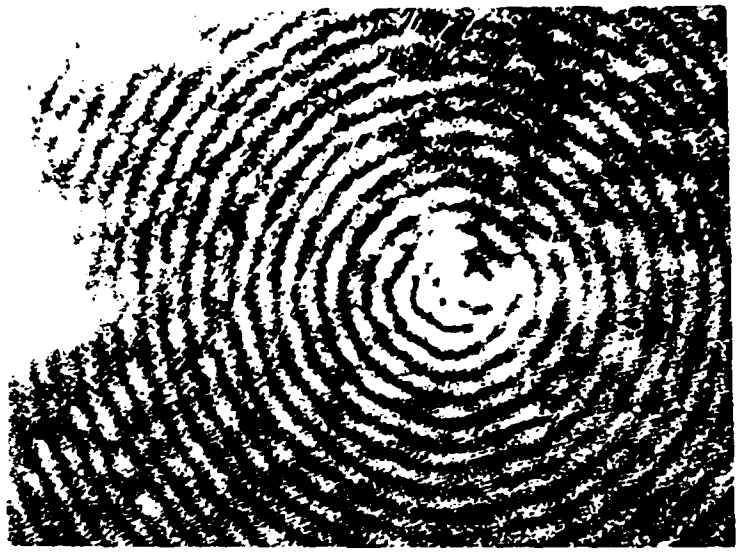

Photograph 6.24

11^{o} countertilt. $W_{22} = -.419\lambda$ $(-.377\lambda, -.463\lambda)$

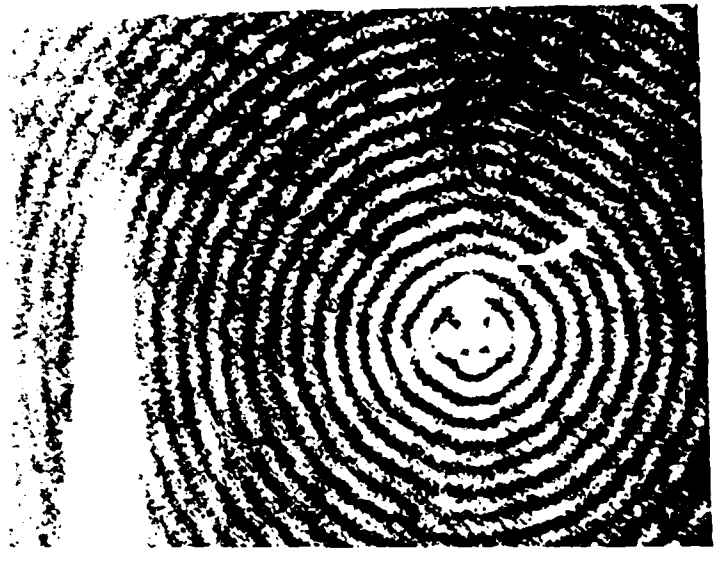

Photograph 6.25

12^{o} tilt same direction. $W_{22} = -.419\lambda$ $(-.377\lambda, -.463\lambda)$

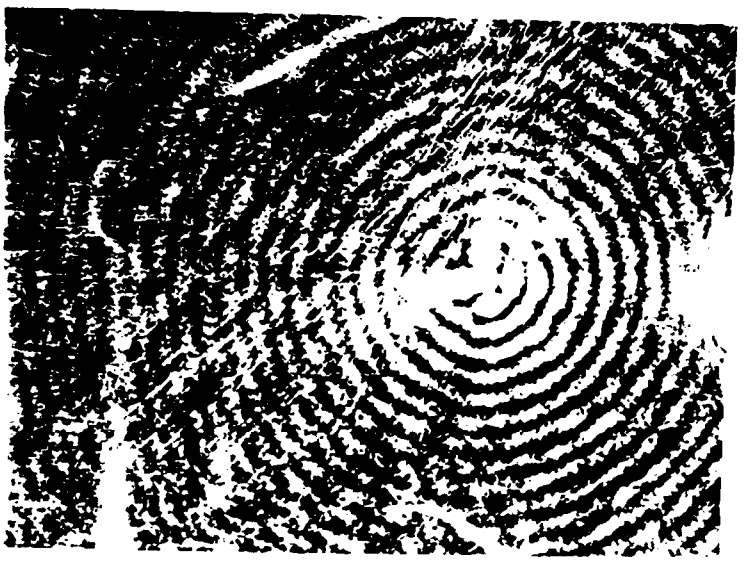

Photograph 6.26

13^{o} countertilt. $W_{22} = -.509\lambda$ ($-.463\lambda$, $-.557\lambda$)

Photograph 6.27

13^{o} tilt same direction. $W_{22} = -.509\lambda$ ($-.463\lambda$, $-.557\lambda$)

Photograph 6.28

14^{o} countertilt. $W_{22} = -.606\lambda$ ($-.557\lambda$, $-.657\lambda$)

Photograph 6.29

14^{o} tilt same direction. $W_{22} = -.606\lambda$ ($-.557\lambda$, $-.657\lambda$)

Photograph 6.30

15^{o} countertilt. $W_{22} = -.710\lambda$ ($-.657\lambda$, $-.765\lambda$)

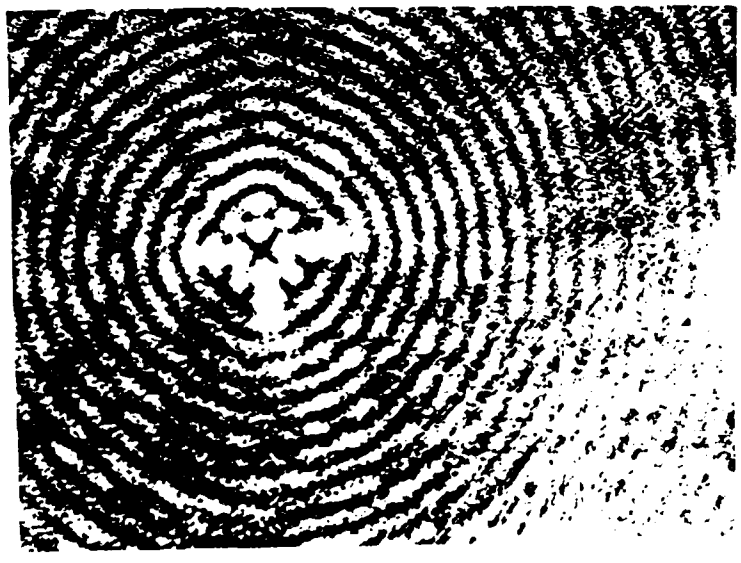

Photograph 6.31

15^{o} tilt same direction. $W_{22} = -.710\lambda$ ($-.657\lambda$, $-.765\lambda$)

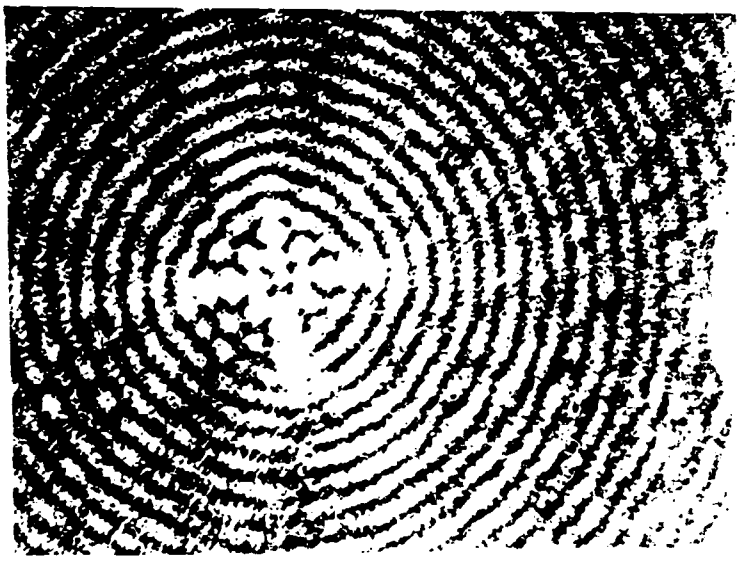

Photograph 6.32

16^{o} countertilt. W_{22} = -.821λ (-.765λ, -.880λ)

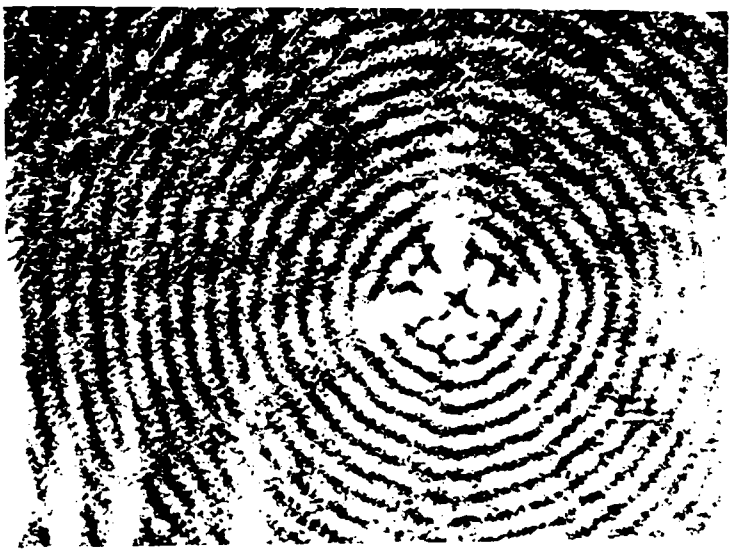

Photograph 6.33

16^{o} tilt same direction. W_{22} = -.821λ (-.765λ, -.880λ)

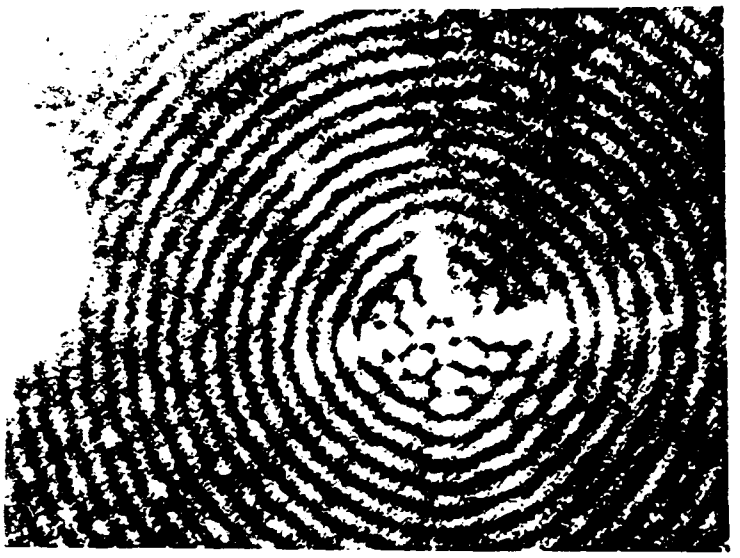

Photograph 6.34

17° countertilt. $W_{22} = -.940\lambda$ ($-.880\lambda$, -1.002λ)

Photograph 6.35

17° tilt same direction. $W_{22} = -.940\lambda$ ($-.880\lambda$, -1.002λ)

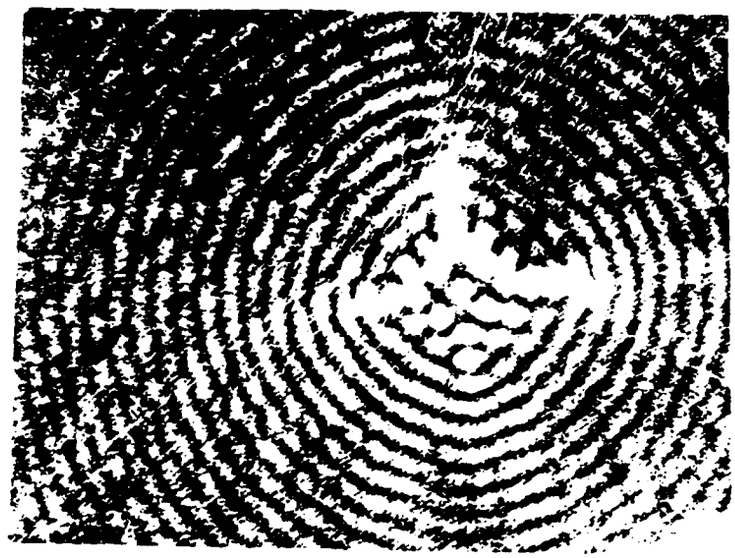

Photograph 6.36

18^{o} countertilt. $W_{22} = -1.065\lambda$ $(-1.002\lambda, -1.131\lambda)$

Photograph 6.37

18^{o} tilt same direction. $W_{22} = -1.065\lambda$ $(-1.002\lambda, -1.131\lambda)$

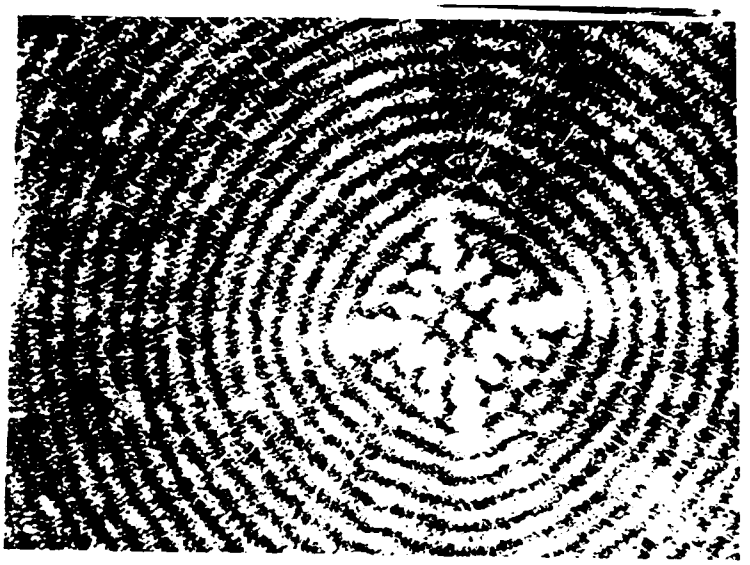

Photograph 6.38

19° countertilt. W_{22} = -1.198λ (-1.131λ, -1.267λ)

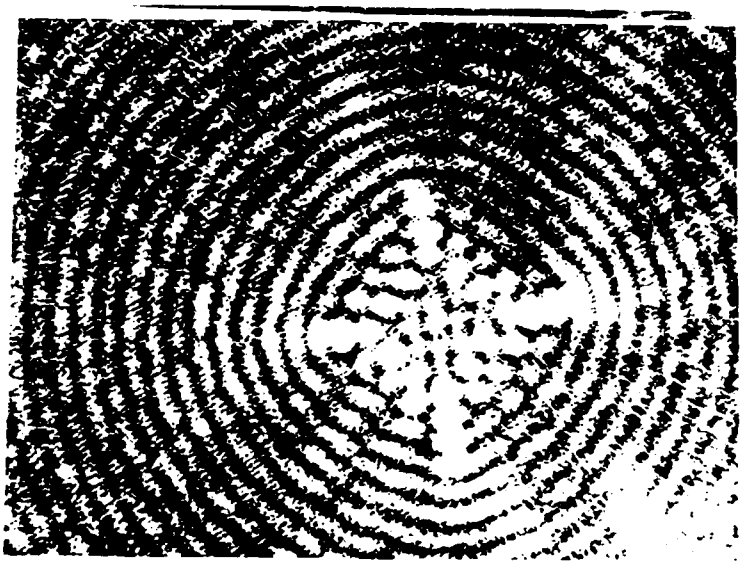

Photograph 6.39

20° countertilt. W_{22} = -1.338λ (-1.267λ, -1.411λ)

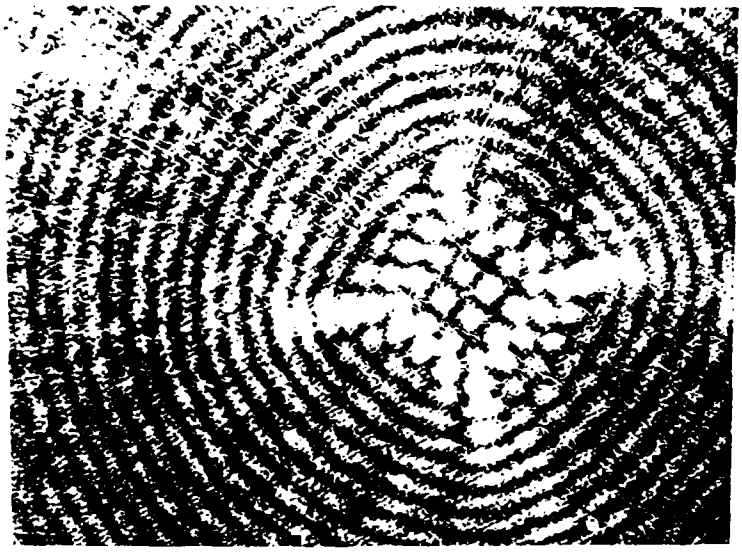

Photograph 6.40

21° countertilt. W_{22} = -1.485λ (-1.411λ, -1.562λ)

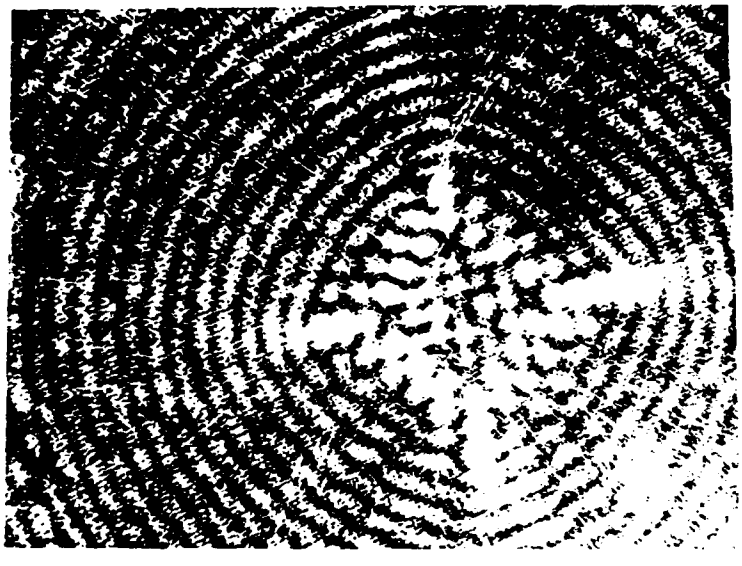

Photograph 6.41

22° countertilt. W_{22} = -1.640λ (-1.562λ, -1.720λ)

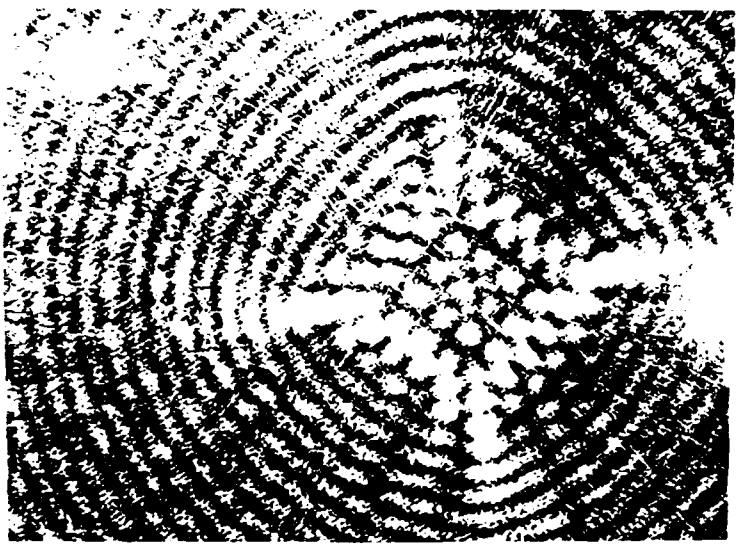

Photograph 6.42

23° countertilt. W_{22} = -1.801λ (-1.720λ, -1.885λ)

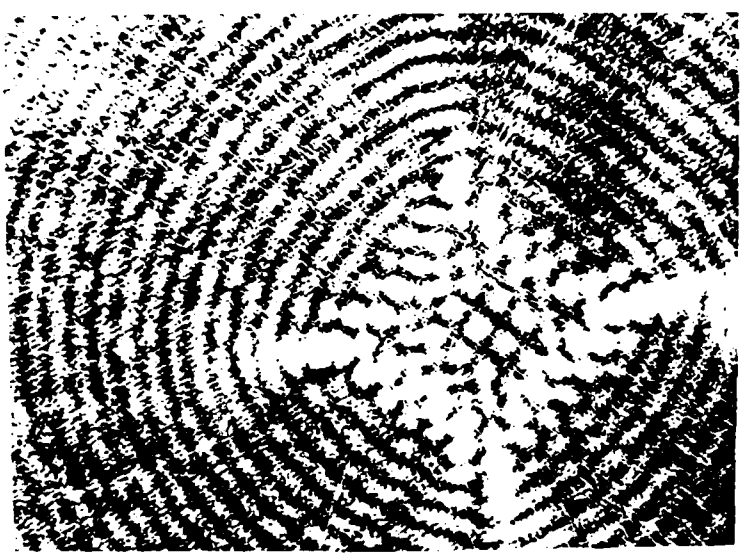

Photograph 6.43

24° countertilt. W_{22} = -1.970λ (-1.885λ, -2.057λ)

Photograph 6.44

25° countertilt. W_{22} = -2.146λ (-2.057λ, -2.237λ)

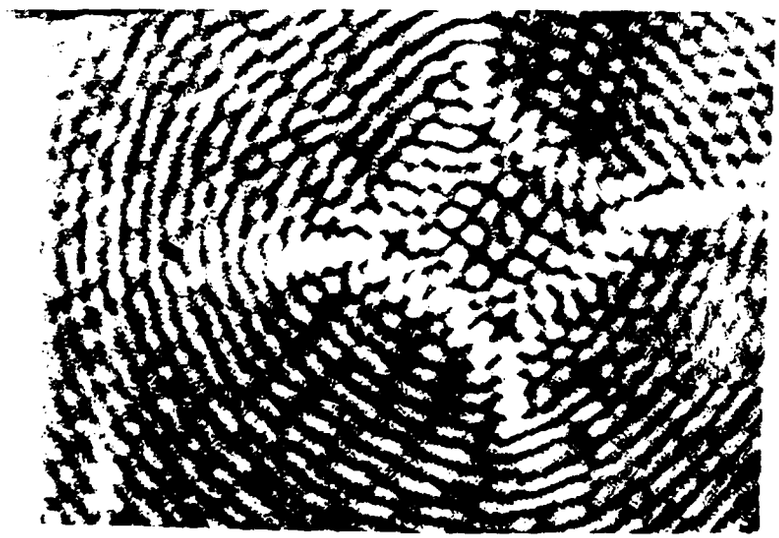

Photograph 6.45

26° countertilt. W_{22} = -2.329λ (-2.237λ, -2.423λ)

Photograph 6.46

27° countertilt. W_{20} = -2.519λ (-2.423λ, -2.617λ)

Photograph 6.47

28° countertilt. W_{20} = -2.717λ (-2.617λ, -2.818λ)

Photograph 6.48

29° countertilt. W_{22} = -2.921λ (-2.818λ, -3.026λ)

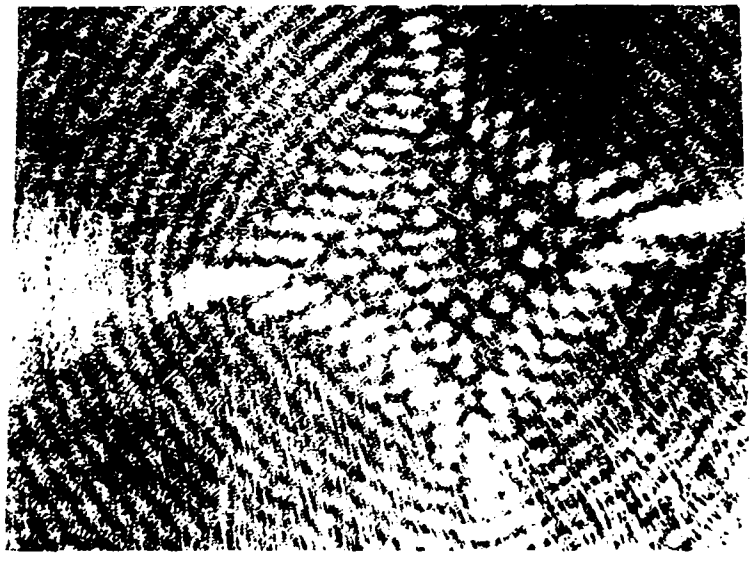

Photograph 6.49

30° countertilt. W_{22} = -3.133λ (-3.026λ, -3.242λ)

There are a number of important features in these photographs. The first thing one notices is the lack of distinction between patterns produced by countertilting or tilting in the same direction. Coma has no noticable effect on the images. This may be due to the difference in magnitude. At 18° tilt the amount of astigmatism is -1.065λ. The amount of coma at that same angle is a mere $-.135\lambda$. Astigmatism breaks up the ring structure into separate nodules. The disintegration of the rings begins in the center of the diffraction pattern. The greater the amount of astigmatism the greater the number of fractured rings.

A ring will break up in a predictable way. If the number of the ring (counting from the center) is n, then the ring will split into 4n nodules and form a square of n + 1 nodules per side.

To describe the process of ring break up, it is convenient to define some new terms. The first effect of astigmatism on a given ring is to distort it from its circular shape. The ring is pushed out at points on the top and bottom and left and right. These points are spaced by right angles. As such, they suggest the directions north, south, east and west, and will be referred to as **compass points.** The compass point at the top of the photograph (the arbitrary "up" direction) will be designated **north.** A ring exhibiting departure from circular shape with the appearance of compass points will be said to be **distorted.**

After the ring becomes distorted, an increase in astigmatism will cause **lobing.** The width of the ring is no longer uniform, but concentrated in regions which will become **nodules** -- remnants of the ring

when finally and fully split. The actual point of **ring break-up** will be defined as when at least half of the ring is established into separate nodules. The region inside the most newly broken ring will be called the **aberrated area.**

The analysis of some sample photographs will fortify these concepts. Photograph 6.20 (0^{o} tilt) shows the first ring slightly distorted. This is evidence of presence of background (positive) astigmatism. Photograph 6.21 is a very symmetric set of concentric rings indicating near absence of astigmatism. Photographs 6.22 through 6.27 chronicle the increased lobing in the first ring to eventual ring break-up at 13^{o} tilt. The difference between lobing and ring break-up is seen in photographs 6.38 and 6.39. At 19^{o} tilt the fourth ring shows definite lobing. At 20^{o} tilt the fourth ring has broken up into distinct nodules. Notice that for large amounts of astigmatism (over 1λ), distortion extends far beyond the region of broken rings.

The breakup of the ring structure has a linear dependence on the amount of astigmatism at the outer edge of the obstacle (W_{22}). A review of the photographs shows the first ring disintegrates between 12^{o} and 13^{o} tilt. The table below lists the angles for which different rings break up. If one plots the ring number versus the aberration coefficient W_{20} at which the ring breaks up, one sees the linear relationship. (The error bars represent the $\pm$ $.5^{o}$ tilt angle uncertainty.) This plot, though, is misleading. The abscissa is uniformly spaced. Spatially the rings are not evenly distributed. Plotting the required astigmatism at ring breakup as a function of

the radial distance from the center of the spot provides a much better perspective on the domain of influence of the aberration.

Table 6.20

Required Countertilt Angles for Diffraction Pattern Ring Break-up

Ring Number	Tilt Angle	W_{22} (wavelengths)
1	12 - 13°	-.419 - -.509
2	15°	-.710
3	18°	-1.065
4	20°	-1.338
5	22°	-1.64
6	24°	-1.97
7	25°	-2.146
8	27°	-2.519
9	29°	-2.921

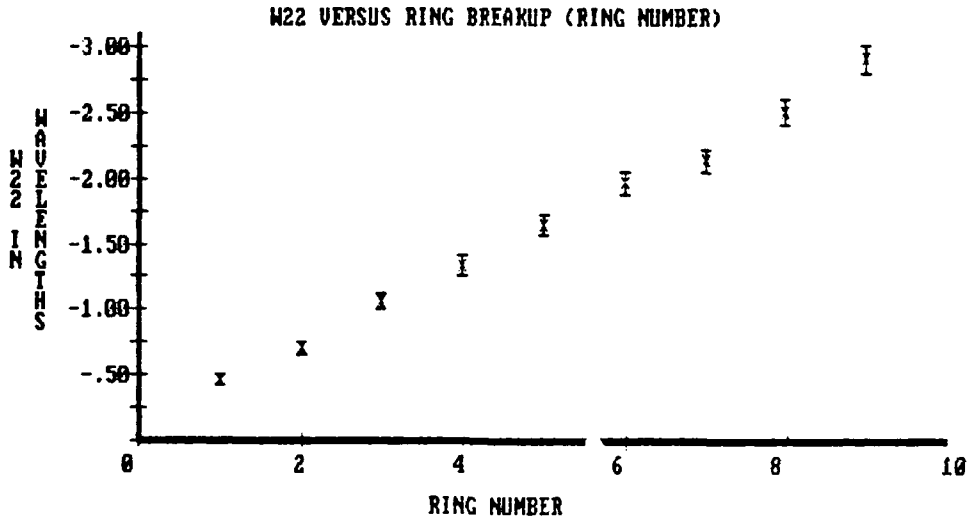

Graph 6.18

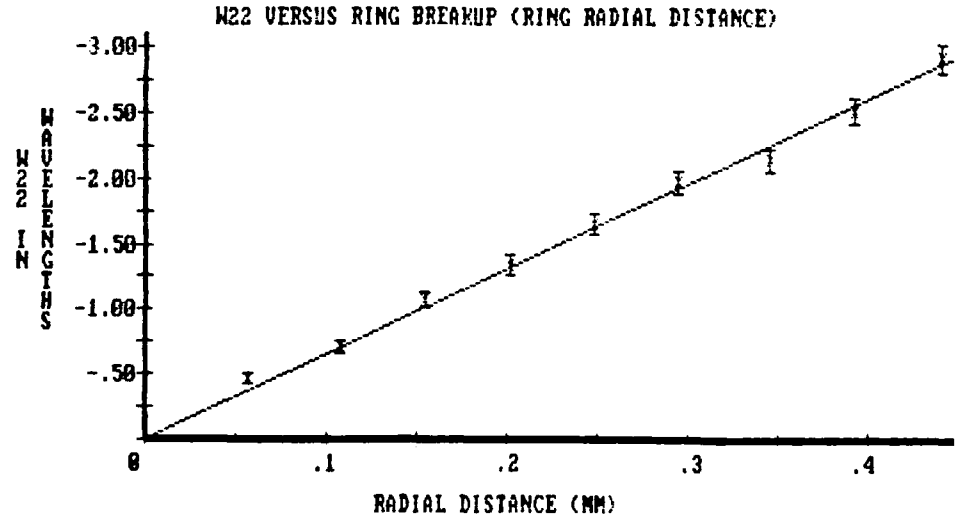

Graph 6.19

The plotted line is the best fit to the data by minimizing the root mean square deviation. One can multiply the radial distance by the constant kd/2z and obtain the argument for the J_0 Bessel function for the unaberrated case. A graph of W_{22} as a function of the Bessel function argument appears below. Graphs 6.19 and 6.20 demonstrate the radius of the region of ring break-up expands linearly with increased

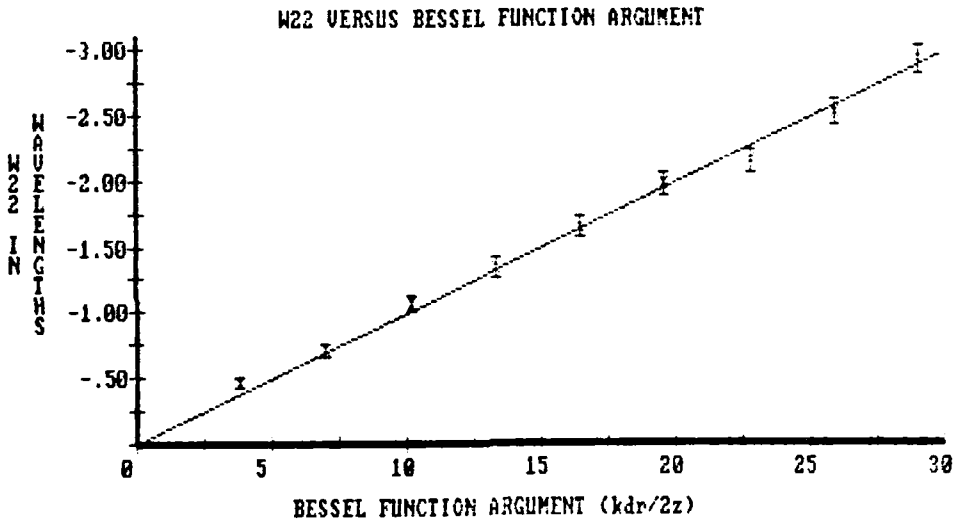

Graph 6.20

astigmatism. In particular when the aberration coefficient W_{22} corresponds to a parameter $x = \frac{kdr}{2z}$ which is a maximum of $J_0(x)$, the ring at distance r will break up.

The position of the outermost broken ring is a very noticable and convenient measure of astigmatism present in the incident beam. There are, however, subtle astigmatic effects which bear mention. In the unaberrated diffraction pattern the region of highest intensity is the

central spot. As astigmatism is introduced this region moves out from the center. For example, Photographs 6.24 through 6.29 chronicle the shift of maximum intensity from the center to the first (broken) ring. At $W_{22} = -.71\lambda$ (Photograph 6.30) the central spot has entirely disappeared. Photographs 6.34 and 6.35 show at $W_{22} = -.94\lambda$ the second (broken) ring is becoming the most intense area. The central spot is reappearing and the first ring is dimming. At $W_{22} = -1.065\lambda$ (Photograph 6.36), the third ring has split, the second ring is the most intense, the first ring has disappeared and the central maximum is bright. This pattern continues through the remaining photographs. As the amount of astigmatism increases the area of greatest intensity spreads out from the center like the crest of a wave. Ahead of this crest distortion occurs and immediately in front of it ring break-up takes place. This crest is composed of either one or two rings. Immediately behind this maximum intensity "wave," there is a dark region. The broken rings left behind by the crest form a checkerboard pattern. The center and even rings, and the odd rings wax and wane alternately. All these areas of the pattern are characteristic of the amount of astigmatism present. This will be important when studying the diffraction patterns of annular apertures where only the region around the central spot remains intact.

The central spot first becomes dark when $W_{22} = -.71\lambda$. The cycle of having a dark center occurs with added multiples of $-.808\lambda$ ($\pm .035\lambda$).

An interesting feature of Photographs 6.40 - 6.49 is the concentration of intensity at the compass points of distorted rings. This concentration extends beyond the region where ring break-up takes

place. The ultimate astigmatic diffraction pattern seems to be a bright diamond outline with spikes at the compass points.

The photographed patterns seem to be slightly canted. Using the compass analogy, they don't point to true north. A certain amount of the angular deviation may stem from the optics of the Bausch and Lomb stereo viewer. However, photographs taken using just a mounted camera back also revealed a slight angle of tilt. The origin of this tilt may lie in the background astigmatism. The orientations of the planes of symmetry of the astigmatism produced by the plane parallel plates lie in the vertical and horizontal directions. The background astigmatism is not necessarily oriented in these directions. The diffraction patterns are the result of the combination of these two aberration sources. A difference in orientations may create a tilted pattern. If this is true and if the tilt angle is characteristic of the individual orientations, this may provide the means of determining an unknown angle of orientation. One could introduce astigmatism of known orientation and observe the combination.

The diffraction pattern behind a circular obstacle for the unaberrated case does not change shape when viewed at different optical axis distances. The pattern with astigmatism present is also constant in shape. The following photographs show the diffraction patterns for three different distances, .35m, .60m and 3m. The first photograph was taken with magnification 7X; the remaining two with magnification 6X. The patterns are identical.

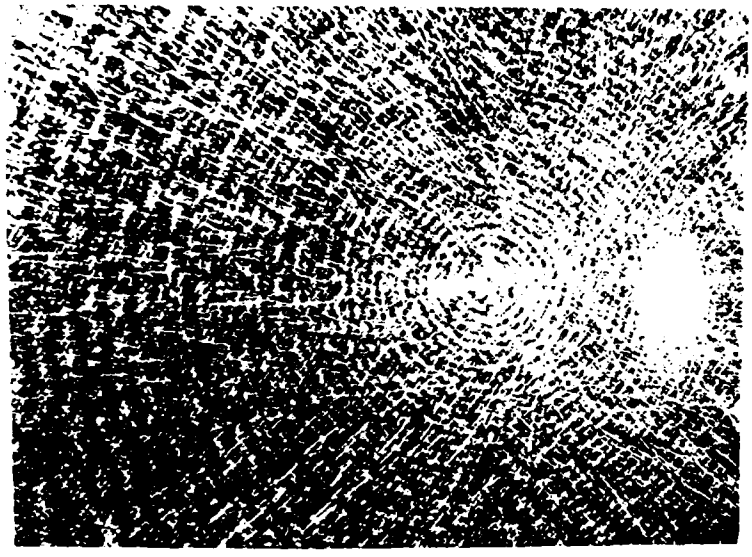

Photograph 6.50

.35m behind 5/16" diameter obstacle.
15° countertilt. W_{22} = -.701λ. 1/2 sec. exposure.

Photograph 6.51

.60m behind 5/16" diameter obstacle.
15° countertilt. W_{22} = -.701λ. 1/2 sec. exposure.

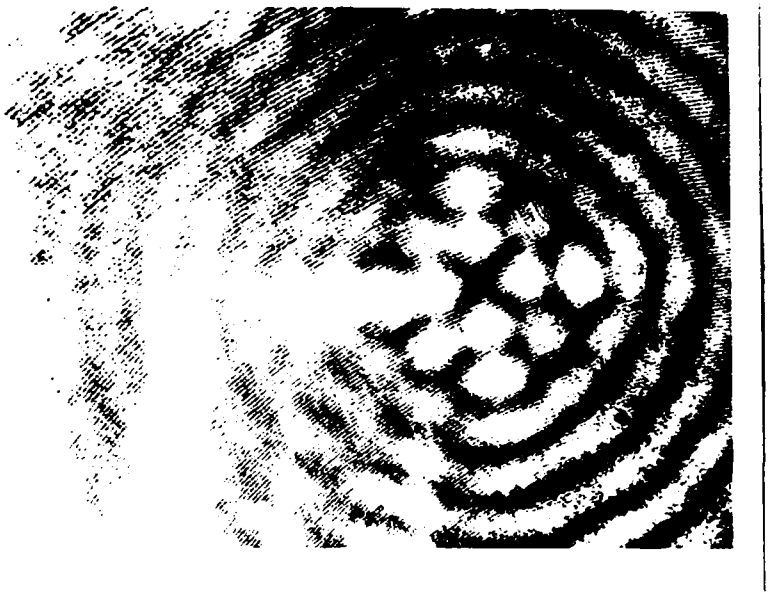

Photograph 6.52

3m behind 5/16" diameter obstacle.
15° countertilt. $W_{22} = -.701\lambda$. 1/2 sec. exposure.

The fact the shape of the diffraction pattern for the circular obstacle is independent of optical axis distance z means Graph 6.20 (W_{22} as a function of the Bessel function argument kdr/2z) is valid for all z. One can determine the amount of astigmatism present by observing the pattern for a given obstacle at any distance.

Research reveals that the shape of the diffraction pattern is also independent of obstacle diameter. What determines the eventual diffraction image is the amount of astigmatism at the edge of the obstacle (W_{22}). The following photographs of patterns produced by the 3/16 inch and 1/2 inch diameter obstacles demonstrate this. The first two photographs show patterns very similar to Photograph 6.30

(W_{22} = -.701λ). The remaining two photographs correspond closely to Photograph 6.40 (W_{22} = -1.485λ).

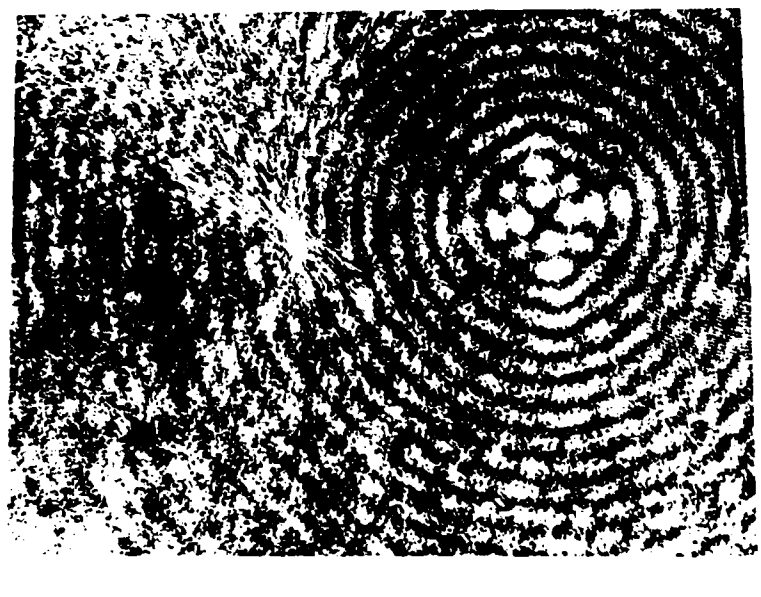

Photograph 6.53

.60m behind 3/16" diameter obstacle. 24° countertilt.
W_{22} = -.647λ (-.616λ, -.678λ), Magnification 6X. 1/4 sec. exposure.

Photograph 6.54

3m behind 1/2" diameter obstacle. 9° countertilt.
W_{22} = -.647λ (-.566λ, -.732λ), Magnification 4X. 1/2 sec. exposure.

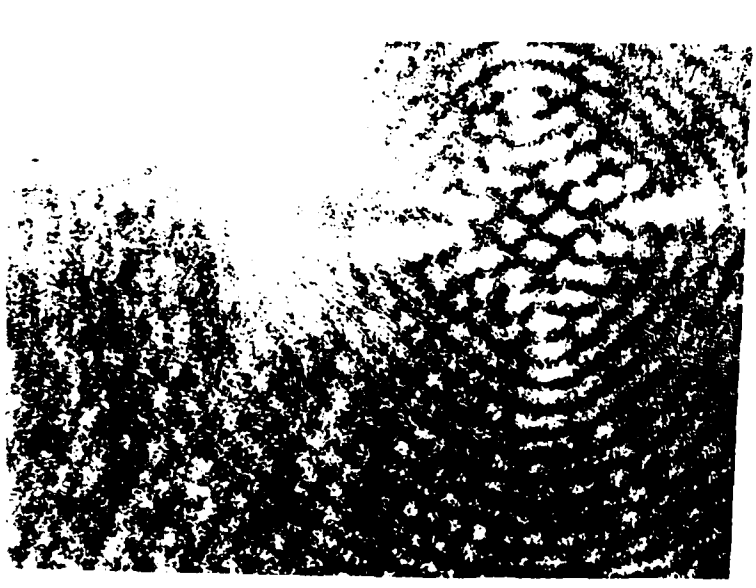

Photograph 6.55

.50m behind 3/16" diameter obstacle. 35° countertilt.
W_{22} = -1.485λ (-1.441λ, -1.531λ), Magnification 6X. 1/8 sec. exposure.

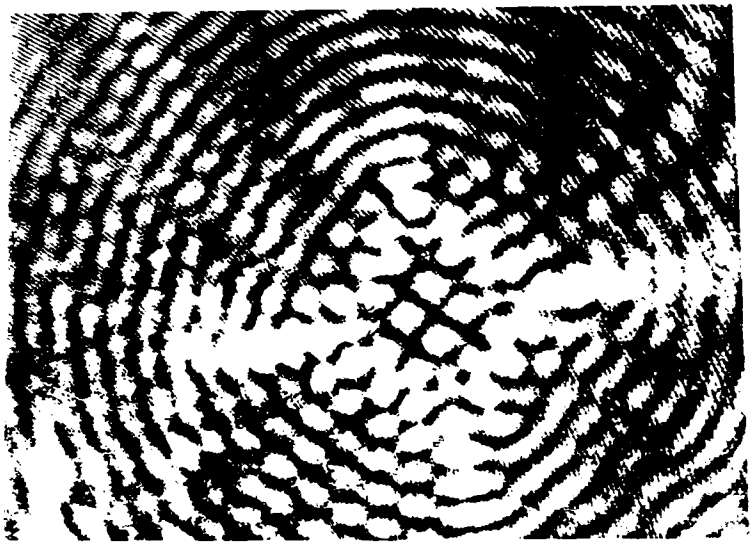

Photograph 6.56

3m behind 1/2" diameter obstacle. 13° countertilt.
W_{22} = -1.455λ (-1.338λ, -1.577λ), Magnification 6X. 1/2 sec. exposure.

There is close agreement in the amount of astigmatism for the three obstacle diameters. The first series of photographs give W_{22} within .05λ and the second series within .03λ. Comparisons of photographs not reproduced here gave results consistently within .05λ.

There is an obvious application of the above. A catalog of diffraction patterns for some arbitrary obstacle diameter with the corresponding amounts of astigmatism can be produced very simply. (For example, Photographs 6.20 - 6.49 could be used.) To find the amount of astigmatism in a test beam, one need only compare the diffraction pattern behind any sized circular obstacle to those in the catalog. The coefficient W_{22} is readily determined.

Annular Aperture

The diffraction pattern behind an annular aperture is a combination of diffraction effects from the inner and outer edges. Each edge contributes its own Arago spot and ring pattern. It is instructive to purposely offset the two patterns and observe how each changes when astigmatism is introduced. The following series of photographs shows the diffraction patterns of a 1/2 inch diameter obstacle with a 5/8 inch diameter aperture separated by 1.1cm. The spot on the left is that produced by the aperture. All the photographs were taken at a viewing distance of 2 meters and magnified four times with exposure times of 1 second.

Photograph 6.57

1/2 diameter obstacle with 5/8" diameter aperture.
5^{o} countertilt.

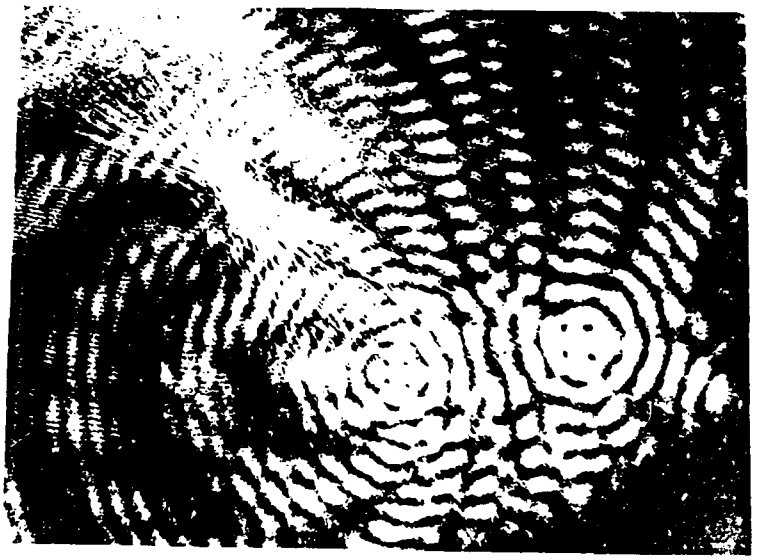

Photograph 6.58

1/2" diameter obstacle with 5/8" diameter aperture.
6^{o} countertilt.

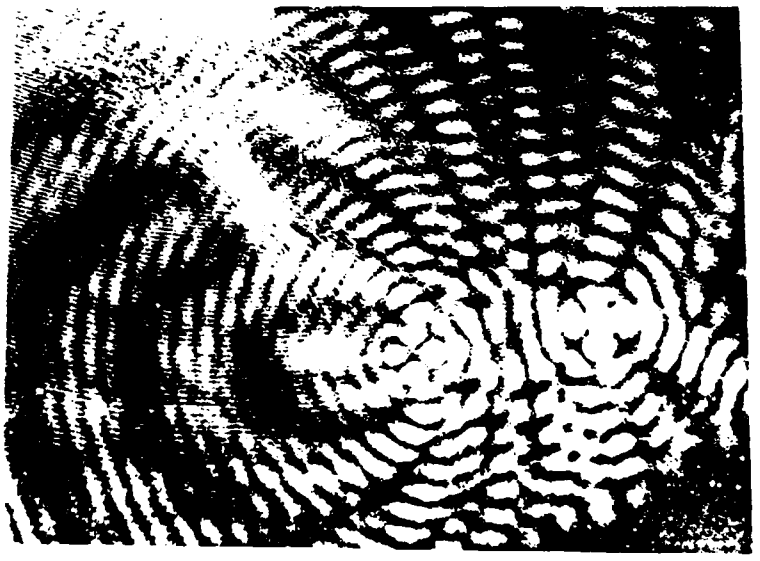

Photograph 6.59

1/2" diameter obstacle with 5/8" diameter aperture.
7^{o} countertilt.

Photograph 6.60

1/2" diameter obstacle with 5/8" diameter aperture.
8° countertilt.

Photograph 6.61

1/2" diameter obstacle with 5/8" diameter aperture.
9° countertilt.

Photograph 6.62

1/2" diameter obstacle with 5/8" diameter aperture.
10° countertilt.

The table below compares the coefficients of astigmatism from the above photographs to the coefficients from similar patterns from the circular obstacle case.

Table 6.21

Astigmatism Coefficients of Off-set Diffraction Patterns

1/2" obstacle		5/16" obstacle comparison	
Countertilt Angle	W_{22} (wavelength)	Countertilt Angle	W_{22} (wavelength)
6°	-.233	10°	-.261
7°	-.352	11°	-.337
8°	-.492	13°	-.509
9°	-.647	15°	-.710
10°	-.821	17°	-.940

5/8" aperture		5/16" obstacle comparison	
Countertilt Angle	W_{22} (wavelength)	Countertilt Angle	W_{22} (wavelength)
6°	-.419	12°	-.419
7°	-.606	14°	-.606
9°	-1.065	19°	-1.198

(The diffraction patterns from the aperture for countertilt angles of 8° and 10° could not be determined.) The individual patterns are

characteristic of the different amounts of astigmatism at the inner and outer edges of the aperture.

A system containing an annular aperture will have offset edge diffraction patterns unless the obstacle is perfectly centered in the aperture. If the purpose of the obstacle is to produce a pattern to measure the degree of astigmatism in a test beam, a separation of the two diffraction images may be desired. The two patterns provide a double measurement for astigmatism.

As seen in Photographs 6.60 and 6.62, when the offset patterns are close and the amount of astigmatism large a great deal of interference occurs. This interference is the source of the very complex structures are observed when an astigmatic beam illuminates a perfectly centered annular aperture. The following photographs show diffraction patterns produced by a variety of annular apertures.

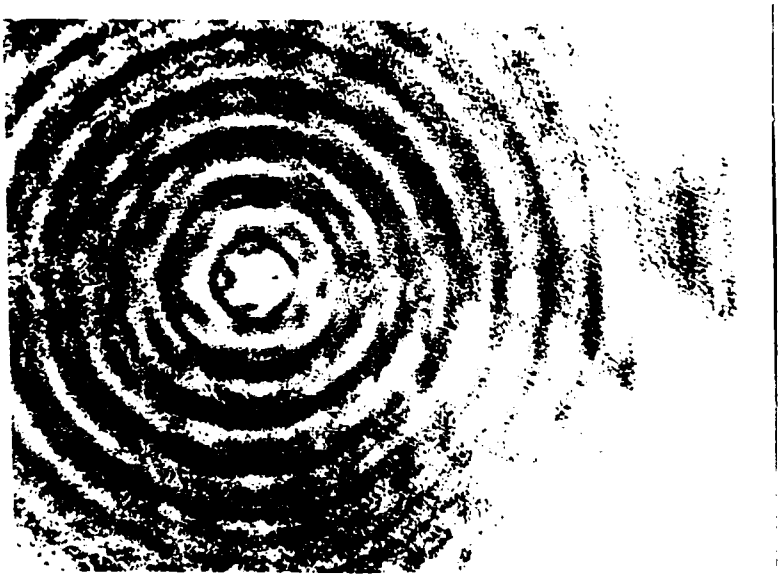

Photograph 6.63
3/16" diameter obstacle with 5/8" diameter aperture.
ε = .3. Viewing distance: 2 - 2.2m. Magnification 4X.
Exposure time 1/4 second. 7° countertilt. Minimum on axis.

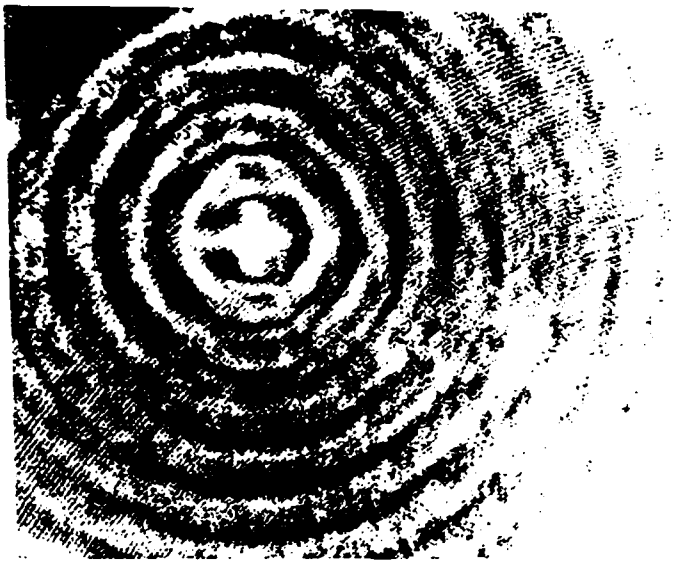

Photograph 6.64
3/16" diameter obstacle with 5/8" diameter aperture.
ε = .3. Viewing distance: 2 - 2.2m. Magnification 4X.
Exposure time 1/4 second. 7° countertilt. Maximum on axis.

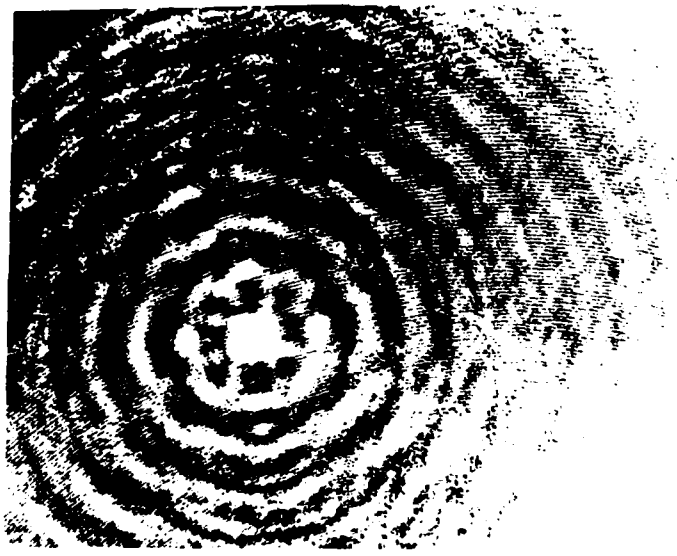

Photograph 6.65
3/16" diameter obstacle with 5/8" diameter aperture.
ε = .3. Viewing distance: 2 - 2.2m. Magnification 4X.
Exposure time 1/4 second. 10° countertilt. Minimum on axis.

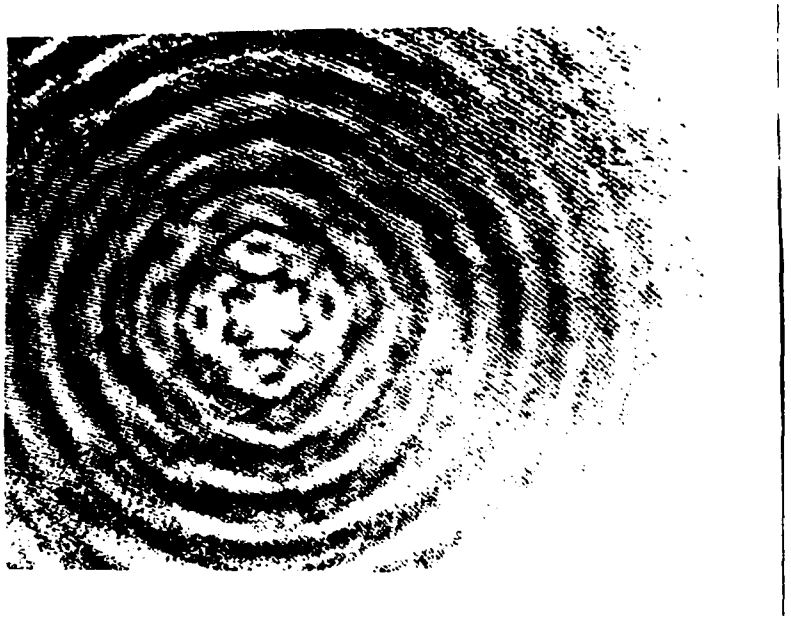

Photograph 6.66
3/16" diameter obstacle with 5/8" diameter aperture.
ε = .3. Viewing distance: 2 - 2.2m. Magnification 4X.
Exposure time 1/4 second. 10^{o} countertilt. Maximum on axis.

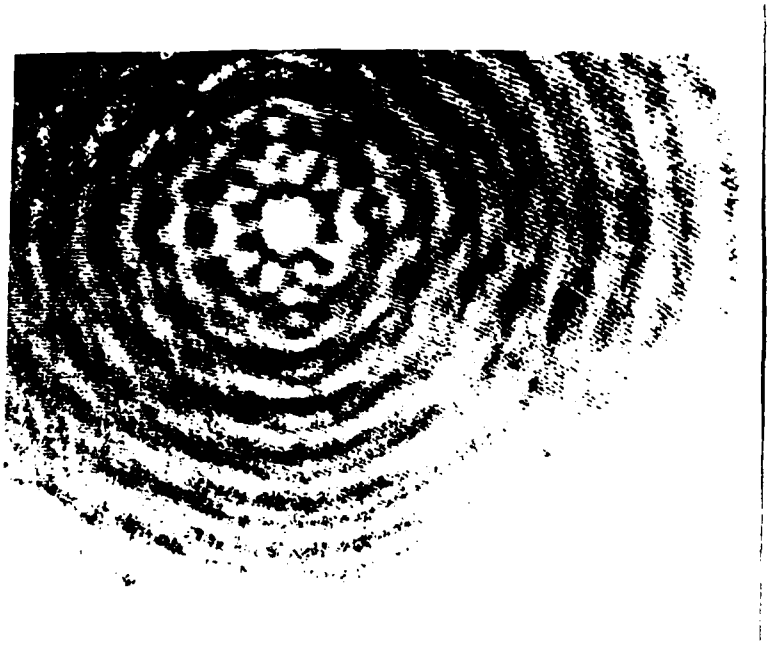

Photograph 6.67
3/16" diameter obstacle with 5/8" diameter aperture.
ε = .3. Viewing distance: 2 - 2.2m. Magnification 4X.
Exposure time 1/4 second. 12^{o} countertilt. Minimum on axis.

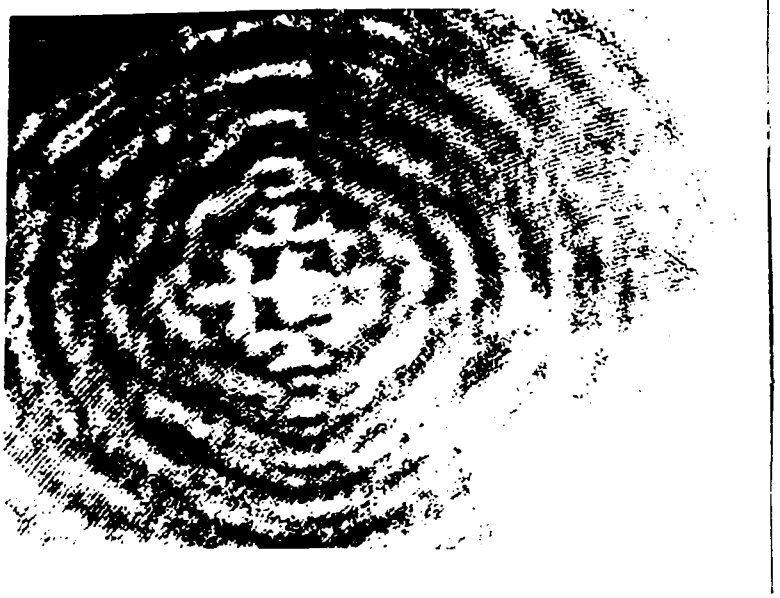

Photograph 6.68
3/16" diameter obstacle with 5/8" diameter aperture.
ε = .3. Viewing distance: 2 - 2.2m. Magnification 4X.
Exposure time 1/4 second. 12^{o} countertilt. Maximum on axis.

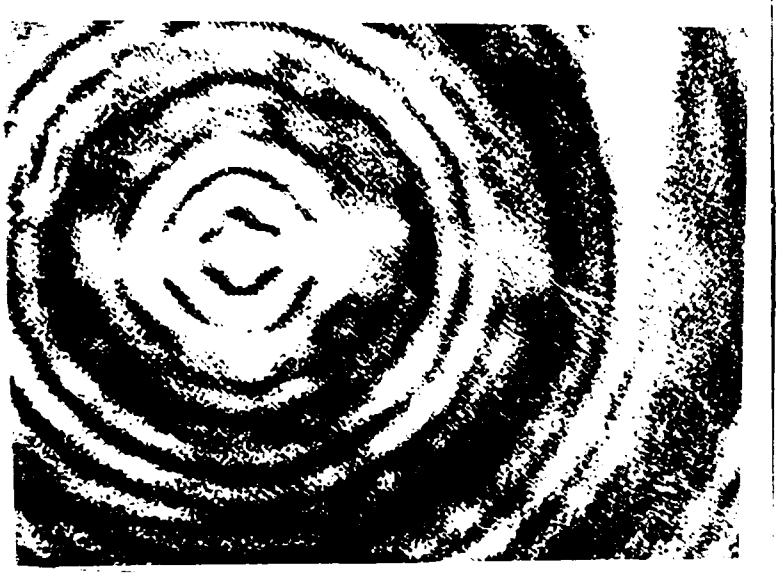

Photograph 6.69
5/16" diameter obstacle with 1/2" diameter aperture.
ε = .625. Viewing distance: 2 - 2.05m. Magnification 6X.
Exposure time 1 second. 10^{o} countertilt. Minimum on axis.

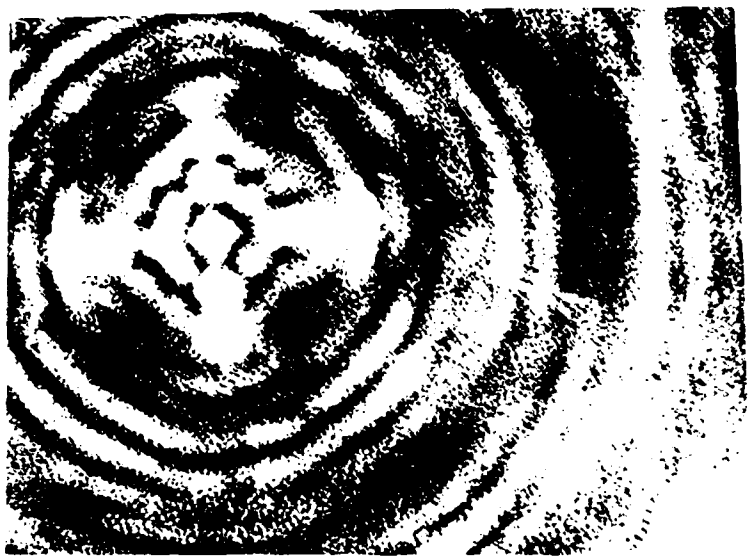

Photograph 6.70
5/16" diameter obstacle with 1/2" diameter aperture.
ε = .625. Viewing distance: 2 - 2.05m. Magnification 6X.
Exposure time 1 second. 11° countertilt. Maximum on axis.

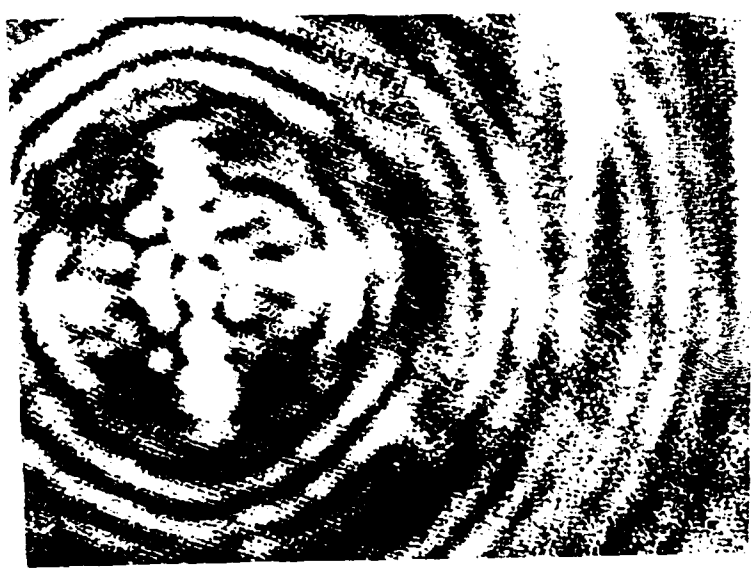

Photograph 6.71
5/16" diameter obstacle with 1/2" diameter aperture.
ε = .625. Viewing distance: 2 - 2.05m. Magnification 6X.
Exposure time 1 second. 12° countertilt. Maximum on axis.

Photograph 6.72
5/16" diameter obstacle with 1/2" diameter aperture.
ε = .625. Viewing distance: 2 - 2.05m. Magnification 6X.
Exposure time 1 second. 13^{o} countertilt. Minimum on axis.

Photograph 6.73
5/16" diameter obstacle with 1/2" diameter aperture.
ε = .625. Viewing distance: 2 - 2.05m. Magnification 6X.
Exposure time 1 second. 13^{o} countertilt. Maximum on axis.

Photograph 6.74
5/16" diameter obstacle with 1/2" diameter aperture.
ε = .625. Viewing distance: 2 - 2.05m. Magnification 6X.
Exposure time 1 second. 14° countertilt. Minimum on axis.

Photograph 6.75
5/16" diameter obstacle with 1/2" diameter aperture.
ε = .625. Viewing distance: 2 - 2.05m. Magnification 6X.
Exposure time 1 second. 14° countertilt. Maximum on axis.

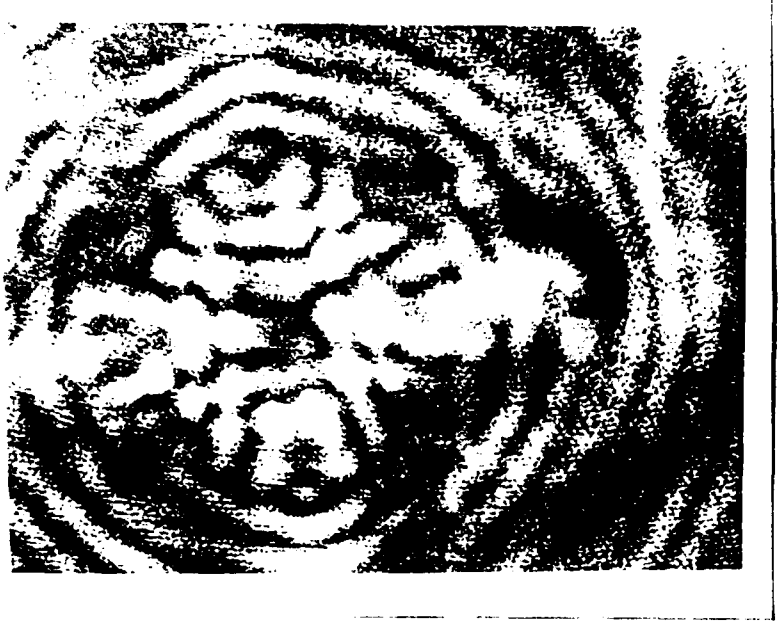

Photograph 6.76
5/16" diameter obstacle with 1/2" diameter aperture.
ε = .625. Viewing distance: 2 - 2.05m. Magnification 6X.
Exposure time 1 second. 15° countertilt. Minimum on axis.

Photograph 6.77
5/16" diameter obstacle with 1/2" diameter aperture.
ε = .625. Viewing distance: 2 - 2.05m. Magnification 6X.
Exposure time 1 second. 15° countertilt. Maximum on axis.

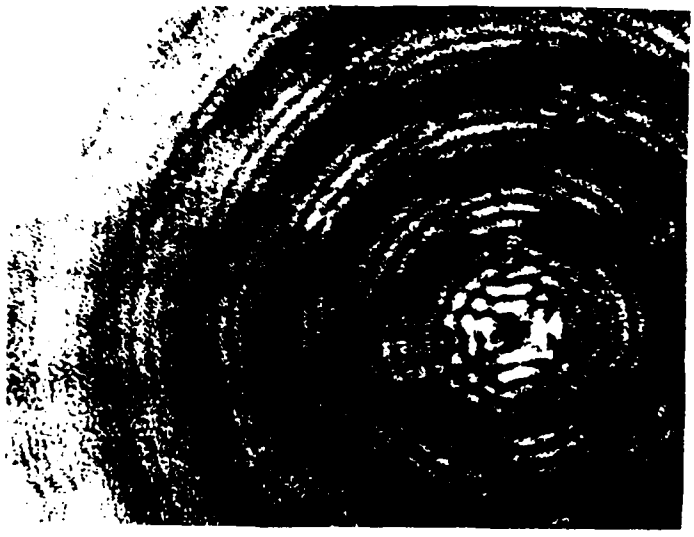

Photograph 6.78
3/16" diameter obstacle with 7mm diameter aperture.
= .68. Viewing distance: .6 - .65m. Magnification 4X.
Exposure time 1 second. 22° countertilt. Minimum on axis.

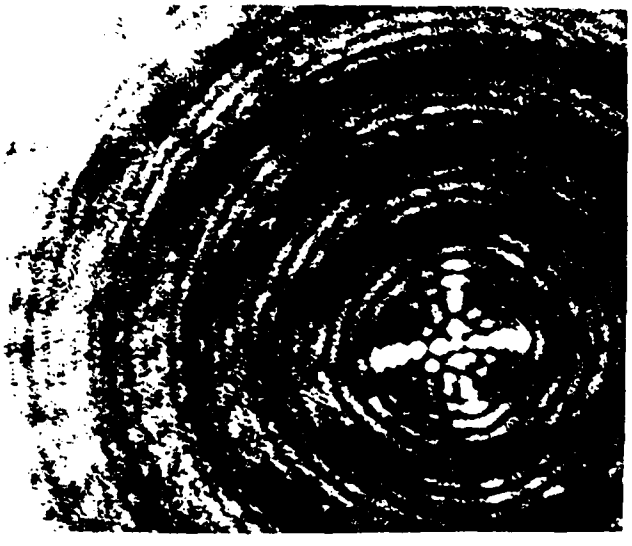

Photograph 6.79
3/16" diameter obstacle with 7mm diameter aperture.
ε = .68. Viewing distance: .6 - .65m. Magnification 4X.
Exposure time 1 second. 22° countertilt. Maximum on axis.

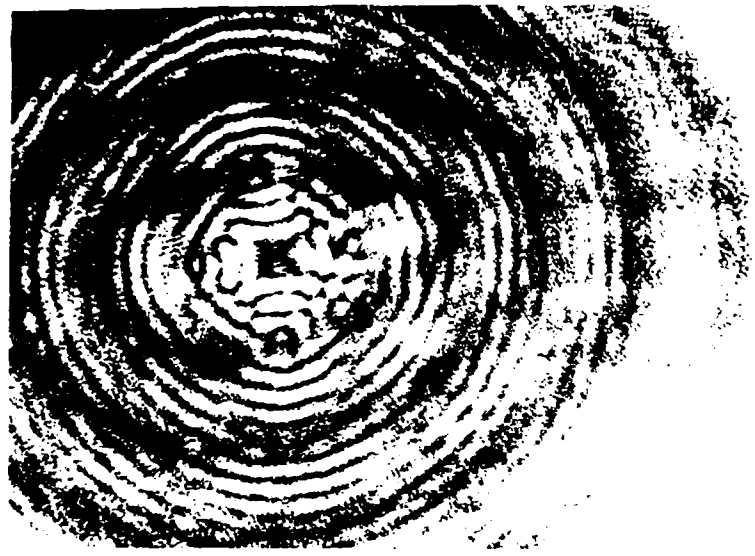

Photograph 6.80
3/16" diameter obstacle with 7mm diameter aperture.
ε = .68. Viewing distance: .6 - .65m. Magnification 4X.
Exposure time 1 second. 24° countertilt. Minimum on axis.

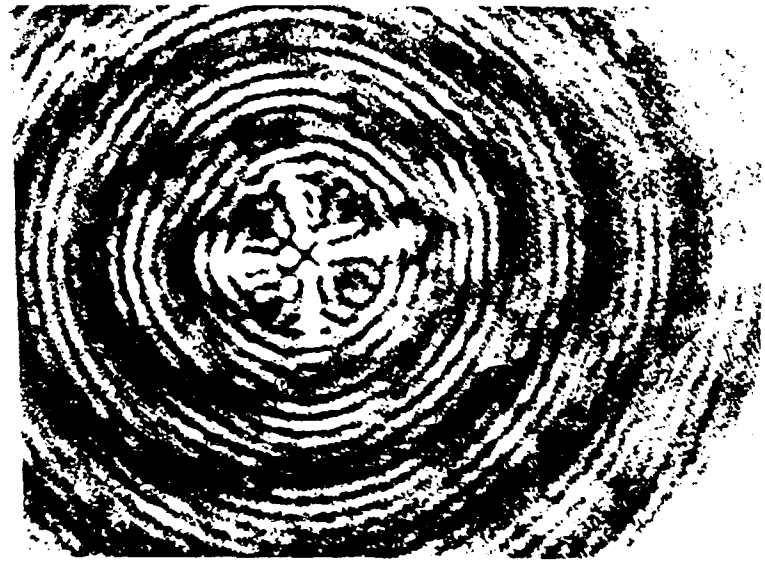

Photograph 6.81
3/16" diameter obstacle with 7mm diameter aperture.
ε = .68. Viewing distance: .6 - .65m. Magnification 4X.
Exposure time 1 second. 24° countertilt. Maximum on axis.

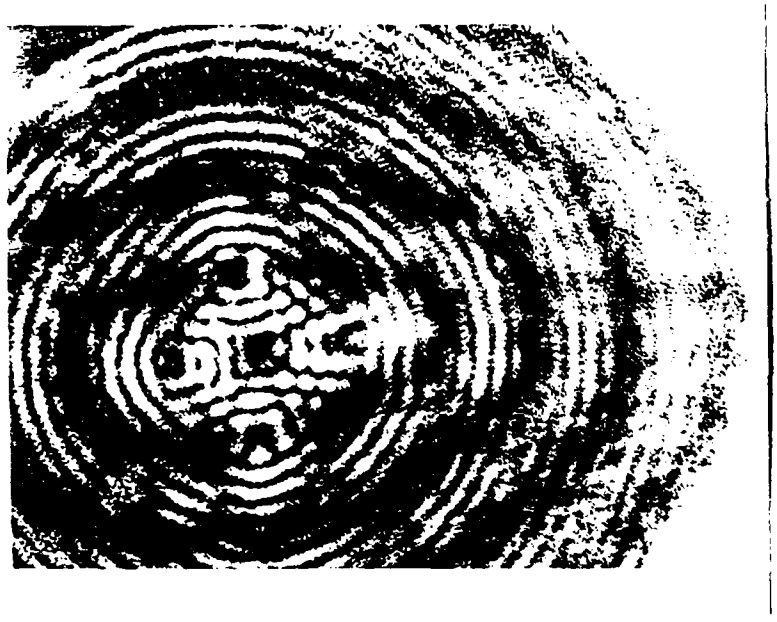

Photograph 6.82
3/16" diameter obstacle with 7mm diameter aperture.
ϵ = .68. Viewing distance: .6 - .65m. Magnification 4X.
Exposure time 1 second. 26° countertilt. Minimum on axis.

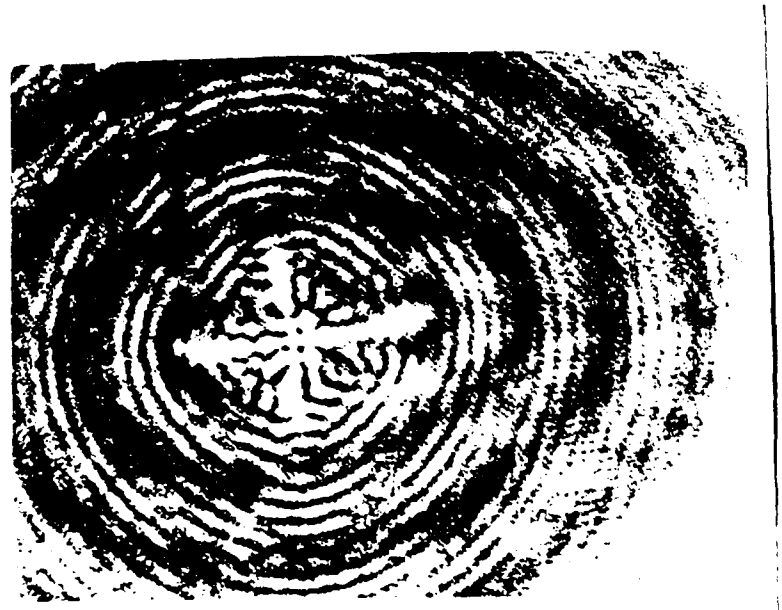

Photograph 6.83
3/16" diameter obstacle with 7mm diameter aperture.
ϵ = .68. Viewing distance: .6 - .65m. Magnification 4X.
Exposure time 1 second. 26° countertilt. Maximum on axis.

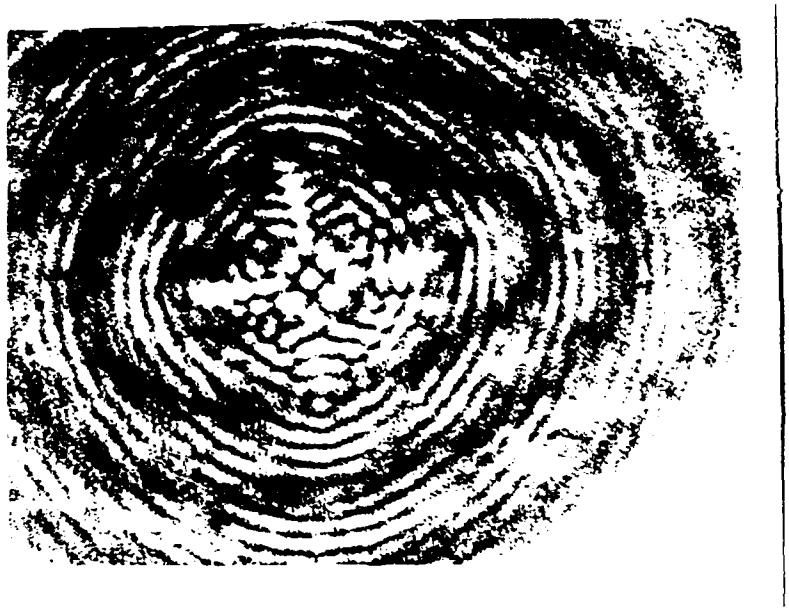

Photograph 6.84
3/16" diameter obstacle with 7mm diameter aperture.
ε = .68. Viewing distance: .6 - .65m. Magnification 4X.
Exposure time 1 second. 28° countertilt. Maximum on axis.

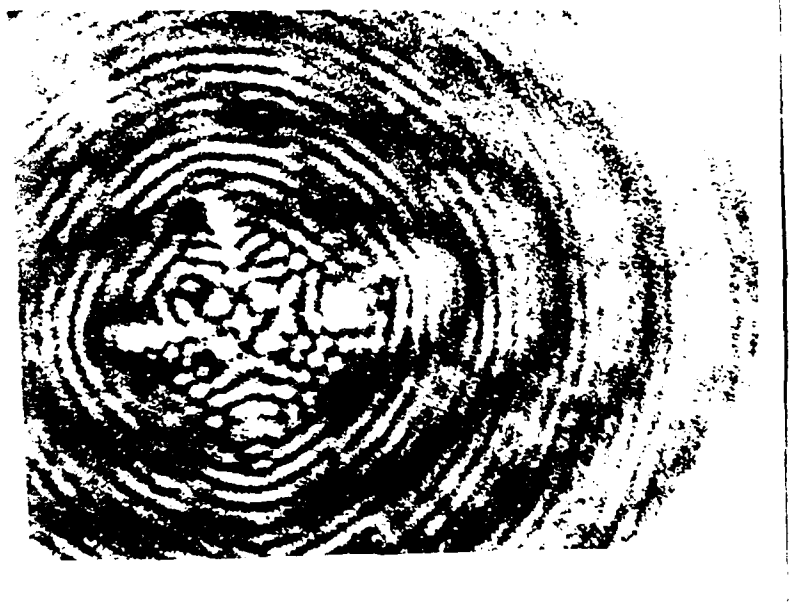

Photograph 6.85
3/16" diameter obstacle with 7mm diameter aperture.
ε = .68. Viewing distance: .6 - .65m. Magnification 4X.
Exposure time 1 second. 30° countertilt. Maximum on axis.

Photograph 6.86
1/2" diameter obstacle with 5/8" diameter aperture.
ε = .8. Viewing distance: 2.05 - 2.15m. Magnification 6X.
Exposure time 1 second. 9° countertilt. Minimum on axis.

Photograph 6.87
1/2" diameter obstacle with 5/8" diameter aperture.
ε = .8. Viewing distance: 2.05 - 2.15m. Magnification 6X.
Exposure time 1 second. 10° countertilt. Minimum on axis.

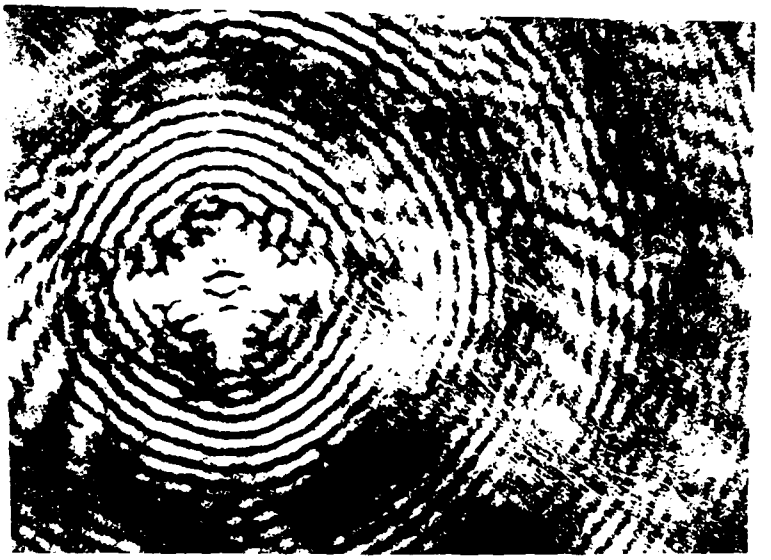

Photograph 6.88
1/2" diameter obstacle with 5/8" diameter aperture.
ε = .8. Viewing distance: 2.05 - 2.15m. Magnification 6X.
Exposure time 1 second. 10° countertilt. Maximum on axis.

Photograph 6.89
1/2" diameter obstacle with 5/8" diameter aperture.
ε = .8. Viewing distance: 2.05 - 2.15m. Magnification 6X.
Exposure time 1 second. 12° countertilt. Maximum on axis.

The diffraction patterns behind annular apertures with high obscuration ratios are quite similar to those produced by a circular obstacle. The resemblance decreases as the obscuration ratio does. The outer areas of the aberrated region cease to show lobing and ring break-up but give way to intricate symmetries. When the obscuration ratio is as low as .3 none of the structures seen in the circular obscuration case are manifested.

An effect seen in the unaberrated case seems to be exaggerated when astigmatism is present. This is the dramatic change in the overall pattern from the position at a maximum on axis to a minimum on axis. Photographs 6.65 and 6.66, 6.67 and 6.68, 6.74 and 6.75, and 6.80 and 6.81 are good examples of this effect. Because the patterns can vary to such a large extent a catalog of diffraction patterns, as suggested for the circular obscuration, is impractical. The changes go through cycles corresponding to the cycles of on-axis extrema. The pattern at any viewing distance z will be associated with a given point in the cycle and so the shape of the pattern will be repeated many times as one moves along the optical axis.

This change from maximum to minimum must be taken into account when comparing the annular aperture photographs to the circular obstacle photographs. For example Photograph 6.87 shows the pattern behind an annular aperture of obscuration ratio .8 at an on-axis minimum. (It is clear this is a minimum on axis because the number and extent of tne bright rings in the center is maximum. Compare this to Photograph 6.19.) The prominent central feature is the absence of the bright central spot and the four very bright nodules composing the

split first ring. This is reminiscent of Photograph 6.30 corresponding to $W_{22} = -.71\lambda$. However, this is incorrect. The last broken ring in Photograph 6.87 is the third and the fourth ring shows severe lobing. This is suggestive of Photograph 6.38 corresponding to $W_{22} = -1.198\lambda$. A comparison of Photograph 6.88 to the circular obstacle photographs confirms this. In this photograph the center spot is bright and the similarity to Photograph 6.38 is immediately apparent. A good rule of thumb when comparing photographs of annular aperture diffraction patterns to circular obscuration diffraction patterns is to count broken rings if the pattern is at an on-axis minimum and match interior patterns when at an on-axis maximum. Table 6.22 lists the results of a comparison of some photographs from 6.70 - 6.90 to photographs 6.20 - 6.49. The figures in parentheses represent the high and low limits to W_{22} based upon an uncertainty in tilt angle measurement of $\pm$ .5°. The preceeding table shows that the astigmatism at the outer edge of the annular aperture drives the diffraction pattern.

Apertures of similar obscuration ratios exhibit similar diffraction patterns with similar amounts of astigmatism. Photograph 6.74 corresponds to $\varepsilon = .625$ and $W_{22} = -1.704\lambda$ at the outer edge. This pattern compares very closely to Photograph 6.81 with $\varepsilon = .68$ and $W_{22} = -1.51\lambda$ at the outer edge. Photograph 6.72 with $W_{22} = -1.97\lambda$ is similar to Photograph 6.83 with $W_{22} = -1.79\lambda$.

It was suggested in Chapter 3 that annular apertures with high obscuration ratios are better suited for aberration studies. This is due to the larger number of rings in the beat envelopes. More of the ring structure stays intact between modulations so any deviations in

Table 6.22

Determination of Astigmatism Present in Annular Aperture Diffraction Patterns by Comparison to Circular Obstacle Diffraction Patterns

Annular Aperture			Circular Obstacle	
	W_{22} (wavelengths)			
Photograph	Inner Edge	Outer Edge	Comparison to Photograph Number	W_{22} (wavelengths)
6.70	-.337 (-.298,-.377)	-1.014 (-.916,-1.118)	6.36	-1.065 (-1.002,-1.131)
6.78	-.528 (-.500,-.557)	-1.254 (-1.193,-1.316)	6.39	-1.338 (-1.267,-1.411)
6.79	-.528 (-.500,-.557)	-1.254 (-1.193,-1.316)	6.39	-1.338 (-1.267,-1.411)
6.80	-.647 (-.616,-.678)	-1.510 (-1.444,-1.578)	6.40	-1.485 (-1.411,-1.562)
6.81	-.647 (-.616,-.678)	-1.510 (-1.444,-1.578)	6.40	-1.485 (-1.411,-1.562)
6.83	-.776 (-.743,-.810)	-1.790 (-1.718,-1.863)	6.42	-1.801 (-1.720,-1.885)
6.84	-.916 (-.880,-.952)	-2.091 (-2.014,-2.170)	6.43	-1.970 (-1.885,-2.057)
6.85	-1.065 (-1.027,-1.104)	-2.415 (-2.332,-2.499)	6.45	-2.519 (-2.423,-2.617)
6.86	-.647 (-.566,-.732)	-1.065 (-.940,-1.198)	6.36	-1.065 (-1.002,-1.131)
6.87	-.821 (-.732,-.916)	-1.338 (-1.198,-1.485)	6.37	-1.198 (1.131,-1.267)
6.88	-.821 (-.732,-.916)	-1.338 (-1.198,-1.485)	6.38	-1.338 (-1.267,-1.411)
6.89	-1.226 (-1.118,-1.338)	-1.970 (-1.801,-2.146)	6.42	-1.801 (-1.720,-1.885)
6.90	-1.226 (-1.118,-1.338)	-1.970 (-1.801,-2.146)	6.43	-1.970 (-1.885,-2.057)

the ring pattern is easier to spot. This raises the question, can the amount of astigmatism be determined from patterns of an annular aperture with a low obscuration ratio? The answer is a guarded yes. A rough measure of the aberration present is possible. The region of aberration extends a distance out from the center of the diffraction pattern. This radial distance can be measured and compared to the radial distance for ring breakup found in the previous section.

To prepare the following table, the average radii of the regions of aberration for photographs of the 3/16 inch diameter obstacle with a 5/8 inch diameter aperture were measured. (The aberrated region was taken as the area out to the last bright band which showed looping or separation in the band. For example, in Photograph 6.66 this was the third band from the center.) These were compared to the known ring

Table 6.23

Radii of Aberrated Areas in Diffraction Patterns
Behind an Annular Aperture with $\varepsilon = .3$

Tilt angle	W_{22} at outer edge (λ)	Radius of aberrated area (mm)	$\frac{kdr}{2z}$
7	-.606 (-.509,-.710)	.17	6.69
8	-.821 (-.710,-.940)	.195	7.68
10	-1.338 (-1.198,-1.485)	.33	13.00
12	-1.970 (-1.801,-2.146)	.45	17.73
14	-2.717 (-2.519,-2.921)	.56	22.10

spacing for the annular aperture with no aberrations present. The actual radial distance of the extent of the region of aberration was calculated. The Bessel function argument kdr/2z was calculated also.

The results from the table are plotted against the line found in Graph 6.20. The points suggest a line of steeper slope than that from Graph 6.20. Recall the line plotted in Graph 6.20 corresponded to the radius of the aberrated area when defined as the region of broken rings. The distance which correlates to this radius in the annular aperture case seems to be different from that measured in Table 6.23. A new line with a different slope should enable one to determine W_{22} from measurements of the diffraction patterns of an annular aperture with a low obscuration ratio.

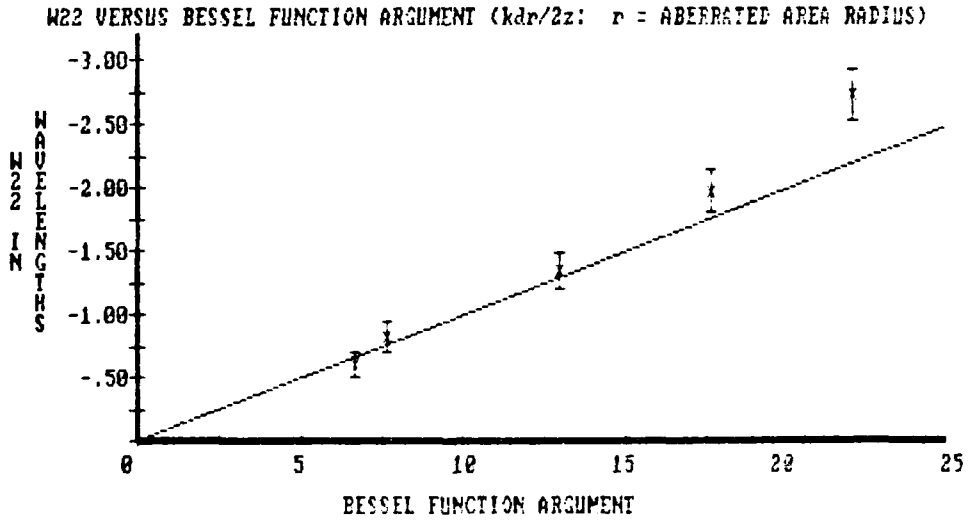

Graph 6.21

An interesting feature is seen in the photographs for the annular aperture. The center of the diffraction pattern often contains a + or x structure. These are seen quite readily in the photographs below.

Photograph 6.90

3/16" diameter obstacle with 5/8" diameter aperture.
Viewing distance 2m. 8^{o} countertilt.

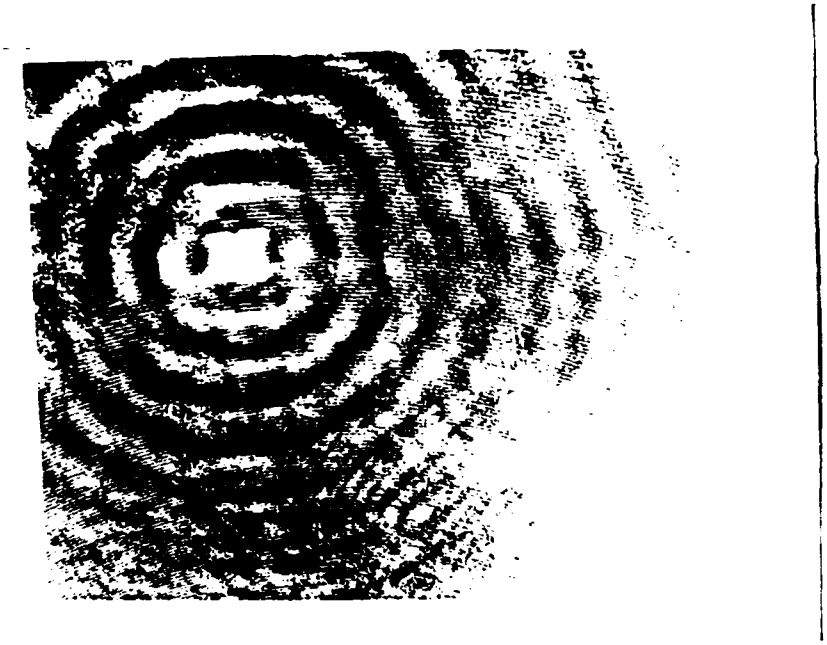

Photograph 6.91

3/16" diameter obstacle with 5/8" diameter aperture.
Viewing distance 2.05m. 8^{o} countertilt.

The structures are also seen in Photographs 6.63, 6.64, 6.67, 6.68, 6.78 and 6.79. In these last two instances the + and x are dark structures at the center. These seem to be related to the positions of maxima and minima on axis. A bright + appears to be composed of the bright central spot and the first broken ring. A bright x looks to be made of the bright central spot and the northeast, southeast, southwest and northwest nodules in the second broken ring. Minimum intensities in these areas give rise to the dark structures.

Astigmatism, like spherical aberration and defocus, shifts the position of on-axis extrema. This was verified using the same procedure as for the previously mentioned aberrations. The first run involved the shift of the 7^{th} order minimum at 65cm behind an annular

aperture composed of a 3/16 inch diameter obstacle with a 7mm diameter aperture separated by 1cm. The second run involved the shift of the 23rd order minimum at 66.5cm behind a 3/16 inch diameter obstacle with a 10mm diameter aperture separated by .8cm. The graphs below plot the data points for each run. The line is the line of best fit by minimizing the root mean square deviations.

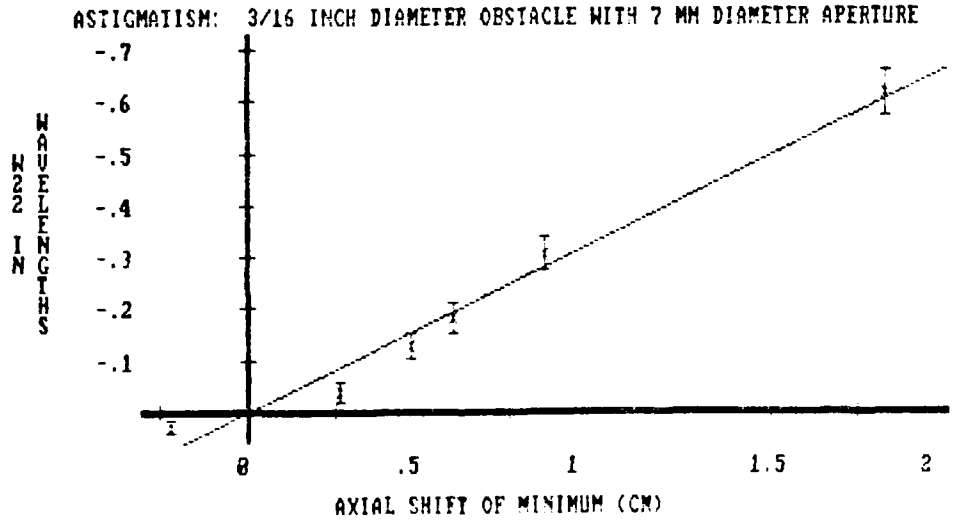

Graph 6.22

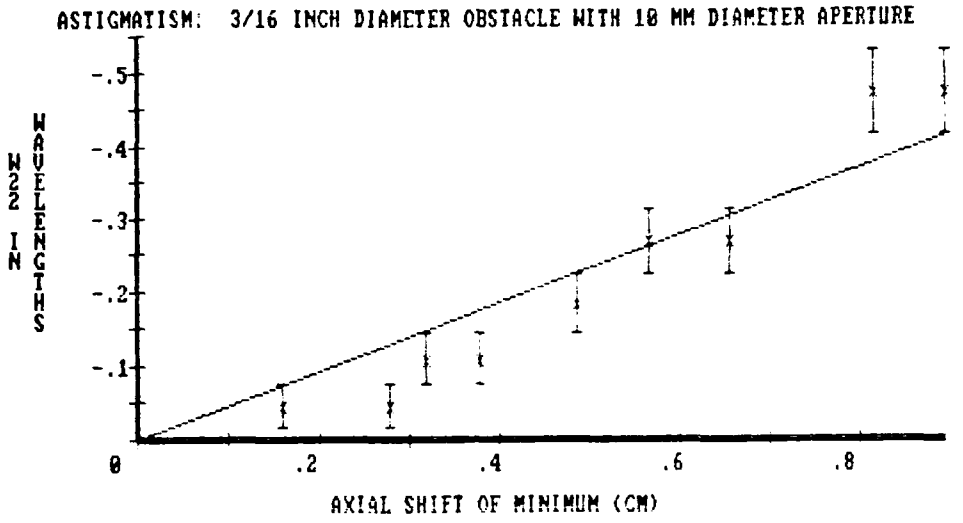

Graph 6.23

The coefficients W_{22} from Graph 6.23 seems to go as the square of the axial shift. However, the linear plots have an attractive feature. The ratio of the radii for the two apertures used is .7. The ratio of slopes of the best fit lines in the graphs is .723. The data does not fit a formula like that found for defocus and spherical aberration:

$$W_{22} = \frac{n}{c}\frac{\Delta z}{z'} \qquad \text{(VI-12)}$$

where n is the order of the minimum and c is a constant presumably dependent upon r.

The complex astigmatic patterns produced with high angles of countertilt make measurements of on-axis shifts very difficult. A more conclusive test of the effect of astigmatism on the positions of axial extrema should limit itself to small amounts of the aberration.

For now it is sufficient to note negative astigmatism causes a shift on axis in the negative z direction.

There are two reasons not to use the shift of extrema to measure astigmatism. The first reason is that the change in the overall diffraction pattern is an accurate and sufficient gauge of aberration present. The second is that both defocus and spherical aberration, which have little effect on the pattern, cause axial shifting. Measuring the shift alone could lead to an erroneous measure for W_{22} if W_{20} and W_{40} are not accounted for.

Notes

[1] Warren J. Smith, Modern Optical Engineering (New York: McGraw-Hill, 1966), p. 82.

Chapter 7

CONCLUSIONS

The most important result of the theoretical and experimental treatment in this thesis is almost trivial. The ultimate diffraction pattern behind a circular obstacle or an annular aperture depends entirely on the physical state of the incident wave at the edges. This is seen repeatedly in the formulas from chapters 3 and 4. The disturbance function at points in image space contains phase terms, Gaussian terms, aberration terms and zero-order Bessel functions which all have arguments dependent upon the radii of the edges. By understanding the physics at these boundaries one gains insight into the diffraction process and its results.

Summary

The diffraction patterns predicted by the theory of chapters 3 and 4 agreed very closely to the experimental findings, typically with less than 5% deviation. The intensity distribution in the near field region close to the optical axis can be described with excellent accuracy by the formulas reviewed at the end of Chapter 4. These formulas depend only on the zero order Bessel function so the computation of the intensity at a given point is substantially reduced from

that requiring the use of unwieldy Lommel functions. The periodicity of the Bessel function provides an explanation of the modulated ring structure observed in annular aperture diffraction patterns in terms of beat envelopes.

The theory of Chapter 4 was very successful in predicting the shift of on-axis extrema behind an annular aperture with the introduction of defocus in the incident beam. Measuring this shift is a very effective method of determining defocus. This method should work for spherical aberration also, but the maximum amount of spherical aberration created from the apparatus produced expected shifts less than the experimental error. It was found that astigmatism will shift the positions of the axial maxima and minima as well. In all the above cases, if the aberration coefficient is negative the shift will be in the minus z direction.

Astigmatism produces very distinct changes in the diffraction patterns of a circular obstacle. The effect of the aberration is seen in the first ring of diffraction pattern at values of W_{22} as low as $-.1\lambda$. This is when the first ring starts to concentrate its intensity at four compass points -- the vertices of a diamond. As the aberration is increased, the first ring breaks up into four separate spots when W_{22} is approximately $-.4\lambda$. In general the n^{th} ring from the center will break up into 4n points forming a diamond with n+1 points on a side. This region of broken rings constitutes an area where aberration effects are manifest. From the radius of this region, the amount of astigmatism can be calculated. The radius and W_{22} are related linearly. The same amount of astigmatism at the

edge of any sized circular obstacle will produce the same aberrated image.

An annular aperture with a high obscuration ratio (> .6) subjected to an astigmatic beam will give a diffraction pattern similar to that for the circular obstacle. In this case it is the amount of astigmatism at the outer edge that determines the pattern. Apertures of nearly equal obscuration ratios produce similar diffractions with similar amounts of astigmatism at the outer edges. W_{22} can be calculated by comparing the annular aperture diffraction pattern to those for the circular obstacle. When the obscuration ratio is low, the diffraction pattern is very complex. In this case one can measure the extent of the aberrated region and, in an analogous manner to that for the circular obstacle, find the amount of aberration present.

The astigmatism produced by tilting plane parallel plates drowned out any effects which might have come from coma. A numerical study of coma is necessary. Coma should produce a diffraction image with one plane of symmetry.

The circular obstacle seems best suited to detect the presence of astigmatism and, likely, coma. An annular aperture is required to detect the rotationally symmetric aberrations, defocus and spherical aberration.

Many of the theoretical and experimental results found in this thesis suggest embarkation points for future study.

Suggestions for Further Research

The experimental apparatus did not include any method of measuring the intensity of Arago's spot and the surrounding ring structure. Many theoretical predictions from chapters 3 and 4 involve the intensity of the spot. For example, measuring the intensities of two on-axis maxima will allow one to separate defocus and spherical aberration. A detector to measure this region near the optical axis must be very small. Its dimensions will be guided by the dimensions of the aperture. The smaller the aperture, the larger the detector can be. The detector can be made by masking all but a small area (diameter on the order of 10 to 50 microns) on the detector surface. The detector should allow translation along the z-axis. The detector should be allowed to move in a radial direction to find the intensity peak. This will allow study of the ring structure as well.

The experimental apparatus contained some background astigmatism. The measure of the tilt angles had a half-degree uncertainty. A definitive study of the astigmatic case where the tilt angles can be measured to high accuracy should be made. A catalog of diffraction patterns can be compiled and used in aberration detection.

Another failing in the experimental equipment was the size of the aperture stop at the collimating lens (13/16 inch). If the parallel plates were tilted in the same direction the transmitted beam began to hit the collimating lens off center. If the tilt angle was much greater than 20° the beam began to miss the lens. A larger collimating lens and holder should be used in future set-ups.

Greater tilt in the same direction will allow a larger amount of coma to be introduced. However, since astigmatism goes as the square of the tilt angle while coma is proportional to the angle one expects astigmatism to overshadow coma. Coma should be studied through a numerical study of the Rayleigh-Sommerfeld integral for the circular obscuration.

Once the patterns for coma are determined, a study of combinations of aberrations can be made. The next step should be a study of higher order aberrations.

Eventually a detection system based on these studies can be constructed. The system should include the intensity detector mentioned earlier as well as an optical apparatus to view the overall diffraction pattern. If the optical system to be tested contains deformable elements, a feedback loop is possible to minimize aberrations.

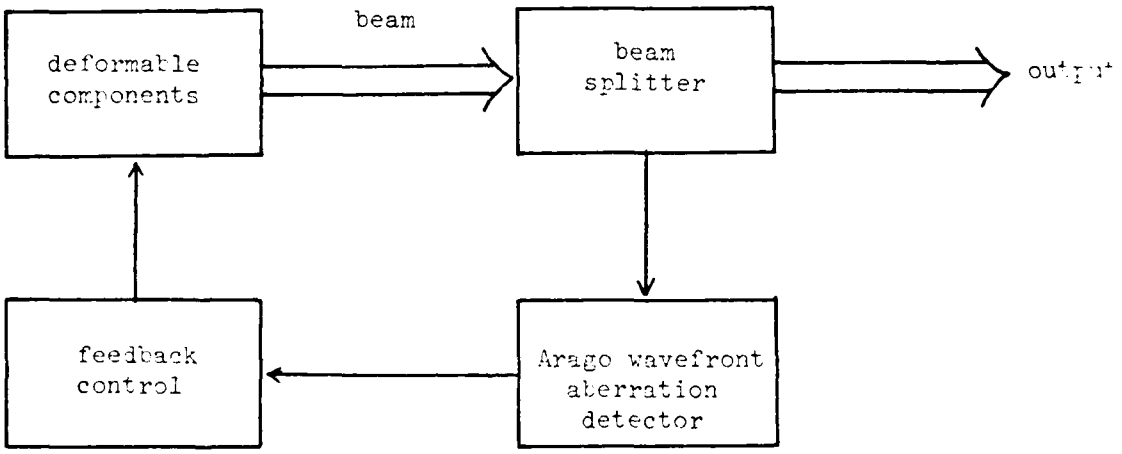

Figure 7.1

Use of an Arago Detection System in a Feedback Loop

The Spot of Arago has a long and interesting history, but so far its practical applications have been few. The use of the spot to detect and measure aberrations will renew its importance.

BIBLIOGRAPHY

Books and Compilations

Arago, Francois Dominique. "Note sur un phenomène remarquable qui s'observe dans diffraction de la lumiere." In Vol. IV of Oeuvres Completes des Memoires, Part III of Notices Scientifiques. Amsterdam: Lees-Museum Bibliothek, 1858.

BASIC - IBM Personal Computer Hardware Reference Library. USA: IBM, 1981.

Born, Max and Emil Wolf. Principles of Optics. 6th ed. Oxford: Pergamon Press, 1980.

Brown, Stanley B., ed. Foundations of Physics. Vol. 7 of The Realm of Science. Louisville: Touchstone Publishing, 1972.

Burke, James. Connections. Boston: Little, Brown and Co., 1978.

Crosland, Maurice. The Society of Arcueil. Cambridge, Mass.: Harvard University Press, 1967.

Fraser, Charles G. Half-hours with Great Scientists. Toronto: University of Toronto Press, 1948.

Fresnel, Augustin. De la Lumière. Paris: Librairie Armand Colin, 1914.

Goodman, Joseph W. Introduction to Fourier Optics. San Francisco: McGraw-Hill, 1968.

Hopkins, H. H. Wave Theory of Aberrations. Oxford: Oxford University Press, 1950.

Jenkins, Francis A. and Harvey E. White. Fundamentals of Optics. 4th ed. New York: McGraw-Hill, 1976.

Miller, Alan R. BASIC Programs for Scientists and Engineers. Berkeley: Sybex, Inc., 1981.

Monk, George S. Light: Principles and Experiments. New York: Dover Publications, 1963.

Rayleigh (Strutt, John William). "Shadows." In his Scientific Papers. Vol. V. New York: Dover Publications, 1964.

_____. "Wave Theory of Light." In his Scientific Papers. Vol. III. New York: Dover Publications, 1964.

Shamos, Morris H., ed. Great Experiments in Physics. New York: Holt, Rinehart and Winston, 1964.

Smith, Warren J. Modern Optical Engineering. New York: McGraw-Hill, 1966.

Sommerfeld, Arnold. Optics. Vol IV of Lectures on Theoretical Physics. New York: Academic Press, 1967.

Strong, John. Concepts of Classical Optics. San Francisco: W. H. Freeman, 1958.

Waldron, R.A. The Wave and Ballistic Theories of Light. London: Frederick Muller, 1977.

Wells, H. G. The Outline of History. Rev. ed. Garden City, New York: International Collectors Library, 1971.

White, Harvey E. Modern College Physics. 6th ed. New York: Van Nostrand Reinhold, 1972.

Journals and Magazines

"The Adventures of a Man of Science." The Leisure Hour, 24 January 1856, pp. 58-61.

Airy, George Biddell. "On the Diffraction of an Annular Aperture." The Philosophical Magazine, 18 (1841): 1-10.

Arkadiew, W. "Die Fresnelschen Beugungerscheinungen." Physikalische Zeitschrift, XIV (1913): 832-835.

Brewster, David. "Francois Arago. His Life and Discoveries." North British Review, 20 (February 1854): 459-500.

Harvey, James E. and James L. Forgham. "The Spot of Arago: New Relevance for an Old Phenomenon." American Journal of Physics, (January 1984).

Hufford, Mason E. "Some New Diffraction Photographs." The Physical Review, III, No. 4 (April 1914): 241-243.

_____. "The Diffraction Ring Pattern in the Shadow of a Circular Object" The Physical Review, VII, No. 5 (May 1916): 545-550.

Johnston, John B. "Projecting Poisson's Spot." The Physics Teacher, 16, No. 3 (March 1978): 179.

Linfoot, E. H. and E. Wolf. "Diffraction Images in Systems with an Annular Aperture." Procedings of the Physical Society, B, No. 66 (1953): 145-149.

Lommel, E. "Die Beugungerscheinungen einer kreisrunden Oeffnung und eines kreisrunden Schirmchens." Abhandlungen der Mathematisch - Physikalischen Classe der Koniglich. Bayerischen Akademie der Wissenschaft, (1898): 233-328.

"M. Arago." Living Age, No. 11, October-December 1846, pp. 140-148.

Pav, Peter Anton. "Eighteenth Century Optics: The Cartesian - Newton Conflict." Applied Optics, 14, No. 12 (December 1975): 3102-3107.

Porter, Alfred W. "On the Formation of Images by Means of an Opaque Disk." The Philosophical Magazine, 27 (April 1914): 673-674.

Potter, Richard. "On the Phenomena of Diffraction in the Centre of the Shadow of a Circular Disc." The Philosophical Magazine, 19 (1841): 151-155.

Raman, C. V. and K. S. Krishnan. "On the Diffraction of Light by Spherical Obstacles." Procedings of the Physical Society, 38 (August 1926): 350-353.

Rankine, A. O. "Demonstration on the Diffraction of Light by a Spherical Obstacle." Procedings of the Physical Society, 37 (August 1925): 267.

Schober, H. and R. Krusche. "Einfacher Demonstrationsversuch zum Poissonschen Fleck." Optik, 30 (1969): 314-317.

Stijns, Erik. "Measuring the Spot Size of a Gaussian Beam with an Oscillating Wire." IEEE Journal of Quantum Electronics, QE-16 (December 1980): 1298-1299.

Welford, W. T. "Use of Annular Apertures to Increase Focal Depth." Journal of the Optical Society of America, 50, No. 8 (August 1960): 749-753.

Other References

"Arago, Francois Jean Dominique." Encyclopedia Britannica. 9th ed.

CRC Handbook of Chemistry and Physics. 62nd ed. Boca Raton, Florida: CRC Press, 1981.

"Deslisle, Joseph Nicholas." The American Cyclopedia. Rev. ed. New York: D. Appleton, 1873.

Harvey, James E. "An Introduction to Aberration Theory." 1983. Class handout. Univ. of New Mexico, Albuquerque.

Jenney, J. A. "Diffraction Disk Imaging Resolution and Image Quality." 29 July 1964. Interdepartmental correspondence, Hughes Aircraft.

"Maraldi, Jacques-Phillipe." La Grand Encyclopedie. Vo. 23. Paris: H. Lamirault et. C^{ic}, 6 August 1896 - 11 August 1898.

"Maraldi, Jean-Dominique." La Grand Encyclopedie. Vo. 23. Paris: H. Lamirault et. C^{ic}, 6 August 1896 - 11 August 1898.

Shakespeare, William. Macbeth. In The Annotated Shakespeare. Ed. A. L. Rowse. New York: Clarkson N. Potter, 1978.

THE SPOT OF ARAGO AND ITS ROLE IN ABERRATION ANALYSIS

Donald Ross Erbschloe, Captain USAF

1983

M.S., Physics

University of New Mexico

AD-A141 983 THE SPOT OF ARAGO AND ITS ROLE IN ABERRATION ANALYSIS 4/4
(U) AIR FORCE INST OF TECH WRIGHT-PATTERSON AFB OH
D R ERBSCHLOE DEC 83 AFIT/CI/NR-84-7T

UNCLASSIFIED F/G 20/6 NL

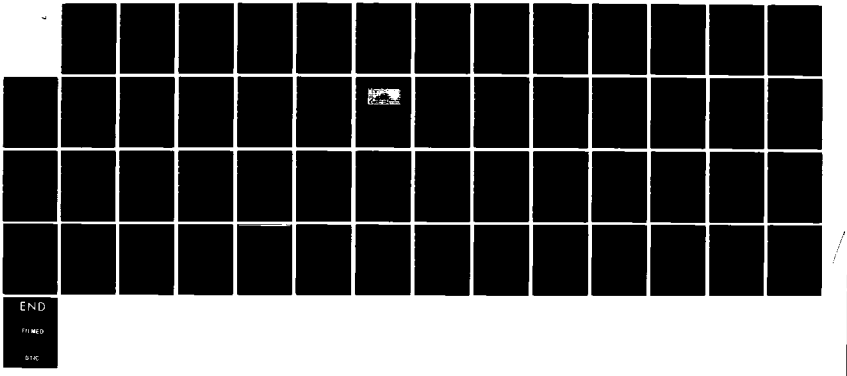

END
FILMED
DTIC

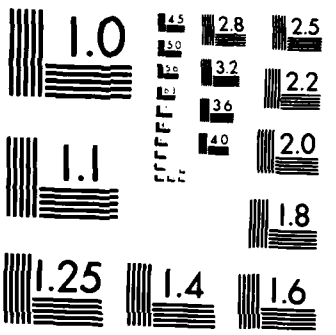

APPENDICES

Appendix 1

THE LIFE AND WORKS OF ARAGO

The great men and women of science are known typically only by their theorems, equations or experiments. Textbooks rarely have the space to provide biographical information beyond an occasional footnote containing dates of birth and death or an amusing anecdote. A sense of history, the personal side of science, is missed in the process. Many scientists led colorful and controversial lives. It would be a particular shame to overlook the life of Dominique Francois Jean Arago.

Arago was born on February 26, 1786 at Estagel, a small village in the eastern Pyrenees near the Mediterranean coast. The village was a halting station for French troops enroute to the army of the Pyrenees. Young Arago was fascinated by the soldiers and once asked an officer what he needed to do to be able to wear such a fine uniform. The reply was to become a student at the Polytechnic School.[1] To prepare for the entrance examination Arago taught himself mathematics from the works of Euler, Legendre, Lagrange and Laplace. He so impressed his examiner, Louis Monge, that he was entered into the school in 1803 with highest commendation.[2]

In 1804 he was appointed as secretary to the Observatory of Paris. Here he met and worked with Laplace and Biot. Arago and Biot

were commissioned in 1806 to complete the measurement of the meridional arc. (The National Convention earlier had adopted the measure of the one ten-millionth part of the quadrant of the meridian passing through Paris as the length of the meter. The complete quadrant could not be measured but it was felt by measuring the arc from Dunkirk through Barcelona to the Balearic Islands and knowing the relative latitudes the total quadrant length could be deduced.)[3] The two Frenchmen, with the aid of two Spanish scientists Chaix and Rodriguez, first measured the distance from the coast of Spain to the island of Ibize. Here Biot and Arago spent months on high mountaintops sending signals by fire to their Spanish counterparts on peaks over a hundred miles distant. They braved severe windstorms, bandits, fatigue and scarce supplies. Biot returned to Paris in 1807 with the preliminary measurements. Arago continued measurements, moving to the summit of Mount Galatzo.[4]

In 1808 Napoleon put his brother Joseph on the throne of Spain which precipitated a war.[5] The natives of the Spanish owned islands where Arago was positioned became convinced the strange fire signals on their mountain peaks at night were messages meant for an invading army. A mob of islanders was dispatched to capture the hapless Frenchman. An assistant got warning to Arago who was able to disguise himself as a peasant. He escaped by joining the ranks of the crowd in pursuit of him. He entrusted his equipment and papers to his still-faithful servants. He made his way to Palma, the island's port. Although he had a ship waiting to take him to safety he stayed until his precious recordings and equipment were returned. By this time the

mob had discovered his charade and to avoid their wrath Arago was obliged to turn himself in to the local authorities. He spent the next two months in prison and used the time to complete calculations on his measurements.[6]

In July of 1808, Rodriguez interceded on Arago's behalf and obtained permission for his passage to Algiers. In Algiers he befriended the Dey, the governor of the city. Soon the young Frenchman set sail for Marseilles. The ship's cargo included two lions meant as presents to the emperor Napoleon. Within sight of the French coast, a Spanish privateer captured the vessel. A casualty of the seizure was one of the lions. Arago was returned to Spain and imprisoned for three months. The Dey learned of the capture and the lion's demise and was outraged. He threatened war if the crew and ship were not set free. Spain had its hands full with France and was not anxious to enter into any other entanglements. The ship departed once more for Marseilles.[7]

Before the vessel made port, a violent storm forced it back out to sea and onto the craggy coast of Sardinia. Sardinia was at war with Algiers and refused to let the ship land to make repairs. The fractured craft found its way to Bougia, a port in northern Africa. The winds were unfavorable for passage to Algiers so Arago decided to travel by land. To make the perilous journey he donned the disguise of a Bedouin. Before Arago arrived in Algiers the Dey was overthrown. The new governor was not friendly to the French and the young scientist avoided incarceration only by the intercession of the Danish consul. Still he suffered through a series of maddening delays.

Finally in July of 1809, three years after he and Biot departed, Arago returned to his native land.[8]

As a reward for his diligence and adventures in the name of science Arago was nominated for entry into the Academié des Sciencès when a vacancy arose. His competition was Simeon Denis Poisson who was being sponsored by Pierre Simon Laplace. Joseph Louis Lagrange led the support for Arago and eventually convinced Laplace to change his endorsement. Arago won and at age 23 became the youngest member ever to be elected to the prestigious body.[9]

The scientific career of Arago was quite varied, involving theoretical works, experimentation, teaching and administration. He taught at the Ecole Polytechnic. As an astronomer at the Royal Observatory he delivered public lectures from 1812 to 1845. In 1816 Arago and Joseph Louis Gay-Lussac founded and co-edited the publication Annalen de Chimie et de Physique. He also helped establish Compte Rendus. When Jean Baptiste Joseph Fourier died in 1830 Arago took over as permanent secretary of the Academie des Sciences.[10] Part of his duties involved writing eloges on members of the Academie. Much of what is known of the lives of Augustin Fresnel, Thomas Young, Alessandro Volta, Andre Marie Ampere, Fourier, Nicolas Leonard Sadi Carnot and others stem from these writings.[11]

Arago was very active politically. From 1830 to 1844 he served in the Chamber of Deputies. During his term he supported the development of steam engines, railroads and lighthouses. He suggested a patent law, boring the Artesian wells at Grenelle and the construction of the museum at Cluny. To promote science he sponsored Louis Jacques

Mande Dageurre and the new field of photography and arranged for the publication of the works of Pierre de Fermat and Laplace. In 1848 France became a republic. Arago was appointed the Minister of War and Marine (a unique combination of two offices). As Minister he put an end to the practice of flogging, improved naval rations and abolished slavery in French colonies. A staunch republican, Arago refused to sign an obligatory oath of allegiance to the new emperor Napoleon III in 1852. The emperor made an exception in Arago's case and the scientist maintained his offices until his death on October 2, 1853.[12]

The collected writings and scientific papers of Arago occupy ten volumes. Below is a short account of some of his scientific achievements. In 1810 he discovered polarization of light when passed through sheets of mica. He and Fresnel showed polarized rays can interfere only when polarized in transverse planes.[13] He demonstrated that refraction of light is independent of the motion of the refracting body. This prompted Fresnel to suggest the Earth drags ether with it.[14] In 1838 Arago proposed the comparison of velocities of light in different media. The corpuscular theory predicted light should travel more rapidly in a medium such as water than in air. The wave theory suggested the opposite. Light would be sent through two tubes, one filled with air, the other with water and onto a rapidly rotating mirror. The difference in transit times through the tubes would result in different incident angles upon the rotating mirror. Jean Bernard Leon Foucault conducted the experiment and found light moved more slowly in water. This was powerful evidence in favor of the wave theory.[15] He studied the bands of Saturn and Jupiter as well as the

polar ice caps of Mars. He made photometric measurements of numerous astronomical bodies. Arago showed a correlation between the changes in the earth's magnetic field and the appearance of the aurora borealis. He was the first to demonstrate that steel could be permanently magnetized by using an electric current and iron filings temporarily so. The Royal Society of London awarded Arago the Copley Medal in 1825 for his exhibition of magnetism in non-ferrous materials. (Other recipients of the award include Humphrey Davy, Hans Christian Oersted, Benjamin Franklin, Joseph Priestley and Poisson.)[16]

In the course of his scientific work Arago had many collaborators. Mention has been made about his work with Young, Poisson, Fresnel, Dageurre, Foucault and Biot. His relation with Biot soured when, while Arago was on a trip away from Paris, Biot attempted to publish results of a joint effort under only his name with but a cursory reference to Arago's help.[17] From 1824 to 1830 Arago and Pierre Louis Dulong performed a series of dangerous experiments on the elastic force of steam. The tests involved heating boilers to the point of bursting.[18] He was the mentor for many scientists in the early nineteenth century. In addition to Foucault and Daguerre, Arago sponsored Urban Jean Joseph Leverrier (who discovered Neptune by studying pertubation on the planet Uranus) and Armand Fizeau.[19]

One intriguing collaboration never transpired. After Napoleon Bonaparte suffered his defeat at Waterloo, he decided to leave Europe and travel to America to devote the remainder of his life to science. He wanted a companion well versed in the sciences to travel with him. His choice was Arago. Arago, though, bordered on chauvinism in the

traditional sense of the word. He refused Napoleon's offer because he wanted France to remain in the forefront of science. The presence of Napoleon in America would sanction the growing field of science there which could only diminish the French scientific authority.[20]

Arago's deeply felt sense of patriotism is his most telling characteristic. It was the impetus for his entry into the Ecole Polytechnic, the launching point for his scientific career. It rendered inevitable his political service to his country. His extraordinary life and works are extensions of that spirit.

Notes

[1] David Brewster, "Francois Arago -- His Life and Discoveries," North British Review, 20, (February 1854), 461.

[2] "Arago, Francois Jean Dominique," Encyclopedia Britannica.

[3] Ibid.

[4] "M. Arago," Living Age, October - December 1846, p. 141.

[5] H. G. Wells, The Outline of History rev. ed. (Garden City: International Collectors Library, 1971), p. 785.

[6] "The Adventures of a Man of Science," The Leisure Hour, 24 January 1856, p. 59.

[7] "M. Arago," op. cit.

[8] "Francois Arago -- His Life and Discoveries," op. cit., p. 464.

[9] "Arago, Francois Jean Dominique," op. cit.

[10] "Francois Arago -- His Life and Discoveries," op. cit., pp. 466-473.

[11] "Arago, Francois Jean Dominique," op. cit.

[12] Ibid.

[13] "Francois Arago -- His Life and Discoveries," op. cit. p. 486.

[14] R. A. Waldren, The Wave and Ballistic Theories of Light (London: Frederick Muller Limited, 1977), pp. 15-16.

[15] Maurice Crosland, The Society of Arcuiel (Cambridge: Harvard University, 1967), pp. 458-459.

[16] "Arago, Francois Jean Dominique," op. cit.

[17] Crosland, op. cit., p. 332.

[18] Ibid., p. 132.

[19] Ibid., p. 454.

[20] "Francois Arago -- His Life and Discoveries," op. cit., p. 468.

Appendix 2

THE SPOT OF ARAGO IN THE SHADOW DURING A SOLAR ECLIPSE

During a solar eclipse the moon acts as an obstacle to the essentially plane waves coming from the sun. The configuration is similar to the circular obstacle case described in Chapter 3. Does this mean the Spot of Arago should be present in the lunar shadow during a solar eclipse? Certainly theory predicts its existence, but this phenomenon has never been recorded. Some possible explanations for this include the spectral distribution of light from the sun, the difference in spot intensity between a spherical and circular obstacle, atmospheric effects, and spot size.

The light from the sun is not monochromatic. It produces a dim multi-colored spot (see Potter's description of the spot in Chapter 2) which for small obstacles must be viewed through a magnifying system. Because the spot produced by sunlight is so insubstantial no one had cause to look for it until Arago. If this carries over into the case of a very large obstacle illuminated by sunlight and observed at very large distance then the situation may be similar to that in 1818. Because the spot is unnoticible to the naked eye no one has looked for it.

The intensity of the spot is also dependent on whether the obstacle was circular or spherical (see the section on Raman and Krishnan's work in Chapter 2). For example, at 50cm behind a 1/4 inch diameter

obstacle the spot intensity for a spherical obstacle is half that for a circular obstacle. At 10cm the spherical obstacle intensity is nine times less that for a circular obstacle.[1] To compare the above results to the case of the moon introduce the quantity $x = \frac{d}{z}$ where d is the diameter of the obstacle and z is the observation distance. The moon's average diameter is 1738.3km and its average distance from the earth is 3.844×10^5km.[2]

$$x = \frac{1738.3\text{km}}{3.844 \times 10^5\text{km}} = 4.522 \times 10^{-3} \qquad \text{(A2-1)}$$

Compare the above to the case of the 1/4 inch obstacle observed at 50cm.

$$x = \frac{.625\text{cm}}{50\text{cm}} = .0125 \qquad \text{(A2-2)}$$

As x decreases the difference in intensities becomes less. Since x for the moon is almost three times less than the result in A2-2 the intensity of the spot produced by the moon should be between one and one half the intensity produced by an equal sized circular obstacle. (This assumes the results by Raman and Krishnan apply to any sized obstacle.) The girth of the moon should have little effect on the observed spot intensity.

Before reaching the surface of the earth the rays diffracted by the lunar edges must pass through the earth's atmosphere. Variations in atmospheric density will introduce phase differences. The cumulative effect of differences may result in destructive interference which diminishes spot intensity. A model to test atmospheric effects

is depicted below. The flame introduces air currents which cause variations in air density with resultant phase differences.

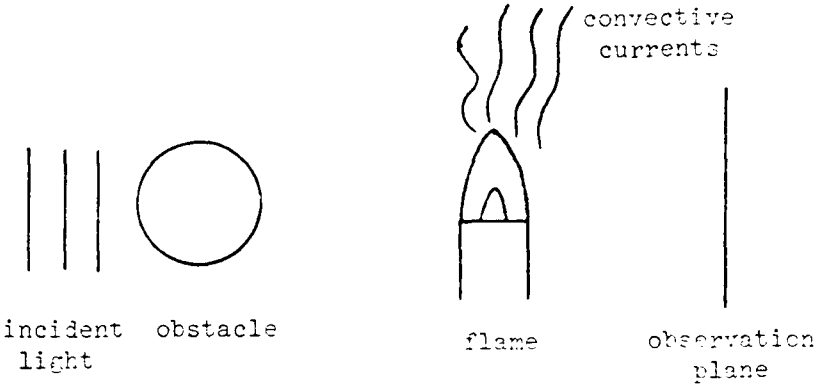

Figure A2.1

Model to Test Atmospheric Effects in Spot

The size of the spot will be affected by the diameter of the obstacle and the observation distance. Taking the radius of the spot as the radial distance to the first intensity minimum in the ring structure, then for the lunar case.

$$\frac{kr_2 d}{2z} = 2.4048$$

$$r_2 = \frac{4.8096z}{kd} \qquad \text{(A2-3)}$$

If one takes λ = 5000A as an average optical wavelength then

$$r_2 = 8.46 \times 10^{-5} m$$

The ratio of the spot size to the shadow size is on the order of 5×10^{-11}. This makes the spot impossibly small to see unless the

observation is made where the center of the shadow hits the earth's surface with some sort of magnifying device.

The spot should exist at the center of the moon's shadow but the effect will be significant only for points in space a much greater distance behind the moon than the earth.

Notes

[1] C. V. Raman and K. S. Krishnan, "On the Diffraction of Light by Spherical Obstacles," Procedings of the Physical Society, 38 (August 1926), 351.

[2] CRC Handbook of Chemistry and Physics, 62nd ed.

Appendix 3

ON AXIS INTENSITY IMMEDIATELY BEHIND AN ANNULAR APERTURE

The maximum intensity on axis behind an annular aperture is found from equation III-37. The argument of the cosine factor for maxima is of the form $(2n + 1)\pi$ where n is an integer. Then the intensity is:

$$I_{max}\ (0,\ 0,\ z_{max}) = A^2\left[\frac{1}{\sqrt{1+\ d^2/4z^2}} + \frac{1}{\sqrt{1+\ d^2/4z^2}}\right]^2 \qquad \text{(A3-1)}$$

with the restriction that Z satisfies:

$$z_{max} = \frac{D^2-d^2}{4\lambda(2n+1)} \qquad n = 0,\ 1,\ 2\ \ldots \qquad \text{(A3-2)}$$

Expression A3-1 forms an upper limit to the oscillations of the intensity on axis.

Likewise the minimum intensities on axis satisfy the relation:

$$I_{min}\ (0,\ 0,\ z_{min}) = A^2\left[\frac{1}{\sqrt{1+\ \frac{D^2}{4z^2}}} - \frac{1}{\sqrt{1+\ \frac{d^2}{4z^2}}}\right]^2 \qquad \text{(A3-3)}$$

with the restriction for Z:

$$z_{min} = \frac{D^2-d^2}{8m\lambda} \qquad m = 1,\ 2,\ 3,\ \ldots$$

In the region where $\frac{d^2}{4z^2} \ll 1$ and $\frac{D^2}{4z^2} \ll 1$ then the upper and

lower bounds to the oscillatory envelope are $4I_0$ and 0.

Consider the region immediately behind the aperture. Here $\frac{d^2}{4z^2}$ and $\frac{D^2}{4z^2}$ are not negligible. For very small z these factors become very large -- becoming the dominant terms in the square roots in the denominators of A3-1 and A3-3. The upper and lower limits of the intensity oscillation envelope both go to zero as Z gets infinitesimally small.

If the obscuration ratio of the aperture is very small (D >> d) then there is a region along the optical axis where the effect from the outer edge is negligible compared to that from the inner edge. Here $\frac{D^2}{4z^2} >> 1$ but $\frac{d^2}{4z^2}$ is not. Then A3-1 and A3-3 become

$$I_{max,min} \simeq A^2 \frac{1}{1+\frac{d^2}{4z^2}} \qquad \text{(A3-4)}$$

which is the result for the circular obscuration alone.

Physically this result is easily explained. As depicted below the cosine obliquity factor for outer edge diffracted rays is much smaller than that for inner edge diffracted rays. The amplitudes of outer edge diffracted rays are diminished into insignificance.

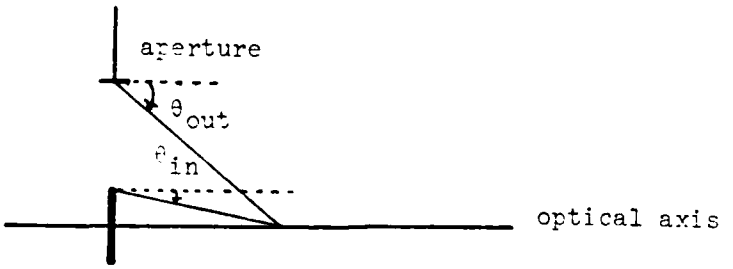

Figure A3.1

Ray Diffracted to Near On-axis Point

The following two graphs show the on axis intensities for the region immediately behind annular apertures with obscuration ratios of 1/100 and 1/1000.

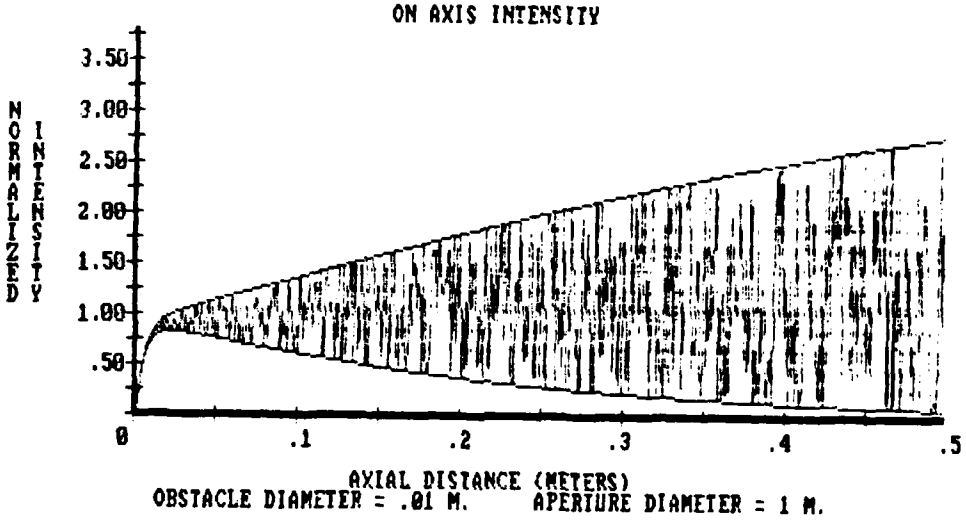

Graph A3.1

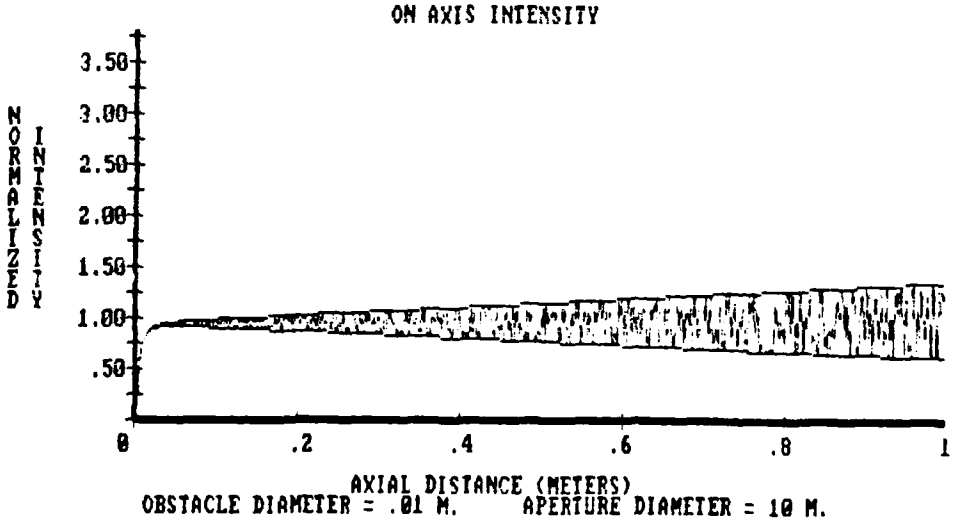

Graph A3.2

The graphs demonstrate that on axis immediately behind an annular aperture (of sufficiently small ε) the intensity pattern is characteristic of a circular obstacle alone. As z increases, the intensity oscillation envelope unfolds and the pattern becomes characteristic of the annular (or circular) aperture.

The off-axis intensity plots for an annular aperture of obscuration ratio 1/1000 are given before for optical axis distances of .5m and 20m. This dramatically shows the circular obscuration behavior for small z and the circular aperture behavior for large z.

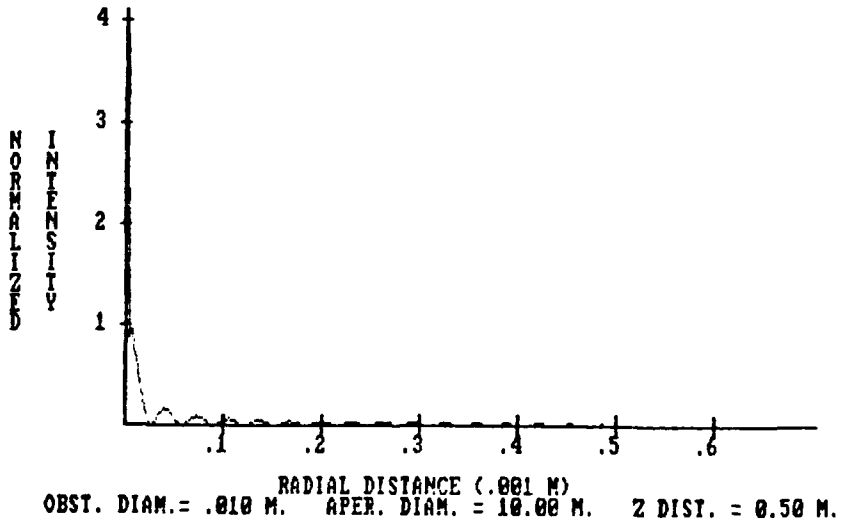

Graph A3.3

Intensity Distribution for Small z

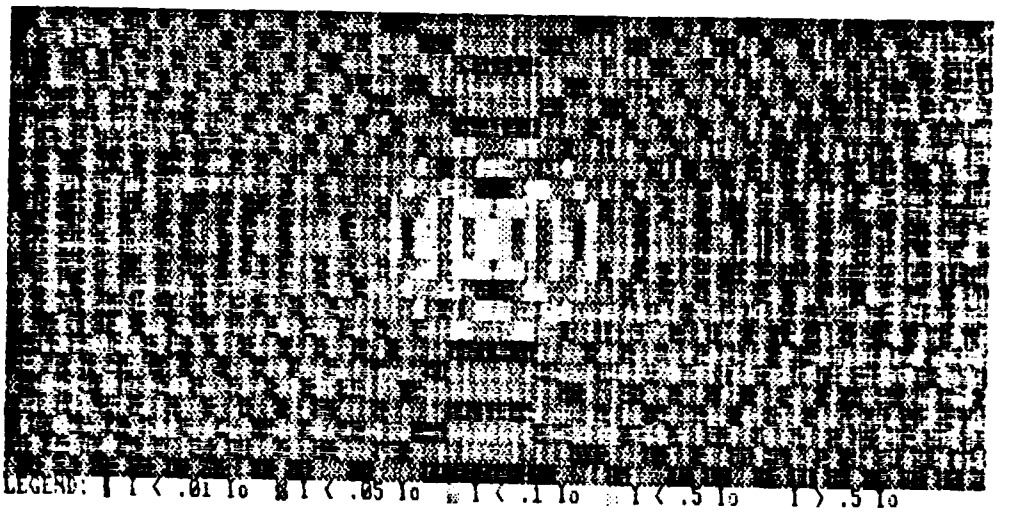

Graph A3.4

Annular Aperture Pattern for Small z

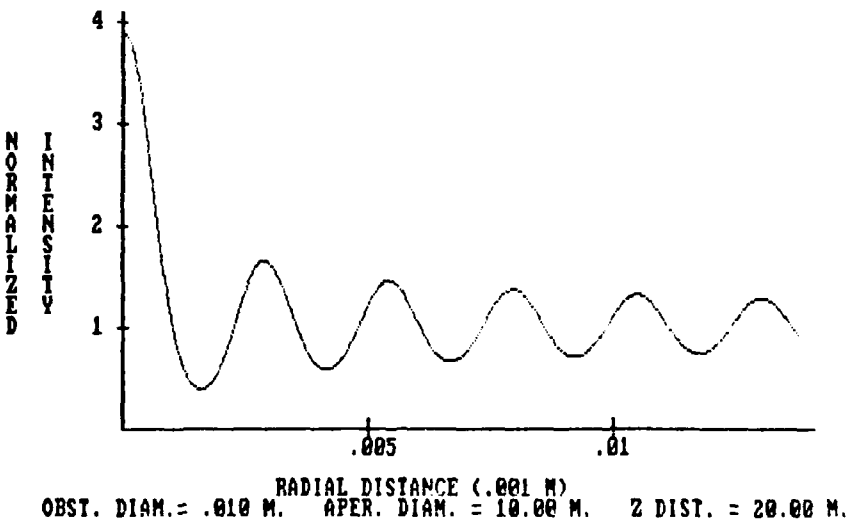

Graph A3.5

Intensity Distribution for Large z

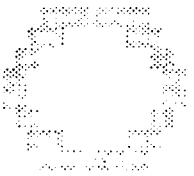

LEGEND: ▮ I < .01 Io ▩ I < .05 Io ▨ I < .1 Io ▒ I < .5 Io I > .5 Io

Graph A3.6

Annular Aperture Pattern for Large z

Appendix 4

MIMICING OF UNABERRATED BEHAVIOR BY WAVES CONTAINING DEFOCUS OR SPHERICAL ABERRATION

One of the important results from Chapter 4 was that the spacing between maxima and minima on axis behind an annular apertue was independent of any aberration present. It was also shown that defocus and spherical aberration shift the positions of extrema. Consider the case where the aberration shifts a maximum (call it the m^{th} order maximum) onto the position of the n^{th} order maximum for the unaberrated case. Can the amount of aberration present be determined?

Assume the aberration present is defocus with aberration coefficient W_{20}. Then if the position of the m^{th} order maximum for aberrated case (z') is the same as the position of the unaberrated n^{th} order maximum (z), one can equate equations III-40 and IV-16:

$$z = \frac{D^2(1-\varepsilon^2)}{4\lambda(2n+1)} = \frac{D^2(1-\varepsilon^2)}{4\lambda(2m+1) - 8W_{20}(1-\varepsilon^2)} = z' \qquad \text{(A4-1)}$$

$$4\lambda(2m + 1) - 8W_{20}(1 - \varepsilon^2) = 4\lambda(2n + 1)$$

$$W_{20} = \frac{(m-n)}{(1-\varepsilon^2)}\ \lambda \qquad \text{(A4-2)}$$

Both m and n are integers so let p = m - n where p must be an integer. Then if defocus is of the form:

$$W_{20} = \frac{P}{(1-\varepsilon^2)} \lambda \qquad \text{(A4-3)}$$

the extrema for the aberrated case are exactly superimposed on the extrema for the unaberrated case. (Equation A4-3 is also the expression obtained by considering the m^{th} order aberrated minimum and the n^{th} order unaberrated minimum. m and n are strictly arbitrary.)

Thus if one takes measurements of axial positions of extrema and compares them to the unaberrated positions and finds them identical, then the proper conclusion drawn is that any defocus present has the form given by equation A4-3. (Clearly the unaberrated case corresponds to $p = 0$.) In this case the amount of defocus can be determined best by intensity considerations.

The corresponding condition for the superposition of extrema for spherical aberration is:

$$W_{40} = \frac{P}{(1-\varepsilon^4)} \lambda \qquad \text{(A4-4)}$$

Appendix 5

ON-AXIS INTENSITY AT Z = $-\frac{d^2}{8W_{20}}$ BEHIND A CIRCULAR OBSCURATION AND ANNULAR APERTURE

On axis the Rayleigh-Sommerfeld integral given by equation IV-3 is reduced to:

$$U(0, z) = \frac{Ak}{iz} e^{ikz} \int_{d/2}^{\infty} e^{ik\left[\frac{1}{2z} + 4\frac{W_{20}}{d^2}\right]r_1^2} r_1 dr_1 \qquad \text{(A5-1)}$$

At $z = -\frac{d^2}{8W_{20}}$, for $W_{20} < 0$, the above is:

$$U(0, -\frac{d^2}{8W_{20}}) = -\frac{8AkW_{20}}{id^2} e^{-ikd^2/8W_{20}} \int_{d/2}^{\infty} e^{ik\left[-\frac{4W_{20}}{d^2} + \frac{4W_{20}}{d^2}\right]r^2}$$

$$x \quad r_1 dr_1$$

$$= -\frac{8AkW_{20}}{id^2} e^{-ikd^2/8W_{20}} \int_{d/2}^{\infty} r_1 dr_1$$

$$= -\frac{4AkW_{20}}{id^2} e^{-ikd^2/8W_{20}} r_1^2 \Big|_{d/2}^{\infty} \qquad \text{(A5-2)}$$

For the circular obscuration case the disturbance function (and therefore the intensity) takes on an infinite value at this particular z.

If the upper limit is not infinite then (A5-2) becomes:

$$U(0, \frac{D^2}{8W_{20}}) = -\frac{4AkW_{20}}{iD^2} e^{-ikd^2/8W_{20}} \left(\frac{D^2}{4} - \frac{d^2}{4}\right)$$

$$= -\frac{A}{i} kW_{20}(1 - \varepsilon^2) e^{-ikd^2/8W_{20}} \qquad (A5-3)$$

The intensity is:

$$I(0, -\frac{D^2}{8W_{20}}) = \left| U(0, -\frac{D^2}{8W_{20}}) \right|^2$$

$$= A^2k^2W_{20}{}^2(1 - \varepsilon^2) \qquad (A5-4)$$

Thus the intensity has a finite value.

An alternate, but related, question is can an on axis maximum occur at $z = -\frac{D^2}{8W_{20}}$ (thus implying infinite intensity)? For this to happen one must satisfy:

$$z = \frac{D^2(1-\varepsilon^2)}{4\lambda(2n+1) - 8W_{20}(1-\varepsilon^2)} = -\frac{D^2}{8W_{20}}$$

$$8W_{20}D^2(1 - \varepsilon^2) = -4\lambda D^2(2n + 1) + 8W_{20}D^2(1 - \varepsilon^2) \qquad (A5-5)$$

or

$$4\lambda D^2(2n + 1) = 0 \qquad (A5-6)$$

which is impossible. Thus the intensity should remain finite in the annular aperture case, in agreement with A5-4.

Appendix 6

SEPARATION OF DEFOCUS AND SPHERICAL ABERRATION BY AXIAL SHIFTING OF MAXIMA WITH DIFFERENT OBSCURATION RATIOS

From equation IV-66 the axial shift from the unaberrated case for the n^{th} maximum behind an annular aperture when both defocus and spherical aberration are present is:

$$\Delta z = \frac{D^2(1-\varepsilon^2)^2}{2} \quad \frac{W_{20} + W_{40}(1+\varepsilon^2)}{\lambda(2n+1)\left[\lambda(2n+1) - 2W_{20}(1-\varepsilon^2) - 2W_{40}(1-\varepsilon^4)\right]} \tag{IV-66}$$

$$\Delta z\left[\lambda(2n+1) - 2W_{20}(1-\varepsilon^2) - 2W_{40}(1-\varepsilon^4)\right] = \frac{D\ (1-\varepsilon^2)^2}{2\ (2n+1)} \times \left[W_{20} + W_{40}(1+\varepsilon^2)\right]$$

$$W_{20} + W_{40}(1+\varepsilon^2) = \frac{2\Delta z\lambda^2(2n+1)^2}{D^2(1-\varepsilon^2)^2} - \frac{\Delta z 4\lambda(2n+1)}{D^2(1-\varepsilon^2)}\ W_{20} - \frac{\Delta z 4\lambda(2n+1)}{D^2(1-\varepsilon^2)^2}\ W_{20}(1+\varepsilon^2)$$

$$(W_{20} + W_{40}(1+\varepsilon^2))\quad \frac{D^2(1-\varepsilon^2) + \Delta z 4\lambda(2n+1)}{D^2(1-\varepsilon^2)}$$

$$= \frac{2\Delta z\lambda^2(2n+1)^2}{D^2(1-\varepsilon^2)}$$

$$W_{20} + W_{40}(1 + \varepsilon^2) = \frac{2\Delta z\lambda^2(2n+1)^2}{(D^2(1-\varepsilon^2) + \Delta z 4\lambda(2n+1))(1-\varepsilon^2)} \qquad \text{(A6-1)}$$

If the axial shifts from two different obscuration ratios are measured, there will be two equations with which to find the two unknowns (W_{20} and W_{40}). Subtracting the two resulting equations and solving for W_{40} yields:

$$W_{40}(\varepsilon_1^2 - \varepsilon_2^2) = \frac{2\Delta z_1 \lambda^2(2n+1)^2}{(D^2(1-\varepsilon_1^2) + \Delta z\ 4\lambda(2n+1))(1-\varepsilon_1^2)} -$$

$$\frac{2\Delta z_2 \lambda^2(2n+1)^2}{(D^2(1-\varepsilon_2^2) + \Delta z_2 4\lambda(2n+1))(1-\varepsilon_2^2)}$$

$$W_{40} = \frac{2\lambda^2(2n+1)^2}{(\varepsilon_1^2-\varepsilon_2^2)(1-\varepsilon_1^2)(1-\varepsilon_2^2)}$$

$$\left[\Delta z_1 D^2(1-\varepsilon_2^2)^2 + \Delta z_1\Delta z_2 4\lambda(2n+1)(1-\varepsilon_2^2) -\right.$$

$$\left.\Delta z_2 D^2(1-\varepsilon_1^2)^2 - \Delta z_1\Delta z_2 4\lambda(2n+1)(1-\varepsilon_1^2)\right]$$

$$\div \left[(D^2(1-\varepsilon_1^2) + \Delta z_1 4\lambda(2n+1))(D^2(1-\varepsilon_2^2) + \Delta z_2 4\lambda(2n+1))\right]$$

$$= \frac{2\lambda^2(2n+1)^2}{(\varepsilon_1^2-\varepsilon_2^2)(1-\varepsilon_1^2)(1-\varepsilon_2^2)}$$

$$x \frac{D^2\left[\Delta z_1(1-\varepsilon_2{}^2)^2 - \Delta z_2(1-\varepsilon_1{}^2)^2\right] + 4\lambda(2n+1)\Delta z_1\Delta z_2(\varepsilon_1{}^2-\varepsilon_2{}^2)}{(D^2(1-\varepsilon_1{}^2) + \Delta z_1 4\lambda(2n+1))(D^2(1-\varepsilon_2{}^2) + \Delta z_2 4\lambda(2n+1))}$$

(A6-2)

The above unwieldy expression has no readily apparent simplification. Substituting back into equation A6-1 yields:

$$W_{20} = \frac{2\lambda^2(2n+1)^2}{(\varepsilon_1{}^2-\varepsilon_2{}^2)(1-\varepsilon_1{}^2)(1-\varepsilon_2{}^2)} \quad \frac{\Delta z_1(1-\varepsilon_2{}^2)(\varepsilon_1{}^2-\varepsilon_2{}^2)}{(D^2(1-\varepsilon_1{}^2) + \Delta z_1 4\lambda(2n+1))} -$$

$$\frac{2\lambda^2(2n+1)^2}{(\varepsilon_1{}^2-\varepsilon_2{}^2)(1-\varepsilon_1{}^2)(1-\varepsilon_2{}^2)}$$

$$x\ (1+\varepsilon_1{}^2)\left[D^2(\Delta z_1(1-\varepsilon_2{}^2)^2 - \Delta z_2(1-\varepsilon_1{}^2)^2) + 4\lambda(2n+1)\right.$$

$$\left. x\ \Delta z_1\Delta z_2(\varepsilon_1{}^2-\varepsilon_2{}^2)\right]$$

$$\div (D^2(1-\varepsilon_1{}^2) + \Delta z_1 4\lambda(2n+1))(D^2(1-\varepsilon_2{}^2) + \Delta z_2 4\lambda(2n+1))$$

$$W_{20} = \frac{2\lambda^2(2n+1)^2}{(\varepsilon_1{}^2-\varepsilon_2{}^2)(1-\varepsilon_1{}^2)(1-\varepsilon_2{}^2)}$$

$$D^2\left[\Delta z_1(1-\varepsilon_2{}^2)^2(1-\varepsilon_1{}^2) - \Delta z_2(1-\varepsilon_1{}^2)^2(1-\varepsilon_2{}^2) -\right.$$

$$\left. 4\lambda(2n+1)\Delta z_1\Delta z_2(\varepsilon_1{}^4-\varepsilon_2{}^4)\right]$$

$$\div (D^2(1-\varepsilon_1{}^2) + \Delta z_1 4\lambda(2n+1))(D^2(1-\varepsilon_2{}^2) + \Delta z_2 4\lambda(2n+1))$$

(A6-3)

Appendix 7

COMPARISON OF CALCULATIONS USING SINGLE PRECISION AND DOUBLE PRECISION NUMBERS

Most of the graphs in this thesis were calculated and plotted using an IBM Personal Computer. The IBM can store numbers with either single or double precision. Using single precision, only six digits are accurate. With double precision, 17 digits are accurate.[1] The drawback to using double precision numbers is the longer program execution time required. For example, a typical run to produce an off axis intensity contour plot took approximately ten minutes with single precision. Double precision required almost twenty minutes for the same run. Because of the large time differences, it is important to ask whether the loss of accuracy using single precision numbers is significant.

To test this, four runs were made. The program calculating the off-axis intensity distribution takes the most time and has the highest number of calculations of the programs used. The maximum and minimum values for the intensity distributions produced using double and single precision were compared. The first two runs used the case of a one centimeter circular obscuration viewed at a distance of one meter. The last two runs used the case of an annular aperture of outer diameter one centimeter and inner diameter .3333 centimeters viewed at the position of an on-axis minimum at .5017 meters.

For the circular obscuration case, 22 points corresponding to the radial distances for maxima and minima up to .7 millimeters from center were compared. The radial distances were calculated to the nearest one and one half microns and the corresponding normalized intensities to the nearest .0001. Of the 22 radial distances only two differed. Likewise only two intensities differed in value. These differences are listed below.

Table A7.1

Comparison of Single Precision Versus Double Precision for Circular Obscuration Run

Extremum Type	Single Precision Calculated Position (mm)	Double Precision Calculated Position (mm)	Difference (mm)
Minimum #4	.237	.238	.001
Minimum #5	.302	.300	-.002

Extremum Type	Single Precision Calculated Intensity	Double Precision Calculated Intensity	Difference
Maximum #5	.4076	.0477	.0001
Maximum #5	.0000	.0001	.0001

The plots for each case reveal no apparent difference.

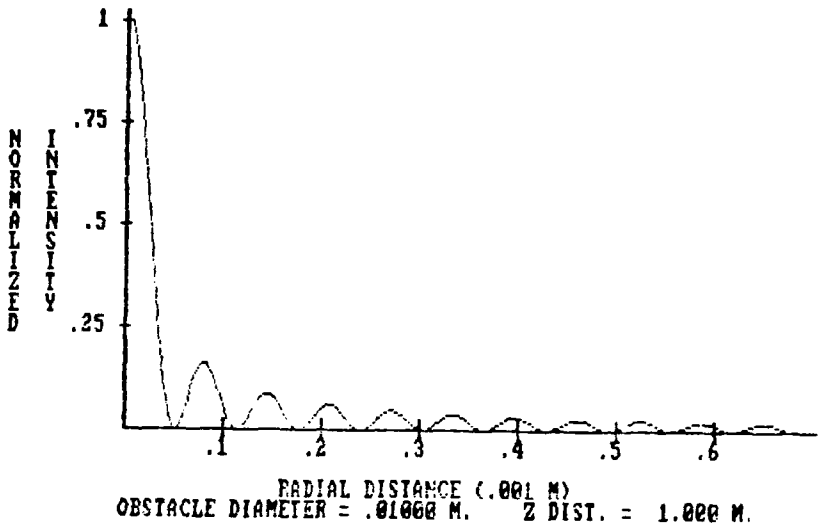

Graph A7.1

Double precision

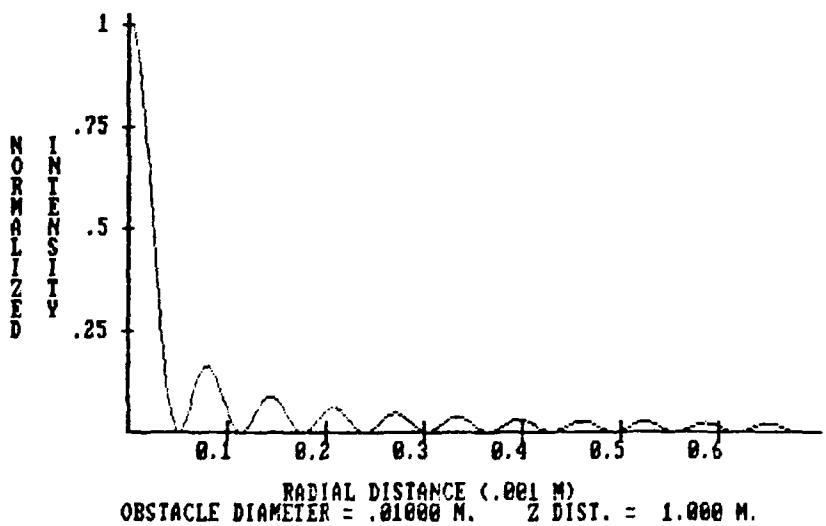

Graph A7.2

Single precision

For the annular aperture case, the first 46 extrema out to a radial distance of 1.1 millimeters were compared. Of the 46 positions 10 differed each by only .001 millimeters. Only two intensities varied. The differences are listed below.

Table A7.2

Comparison of Single Precision Versus Double Precision for Annular Aperture Run

Extremum Type	Single Precision Calculated Position (mm)	Double Precision Calculated Position (mm)	Difference (mm)
Minimum #2	.062	.063	.001
Maximum #3	.132	.133	.001
Maximum #6	.267	.268	.001
Maximum #8	.362	.363	.001
Maximum #9	.417	.418	.001
Minimum #12	.537	.538	.001
Maximum #12	.552	.553	.001
Maximum #13	.607	.608	.001
Minimum #16	.727	.728	.001

Extremum Type	Single Precision Calculated Intensity	Double Precision Calculated Intensity	Difference
Maximum #3	.3158	.3154	.0004
Maximum #9	.0996	.0994	.0002

For this run all position differences were .001mm lower in the single precision case. Still, there is very little change between the two runs.

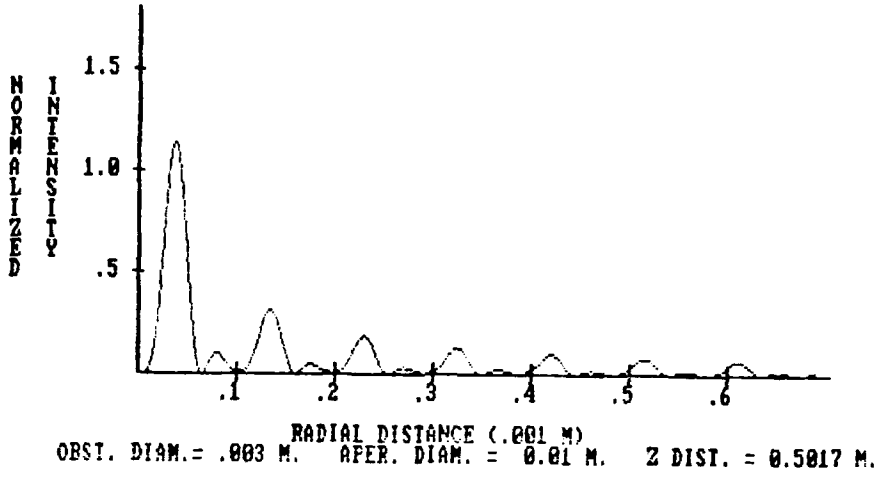

Graph A7.3

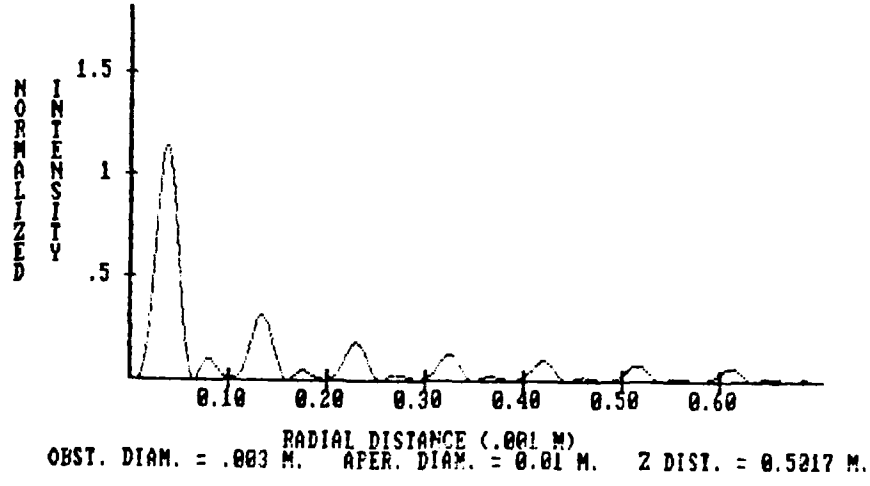

Graph A7.4

These four runs suggest for the degree of accuracy required to produce the plots and graphs, single precision is sufficient.

Notes

[1] BASIC - IBM Personal Computer Hardware Reference Library, 1st ed., pp. 311.

Appendix 8

COMPUTER PROGRAM LISTINGS

The programs listed below were used to study on and off axis intensity patterns behind circular obscurations and annular apertures. The programs are written in advanced BASIC using DOS 1.1 for the IBM Personal Computer. The advanced features of BASIC allowed for graphics with a screen resolution of 200 x 640 pixels.

The first program listed is MAXMIN. This program lists the positions for the maxima and minima on axis behind an annular aperture. The computer prompts (inputs) are self-explanatory. Allowance is made for the presence of defocus, spherical aberration and a displaced obstacle and aperture. The distance along the optical axis is measured from the aperture. If Δz is the separation between the aperture and obstacle, the n^{th} order maximum satisfies:

$$z_{max} = \frac{1}{2}\left[\frac{D^2 - d^2}{4\lambda(2n+1) - 8W_{20}(1-\varepsilon^2) - 8W_{40}(1-\varepsilon^4)} - \Delta z + \sqrt{\left(\Delta z - \frac{D^2 - d^2}{4\lambda(2n+1) - 8W_{20}(1-\varepsilon^2) - 8W_{40}(1-\varepsilon^4)}\right)^2 + \frac{\Delta z D^2}{4\lambda(2n+1) - 8W_{20}(1-\varepsilon^2) - 8W_{40}(1-\varepsilon^4)}}\right] \qquad \text{(A8-1)}$$

The nth order minimum has the same form with (2n + 1) replaced by 2n.

The second program is AXIS.OBS. This program plots the on axis intensity function behind a circular obscurration, using equations IV-43 and III-34.

The third program is AXIS.ANN. This program is the analog of AXIS.OBS for the annular aperture. It employs equation IV-72 for r_2 = 0.

The fourth program is ARAGO.OBS. This provides an intensity contour plot and a radial intensity function plot for the diffraction pattern at a given distance behind a circular obstacle. This program uses equations IV-43 and III-34.

The last program is ARAGO.ANN which yields the plots mentioned above for an annular aperture. Equation IV-72 is used. This program, as well as ARAGO.OBS, includes a subroutine to find Bessel functions of the first kind. The subroutine comes from BASIC Programs for Scientists and Engineers by Miller.[1]

```
1 '    PROGRAM:  MAXMIN
2 '
5 DIM MAX(21),MIN(21)
10 ' MAXIMA AND MINIMA ON AXIS--UNIFORM BEAM, NO ABERRATIONS
20 KEY OFF
30 CLS
40 PRINT
50 PRINT "THIS PROGRAM PROVIDES A LISTING OF MAXIMA AND MINIMA ON AXIS
60 PRINT "BEHIND A TARGET CONSISTING OF A DISPLACED OBSTACLE AND APERTURE.
70 PRINT "WE ASSUME A WAVELENGTH OF 6328 ANGSTROMS.
80 PRINT
90 PRINT "INPUTS ARE SEPARATION OF OBSTACLE AND APERTURE, DIAMETERS OF
100 PRINT "OBSTACLE AND APERTURE, AND ABERRATION COEFFICIENTS.
110 PRINT
120 INPUT "INPUT THE SEPARATION OF OBSTACLE AND APERTURE IN METERS";DELZ
130 PRINT
140 INPUT "INPUT THE DIAMETER OF THE APERTURE IN METERS";DD
150 PRINT
160 INPUT "INPUT THE DIAMETER OF THE OBSTACLE IN METERS";D
165 EPS = D/DD
170 PRINT
172 INPUT "INPUT AMOUNT OF DEFOCUS IN TERMS OF WAVELENGTHS";DFC
174 PRINT
176 INPUT "INPUT AMOUNT OF SPHERICAL ABERRATION IN TERMS OF WAVELENGTH";SA
178 PRINT
180 INPUT "DO YOU WISH A PRINT OUT ON SCREEN (Y/N)";PRT$
190 IF PRT$ = "Y" THEN PRT = 1 ELSE PRT = 0
191 '
192 '  CALCULATE MAXIMA AND MINIMA USING EQUATIONS A8-1 AND A8-2.
193 '
195 LAM = 6.328E-07
196 W020 = DFC*LAM
197 W040 = SA*LAM
200 COEF1 = DD*DD - D*D
210 COEF2 = DD*DD
215 COEF3 = 2*W020*(1-EPS*EPS) + 2*W040*(1-EPS*EPS*EPS*EPS)
220 FOR N = 0 TO 40
222 COEF5 = LAM*(2*N+1) - COEF3
224 COEF6 = LAM*2*N - COEF3
250 MAX(N+1) = (COEF1/(4*COEF5) - DELZ + SQR((DELZ-COEF1/(4*COEF5))^2 + COEF2*
    DELZ/COEF5))/2
255 IF N = 0 GOTO 270
260 MIN(N+1) = (COEF1/(4*COEF6) - DELZ + SQR((DELZ-COEF1/(4*COEF6))^2 + COEF2*
    DELZ/COEF6))/2
270 IF PRT = 0 GOTO 300
280 PRINT N,MAX(N+1),MIN(N+1)
300 NEXT N
301 '
302 '  PRINT OUT RESULTS
303 '
310 LPRINT "MAXIMA AND MINIMA ON AXIS:
320 LPRINT
330 LPRINT "SEPARATION OF OBSTACLE AND APERTURE = ";DELZ;" M."
340 LPRINT
```

```
350 LPRINT "DIAMETER OF APERTURE = "3DD" M.     DIAMETER OF OBSTACLE = "ID" M.
360 LPRINT
365 LPRINT "DEFOCUS = "3FC" WAVELENGTHS      SPHERICAL ABERRATION = "3SA" WAV
ELENGTHS"
366 LPRINT
370 LPRINT "ORDER (N)        Z(MAXIMA)          Z(MINIMA)"
380 LPRINT "----------       ---------          ---------"
390 FOR N = 1 TO 41
400 LPRINT USING "   ##            ###.####            ###.####";N-1,MAX(N) MIN(N)

410 NEXT N
420 PRINT
430 INPUT "DO YOU WISH TO MAKE ANOTHER RUN (Y/N)";D$
440 IF D$ = "Y" THEN GOTO 10 ELSE END
```

```
1 '  PROGRAM: AXIS.OBS
2 '
10 CLS
20 KEY OFF
30 PRINT
40 PRINT "THIS PROGRAM CALCULATES THE INTENSITY ON AXIS BEHIND AN CIRCULAR
50 PRINT "OBSTACLE
60 PRINT
70 PRINT "WE ASSUME A WAVELENGTH OF 6328 ANGSTROMS.
80 PRINT
100 '
101 '   INPUT PARAMETERS
102 '
110 INPUT "WHAT IS THE MAXIMUM DISTANCE BEHIND THE SCREEN TO BE CALCULATED";ZMAX

140 PRINT
145 INPUT "WHAT IS THE MINIMUM DISTANCE BEHIND THE SCREEN TO BE CALCULATED";ZMIN

146 PRINT
147 Z1 = ZMAX - ZMIN
150 '
151 '   CALCULATE THE RANGE ALONG THE OPTICAL AXIS TO BE PLOTTED
152 '
155 Z1 = ZMAX - ZMIN
160 INPUT "WHAT IS THE DIAMETER OF THE OBSTACLE (METERS)";D
170 PRINT
190 PRINT: INPUT "WHAT IS THE COEFFICIENT FOR DEFOCUS IN TERMS OF WAVELENGTH";W1

195 W020 = 6.328E-07 * W1
200 PRINT: INPUT "WHAT IS THE COEFFICIENT FOR SPHERICAL ABERRATION IN TERMS OF W
AVELENGTH";W2
210 W040 = 6.328E-07 * W2
220 PRINT: INPUT "WHAT IS THE GAUSSIAN CONSTANT";GC
230 '
231 ' CALCULATE THE GAUSSIAN FACTOR
232 '
240     GF1 = EXP(-GC/4)
890 '
891 ' TRANSFER TO COLOR DISPLAY
892 '
900 PRINT: INPUT "MAKE SURE VIDEO SCREEN IS ON AND HIT RETURN WHEN READY" ARB$
910 DEF SEG = 0
920 POKE &H410,(PEEK(&H410) AND &HCF) OR &H10
930 SCREEN 1,0,0,0 : SCREEN 0: WIDTH 80
940 LOCATE ,,1,6,7 : DEF SEG
950 GOTO 1000
960 '
961 ' TRANSFER BACK TO MONOCHROME
962 '
970 DEF SEG = 0
980 POKE &H410, (PEEK(&H410) OR &H30)
990 SCREEN 0: WIDTH 40: WIDTH 80: LOCATE ,,1,12,13: DEF SEG: GOTO 1770
1000 '
1001 '   PLOT THE AXES
1002 '
1005 CLS
1010 SCREEN 2
1020 FOR I = 1 TO 20
1030 LOCATE I,12
```

```
1040 PRINT CHR$(179);
1050 NEXT I
1060 LOCATE 21,12
1070 PRINT CHR$(192)
1080 FOR I = 1 TO 65
1090 LOCATE 21,12+I
1100 PRINT CHR$(196);
1110 NEXT I
1120 '
1121 '  LABEL Y AXIS
1122 '
1125 LOCATE 16,9
1130 PRINT 1;CHR$(197)
1140 LOCATE 11,9
1150 PRINT 2;CHR$(197)
1160 LOCATE 6,9
1170 PRINT 3;CHR$(197)
1180 LOCATE 1,9
1190 PRINT 4;CHR$(197)
1200 FOR I = 1 TO 9
1210 LOCATE 6+I,5
1220 ON I GOTO 1230,1250,1270,1290,1250,1310,1230,1270,1330
1230 PRINT "I"
1240 GOTO 1340
1250 PRINT "N"
1260 GOTO 1340
1270 PRINT "T"
1280 GOTO 1340
1290 PRINT "E"
1300 GOTO 1340
1310 PRINT "S"
1320 GOTO 1340
1330 PRINT "Y"
1340 NEXT I
1350 '
1351 '  CALCULATION AND PLOTTING OF THE INTENSITY FUNCTION USING EQUATION A10-3
1352 '
1355 Z = Z1/540
1360 FOR I = 1 TO 540
1405     AB2 = (1-16*W040*(ZMIN+Z*I)/(D*D))/(1+8*W020*(ZMIN+Z*I)/(D*D))
1410     X = 92 + I
1420     Y = 164 - CINT(AB2*AB2*GF1*GF1*40)
1425     IF I = 1 GOTO 1440
1430     LINE (X,Y)-(XO,YO)
1440     XO = X
1450     YO = Y
1460 NEXT I
1500 '
1501 '  LABEL X AXIS
1502 '
1530 POW = INT(LOG(Z1)/LOG(10))
1540 SCALE = Z1/10^POW
1550 IF SCALE < 4 THEN FACT = 2 ELSE FACT = 1
1560 UNIT = 46/(SCALE * FACT)
1570 FOR I = 1 TO INT(SCALE * FACT)
1580 LOCATE 21,12 + I*UNIT
1590 PRINT CHR$(197)
```

```
1600 LOCATE 22,7 + I*UNIT
1610 PRINT ZMIN+I*10^POW/FACT
1620 NEXT I
1630 LOCATE 23,20
1640 PRINT "AXIAL DISTANCE (METERS)"
1650 LOCATE 24,5
1660 PRINT "DIAMETER OF OBSCURATION = "10" M.     W20 = ";W1;"LAMBDA";
1670 LOCATE 25,5
1680 PRINT "W0 = ";W0;"LAMBDA     GAUSSIAN CONSTANT = ";GC;
1730 LOCATE 1,1
1740 '
1741 '  PAUSE TO ALLOW PRINTING OF PLOT
1742 '
1745 FOR I    1 TO 3000
1750 NEXT I
1760 GOTO 970
1770 CLS
1780 INPUT "DO YOU WISH TO MAKE ANOTHER RUN (Y/N)";D$
1790 IF D$ = "N" THEN END ELSE GOTO 130
```

```
1 '  PROGRAM: AXIS.ANN
2 '
10 CLS
20 KEY OFF
30 PRINT
40 PRINT "THIS PROGRAM CALCULATES THE INTENSITY ON AXIS BEHIND AN ANNULAR
50 PRINT "APERTURE
60 PRINT
70 PRINT "WE ASSUME A WAVELENGTH OF 6328 ANGSTROMS.
80 PRINT
100 '
101 '  INPUT PARAMETERS
102 '
110 INPUT "WHAT IS THE MAXIMUM DISTANCE BEHIND THE SCREEN TO BE CALCULATED";ZMAX

140 PRINT
145 INPUT "WHAT IS THE MINIMUM DISTANCE BEHIND THE SCREEN TO BE CALCULATED";ZMIN

146 PRINT
147 Z1 = ZMAX - ZMIN
150 '
151 '  CALCULATE THE RANGE ALONG THE OPTICAL AXIS TO BE PLOTTED
152 '
155 Z1 = ZMAX - ZMIN
160 INPUT "WHAT IS THE DIAMETER OF THE INNER OBSCURATION (METERS)";
170 PRINT
190 PRINT: INPUT "WHAT IS THE COEFFICIENT FOR DEFOCUS IN TERMS OF WAVELENGTH";W1

195 W020 = 6.328E-07 * W1
200 PRINT: INPUT "WHAT IS THE COEFFICIENT FOR SPHERICAL ABERRATION IN TERMS OF W
AVELENGTH";W2
210 W040 = 6.328E-07 * W2
220 PRINT: INPUT "WHAT IS THE GAUSSIAN CONSTANT";GC
230 '
231 ' CALCULATE THE GAUSSIAN FACTOR
232 '
240     GF1 = EXP(-GC/4)
260     GF2 = EXP(-GC*D*D/(4*DD*DD))
890 '
891 ' TRANSFER TO COLOR DISPLAY
892 '
900 PRINT: INPUT "MAKE SURE VIDEO SCREEN IS ON AND HIT RETURN WHEN READY";ARB$
910 DEF SEG = 0
920 POKE &H410,(PEEK(&H410) AND &HCF) OR &H10
930 SCREEN 1,0,0,0 : SCREEN 0: WIDTH 80
940 LOCATE ,,1,6,7 : DEF SEG
950 GOTO 1000
960 '
961 ' TRANSFER BACK TO MONOCHROME
962 '
970 DEF SEG = 0
980 POKE &H410, (PEEK(&H410) OR &H30)
990 SCREEN 0: WIDTH 40: WIDTH 80: LOCATE ,,1,12,13: DEF SEG: GOTO 1770
1000 '
1001 '  PLOT THE AXES
1002 '
1005 CLS
1010 SCREEN 2
```

```
1020 FOR I = 1 TO 20
1030 LOCATE I,12
1040 PRINT CHR$(179);
1050 NEXT I
1060 LOCATE 21,12
1070 PRINT CHR$(192)
1080 FOR I = 1 TO 66
1090 LOCATE 21,12+I
1100 PRINT CHR$(196);
1110 NEXT I
1120 '
1121 '  LABEL Y AXIS
1122 '
1125 LOCATE 16,9
1130 PRINT 1;CHR$(197)
1140 LOCATE 11,7
1150 PRINT 2;CHR$(197)
1160 LOCATE 6,9
1170 PRINT 3;CHR$(197)
1180 LOCATE 1,9
1190 PRINT 4;CHR$(197)
1200 G$ = "NORMALIZE": H$ = "INTENSITY"
1210 FOR I = 1 TO 9
1220 LOCATE 6+I,3
1230 PRINT MID$(G$,I,1);
1240 LOCATE 6+I,6
1250 PRINT MID$(H$,I,1);
1260 NEXT I
1270 LOCATE 16,3
1280 PRINT "D";
1350 '
1351 '  CALCULATION AND PLOTTING OF THE INTENSITY FUNCTION USING EQUATION A10-4
1352 '  KK = WAVE NUMBER
1353 '
1355 Z = Z1/540
1360 FOR I = 1 TO 540
1370     COEF4 = 4*Z*Z*GC*GC/(DD*DD*DD*DD*KK*KK)
1390     C = COS(1241147!*((DD*DD - D*D)/(ZMIN+Z*I) + 8*W020*(1-D*D/(DD*DD)) +
           32*W040*(1-D*D*D*D/(DD*DD*DD*DD))))
1400     AB1 = (1-16*W040*(ZMIN+Z*I)/(DD*DD))/((1+8*W020*(ZMIN+Z*I)/(DD*DD))*SQR
(1+DD*DD/(4*(ZMIN+Z*I)*(ZMIN+Z*I))))
1405     AB2 = (1-16*W040*(ZMIN+Z*I)*D*D/(DD*DD*DD*DD))/((1+8*W020*(ZMIN+Z*I)*D*
D/(DD*DD*DD*DD))*SQR(1+D*D/(4*(ZMIN+Z*I)*(ZMIN+Z*I))))
1406     COEF1 = AB1*AB1*GF1*GF1
1407     COEF2 = AB2*AB2*GF2*GF2
1408     COEF3 = 2*GF1*GF2*AB1*AB2*C
1410     Y = 95 - I
1420     Y = 164 - CINT((COEF1 + COEF2 - COEF3)/(1+COEF4)*40)
1425     IF I = 1 GOTO 1440
1430     LINE (X,Y)-(XO,YO)
1440     XO = X
1450     YO = Y
1460 NEXT I
1500 '
1501 '  LABEL X AXIS
1502 '
```

```
1530 POW = INT(LOG(Z1)/LOG(10))
1540 SCALE = Z1/10^POW
1550 IF SCALE < 4 THEN FACT = 2 ELSE FACT = 1
1560 UNIT = 66/(SCALE * FACT)
1570 FOR I = 1 TO INT(SCALE * FACT)
1580 LOCATE 21,12 - I*UNIT
1590 PRINT USING "#";I
1600 LOCATE 22,9 + I*UNIT
1610 PRINT USING "#";I/10 ^POW/FACT
1620 NEXT I
1630 LOCATE 24,30
1640 PRINT "AXIAL DISTANCE (METERS)";
1650 LOCATE 25,7
1660 PRINT USING "OBS. DIAM. = #.### M.   APER. DIAM. = # ##  M.   GAUSSIAN CON
ST. = #.#";1.2D,GC;
1670 'LOCATE 23,3
1680 'PRINT "      W020 = ";W1;"LAMBDA   W040 = ";W2;"LAMBDA    GAUSSIAN CONSTAN
T = ";GC;
1730 LOCATE 1,1
1740 '
1741 '  PAUSE TO ALLOW PRINTING OF PLOT
1742 '
1745 FOR I = 1 TO 3000
1750 NEXT I
1760 GOTO 970
1770 CLS
1780 INPUT "DO YOU WISH TO STORE THE PLOT ON DISK (Y/N)";A$
1790 IF A$ = "N" GOTO 1900
1800 '
1801 '  ROUTINE TO STORE PLOT
1802 '
1805 PRINT
1810 INPUT "WHAT IS THE NAME YOU WISH TO STORE THE PLOT UNDER";F1$
1820 FILNAM$ = "B:"+F1$
1830 DEF SEG = &HB800
1840 BSAVE FILNAM$,0,&H4000
1900 INPUT "DO YOU WISH TO MAKE ANOTHER RUN (Y/N)";D$
1910 IF D$ = "N" THEN END ELSE GOTO 130
```

```
1 '   PROGRAM: ARAGO.OBS
2 '
10 KEY OFF
15 DIM INTEN(110)
20 CLS
30 PRINT
40 PRINT "ARAGO PLOTTING ROUTINE:
50 PRINT
60 PRINT "THIS PROGRAM WILL GIVE A CONTOUR PLOT OF THE SPOT OF ARAGO AT A
70 PRINT "CHOSEN DISTANCE BEHIND AN OPAQUE CIRCULAR TARGET.
80 PRINT
90 PRINT "THIS PROGRAM ASSUMES A WAVELENGTH OF 6328 ANGSTROMS.  INPUTS ARE
100 PRINT "THE OBSTACLE DIAMETER, THE TOTAL RADIAL DISTANCE OFF THE
110 PRINT "OPTICAL AXIS FOR COMPUTATION, THE ABERRATION COEFFICIENTS FOR DEFOCUS

120 PRINT "AND SPHERICAL ABERRATION, THE GAUSSIAN CONSTANT AND THE DISTANCES Z1
125 PRINT "AND Z2 (MEASURED FROM THE APERTURE AND OBSTACLE RESPECTIVELY).
130 PRINT
140 PRINT
150 INPUT "INPUT THE TOTAL RADIAL DISTANCE TO BE CALCULATED (IN METERS)";R1
160 PRINT
170 INPUT "INPUT THE OBSTACLE DIAMETER";D
190 PRINT
195 INPUT "INPUT THE DISTANCE Z2 FROM OBSTACLE TO VIEWING PLANE (IN METERS)";Z2
200 PRINT
210 INPUT "INPUT THE COEFFICIENT OF DEFOCUS IN TERMS OF WAVELENGTH";W1
220 W020 = 6.328E-07 * W1
230 PRINT
240 INPUT "INPUT THE COEFFICIENT OF SPHERICAL ABERRATION IN TERMS OF WAVELENGTH"
;W2
250 W040 = 6.328E-07 * W2
260 PRINT
270 INPUT "INPUT THE GAUSSIAN CONSTANT";GC
280 PRINT
290 INPUT "DO YOU WANT TO SAVE THE CONTOUR PLOT ON DISK (Y/N)";CPLOT$
300 IF CPLOT$ = "N" GOTO 330
310 PRINT : INPUT "WHAT IS THE NAME OF THE FILE TO STORE THE PLOT UNDER";F1$
320 FIL1$ = "B:"+F1$
330 PRINT
340 INPUT "DO YOU WANT TO SAVE THE INTENSITY PLOT ON DISK (Y/N)";IPLOT$
350 IF IPLOT$ = "N" GOTO 410
360 PRINT: INPUT "WHAT IS THE NAME OF THE FILE TO STORE THE PLOT UNDER";F2$
370 FIL2$ = "B:" + F2$
380 ON ERROR GOTO 390
390 RESUME NEXT
400 PRINT: INPUT "DO YOU WISH TO BYPASS THE CONTOUR PLOT (Y/N)";PBY$
401 '
402 '  CALCULATE ABERRATION AND GAUSSIAN FACTORS
403 '
410 PI = 3.14159
418 AB2 = 1/(1+8*W020*Z2/(D*D))
420 AB4 = 1-16*W040*Z2/(D*D)
421 GF2 = EXP(-GC/4)
425 COEF2 = AB4*GF2*GF2/(AB2*AB2)
429 IO =  COEF2
430 PRINT : PRINT "COMPUTING ..."
500 D2 = 0
```

```
510 R = R1/320
520 FOR I = 1 TO 440
530 '
531 '  CALCULATE ARGUMENT FOR BESSEL FUNCTION AND EVALUATE RADIAL INTENSITY
      FUNCTION
532 '
535 X = (D + I * 8 * PI)/(6.328E-07 * Z2)
540 GOSUB 8000
550 INTEN(I) = COEF2*J7*J7
560 NEXT I
570 CLS
890 '
891 ' TRANSFER TO COLOR DISPLAY
892 '
900 PRINT: INPUT "MAKE SURE VIDEO SCREEN IS ON AND HIT RETURN WHEN READY";A$
910 DEF SEG = 0
920 POKE &H410,(PEEK(&H410) AND &HCF) OR &H10
930 SCREEN 1,0,0,0 : SCREEN 0: WIDTH 80
940 LOCATE ,,1,0,7 : DEF SEG
950 GOTO 995
960 '
961 ' TRANSFER BACK TO MONOCHROME
962 '
970 DEF SEG = 0
980 POKE &H410, (PEEK(&H410) OR &H30)
990 SCREEN 0: WIDTH 40: WIDTH 80: LOCATE ,,1,12,13: DEF SEG: GOTO 1950
995 SCREEN 2: WIDTH 80
1000 IF PBY$ = "Y" THEN GOTO 1200
1001 '
1002 '  CONTOUR PLOTTING ROUTINE.  FIND INTENSITY AT RADIAL DISTANCE FROM
       SCREEN CENTER (100,320).
1003 '
1004 FOR I = 1 TO 80
1005 FOR J = 1 TO 24
1007 J1 = J+1.7
1010 R2 = CINT(SQR((170-J1*8)*(170-J1*8) + (320-I*8)*(320-I*8)))
1012 IF R2 < 1 THEN R2 = 1
1015 GOSUB 2030
1020 ON DUM GOTO 1030,1050,1070,1090,1110
1030 A$ =CHR$(0)
1040 GOTO 1150
1050 A$ = CHR$(176)
1060 GOTO 1150
1070 A$ = CHR$(177)
1080 GOTO 1150
1090 A$ = CHR$(178)
1100 GOTO 1150
1110 A$ = CHR$(219)
1150 LOCATE J,I
1160 PRINT A$;
1170 NEXT J
1175 NEXT I
1177 GOSUB 2000
1180 '
1181 '  PAUSE FOR PRINTING AND STORING OF PLOT.
1182 '
1183 FOR K = 1 TO 5000: NEXT K
1185 IF CPLOT$ = "N" GOTO 1200
1190 DEF SEG= &HB800
1195 BSAVE FIL1$,0,&H4000
```

```
1200 '
1201 '  DRAW AXES
1202 '
1205 CLS
1210 FOR I = 1 TO 20
1220 LOCATE I,12
1230 PRINT CHR$(179);
1240 NEXT I
1250 LOCATE 21,12
1260 PRINT CHR$(192);
1270 FOR I = 1 TO 58
1280 LOCATE 21,12+I
1290 PRINT CHR$(196);
1300 '
1301 '  LABEL Y AXIS
1302 '
1305 NEXT I
1310 LOCATE 16,7
1320 PRINT .25;CHR$(197)
1330 LOCATE 11,8
1340 PRINT .5;CHR$(197)
1350 LOCATE 6,7
1360 PRINT .75;CHR$(197)
1370 LOCATE 1,9
1380 PRINT 1;CHR$(197)
1390 FOR I = 1 TO 9
1400 LAB1$ = "NORMALIZE": LAB2$ = "INTENSITY"
1410 FOR I = 1 TO 9
1420 LOCATE 6+I,3
1430 PRINT MID$(LAB1$,I,1);
1440 LOCATE 6+I,6
1450 PRINT MID$(LAB2$,I,1);
1460 NEXT I
1470 LOCATE 16,3
1480 PRINT "0";
1530 '
1531 '  LABEL X AXIS
1532 '
1540 LOCATE 24,25
1550 PRINT "RADIAL DISTANCE (.001 M)";
1560 '
1561 '  PLOT RADIAL INTENSITY FUNCTION
1562 '
1563 DDD = 1250 * R1
1570 POW = INT(LOG(DDD)/LOG(10))
1580 SCALE = DDD/10^POW
1590 IF SCALE < 4 THEN FACT = 2 ELSE FACT = 1
1600 UNIT = 30/(SCALE * FACT)
1610 FOR I = 1 TO INT(SCALE * FACT)
1620 LOCATE 21,12 + I*UNIT
1630 PRINT CHR$(197)
1640 LOCATE 22,10 + I*UNIT
1650 PRINT I*10^POW/FACT
1660 NEXT I
1665 Y0 = 164 - CINT(I0*160)
1666 X0 = 93
```

```
1670 FOR I = 1 TO 440
1680 Y = 164 - CINT(INTEN(I) * 160)
1685 X = 93 + I
1695 LINE (X,Y)-(XO,YO)
1700 XO = X
1705 YO = Y
1710 NEXT I
1720 LOCATE 25,2
1730 PRINT USING "          OBSTACLE DIAMETER = .##### M.     Z DIST. = ##.### M.
   ";D,Z2;
1735 LOCATE 1,1
1740 FOR I = 1 TO 5000
1745 NEXT I
1750 IF IPLOT$ = "N" GOTO 1800
1760 '
1761 '  STORE INTENSITY PLOT ON DISK
1762 '
1765 DEF SEG= &HB800
1770 BSAVE FIL2$,0,&H4000
1800 PRINT: INPUT "DO YOU WISH A LISTING OF THE INTENSITIES(Y/N)";D1$
1810 IF D1$ = "Y" THEN GOTO 1820 ELSE GOTO 1940
1820 LPRINT:LPRINT:LPRINT:LPRINT:LPRINT:LPRINT:LPRINT:LPRINT :LPRINT
1830 LPRINT : LPRINT : LPRINT : LPRINT : LPRINT : LPRINT : LPRINT
1840 LPRINT "RADIAL DISTANCE(MM)    INTENSITY    EXTREMUM TYPE
1850 LPRINT "--------------------    ---------    ------------
1855 IF IO - INTEN(1) > 0 THEN EXT$ = "MAXIMUM" ELSE EXT$ = "MINIMUM"
1860 LPRINT USING "       #.###                #.###";0,IO;
1865 LPRINT "         ";EXT$
1869 SIGN = SGN(IO-INTEN(1))
1870 FOR I = 1 TO 439
1880 IF SGN(INTEN(I+1)-INTEN(I)) = SIGN GOTO 1930
1890 IF SIGN > 0 THEN EXT$ = "MAXIMUM" ELSE EXT$ = "MINIMUM"
1900 SIGN = SGN(INTEN(I+1)-INTEN(I))
1910 LPRINT USING "       #.###                #.####";I*R*1000,INTEN(I);
1920 LPRINT "         ";EXT$
1930 NEXT I
1940 GOTO 970
1950 CLS
1960 INPUT "DO YOU WISH TO MAKE ANOTHER RUN (Y/N)";D$
1970 IF D$ = "N" THEN END ELSE GOTO 130
2000 '
2001 '  LABEL CONTOUR PLOT
2002 '
2005 LOCATE 24,1
2010 PRINT " LEGEND: ";CHR$(221);" I < .002 Io  ";CHR$(178);" I < .01 Io  ";CHR$
(177);" I < .05 Io  ";CHR$(176);" I < .2 Io  ";CHR$(0);" I > .2 Io";
2020 RETURN
2030 '
2031 '  FIND SHADING FOR CONTOUR PLOT POINTS
2032 '
2035 IF INTEN(R2) > .002 GOTO 2060
2040 DUM = 5
2050 RETURN
2060 IF INTEN(R2) > .01 GOTO 2090
2070 DUM = 4
2080 RETURN
2090 IF INTEN(R2) > .05 GOTO 2120
2100 DUM = 3
2110 RETURN
```

```
2120 IF INTEN(R2) > .2 GOTO 2150
2130 DUM = 2
2140 RETURN
2150 DUM = 1
2160 RETURN
8000 '
8001 ' SUBROUTINE TO FIND BESSEL FUNCTIONS OF THE FIRST KIND
8002 '
8010 T1 = 9.999999E-06
8020 PI = 3.14159
8030 X2 = X + X
8040 IF ((X=0) AND (D9=1)) THEN 8240
8050 IF (X > 15) THEN 8260
8060 IF (D9 <> 0) THEN 8090
8070 S6 = 1
8080 GOTO 8130
8090 X3 = X
8100 X = D9 + 1
8110 GOSUB 8290
8120 X = X3
8130 S6 = (X/2)^D9/G5
8140 T3 = S6
8150 I% = 0
8160 IF ABS(T3) <= ABS(S6*T1) THEN 8220
8170 I% = I% + 1
8180 T4 = T3
8190 T3 = -T4 * X2 * .25/(I% * (D9 + I%))
8200 S6 = S6 + T3
8210 GOTO 8160
8220 J7 = S6
8230 RETURN
8240 J7 = 0
8250 RETURN
8260 ' ASYMPTOTIC EXPANSION
8270 J7 = SQR(2/(PI * X)) * COS(X-PI/4-D9*PI/2)
8280 RETURN
8290 'GAMMA FUNCTION
8300 IF (X<0) THEN GOTO 8350
8310 Y = X + 2
8320 G2 = SQR(2*PI/Y) * EXP(Y*LOG(Y) + (1-1/(30*Y*Y))/(12*Y)-Y)
8330 G5 = G2/(X*(X+1))
8340 RETURN
8350 'NEGATIVE ARGUMENT
8360 K5% = 0
8370 G3 = X
8380 IF (X >= 0) THEN GOTO 8420
8390 K5% = K5% + 1
8400 X = X + 1
8410 GOTO 8380
8420 GOSUB 8290
8430 FOR J = 1 TO K5%
8440 X = X - 1
8450 G5 = G5/X
8460 NEXT J
8470 X = G3
8480 RETURN
```

```
1 '  PROGRAM: ARAGO.ANN
2 '
10 KEY OFF
15 DIM INTEN(440)
20 CLS
30 PRINT
40 PRINT "ARAGO PLOTTING ROUTINE:
50 PRINT
60 PRINT "THIS PROGRAM WILL GIVE A CONTOUR PLOT OF THE SPOT OF ARAGO AT A
70 PRINT "CHOSEN DISTANCE BEHIND AN ANNULAR TARGET.  THE APERTURE AND OBSTACLE
75 PRINT "CAN BE DISPLACED.
80 PRINT
90 PRINT "THIS PROGRAM ASSUMES A WAVELENGTH OF 6328 ANGSTROMS.  INPUTS ARE
100 PRINT "THE INNER AND OUTER DIAMETERS, THE TOTAL RADIAL DISTANCE OFF THE
110 PRINT "OPTICAL AXIS FOR COMPUTATION, THE ABERRATION COEFFICIENTS FOR DEFOCUS

120 PRINT "AND SPHERICAL ABERRATION, THE GAUSSIAN CONSTANT AND THE DISTANCES Z1
125 PRINT "AND Z2 (MEASURED FROM THE APERTURE AND OBSTACLE RESPECTIVELY).
130 PRINT
140 PRINT
150 INPUT "INPUT THE TOTAL RADIAL DISTANCE TO BE CALCULATED (IN METERS)";R1
160 PRINT
170 INPUT "INPUT THE APERTURE DIAMETER";DD
172 PRINT
174 INPUT "INPUT THE OBSTACLE DIAMETER";D
176 EPS = D/DD
180 PRINT
185 INPUT "INPUT THE DISTANCE Z1 FROM APERTURE TO VIEWING PLANE (IN METERS)";Z1
190 PRINT
195 INPUT "INPUT THE DISTANCE Z2 FROM OBSTACLE TO VIEWING PLANE (IN METERS)";Z2
200 PRINT
210 INPUT "INPUT THE COEFFICIENT OF DEFOCUS IN TERMS OF WAVELENGTH";W1
220 W020 = 6.328E-07 * W1
230 PRINT
240 INPUT "INPUT THE COEFFICIENT OF SPHERICAL ABERRATION IN TERMS OF WAVELENGTH"
;W2
250 W040 = 6.328E-07 * W2
260 PRINT
270 INPUT "INPUT THE GAUSSIAN CONSTANT";GC
280 PRINT
290 INPUT "DO YOU WANT TO SAVE THE CONTOUR PLOT ON DISK (Y/N)";CPLOT$
300 IF CPLOT$ = "N" GOTO 330
310 PRINT: INPUT "WHAT IS THE NAME OF THE FILE TO STORE THE PLOT UNDER";F1$
320 FIL1$ = "B:" + F1$
330 PRINT
340 INPUT "DO YOU WANT TO SAVE THE INTENSITY PLOT ON DISK (Y/N)";IPLOT$
350 IF IPLOT$ = "N" GOTO 380
360 PRINT: INPUT "WHAT IS THE NAME OF THE FILE TO STORE THE PLOT UNDER";F2$
370 FIL2$ = "B:" + F2$
380 ON ERROR GOTO 390
390 RESUME NEXT
400 PRINT: INPUT "DO YOU WISH TO BYPASS THE CONTOUR PLOT (Y/N)";PDY$
401 '
402 '  CALCULATE ABERRATION AND GAUSSIAN FACTORS
403 '
410 PI = 3.14159
```

```
417 AB1 = (1+8*W020*Z1/(DD*DD)
418 AB2 = (1+8*W020*Z2/(DD*DD))
419 AB3 = 1+16*W040*Z1/(DD*DD)
420 AB4 = 1+16*W040*Z2*D*D/(DD*DD*DD*DD)
421 GF1 = EXP(-G0/4)
422 GF2 = EXP(-G0*D*D/(4*DD*DD))
423 C = COS(12.57*(DD*DD/Z1 - D*D/Z2) - 8*W020*(1-D*D/(DD*DD)) + 8*W040*(1-
    D*D*D*D/(DD*DD*DD*DD)))
424 COEF1 = AB3*GF1*GF1/(AB1*AB1)
425 COEF2 = AB4*GF2*GF2/(AB2*AB2)
426 COEF3 = 2*GF1*GF2*(1-8*W040*(1-D*D/(DD*DD)))*C/(AB1*AB2)
429 I0 = COEF1 + COEF2 - COEF3
430 PRINT : PRINT "COMPUTING ..."
500 D9 = 0
510 R = R1/320
520 FOR I = 1 TO 440
525 FOR J = 1 TO 2
526 IF J = 1 GOTO 530
527 Z = Z2
528 TEMP = EPS
529 GOTO 535
530 '
531 '  CALCULATE ARGUMENT FOR BESSEL FUNCTION AND EVALUATE RADIAL INTENSITY
     FUNCTION
532 '
535 X = (DD * TEMP * I * R * PI)/(6.328E-07 * Z)
540 GOSUB 8000
541 IF J = 1 THEN TEMP2 = J7 ELSE GOTO 550
542 GOTO 559
550 INTEN(I) = COEF1*TEMP2*TEMP2 + COEF2*J7*J7 - COEF3*TEMP2*J7
559 NEXT J
560 NEXT I
570 CLS
890 '
891 ' TRANSFER TO COLOR DISPLAY
892 '
900 PRINT: INPUT "MAKE SURE VIDEO SCREEN IS ON AND HIT RETURN WHEN READY";ARB$
910 DEF SEG = 0
920 POKE &H410,(PEEK(&H410) AND &HCF) OR &H10
930 SCREEN 1,0,0,0 : SCREEN 0: WIDTH 80
940 LOCATE ,,1,6,7 : DEF SEG
950 GOTO 995
960 '
961 ' TRANSFER BACK TO MONOCHROME
962 '
970 DEF SEG = 0
980 POKE &H410, (PEEK(&H410) OR &H30)
990 SCREEN 0: WIDTH 40: WIDTH 80: LOCATE ,,1,12,13: DEF SEG: GOTO 1950
995 SCREEN 2: WIDTH 80
1000 IF PBY$ = "Y" GOTO 1200
1001 '
1002 '  CONTOUR PLOTTING ROUTINE.  FIND INTENSITY AT RADIAL DISTANCE FROM
        SCREEN CENTER (100,320).
1003 '
1004 FOR I = 1 TO 80
1005 FOR J = 1 TO 24
1007 J1 = J*1.7
1010 R2 = CINT(SQR((170-J1*8)*(170-J1*8) + (320-I*8)*(320-I*8)))
```

```
1012 IF R2 < 1 THEN R2 = 1
1015 GOSUB 2020
1020 ON DUM GOTO 1030,1050,1070,1090,1110
1030 A$ =CHR$(0)
1040 GOTO 1130
1050 A$ = CHR$(127)
1060 GOTO 1130
1070 A$ = CHR$(177)
1080 GOTO 1130
1090 A$ = CHR$(178)
1100 GOTO 1130
1110 A$ = CHR$(219)
1150 LOCATE J,I
1160 PRINT A$;
1170 NEXT J
1175 NEXT I
1177 GOSUB 2000
1180 '
1181 '  PAUSE FOR PRINTING AND STORING OF PLOT.
1182 '
1183 FOR K = 1 TO 5000: NEXT K
1185 IF CPLOT$ = "N" GOTO 1200
1190 DEF SEG= &HB800
1195 BSAVE FIL1$,0,&H4000
1200 '
1201 '  DRAW AXES
1202 '
1205 CLS
1210 FOR I = 1 TO 20
1220 LOCATE I,12
1230 PRINT CHR$(179);
1240 NEXT I
1250 LOCATE 21,12
1260 PRINT CHR$(192)
1270 FOR I = 1 TO 56
1280 LOCATE 21,12+I
1290 PRINT CHR$(196);
1300 '
1301 '  LABEL Y AXIS
1302 '
1305 NEXT I
1310 LOCATE 16,9
1320 PRINT 1;CHR$(197)
1330 LOCATE 11,9
1340 PRINT 2;CHR$(197)
1350 LOCATE 6,9
1360 PRINT 3;CHR$(197)
1370 LOCATE 1,9
1380 PRINT 4;CHR$(197)
1390 FOR I = 1 TO 9
1400 LAB1$ = "NORMALIZE": LAB2$ = "INTENSITY"
1410 FOR I = 1 TO 9
1420 LOCATE 5+I,7
1430 PRINT MID$(LAB1$,I,1);
1440 LOCATE 6+I,6
```

```
1440 PRINT MID$(LAB2$,I,1);
1460 NEXT I
1470 LOCATE 16,3
1480 PRINT "D";
1530 '
1531 '  LABEL X AXIS
1532 '
1540 LOCATE 24,25
1550 PRINT "RADIAL DISTANCE (.001 M)";
1560 '
1561 '  PLOT RADIAL INTENSITY FUNCTION
1562 '
1565 DDD = 1250 * R1
1570 POW = INT(LOG(DDD)/LOG(10))
1580 SCALE = DDD/10^POW
1590 IF SCALE < 4 THEN FACT = 2 ELSE FACT = 1
1600 UNIT = 30/(SCALE * FACT)
1610 FOR I = 1 TO INT(SCALE * FACT)
1620 LOCATE 21,12 + I*UNIT
1630 PRINT CHR$(197)
1640 LOCATE 22,10 + I*UNIT
1650 PRINT I*10^POW/FACT
1660 NEXT I
1665 YO = 164 - CINT(IO*40)
1666 YO = 93
1670 FOR I = 1 TO 440
1680 Y = 164 - CINT((INTEN(I) * 160)/4)
1685 X = 93 + I
1695 LINE (X,Y)-(XO,YO)
1700 XO = X
1705 YO = Y
1710 NEXT I
1720 LOCATE 25,6
1730 PRINT USING "O.D.= .### M.    I.D. = .#### M.    Z DIST. = #.### M.  GAUSS. C
INST. = #.##";DD,D,Z1,GC;
1735 LOCATE 1,1
1740 FOR I = 1 TO 5000
1745 NEXT I
1750 IF IPLOT$ = "N" GOTO 1800
1760 '
1761 '  STORE INTENSITY PLOT ON DISK
1762 '
1765 DEF SEG= &HB800
1770 BSAVE FIL2$,0,&H4000
1800 PRINT: INPUT "DO YOU WISH A LISTING OF THE INTENSITIES(Y/N)";D1$
1810 IF D1$ = "Y" THEN GOTO 1820 ELSE GOTO 1940
1820 LPRINT:LPRINT:LPRINT:LPRINT:LPRINT:LPRINT:LPRINT:LPRINT :LPRINT
1830 LPRINT : LPRINT : LPRINT : LPRINT : LPRINT : LPRINT : LPRINT
1840 LPRINT "RADIAL DISTANCE(MM)    INTENSITY    EXTREMUM TYPE
1850 LPRINT "--------------------    ---------    ------------
1855 IF IO - INTEN(1) > 0 THEN EXT$ = "MAXIMUM" ELSE EXT$ = "MINIMUM"
1860 LPRINT USING "       #.###                #.###";O,IO;
1865 LPRINT "          ";EXT$
1869 SIGN = SGN(IO-INTEN(1))
1870 FOR I = 1 TO 439
1880 IF SGN(INTEN(I+1)-INTEN(I)) = SIGN GOTO 1930
1890 IF SIGN > 0 THEN EXT$ = "MAXIMUM" ELSE EXT$ = "MINIMUM"
1900 SIGN = SGN(INTEN(I+1)-INTEN(I))
1910 LPRINT USING "       #.###                #.####";I*R*1000,INTEN(I);
1920 LPRINT "          ";E
1930 NEXT I
```

```
1940 GOTO 970
1950 CLS
1960 INPUT "DO YOU WISH TO MAKE ANOTHER RUN (Y/N)";D$
1970 IF D$ = "N" THEN END ELSE GOTO 130
2000 '
2001 '  LABEL CONTOUR PLOT
2002 '
2005 LOCATE 24,1
2010 PRINT "LEGEND: ";CHR$(221);" I < .01 Io  ";CHR$(178);" I < .05 Io  ";CHR$(1
77);" I < .1 Io  ";CHR$(176);" I < .5 Io  ";CHR$(0);" I > .5 Io";
2020 RETURN
2030 '
2031 '  FIND SHADING FOR CONTOUR PLOT POINTS
2032 '
2035 IF INTEN(R2) > .002 GOTO 2060
2040 DUM = 5
2050 RETURN
2060 IF INTEN(R2) > .05 GOTO 2090
2070 DUM = 4
2080 RETURN
2090 IF INTEN(R2) > .1 GOTO 2120
2100 DUM = 3
2110 RETURN
2120 IF INTEN(R2) > .5 GOTO 2150
2130 DUM = 2
2140 RETURN
2150 DUM = 1
2160 RETURN
8000 '
8001 ' SUBROUTINE TO FIND BESSEL FUNCTIONS OF THE FIRST KIND
8002 '
8010 T1 = 9.999999E-06
8020 PI = 3.14159
8030 X2 = X * X
8040 IF ((X=0) AND (D9=1)) THEN 8240
8050 IF (X > 15) THEN 8260
8060 IF (D9 <> 0) THEN 8090
8070 S6 = 1
8080 GOTO 8140
8090 X3 = X
8100 X = D9 + 1
8110 GOSUB 8290
8120 X = X3
8130 S6 = (X/2)^D9/G5
8140 T3 = S6
8150 I% = 0
8160 IF ABS(T3) <= ABS(S6*T1) THEN 8220
8170 I% = I% + 1
8180 T4 = T3
8190 T3 = -T4 * X2 * .25/(I% * (D9 + I%))
8200 S6 = S6 + T3
```

END

FILMED

2-85

DTIC